91-03

Numerical Assessment Of Three-Dimensional Rigid Pavement Joints Under Impact Loads

Minnesota Department of Transportation

Dept. of Civil and Mineral Engineering
University of Minnesota

REPORT DOCUMENTATION PAGE	1. Report No. MN/RD - 91/03	2.	3. Recipient's Accession No.

4. Title and Subtitle Numerical Assessment Of Three-Dimensional Rigid Pavement Joints Under Impact Loads	5. Report Date August, 1990 6.
7. Author(s) Amir Koubaa, Prof. Theodor Krauthammer	8. Performing Organization Rept. No. 9RD0004
9. Performing Organization Name and Address University of Minnesota Dept. of Civil and Mineral Engineering 122 Civil and Mineral Engineering Bldg. 500 Pillsbury Drive, S.E. Minneapolis, MN 55455-0220	10. Project/Task/Work Unit No. 11. Contract(C) or Grant(G) No. (C) 64988 (G)
12. Sponsoring Organization Name and Address Minnesota Department of Transportation Materials and Research Laboratory 1400 Gervais Avenue Maplewood, Minnesota 55109	13. Type of Report & Period Covered Final Report 1988-1990 14.

15. Supplementary Notes

16. Abstract (Limit: 200 words)

This study was conducted with the aim of improving the state of knowledge on the behavior of joints in concrete pavements, and to explore the feasibility of developing a non-destructive testing technique based on frequency response of dynamically loaded joints. One of the objectives of this study was to numerically investigate the existence of a relationship between load transfer capacity of a joint in rigid pavements and its dynamic response. The approach adapted for the present study is based on a numerical model which accurately represents the mechanism of shear transfer in reinforced concrete members implemented it in a commercially available finite element code. That tool is then used for the analysis of two models which consisted of various joint conditions. One model represented an ideal condition of full load transfer across a joint, while the other model was used to simulate variable load transfer conditions. The results obtained are analyzed in the time and frequency domains. These results provided a comprehensive description of the joint response characteristics, and enabled the derivation of a clear relationship between the response frequencies and the joint's shear transfer capabilities. The results may be used as the starting point for the development of a precise/non-destructive testing method for a wide range of cases in which shear transfer across discontinuities in concrete systems is a principal load resisting mechanism. Specific conclusions and recommendations on future developments have been provided.

17. Document Analysis a.Descriptors
Frequency Analysis
Impact Testing
Pavement Joints

b.Identifiers/Open-Ended Terms

c.COSATI Field/Group

18. Availability Statement No restrictions. This document is available through the National Technical Information Services, Springfield, VA 22161	19. Security Class (This Report) Unclassified 20. Security Class (This Page) Unclassified	21. No. of Pages 182 22. Price

NUMERICAL ASSESSMENT OF THREE-DIMENSIONAL RIGID PAVEMENT JOINTS UNDER IMPACT LOADS

Final Report

Prepared by

Amir Koubaa

Prof. Theodor Krauthammer

Department of Civil and Mineral Engineering
University of Minnesota

Submitted to

Research Administration and Development Section
Office of Materials and Research
Minnesota Department of Transportation

August 1990

TABLE OF CONTENTS

CHAPTER 3 APPROACH OF THE STUDY

CHAPTER 4 RESULTS

List of Tables

List of Figures

ACKNOWLEDGEMENTS

This research was sponsored by the Minnesota Department of Transportation under Grant No. MNDOT/64988 T.O #39

I wish to express my gratitude to my advisor, Dr. Theodore Krauthammer for his patience, encouragement, guidance, and assistance during the preparation of this thesis. I would like also to thank professors C. French and H. Jenkins for participating on my examination committee.

I would like to thank Hussein Shanaa and Dipanker Chandra for their valuable help and guidance. Special thanks to Mr. Greg Sherar of the computer group in the department of Civil and Mineral Engineering at the University of Minnesota. Special thanks is extended to Pandu Kulkarni, Iyad Alsamsam, Steve Olson, Paul Bergson, Lucio Palmieri and Brahim Mezghani.

Finally I would like to thank my wife Zahira and my father Taoufik for their patience, support, perseverance and understanding, through all of this, my love and affection.

EXECUTIVE SUMMARY

This study was conducted for the Minnesota Department of Transportation with the aim of improving the state of knowledge on the behavior of joints in concrete pavements, and to explore the feasibility of developing a non-destructive testing technique based on frequency response of dynamically loaded joints. One of the objectives of this study was to numerically investigate the existence of a relationship between load transfer capacity of a joint in rigid pavements and its dynamic response, and the obtained results confirm the existence of such a relationship.

The approach adapted for the present study is based on a numerical model which accurately represents the mechanism of shear transfer in reinforced concrete members implemented it in a commercially available finite element code. That tool is then used for the analysis of two models which consisted of various joint conditions. One model represented an ideal condition of full load transfer across a joint, while the other model was used to simulate variable load transfer conditions. The results obtained are analyzed in the time domain for understanding the pavement behavior and also in the frequency domain by using Fast Fourier Transformation for relating the condition of a joint to the frequency response. These results provided a comprehensive description of the joint response characteristics, and enabled the derivation of a clear relationship between the response frequencies and the joint's shear transfer capabilities. The results may be used as the starting point for the development of a precise non-destructive testing method for a wide

range of cases in which shear transfer across discontinuities in concrete systems is a principal load resisting mechanism.

Specific conclusions and recommendations on future developments and corresponding parametric studies have been provided.

CHAPTER 1

INTRODUCTION

1.1 Objectives of the study

Pavement characterization is of critical importance in the resources allocation for rehabilitating the deteriorating highway infrastructure. It has been recognized that cracks and joints in concrete pavements have a significant effect on the mechanical responses of pavements. There have been various attempts, both experimental and numerical, for studying the performance of concrete pavements. While nondestructive testing methods and empirical procedures are common, a move toward more rational methods that consider the dynamic response for assessing pavement integrity is also evident. In a previous study by Krauthammer and Western '88, it was shown that the shear transfer across a rigid pavement joint can be described accurately by a shear stress vs a shear slip relationship. A deterioration in the joint shear transfer capability was correlated to a reduction in the joint shear stiffness.

The objective of this study was to analyze the effects of joint shear transfer on pavement behavior and to investigate the feasibility of relating the joint deterioration to the response frequency, which is based on a Fourier synthesis of a solution for dynamic impulsive loading of a layered pavement.

1.2 Scope of the study

This study focuses on the relationship between shear transfer capabilities and the frequency domain response. The approach adapted here is to apply a finite element code for analyzing concrete pavement systems by evaluating jointed rigid pavements that were defined by a load transfer model that represents the mechanism of shear transfer across rigid pavement joints. The joint response is then analyzed both in the time domain and in the frequency domain, and a correlation between these results is presented.

The cases considered in this study are: 1. Two pavement slabs which consist of concrete and base material with the joint mechanism connecting the two, and 2. One slab that has an overall dimension of the two previous combined slabs laying on the same base material. This case represents a perfect joint in which no discontinuity exists.

CHAPTER 2

BACKGROUND

2.1 Finite Element Approach

Previous studies were conducted to investigate the behavior of pavement slabs. It was noticed in studies by Chou '81, '84 that the joint shear transfer capability had a major influence on the stresses when the load was applied in the joint region, and that stresses in the slab were reduced when higher joint efficiency values were used. The joint efficiency is recognized as a physical property of the joint, and is defined as the ratio of the deflection of the unloaded side to deflection of the loaded side of the joint.

Researchers employed the finite element method (FEM) for studying the performance of pavements and the relationships to design applications. For example Huang and Wang '78 studied the effect of loading position, efficiency of load transfer and loss of subgrade contact on critical stresses due to the modulus subgrade reaction, k, in rigid pavements, and their approach was similar to the procedure used in other studies.

In the studies by Tabatabaie and Barenberg '78, '80, the development, verification and the application of a finite element model were reported. Their model was based on the classical theory for medium-thick plate (concrete slabs on stabilized base and overlay) on Winckler foundation in order to analyze one of the two layered concrete pavements with joints or cracks, including the effect of load transfer systems due

to dowel bars and aggregate interlock. In the same study, they used similar assumption as in the works by Chou '81 and Huang and Wang '78 for the subgrade reaction. It was later modified by Ioannidis, Barenberg and Thompson '84 where the concept of the Resilient Modulus of the subgrade reaction, K_r, was introduced because the response of subgrade under repeated impulsive loads. Krauthammer and Western '88 investigated joint shear transfer effects on pavement performance using the finite element method. In that study, they employed an explicit shear-stress shear slip relationship for representing the shear transfer across a rigid pavement joint.

The finite element method (FEM) is also employed in this study. It is an approximate, but highly effective, numerical method for solving structural problems, where the actual continuous structure is replaced by an idealized structure composed of discrete elements connected together at nodes. The FEM is based on displacement fields, or stress patterns, within an element and by using variational principles (for example, the energy method), for deriving the stiffness matrix that relates the nodal forces to the nodal displacements. Cook, Malkus and Plesha '89 specified that the FEM analysis usually involves the following steps:

1. Divide the structure into small finite elements.
2. Formulate the material properties of each element.
3. Assemble the elements together to obtain the finite element structural model.
4. Apply the loading pattern to the model.

5. Specify the boundary conditions by constraining specific nodes from moving in certain directions.
6. Solve the simultaneous linear algebraic equations to find the degree of freedom of the nodes.
7. Find the strains, stresses, deflections from the degrees of freedom of the nodes.

The reader can find extensive information on the method also in other books (e.g. by Bathe '82). For this study, it was decided to employ the commercially available finite element code, ADINA '81. Although ADINA was not developed to be used specifically for pavement analysis, it is similar to many general purpose codes and it could be employed in a design office environment.

The approach for this study is similar to recent studies on dynamic soil structure interaction in which the rigid pavement is considered to be a reinforced concrete system placed on a soil foundation. The background information on structural dynamics can be obtained from Newmark and Roseinblueth '71, on reinforced concrete structures from Park and Pauley '75, and on foundation dynamics from either Barkan '62 or by Richart, Hall, and Woods '70.

The loading conditions that were employed for a parallel experimental study were generated by a drop weight machine for obtaining high loading rates. Unfortunately, a standard technique for testing concrete systems under impact does not exist, and this method can not be

compared to others. These general loading conditions are later used for the finite element analysis based on the time histories that were obtained experimentally. The drop weight machine was placed on top of a load cell that was connected to a high speed data acquisition, as described by Palmieri '90.

2.2 Loading on Pavements

In structural analysis, it is essential to identify the loading pattern, the loading intensity and type (static or dynamic, concentrated or distributed) and time history.

Loading on pavements comes from the wheels of vehicles, and this loads depends on:

- Weight of the vehicle
- Number of wheels under the vehicle and their distributions
- Tire-pavement contact area
- Speed
- Road conditions

Because of the variety of traffic loads on pavements (loading configurations and intensities) and the difficulty of accounting for every loading situation, several methods were introduced to simulate the traffic loading such as :

- Equivalent single wheel loads (ESWL) and equivalent wheel load factor (EWLF)

- Equivalent axle load (EAL)
- Falling weight deflectometer (FWD)
- Dynaflect or Road Rater

The background information on ESWL, EWLF and EAL can be obtained from the book by Yoder and Witczak '75. The interpretation and the analysis of the data obtained from the Road Rater were somewhat difficult (because of the spurious resonances in pavement layers), as reported by Selby, Davis and Mamlouk '85, and the loading patterns do not accurately represent the traffic loading. Hoffman and Thompson '82 reported that the FWD test yielded good correlations with pavement deflection when subjected to traffic loading. The FWD consists of a large mass which falls vertically under gravity onto a spring loaded plate resting on the pavement surface. Four different masses may be used, 110, 220, 440 and 660 lbs which can be dropped from heights varying from 0.5 to 15 inches, producing a load that varies from 1,500 to 24,000 lbs. The load pulses have a half-sine wave shape with a duration of about 25 to 30 milliseconds (Fig 2.1). Such loads induce deflections in the pavement surface which are obtained from integrating the measured velocities over the pulse duration. However, the time history of a truck, traveling at 50 mph, shows a load duration of about 100 milliseconds which may indicate that the FWD test may not simulate accurately traffic loads (Hoffman and Thompson '82).

2.3 Concrete Strength Parameters

In pavement engineering, the properties of concrete that are of the most interest are :

- Concrete compressive strength, f'_c
- Modulus of rupture (MR) determined by flexural test
- Modulus of elasticity, E_c
- Poisson's ratio, ν_c

2.3.1 Determination of f'_c

The compressive strength of concrete, f'_c, depends on the mix proportions, water-cement ratio, cement type, conditions of mixing, aggregate character and gradation, size and shape of test specimen, temperature, curing condition and the age of the concrete. The value of f'_c is generally determined experimentally by testing cylinders made in the laboratory or in the field, cores of hardened concrete cut from a structures, or cubes. Detailed descriptions are given by Park and Pauley '75 or by Wang and Salmon '85.

2.3.2 Modulus of Rupture: MR

Modulus of rupture, MR, is the tensile strength of concrete determined by the flexural strength of a beam and is measured in accordance with ASTM '75 standard procedure. The test specimen has the dimension of 6"x6"x18" and is usually tested after 7, 14, 28 or 90 days after being casted from the design mix (Wang and Salmon '85).

The value of MR is obtained according to the following formula:

$$MR = M*c/I \qquad (2.1)$$

in which

M = maximum bending moment (in-lb)

c = distance from the neutral axis to the extreme fiber in tension (in)

I = moment of inertia of the beam cross section with respect to the neutral axis (in^4)

An approximate relationship between the modulus of rupture and compressive strength of concrete is given by Park and Pauley '75 or by Wang and Salmon '85.

$$MR = K * f'_c \qquad (2.2)$$

where K is a constant ranging from 7 to 13 and with common values between 8 to 10.

It's recommended by the ACI 318-89 code (section 9.5.2.3) for normal weight concrete to use a K value of 7.5 and for light weight concrete to multiply the value of MR by 0.75.

2.3.3 Modulus of Elasticity:

The modulus of elasticity of concrete varies with the strength and it depends on the age of the concrete, properties of aggregates and cement used, loading rate and specimen type and size, (Wang and Salmon '85). For normal weight concrete E_c can be determined, according to Pauw '60, by the equation

$$E_c = 57000 \sqrt{f'_c} \quad (psi) \qquad (2.3)$$

This equation gives the modulus of elasticity under static loads. Under dynamic conditions, the value of modulus of elasticity can be up to

twice the static value. Park and Pauley '75 reported that under dynamic loading, the modulus of elasticity can be up to 1.62 the static value for low strength concrete (2.5 ksi) and 1.4 for high strength concrete (6.5 ksi). However in this study no dynamic enhancement factor was used for the modulus of elasticity values.

2.3.4 Poisson's Ratio, ν

Poisson's ratio, ν, is the ratio of lateral strain, ϵ_l, to the axial strain, ϵ_a, in the direction of the applied uniaxial load. A value of ν between 0.15 and 0.20 is usually determined, however values between 0.1 and 0.3 have been reported. Poisson's ratio is generally considered lower for high-strength concrete (Park and Pauley '75). A value of 0.28 was selected in this study, as used by Tabatabaie and Barenberg '80.

2.4 Behavior of Reinforced Concrete Members in Shear

Almost all the structural members, with the exception of members in pure bending, should establish mechanisms to transfer shear. Shear transfer is influenced by the material under consideration, configuration and geometry of the structure. The shear behavior for homogeneous material is well defined because of the simplicity of the material. For cementinious materials, the shear behavior is more complicated because such materials are less understood. For composite material (e.g. reinforced concrete) this problem is at least as complicated.

In reinforced concrete members, shear transfer relies significantly on the tensile and compressive strength of the concrete. Therefore, not

surprisingly, shear failure is generally nonductile (Park and Pauley '75). The transfer of shear in reinforced concrete members is accomplished in different manners, and the behavior of the concrete structures depends mainly on the method of shear transfer. The main types of shear transfers are as follows:

- Shear transfer due to concrete shear force, V_c: This type of shear transfer occurs due to shearing stresses which will interact with tensile and compressive stresses to produce principal stresses. These principal stresses are responsible for the formation of inclined cracks and the concrete crushing.

- Interface shear transfer, V_a: This is also called aggregate interlock which can be adequately described on the micro-level, as reported by Walraven and Reinhard '81. The shear transfer mechanism relies predominantly on the aggregate interlock which is essentially responsible for the transmission of only shear stresses across a crack or a joint due to the irregular interlocking of the aggregate along the concrete surfaces on each side of the crack or joint. Tabatabaie and Barenberg '78 reported that the joints or cracks must be pressed tightly together for transmitting shear.

- Dowel action, V_d: This is accomplished by reinforcing bars crossing a crack or a joint which will provide resistance to the shearing displacements by the doweling force. Dowel bars are responsible for both shearing stresses and moments as shown in the works by Tabatabaie and

Barenberg '78.

- Arch action : This action is particularly for deep beams which transmit loads to the supports. In slabs, The arch action may occur around interior columns.

- Beam action: This is provided by the cracks induced by the load which will result in the division of the tension zone into small blocks, with each one acting as a cantilever. The cantilever action results from the increase of the tensile force between adjacent cracks, shear displacements at the faces of cracks and the induction of dowel forces across the flexural reinforcement (Park and Pauley '75).

- Shear reinforcement: This is provided by the vertical or inclined stirrups. The shear reinforcement restrict the enlargement of cracks that can reduce the shear interlock transfer.

All of the above mechanisms participate in the shear resistance. For a rectangular beam without shear reinforcement, it was reported by Talar '74 that after an inclined crack has formed, each of the following mechanisms contribute to the shear resistance according to the following ranges:

Dowel Action	15 to 25 %
Uncracked concrete compression zone	20 to 40 %
Aggregate interlock	33 to 50 %

For beams, shear failures are characterized by the occurrence of inclined cracks which develop, grow and then initiate failure due to the relative magnitude of shearing stress, v_c, and the flexural stress, f_t. The expressions of v_c and f_t are :

$$v_c = \frac{V}{b_w\ d} \tag{2.4}$$

$$f_t = K_2\ \frac{M}{b\ d^2} \tag{2.5}$$

in which:

b_w = Width of the beam web (in)

b = Width of the beam flange (in)

d = Effective depth (in)

V = Shear force (lbs)

M = Moment (lbs-in)

K_1, K_2 = Coefficients that depends on beam geometry, loading type and reinforcement ratio

For a rectangular beam, the ratio of v_c and f_t is

$$\frac{f_t}{v_c} = \frac{K_2}{K_1}\ \frac{M}{V\ d} = \frac{K_3\ M}{V\ d} \tag{2.6}$$

When beams are subjected to concentrated load, we have the following equation :

$$M = V * a \tag{2.7}$$

where :

a = shear span

Combining Equation (2.6) and (2.7) we obtain :

$$\frac{f_t}{v_c} = K_3 \frac{a}{d} \qquad (2.8)$$

It was reported by Bresler and MacGregor '76 that the ratio a/d has a major influence on the shear strength and the inclined cracking load.

2.5 Soil Strength Parameters

The base material belongs to the dense category of sand-gravel, which gives a range of modulus of elasticity, E_{sb}, values of 5,000 to 25,000 psi (Das '84). A value of 10,500 psi was used in this study. In dynamic analysis, the modulus of elasticity can be up to 1.5 times the static value, as discussed by Newmark and Rosenblueth '71. In this model, no dynamic factor was used for the soil material properties. The value of Poisson's ratio ranges from 0.15 to 0.35 for subsoils, and a typical value of 0.25 was adapted in this model (Das '84).

2.6 Joints

Joints are locations where discontinuities in slabs occur. They are placed in concrete pavements to permit contraction and expansion of the pavement for relieving the stresses due to temperature changes, moisture changes, friction and to facilitate construction (AASHTO '86).

Joints can be divided into four categories, as given by Yoder and Witczack '75:

- **Contraction joints**: Contraction joints are placed to control cracking of concrete slab due to tensile stresses from moisture,

temperature, friction and shrinkage. If contraction joints are not placed, random cracking will occur on the surface of the slabs, as reported in AASHTO '86. To make sure that cracking will occur at a certain location, a groove is cut at that location, and the joint may not be doweled. The load transfer is accomplished by grain interlock of the lower cracked portion of the slab or by dowel action if dowel bars are present. This type of joint will not relieve expansion stresses (Yoder and Witczack '75).

If dowel bars are present, generally spaced at the middepth of the slab, it is important to use smooth bars and to lubricate at least half of the length of bars since the slabs are moving in relation to one another in the longitudinal direction (Yoder and Witczak '75). The joint may be formed by sawing the concrete after pouring, but without leaving marks on the concrete or displacing pieces of aggregates. To form a groove, a metal or fiber strip is placed in the uncured concrete and removed as soon as the initial set of the concrete has occurred.

- **Expansion joints**: Expansion joints are used primarily to provide space for the expansion of the pavements which causes the development of compressive stresses. The compressive stresses in slabs may cause the buckling of the pavements as reported in AASHTO '86. These joints are constructed with a clean break throughout the depth of the slab to permit the expansion of the slabs. The openings between slabs is usually set to 3/4 inches although in some cases a value of 1.0 inch should be used. Aggregate interlock does not exist in this case so load transfer should

be provided by dowel bars which must be smooth and lubricated. An expansion cup is mandatory to provide sliding of the bars during expansion(Yoder and Witczak '75).

Expansion joint for highways are susceptible to pumping action, the ejection of water and subgrade materials through joints or cracks at the edges of the pavements due to the accumulation of free water, therefore many states have stopped their construction. Some studies reported that high expansion stresses are influenced by the type of coarse aggregate and their source. This may lead to the use of expansion joints along with low thermal expansion type of aggregates. Some states are still using expansion joints, and other states use them in lieu of contraction joints (Yoder and Witczak '75).

- **Construction joints**: Construction joints are usually used to facilitate construction and contain dowel bars to transfer the load across the joint (AASHTO '86). These joints are used also at the transition between the old pavement and the construction such as the end of the day's pour. But construction joint are often used in highway work, and keyed construction joints are used in airfield pavements. Keyed, longitudinal construction joints are not usually tied with dowel bars except for the extreme outer slabs (Yoder and Witczak '75).

- **Hinge or warping joints**: These joints are used to control cracking along the centerline of highway pavements. The type of joint depends primarily upon the method of pouring the concrete slab. Keyed

joint are usually built when "a line at a time" construction is used. To make sure that the key is transferring load, tie bars are used to tie keyed joints together. When two-lane construction is used, the dummy groove joint type is the most convenient longitudinal warping joint to be used. For this type, tie bars are used to assure aggregate interlock (Yoder and Wictzak '75).

2.7 Joint Efficiency

Non destructive deflection testing methods are used to evaluate the structural capacity and the situ load transfer capacity of rigid pavement joints. AASHTO '86 reported that nondestructive deflection tests are efficient tool to evaluate the actual performance of the joints in the fields relative to their expected performance in the design phase. The amount of load transferred across a rigid pavement joint is related directly to the flexural slab stress near the joint. The joint efficiency, which is a physical property of the joint, measures the load transfer capability by the deflection efficiency J.E. which is expressed by the following formula :

$$J.E. = \frac{d_u}{d_l} \; 100 \qquad (2.9)$$

where

d_u = deflection at the joint or crack of the unloaded side

d_l = deflection at the joint or crack of the loaded side

The joint deflection efficiency values are between 0 to 100%, as shown in figure 2.2. If there is no load transfer, the stresses and the

deflection in the loaded slab side are increased and may cause the breakup and the loss of serviceability of the slab. Foxworthy '85 reported that the joint shear efficiency is influenced by temperature changes, magnitude of applied load, soil characteristics, moisture and shrinkage.

2.8 Wave Propagation

Dynamic problems are categorized as wave propagation problem or as structural dynamic problem. In the case of wave propagation problem, the loading is an impact or blast, which will result in high frequencies. In such case, the most interest is in the effect of stress waves (Cook, Malkus, Plesha '89).

When subjected to a dynamic loads, three different types of waves are propagating:

1. **P-wave**:This wave is called a dilatational wave or primary wave. The dilatational wave does not involve rotation and is a body wave (Rinehart '75). The P-wave velocity has a velocity of c_1 which is given by the following equation:

$$c_1 = \sqrt{\left(\frac{\lambda + 2\,G}{\rho} \right)} \tag{2.10}$$

in which

λ , G = Lame's parameters

$$\lambda = \frac{2\,\nu\,G}{(1 - 2\,\nu)} \tag{2.11}$$

ν = Poisson's ratio

$$G = \frac{E}{2\,(1+\nu)} \qquad (2.12)$$

E = Modulus of elasticity

2. S-wave: This is often called a shear wave or distortion waves. Rinehart '75 describes this type of wave as a body wave which involves rotation and no dilatation and propagates with a velocity ,c_2, of :

$$c_2 = \sqrt{\frac{G}{\rho}} \qquad (2.13)$$

3. R-wave : This is called a Raleigh wave and is a surface wave. The raleigh wave is in function of the shear wave as given by the following expression (Kolsky '63):

$$G = \alpha\, c_2 \qquad (2.14)$$

where α is a function of the Poisson's ratio and varies

from : $\alpha = 0.875$ for $\nu = 0.0$

to : $\alpha = 0.955$ for $\nu = 0.5$

The Raleigh wave and shear wave are not particularly dependant on the Poisson's ratio, However the longitudinal wave is strongly dependant on the Poisson's ratio, as shown by Moore et al '78. The shear wave velocity is usually about 1/2 the longitudinal wave velocity ($C_2 = 0.5\ C_1$), as reported by Rinehart '75.

In concrete and soils, wave velocities are sensitive to the state

of stress, temperature, composition, voids and cracks.

2.9 Time History Analysis: Direct Integration Method

For structural dynamics, wave propagation and nonlinearities problems, the Direct Integration Method (D.I.M) is very useful and necessary. Cook, Malkus and Plesha reported '89 that the D.I.M. is a step-by-step method where a finite difference approximation is used to replace some of the time derivatives term $\{\dot{D}\}$ and $\{\ddot{D}\}$ of the displacement vector $\{D\}$ in the dynamic motion equation:

$$[M]\{\ddot{D}\} + [C]\{\dot{D}\} + [K]\{D\} = \{F(t)\} \qquad (2.15)$$

where

$[M]$ = mass matrix of the structure

$[C]$ = damping matrix of the structure

$[K]$ = stiffness matrix of the structure

$\{D\}$ = displacement vector of the structure

$\{\dot{D}\}$ = first derivative of $\{D\}$ with respect to time

$\{\ddot{D}\}$ = second derivative of $\{D\}$ with respect to time

$\{F(t)\}$ = loading vector of forces applied on the structure

In direct integration method, $\{\dot{D}\}$ and $\{\ddot{D}\}$ are replaced by differences of displacements $\{D\}$ at various instants Δt. The method is to write the equation of motion at a specific instant time $n\Delta t$ in the following expression:

$$[M]\{\ddot{D}\}_n + [C]\{\dot{D}\}_n + [K]\{D\}_n = \{F\}_n \qquad (2.16)$$

in which n denotes the time $n\Delta t$ and Δt is the time step increment.

Cook, Malkus and Plesha '89 reported that the time step increment, Δt, need to satisfy the following stability condition:

$$\Delta t \leq 2/\omega_{max} \tag{2.17}$$

where ω_{max} is the highest natural frequency of the structure which is estimated for linear-displacement case by the following formula:

$$(\omega_{max})_e = 2\ c/L \tag{2.18}$$

in which

c = dilatational wave and is given by equation (2.)

L = the shortest length of linear displacement elements

2.10 Fourier Series and Fast Fourier Transform

Many of the computational problems can be solved by the "Fourier Transform methods" or "Spectral methods". The Fourier transform is simply an efficient computational tool to manipulate data, as discussed in various sources, for example Tolstov '62, Churchill and Brown '78. It can be shown that any function of time f(t) can be represented over the interval $-\pi/w < t < \pi/w$ by a sum of sines and cosines of varying frequencies and amplitudes. This is called the Fourier series of the function and is given by the following equation:

$$f(t) = 1/2\ a_0 + \Sigma(\ a_n \cos(wnt) + b_n \sin(wnt)\ ) \tag{2.19}$$

a_n = amplitude of the cosine wave at a frequency nw (rad/sec)

$$= (w/\pi) \int_{-\pi/w}^{\pi/w} f(t) \cos(nw\tau)\, d\tau \tag{2.20}$$

b_n = amplitude of the sine wave at a frequency nw (rad/sec)

$$= (-w/\pi)\int_{-\pi/w}^{\pi/w} f(t)\ \sin(nw\tau)\ d\tau \qquad (2.21)$$

The sign "=" is not appropriate and it should be "~" , because the above series is not equal to the function f(t) for all t but is equal to the "periodic extension of f(t) over the interval $-\pi/w < t < \pi/w$. The Fourier series is equal to the function f(t) for all t if the f(t) is a periodic function.

Theoretically, it is possible to find a series of sines and cosines that represent any continuous function f(t) for t. If w is made to be very small, then the interval $(-\pi/w, \pi/w)$ will become very large and the Fourier series is obtained as what so called the "Fourier Integral Formula" :

$$f(t) = 1/\pi \int_{0}^{\infty} [\ A(w)\ \cos(wt) + B(w)\ \sin(wt)\ ]dw \qquad (2.22)$$

in which

$$A(w) = \int_{-\infty}^{\infty} f(\tau)\ \cos(w\tau)\ d\tau$$

$$B(w) = \int_{-\infty}^{\infty} f(\tau)\ \sin(w\tau)\ d\tau$$

The above Fourier Integral Formula has a fundamental period of $(-\infty,\infty)$, stated differently: the Fourier Integral Formula represent f(t) in function of cosines and sines of varying amplitude and frequencies. When we use the complex form and by Euler's equation one has:

$$e^{i\vartheta} = \cos \vartheta + i \sin \vartheta \tag{2.23}$$

replacing $\vartheta = wt$ and rewriting equation (2.22)

$$f(t) = \int_{-\infty}^{\infty} F(w)\, e^{-iwt}\, dw \tag{2.24}$$

where F(w) is the fourier transform of f(t) and is given by the following expression:

$$F(w) = \int_{-\infty}^{\infty} f(\ )\, e^{iw\tau}\, d\tau = A(w) + i\, B(w) \tag{2.25}$$

To obtain the Fourier Transform F(w) of complicated cases, one must use numerical integration. A numerical integration of F(W) is called a Discrete Fourier Transform, which requires extensive computational resources. However, for a large array of data, this becomes almost impossible, and a need for approximations arises. Such approximation will result in some inaccuracy, as discussed by Stearns '75. When implemented, this numerical method is called the Fast Fourier Transform (FFT), and it was employed for evaluating the time histories obtained from the finite element analysis.

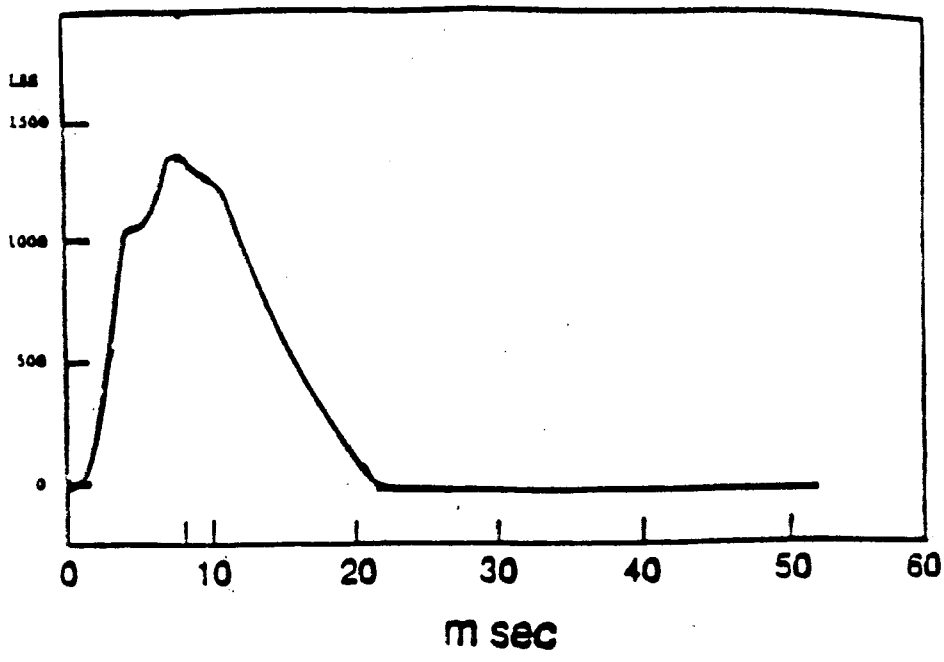

Figure 2.1: Load-Time History

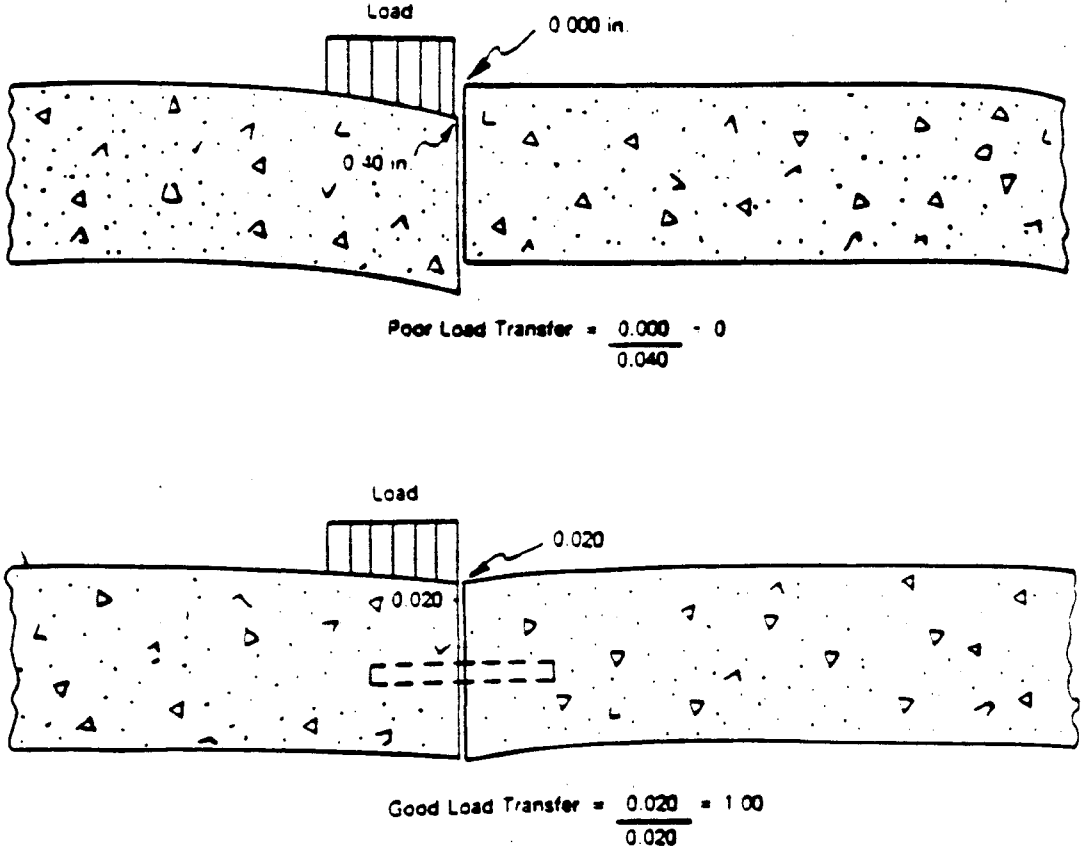

Figure 2.2: Illustration of poor and good load transfer

CHAPTER 3

APPROACH OF THE STUDY

3.1 General

In a study by Krauthammer and Western '88, the joint shear transfer effects on pavement performance were investigated. An explicit shear stress-shear slip relationship was successfully employed for defining the shear transfer across a pavement joint. A deterioration in the joint shear transfer capability has been correlated to a reduction in the joint shear stiffness and it was presented as a decrease in the joint efficiency, as it will be explained next. The present approach was developed to understand the overall behavior of the mechanism of shear transfer across pavement joints and by performing time and frequency analyses of the joint's dynamic response.

In the field, several nondestructive testing methods have been developed to investigate the performance of joints, and the FWD test is one of these widely used methods. This method provides the ratio between the pavement deflection at two points located at equal distances from the joint face on each side. This ratio is defined as the "joint efficiency" which is clearly related to the joint shear transfer capacity. A new joint will correspond to a joint efficiency value close to 1.0, while a dead joint will correspond to a significantly low value of joint efficiency, as shown in Table 3.1. For this study, a loading history was taken from a drop test during a study by Palmieri '90.

The pavement structure was simulated as concrete slabs laying on a soil foundation, and two models were constructed:

- **Model 1**: A concrete slab with dimensions 60 x 30 x 6 in. placed on a 9 inches deep soil layer.
- **Model 2**: Two concrete slabs of 30 x 30 x 6 in. , each, are placed on a 9 inches deep soil layer.

Compressive axial forces, N, were applied to the edges of the slabs, and a dynamic load, F(t), was applied on one side of the joint, as described in the Fig 3.1. The same Hawkins' model employed by Krauthammer and Western '88, was adopted here for the shear transfer mechanism across the joint. Generally for highway conditions, it is reasonable to assume a linear load-deformation relationships for pavements since the traffic-induced stresses are relatively small and within the linear range. Therefore, a linear load-deformation relationship was assumed in this study, although the actual behavior of the concrete and soil material could, under special conditions, be nonlinear.

3.2 Construction of the Finite Element Model

When modeling structural systems, several conditions have to be met:

1) Divide the structure into elements sufficiently small so that the results can adequately approximate the true solution. The aspect ratio, which describes the shape of the element in the assemblage, was kept at 2:1 and was not exceeded so that narrow elements are avoided.

2) Numbering the nodes so that the bandwidth, the largest number difference in all elements of the assemblage, is minimized in order to minimize the storage requirements and the solution time for the overall stiffness matrix.

3) Elements in the area of interest need to be small enough to provide a good resolution of results.

4) The elements at the interfaces of different materials (here, concrete and sand) need to be small enough to represent accurately the material discontinuity.

For the models used in this study, the bottom of concrete was used as the datum. The size and the description of the models used are as follows:

a) Model 1: the size of the concrete slab has a length of 60 inches, a width of 30 inches and a depth of 6 inches. The slab lays on a soil foundation of the same length and width with a depth of 9 inches. This model represent a perfect joint since no discontinuity is present at the middle. At the middle, the elements were small since it is the area of interest, and the corresponding nodes are 3 inches from the center of the slab. The soil was represented by equivalent springs, as will be discussed later (Figures 3.2 to 3.4)

b) Model 2: Two concrete slabs are used, both had a length of 30 inches, a width of 30 inches and a depth of 30 inches. The joint

discontinuity for this model is represented by a gap between the faces of the concrete slabs and by the shear transfer mechanism described later. Both slabs are laying on a base foundation which has the same length and width as the slabs and a depth of 9 inches. The elements at the middle were small enough because the shear model mechanism exits between the faces of the slabs, and because it is the area of interest. The nodes under observation are at 3 inches from the faces of the concrete slabs. (Figures 3.5 to 3.7).

For both models, three dimensional analyses were performed. The concrete elements are rectangular with several sizes depending on the area where they are located. The sizes of concrete elements used were 3×3×1 inches, 3×3×2 inches, 3×6×1 inches, 3×6×2 inches, 6×6×1 inches and 6×6×2 inches. The strength parameters for the concrete were the modulus of elasticity E_c, and the Poisson's ratio, ν_c, of the concrete. The base elements (sand) are assumed to be truss elements with a depth of 9 inches and an area corresponding to the tributary area of the nodes for the element. The modulus of elasticity, E_b, and the Poisson ratio, ν_b, of the sand were the strength parameters of the truss elements.

3.3 Loading on Pavements

In structural analysis, the first step for an analytical study is to identify the loading pattern and the loading intensity; this will include whether the load is point load or distributed pressure and if it is static or dynamic loading. When a dynamic loading is to be used, the load time history must to be known and it is necessary to understand the

effect of such load on the pavement.

A drop weight machine was developed for the parallel experimental study. That machine had a 4 ft tall pole mounted on a steel plate of 12 x 12 in area and a thickness of 3/8 inches. The steel plate was used to distribute the load evenly over the plate area. Two rubber sheets, 1/16 inches in thickness, are placed on top and the bottom of the steel plate to avoid the high acceleration created because of steel-steel contact. A weight of 30 lbs is released from a height of 3 ft. Before the structural tests, a loadcell was placed under the steel plate to record the signal. This method induced a load of 22,500 lbs with a duration of 1.62 milliseconds(msec). This load was simulated as a triangular load over a duration of 1.62 msec and a peak of 22,500 lbs at 0.8 msec as shown in Fig 3.8. However in this study, an older version of the loading pattern was used. This pulse was introduced to have a triangular pulse with a duration of 0.81 msec and a peak of 22,000 lbs at 0.4 msec as shown in Fig 3.9. This load is applied over an area of 12 x 12 in (144 in^2) for simulating the steel plate in the experimental study.

In the experimental study, two rods were used to tie the slab together and to apply a compressive force to the slab. These compressive forces were introduced as a two dimensional pressure applied to the outside edge from each side. Each side had a dimension of 30 x 6 in. Three different values were used 2000, 4000, and 9500 lbs which was distributed over each side area which has the dimension of 30 x 6 in (180 in^2). This was introduced for investigating three different joint conditions:

- Perfect joint
- Dead joint
- New joint

3.4 Damping

Damping plays a key roll in dynamic finite element analysis. The option that was adopted here was that to find the natural frequency, ω_n, of the system from the finite element analysis ADINA and then to calculate the damping at each node using the fact that the critical damping, C_{cr}, is a function of ω_n, the natural frequency of the model.

The value of damping, C, at each node is calculated by the following formula:

$$C = \beta\, C_{cr} = \beta\, (2\, m_E\, \omega_n) = 2\, \beta\, A_E\, L\, \rho_E\, \omega_n \qquad (3.1)$$

in which :

C_{cr} = critical damping of the model

β = % of critical damping

m_E = mass of the element

l_E = depth of the element

ρ_E = density of the element

A_E = area of the model.

For external nodes, The critical damping value was assumed to be 100% . For internal damping, a value of β of 3% for concrete and a value of β of 7% for soils were assumed. For each material, an average weight was assumed as follows: 150 and 105 lb/ft^3 for the concrete and sand

respectively (Manual of Steel Construction '84).

Using ADINA (ADINA Engineering, '81), the value of the lowest frequency of the undamped system was found to be 752 rad/sec, and the damping was calculated in the x, y, z directions. The calculation of the nodal damping data for the external nodes, 1-3, 8-10, 18, 63, 70, 71, 77, 148 and 162 are presented in Table 3.2, and for internal nodes 37-38, 44-45, 51-52, 58-59, 65-66 ,72-73 and 79-80 in Table 3.3.

3.5 Joint Shear Transfer Mechanism

The model employed for simulating the shear transfer mechanism in a joint, proposed by Krauthammer and Western '88, is shown in Figs 3.10-3.11, and is described as follows:

The two sides of the shear plane are connected with two beam elements and then another two beam element are extended out, one from the top which is connected to one slab, and the other is from the bottom and connected to the second slab. Two truss elements are connecting the top and bottom beam elements spaced 3 inches from the center along the joint faces. The truss elements have the material model proposed by Hawkins '74, as it will be discussed later, satisfying the requirements of shear transfer, as described by Park and Pauley '75.

The beam elements on the edges on each shear plane have significantly stiffer modulus of elasticity (ten times stiffer in this case) so that the forces transferred will be distributed evenly through

the slab, and therefore no concentrated forces will result from the use of the mechanism.

3.6 Shear Resistance Function:

Theoretically, if the shear faces are fully efficient, they transfer 50% of the applied load from one slab to the other. This is true if the same deflection is recorded for both slabs and each slab assumes the same portion of the applied load. Yoder and Witczak and '75, reported that for most cases the portion of the load transferred was about 45% of the applied load. However, an explicit model is needed that would be suitable representing this response, and the numerical model was based on studies by Hawkins '74, '81, Mattock and Hawkins '72, Mattock '74, '76, '77, and Walraven and Reinhardt '81. That model is referred to as the "Hawkins shear stress-shear slip model", as described by Murtha and Holland '82. The Hawkins model is a combination of straight lines as shown in Fig 3.12 and defined next:

1. Line OA: In this region the response is elastic and the shear resistance, τ_e, for a slip Δ_1 of 0.004 inch is given by :

$$\tau_e = 165 + 0.157\ f'_c \leq \tau_m/2 \qquad (3.2)$$

For the present case, $f'_c = 3200$ psi, and therefore:

$$\tau_e = 165 + 0.157\ (3200) = 667.4 \text{ psi}$$

Both τ_e and f'_c are in psi and f'_c is the concrete compressive strength. The elastic limit τ_e should be taken no greater than half of τ_m.

2. Line AB: From the point A to B the slope of the curve decreases continuously but it remain positive until a maximum shear resistance, τ_m, is reached at a slip, Δ_2, of 0.012 inch. The maximum shear stress obtained is defined by the following expression:

$$\tau_m = 8 \sqrt{f'_c} + 0.8 \rho_{vt} fy \leq 0.35 f'_c \qquad (3.3)$$

where

f'_c, τ_m, f_y are in psi

$\rho_{vt} = A_1 / A_c$

A_c = cross sectional area (in^2)

A_1 = total area of reinforcement crossing the shear plane (longitudinal reinforcements for vertical slip) (in^2)

f_y = yield strength of the reinforcements crossing the shear plane (psi)

Since no reinforcement is crossing the shear plane the second term is zero; so

$$\tau_m = 8\sqrt{f'_c} = 452.55 \leq 1120 \text{ psi}$$

Since the value of τ_e is greater than $\tau_m/2$ then τ_e is set to be equal to $\tau_m/2$ or 226.3 psi.

3. Line BC : This segment is represented by a horizontal line. The shear capacity will remain constant while the relative shear slip increases to a slip, Δ_3, of 0.024 inch.

4. Line CD : From point C to D the slope will be constant but decreasing and is independent of the amount of steel crossing the shear plane. The slope is given by the following expression:

$$K_u = 2000 + 0.75\ f'_c \qquad (3.4)$$

$$K_u = 2000 + 0.75\ (3200) = 4400 \quad (psi/in)$$

Point D is located at a limiting shear strength, τ_L, which given by:

$$\tau_L = \frac{0.85\ A_{sb}\ f's}{A_c} \qquad (3.5)$$

in which :

A_{sb} = area of bottom reinforcement (in^2)

A_c = area of concrete faces (in^2)

f'_s = tensile strength of bottom reinforcement (psi)

However, no bars were crossing the shear plane, the limiting shear strength, τ_L, will be zero which is unrealistic because of the friction and aggregate interlock that exist at the shear plane. Here it was assumed that τ_L should not be taken less than $\tau_m/2$ so τ_L will be 226.3 psi.

The slip at the limiting strain will be:

$$\Delta_4 = 0.024 + \Delta_L = 0.024 + \tau_L/K_u \qquad (3.6)$$

$$= 0.024 + 226.27/4400 = 0.0754 \text{ inch}$$

5. Line DE: In this portion, the capacity will remain constant at τ_L until failure will occur. For a well-anchored bar, the slip at failure is given by the following formula:

$$\Delta_{max} = \frac{C\ (e^{x}-1)}{120} \qquad (3.7)$$

where

$$x = \frac{900}{2.86\ \sqrt{(f'_c/d_b)}} \qquad (3.8)$$

d_b = average bar diameter crossing the plane (in)

Since no steel bars were crossing the shear plane, the value of x, will be zero and consequently the value for Δ_{max} will be also zero. Therefore, the above equation does not apply to this case. However, at a strain of 0.1 in/in the concrete slabs cannot provide any shear resistance or tension resistance, so a maximum strain of 0.1 in/in was assumed. This corresponds to a slip of 0.6 in., since the strain is defined as the slip divided by the thickness of the shear plane.

3.6.1 Effect of Frictional Forces:

In the above model the frictional effect between the two slabs were not included. In accordance to ACI 318-89 (section 11.7.4.3), a third term will be added to the equation for the max shear strength , τ_m, as follows:

$$\tau_m = 8\ \sqrt{f'_c} + 0.8\ \rho_{vt}\ f_y + \mu\ N/A_g \qquad (3.9)$$

where

μ = coefficient of friction

N = total axial force acting on both sides of the slabs (lbs)

A_g = total shear plane area (in^2)

μ = coefficient of friction

N = total axial force acting on both sides of the slabs (lbs)

A_g = total shear plane area (in^2)

Since the present case represented roughened concrete surfaces in contact, the value of the coefficient of friction is given by the expression:

$$\mu = 0.6\ \lambda \tag{3.10}$$

where $\lambda = 1.0$ for normal weight concrete

However different values of axial forces were used, and for each type of joint a range of values were adopted. For a dead joint, a range from 1000 lbs to 2500 lbs was set, for a deteriorated joint, a range of 4000 to 6000 lbs, and for new joint values between 8800 and 9500 lbs were assumed.

3.6.2 Effect of Axial Compressive Forces on Shear Behavior:

When axial compression is present, the ability of reinforced concrete members to resist shear is improved. This is the result of the motion of the neutral axis to a greater depth which will prevent the widening of cracks, prevent the extension of the cracks in the compression zone, and delay the yielding of transverse reinforcement. The ACI 318-89 code suggests the use of the following equation for the shear capacity when axial compression is present:

$$V_c = 2\left(1+ 0.0005 \frac{N_u}{A_g}\right) \sqrt{f'_c}\, b_w\, d \tag{3.11}$$

and

$$V_c \leq 3.5 \sqrt{f'_c} \sqrt{(1+ \frac{0.002\ N_u}{A_g})}\ b_w\ d \qquad (3.12)$$

instead of

$$V_c = 2 \sqrt{f'_c}\ b_w\ d \qquad (3.13)$$

where :

Vc = nominal shear strength of concrete (psi)

f'_c = compressive strength of concrete (psi)

b_w = width of the cross section (in)

d = effective depth of the cross section (in)

A_g = gross area of the cross section (in^2)

N_u = total axial compressive force (lb)

Based on the ACI Equation (11-4), Krauthammer and Holmquist '84 have suggested an amplification factor, TF, given by the following expression:

$$TF = 1 + 0.0005\ (N_u/A_g) \qquad (3.14)$$

Mattock and Wang '84 reported that the ACI provisions were too conservative when the amplification factor was considered and they suggested the following formula for V_c :

$$V_c = 2 \sqrt{f'_c}\ (1+ \frac{3\ N_u}{A_g\ f'_c})\ b_w\ d \qquad (3.15)$$

with the condition that:

$$V_c \leq 3.5 \sqrt{f'_c} \sqrt{(1+ \frac{0.3\ P}{A_g})}\ b_w\ d \qquad (3.16)$$

$$IF = 1 + \frac{3\ N_u}{A_g\ f'_c} \qquad (3.17)$$

The trust factor, TF, has been successfully used by Holmquist and Krauthammer '84, and for values of f'_c less than 6000 psi, it predicts higher improvement than the IF factor; the trust factor, TF, was adapted in this model.

3.6.3 Dynamic Enhancement Factor:

For dynamic analysis, a strain rate enhancement factor for concrete should be included. Some researchers have adapted two different techniques to implement the influence of rate of strain on the dynamic behavior of reinforced concrete members. One group used the dynamic enhancement factor to increase the material properties, whereas the second group uses an increase in the flexural and shear capacities. Murtha and Crawford '81 proposed that a DEF of 1.5 should be applied to the shear capacities of reinforced concrete members. Kiger and Slawson '84 have also suggested a DEF of 1.5 in the direct shear capacity of reinforced concrete structures when subjected to dynamic loading. Krauthammer et al '86 have used a combined thrust factor and dynamic enhancement factor of 1.4 which was successfully used previously also by Krauthammer and Holmquist '84. Newmark '63, Criswell '70, and Soroushian and Obaseki '86, used a dynamic enhancement factor ranging from 1.2 to 1.4 and applied to the strength properties of concrete members. Ross '83 also used a factor of 1.3 to increase the properties of concrete members. In this model a DEF of 1.5 was used to increase the shear capacity of the joint.

3.7 Stress-Strain Envelope:

In this model the strain is calculated as the slip divided by the length of the thickness of the slabs. The following data were obtained in accordance to the Hawkins model adapted and applying the frictional effect, the effect of axial compression and the dynamic enhancement factor, DEF. these are presented in Tables 3.4-3.6, and Figures 3.13-3.14.

3.8 Model with Changing Joint Shear Transfer:

As was discussed before and reported by Krauthammer and Western '88, a deterioration in the joint can be represented as decrease in the stiffness of the shear transfer. This reduction in the stiffness will result in a decrease in the joint efficiency. Variations of the shear model were used to model the shear transfer in this study. A new joint corresponds to a value of shear transfer stiffness between the slopes of the line from O to B and the line O to A, using a compressive force between 8000 and 9500 lbs as shown in Figure 3.15.

Using a range of 5000 to 7000 lbs for axial forces a new shear stress-strain envelope is obtained. A deteriorated joint corresponds to a slope value between the slopes of lines O to C and the lines O to D as described in Figure 3.16.

Using a range of 1000 to 3000 lbs for axial force represents the third category of joints, the dead joint. A dead joint corresponds to slope between the slopes between O to E and to O to D, as shown in Figure

3.17.

The value of the stiffness of shear transfer was used for the properties of the truss elements connecting the shear planes in the middle as follows :

$$K = A E / L \qquad (3.19)$$

where

A = area of the truss element

L = Length of the truss element

E = Modulus of elasticity of the truss.

New joint:

$402,300 \leq K \leq 610,945$ psi

Joint 7 K = 600,000 psi

Joint 6 K = 450,000 psi

Deteriorated joint:

$183,625 \leq K \leq 381,500$ psi

Joint 5 K = 350,000 psi

Joint 4 K = 240,000 psi

Dead joint:

$3,466 \leq K \leq 180,225$ psi

Joint 3 K = 175,000 psi

Joint 2 K = 140,000 psi

Joint 1 K = 15,600 psi

Since two truss elements were used to transfer the shear, the stiffness of each truss element is half of the K value.

Perfect joint

Model 1 represents the perfect joint case since no discontinuity is present in the middle and the joint is 100% efficient.

In this study the time step increment was found according to equation (2.17) to be 0.00002 sec and a value of 0.00001 sec was used.

Table 3.1: Joint Efficiencies (From Krauthammer and Western '88)

	Poor	Fair	Good	Excellent	Experimental
New	0.80	0.84	0.87	0.93	0.86
Deteriorated	0.71	0.76	0.80	0.88	na
Dead	0.53	0.57	0.60	0.70	na

Table 3.2 External damping

Node Number	Tributary Area in^2	Density lb/ft^4	Length (in)	x-damping C_x , C_y	z-damping C_z
1*	2.25	150/105	0.5/4.5	2.761	0.178
2*	6.75	150/105	0.5/4.5	8.283	0.534
3*	9.00	150/105	0.5/4.5	11.045	0.712
8	2.25	150	1.0	0.761	0.023
9	6.75	150	1.0	2.283	0.069
10	9.00	150	1.0	3.045	0.091
18	9.00	150	1.5	4.566	0.137
63	6.75	150	1.0	4.566	0.137
70	6.75	150	1.0	2.283	0.069
71*	9.00	150/105	0.5/4.5	11.045	0.712
77*	9.00	150/105	0.5/4.5	11.045	0.712
148	9.00	150	1.0	3.045	0.091
162	9.00	150	1.5	6.089	0.183

Table 3.3 Internal damping

Node Number	Tributary Area in^2	Length (in)	Density (lb/ft^4)	Damping β (%)	Damping C_x, C_y, C_z
37*	20.25	0.5/4.5	150/105	3.0/7.0	1.603
38*	27.00	0.5/4.5	150/105	3.0/7.0	2.137
44	20.25	1.0	150	3.0	0.206
45	27.00	1.0	150	3.0	0.274
51	20.25	1.5	150	3.0	0.308
52	27.00	1.5	150	3.0	0.411
58	20.25	2.0	150	3.0	0.411
59	27.00	2.0	150	3.0	0.548
65	20.25	1.0	150	3.0	0.206
66	27.00	1.0	150	3.0	0.274
72*	27.00	0.5/4.5	150/105	3.0/7.0	2.137
73*	36.00	0.5/4.5	150/105	3.0/7.0	2.849
79	27.00	1.0	150	3.0	0.274
80	36.00	1.0	150	3.0	0.365

*Note: Nodes are at the interface between the two materials, concrete and soils.

Table 3.4: Values for Hawkins Shear Model

Slip (in)	Strain (in/in)	Shear Value (psi)
0.004	0.00067	226.27
0.012	0.002	452.56
0.024	0.004	452.56
0.075	0.01256	226.27
0.600	0.100	226.27

Table 3.5 Values of Multiplication Factors on the Shear Stress values

Axial Comp Force(lbs)	Frictional Effect(psi)	Frict. Factor	Trust Factor	DEF* factor	Combined Factor
2000.0	6.67	1.015	1.006	1.5	1.532
6000.0	20.00	1.044	1.017	1.5	1.593
8000.0	26.67	1.059	1.022	1.5	1.623
12000.0	40.00	1.088	1.033	1.5	1.686
17600.0	58.67	1.130	1.049	1.5	1.778
19000.0	63.33	1.140	1.053	1.5	1.801

DEF: Dynamic Enhancement Factor

Table 3.6 Values for Shear model, Boundary shear values

Strain	New Joint		Deteri. Joint		Dead Joint	
	Upper	Lower	Upper	Lower	Upper	Lower
0.00067	407.5	402.3	381.5	367.2	360.4	346.6
0.00200	815.0	804.6	763.0	734.5	720.9	693.3
0.00400	815.0	804.6	763.0	734.5	720.9	693.3
0.01257	407.5	402.3	381.5	367.2	360.4	346.6
0.10000	407.5	402.3	381.5	367.2	360.4	346.6

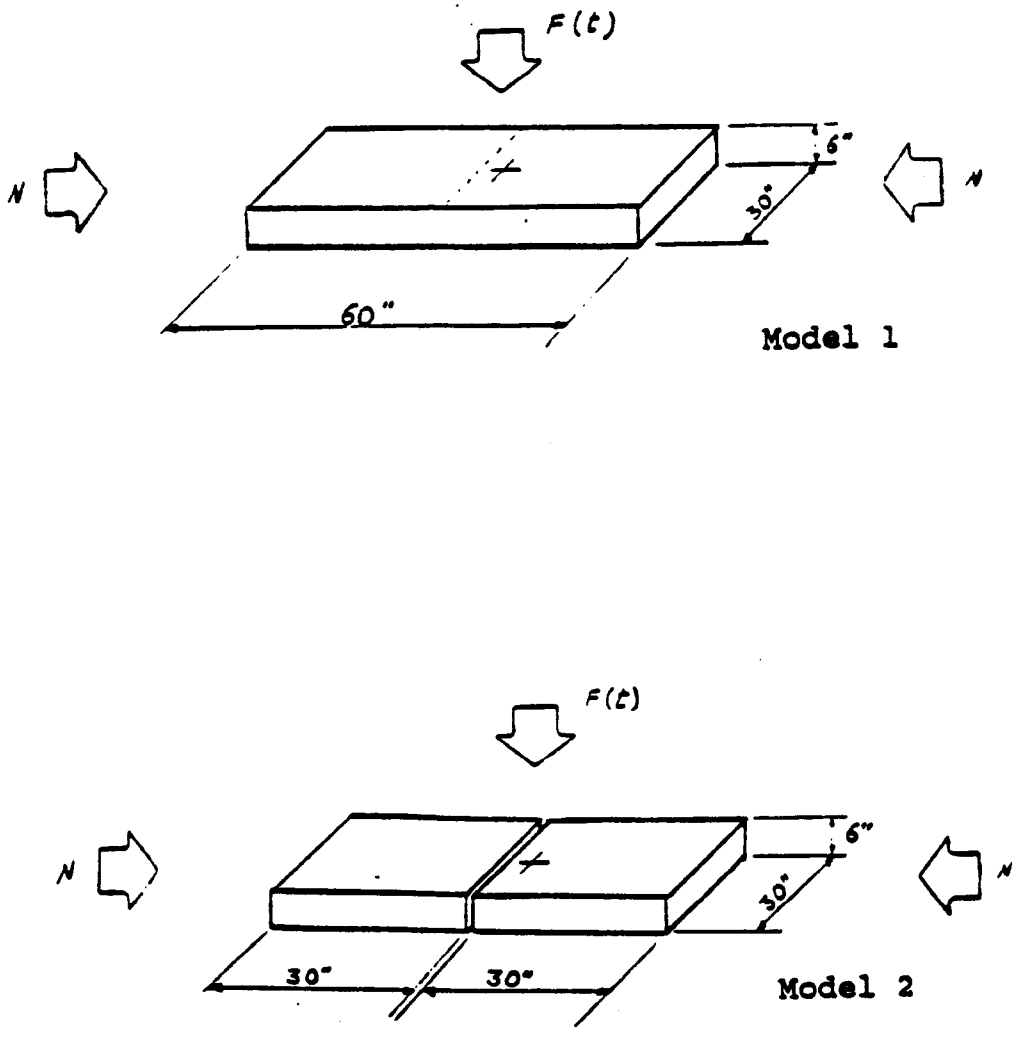

Figure 3.1: Slabs and Force Systems

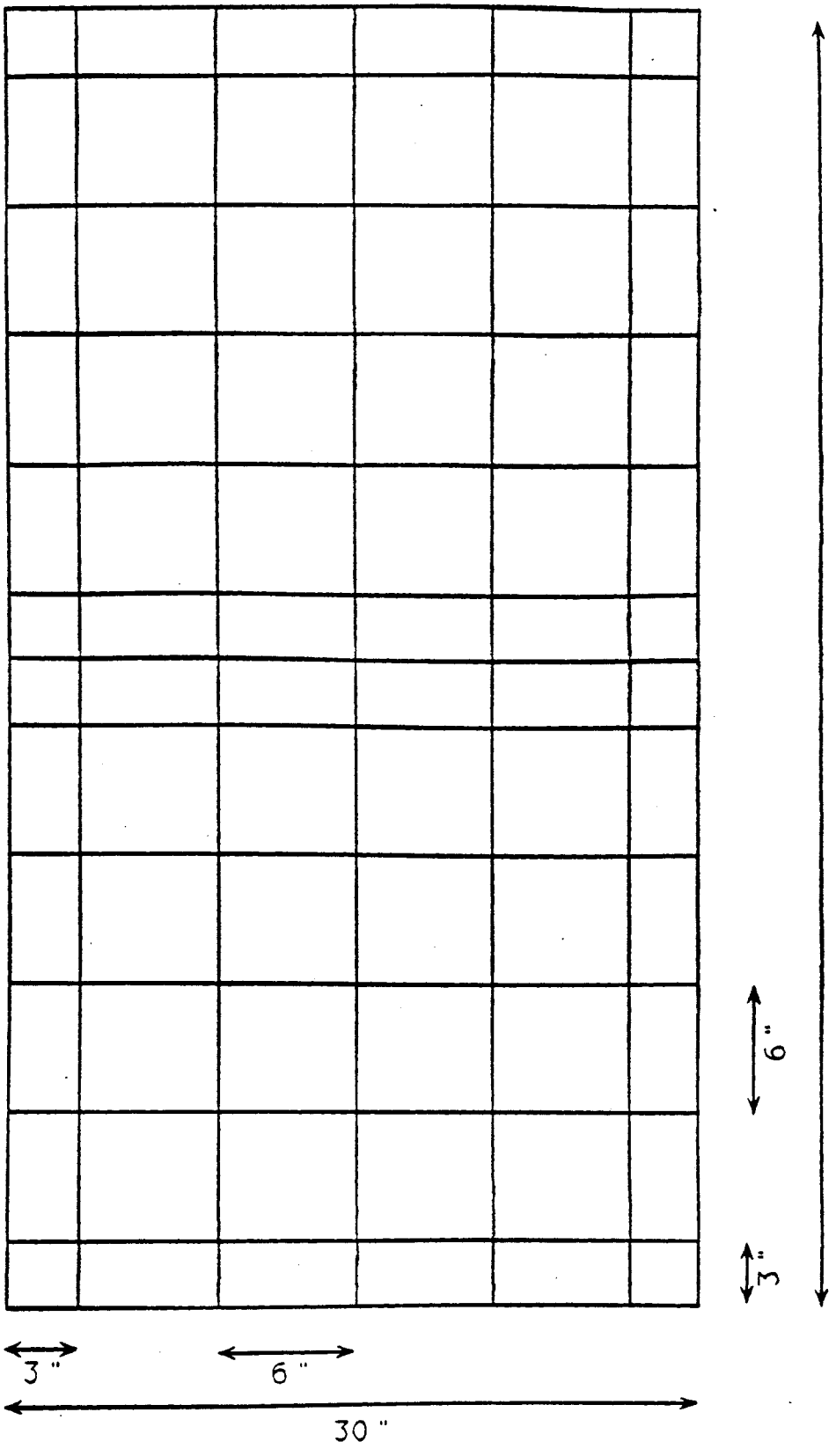

Figure 3.2: Top view for model 1

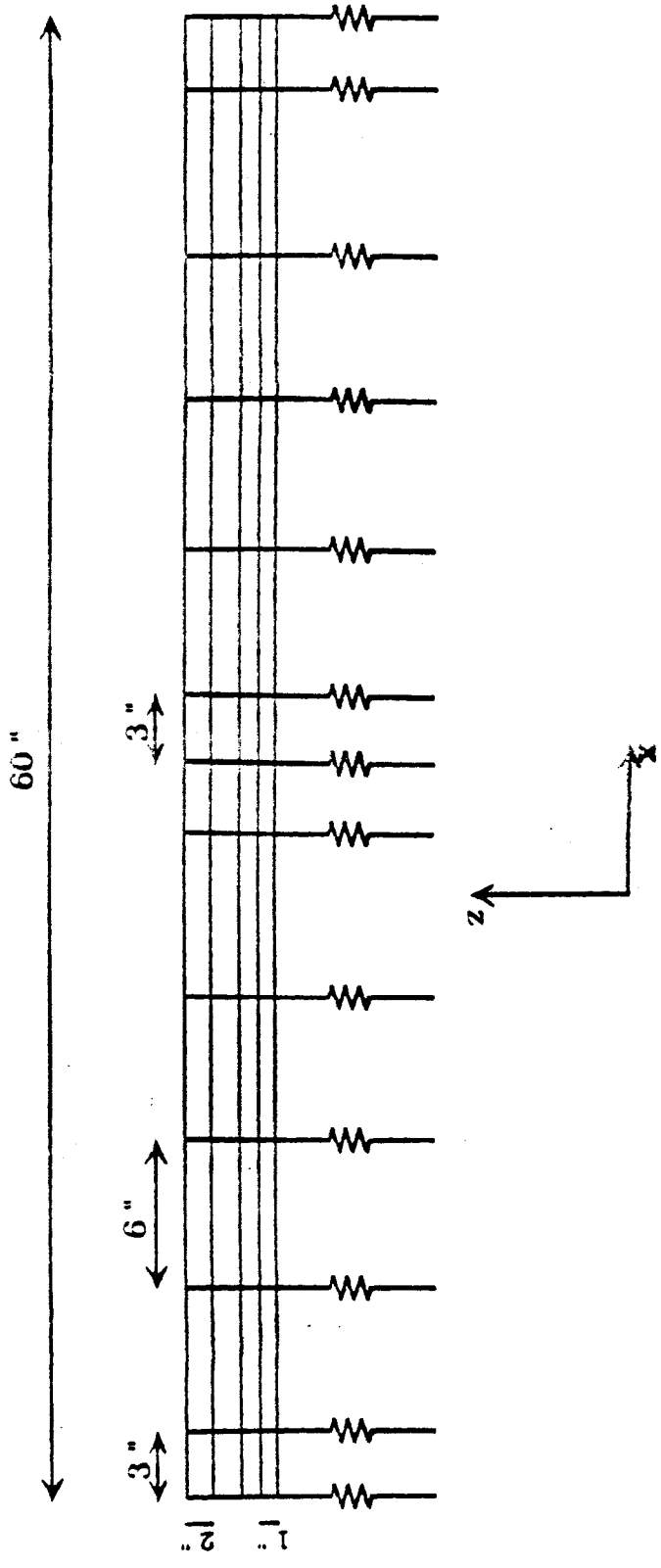

Figure 3.3: Side view for model 2

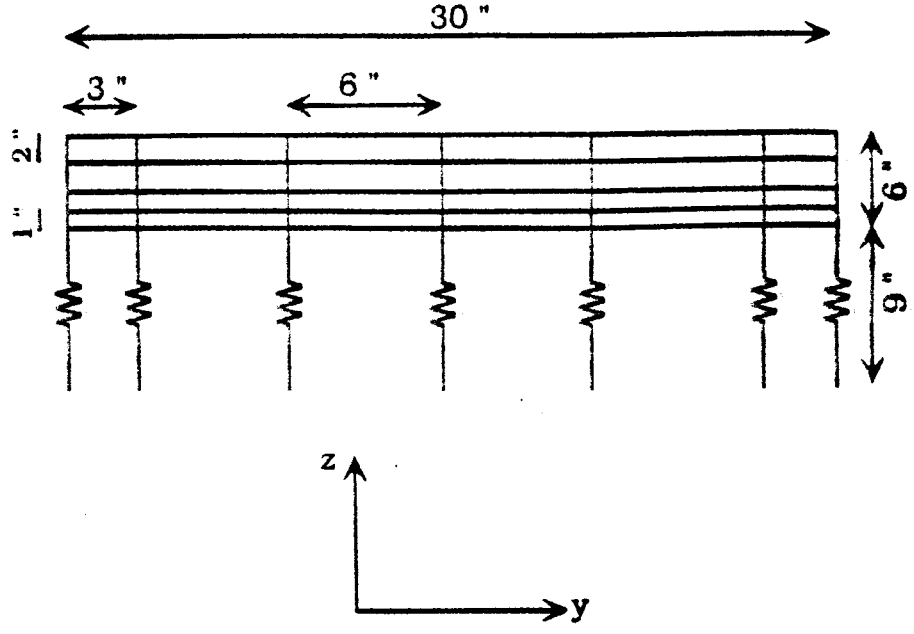

Figure 3.4: Side view for model 1

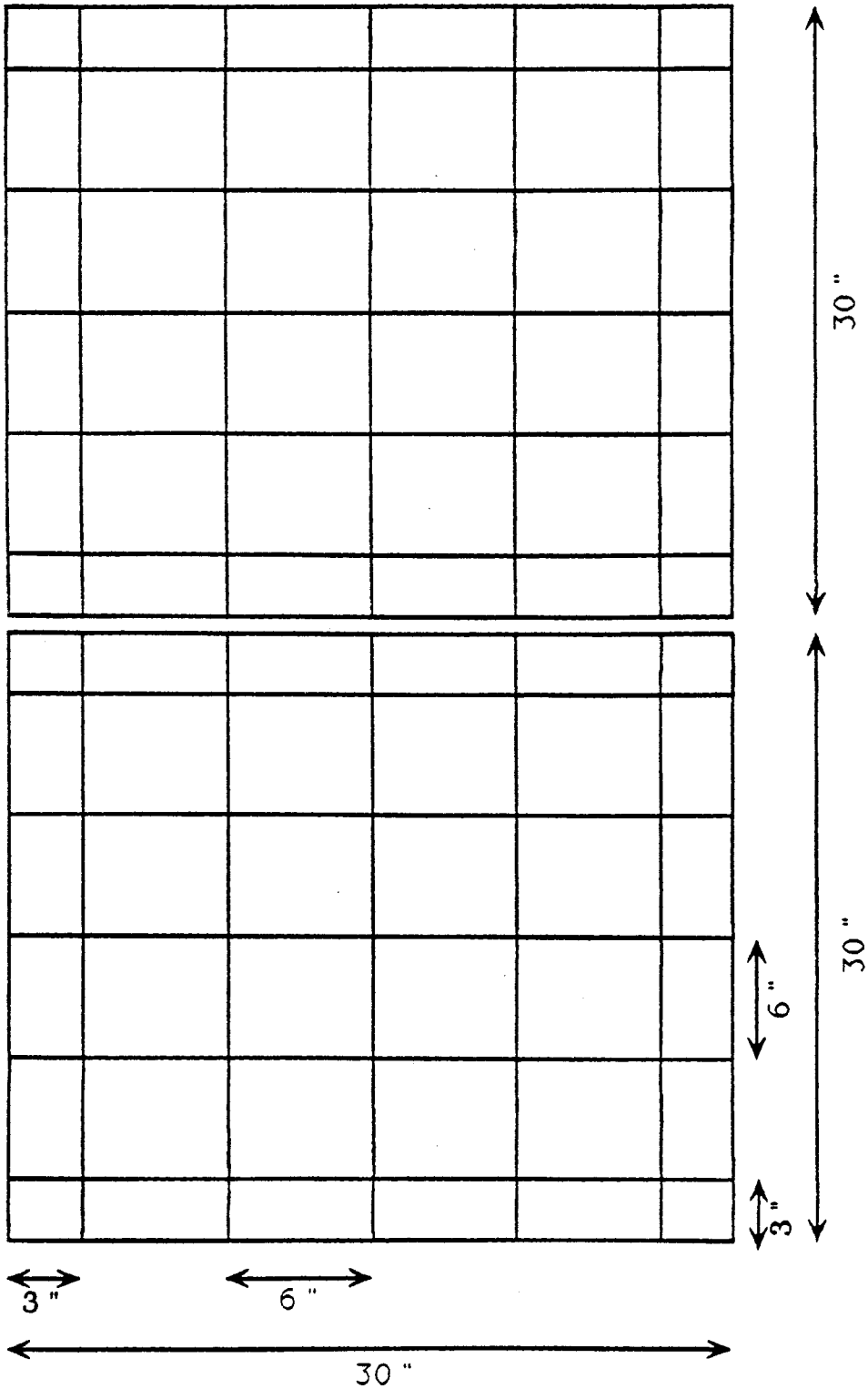

Figure 3.5: Top view for model 2

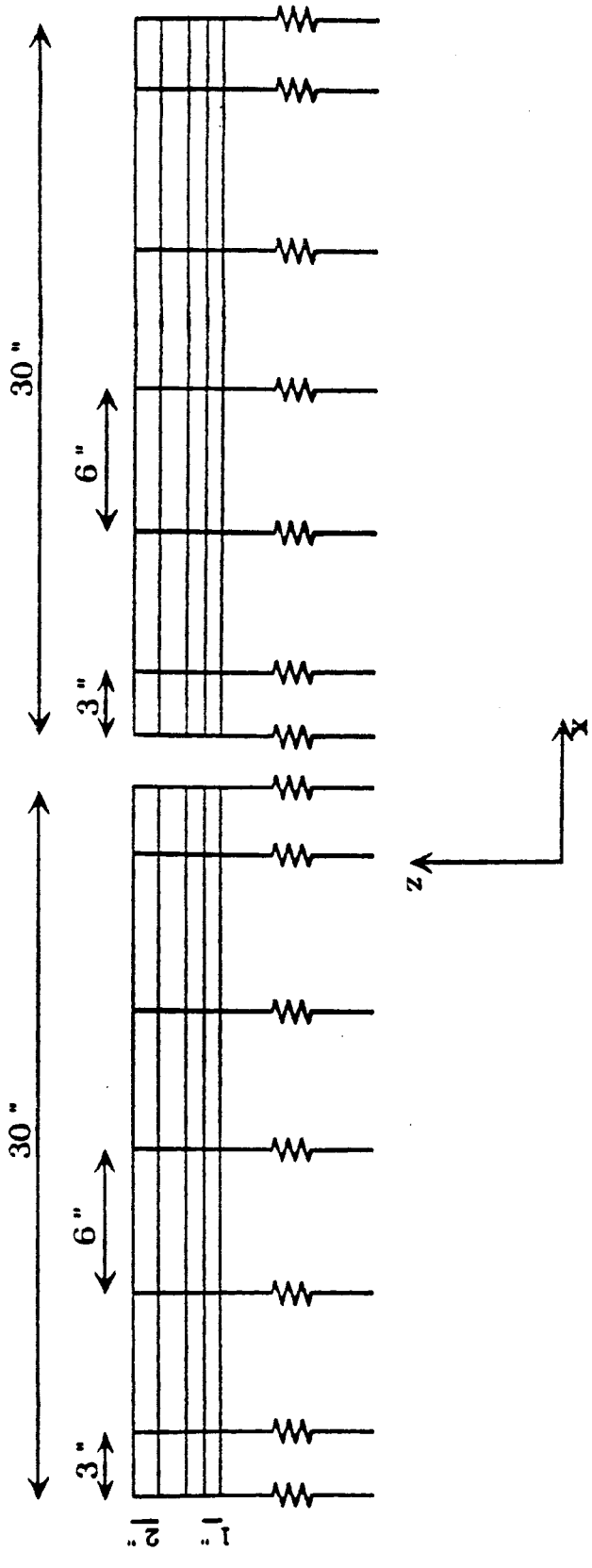

Figure 3.6: Side view for model 2

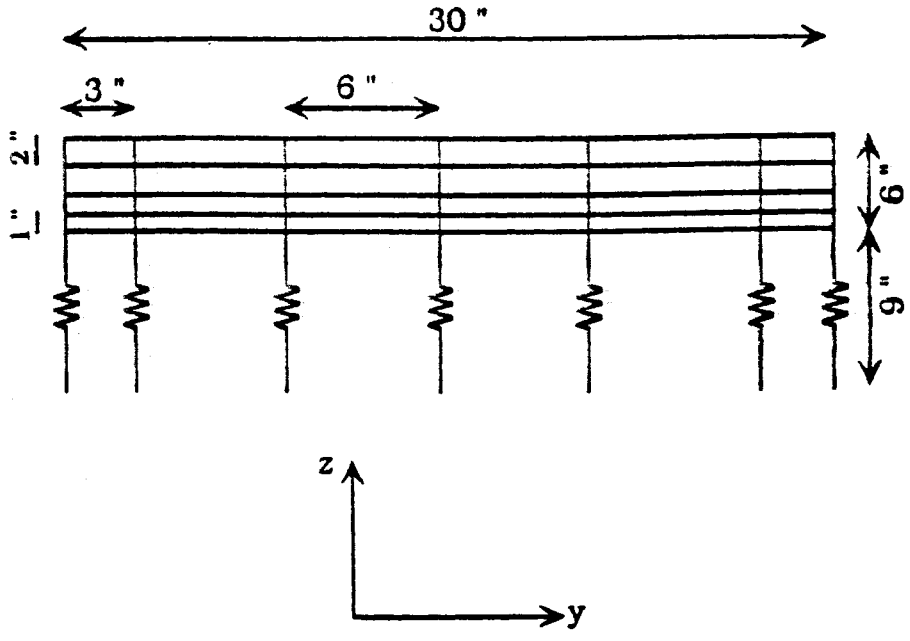

Figure 3.7: Side view for model 2

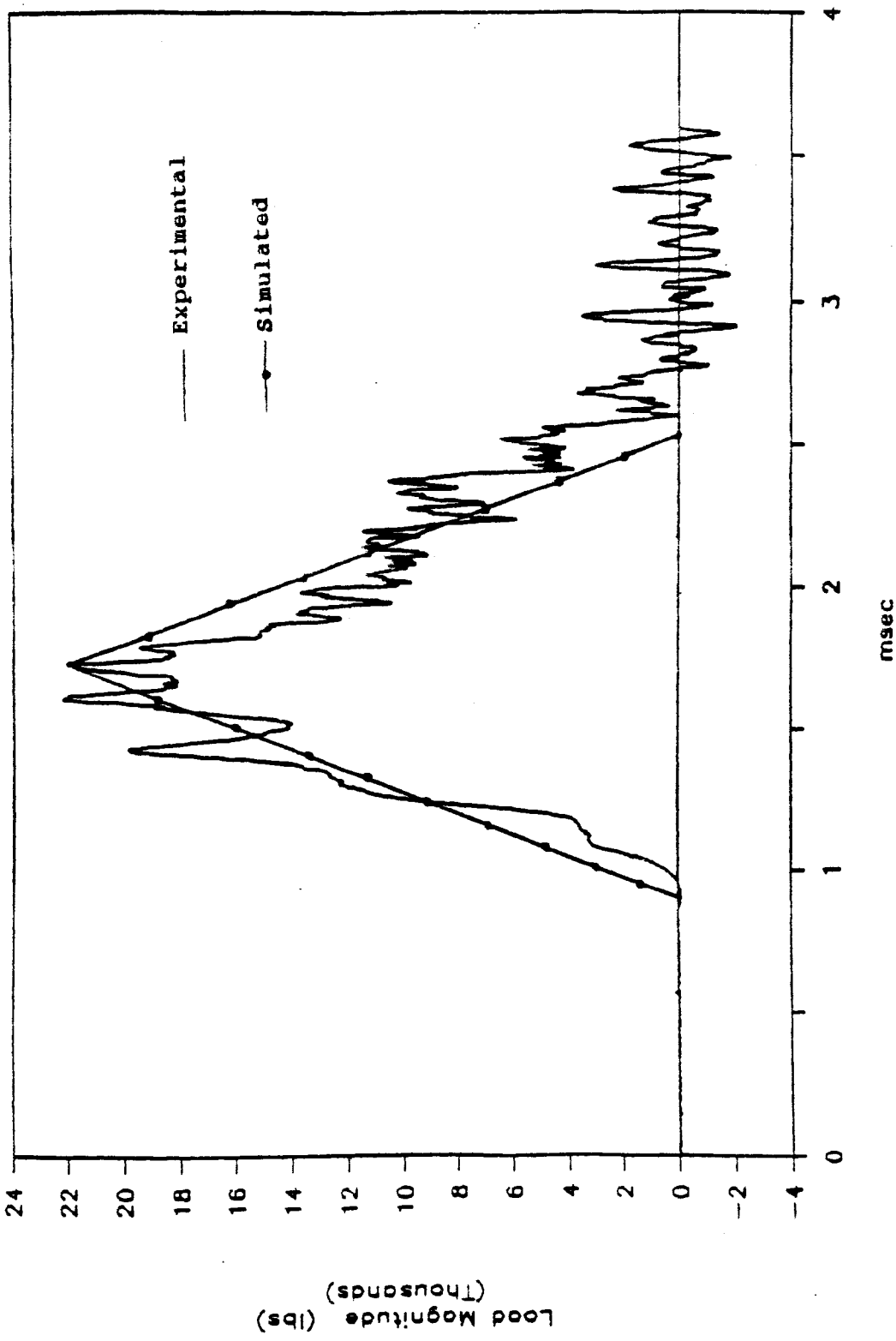

Figure 3.8: Loading Pulse (Test LC 4)

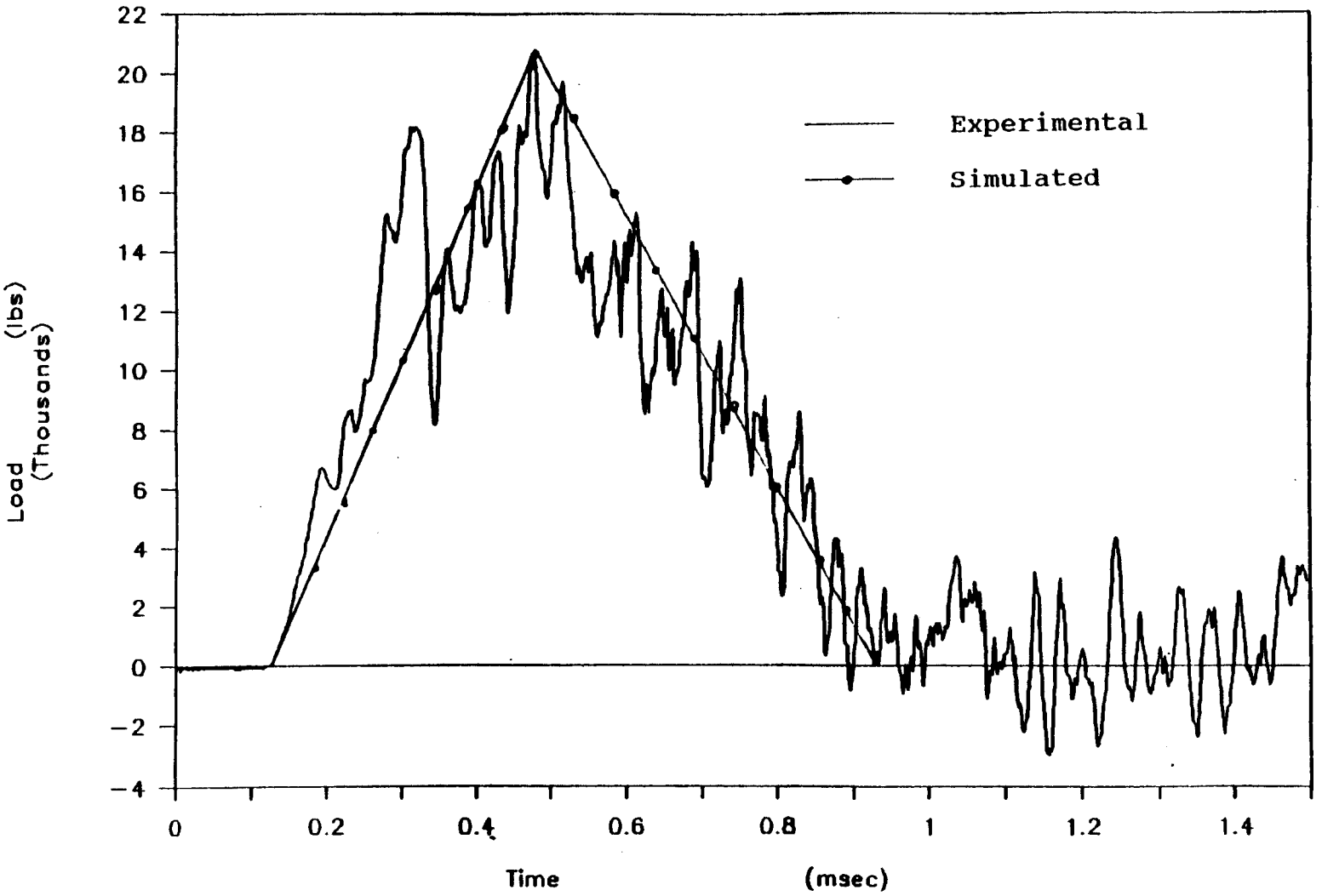

Figure 3.9: Loading Pulse (from a height of 3 ft)

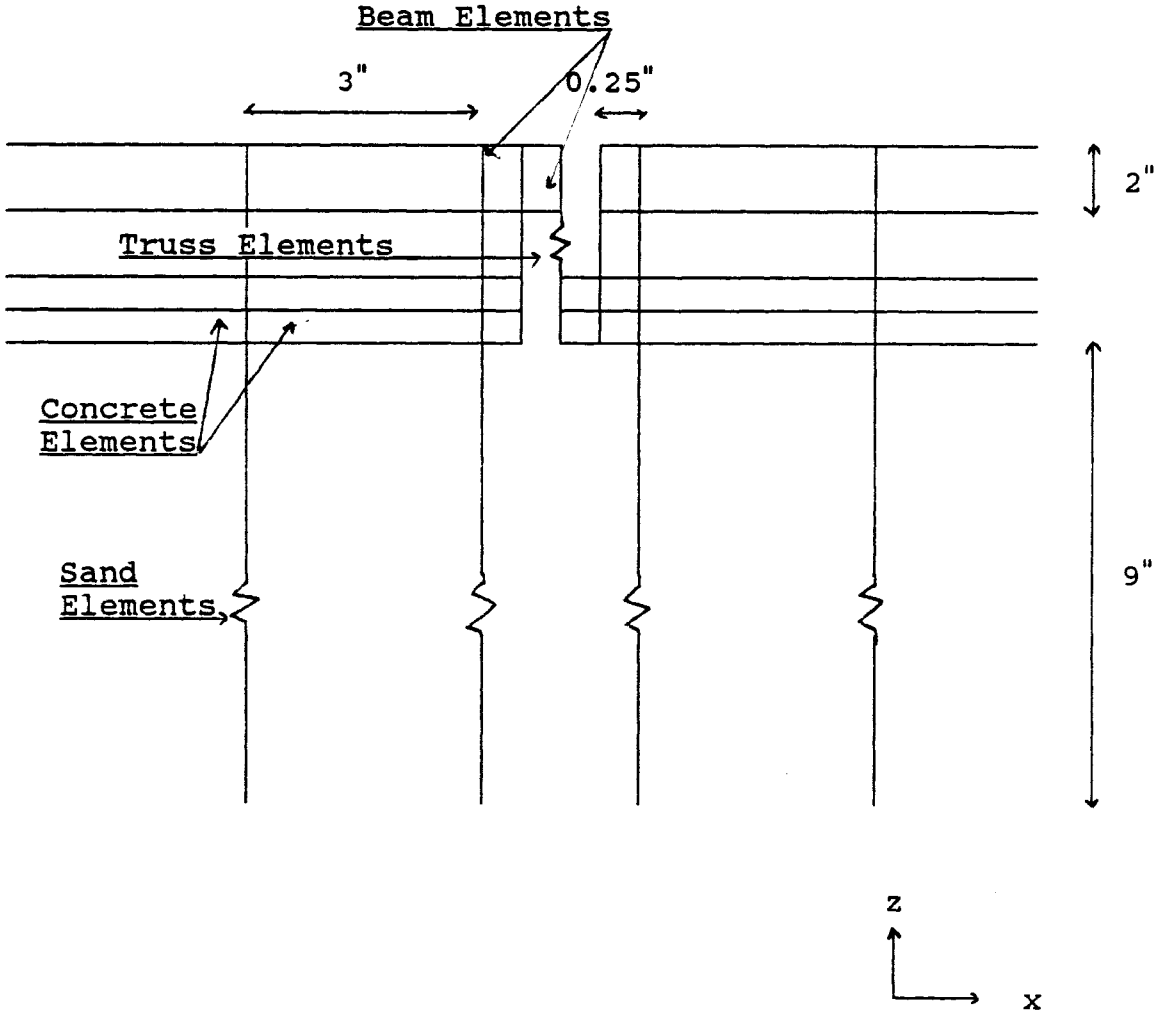

Figure 3.10: Side View of Shear transfer Mechanism

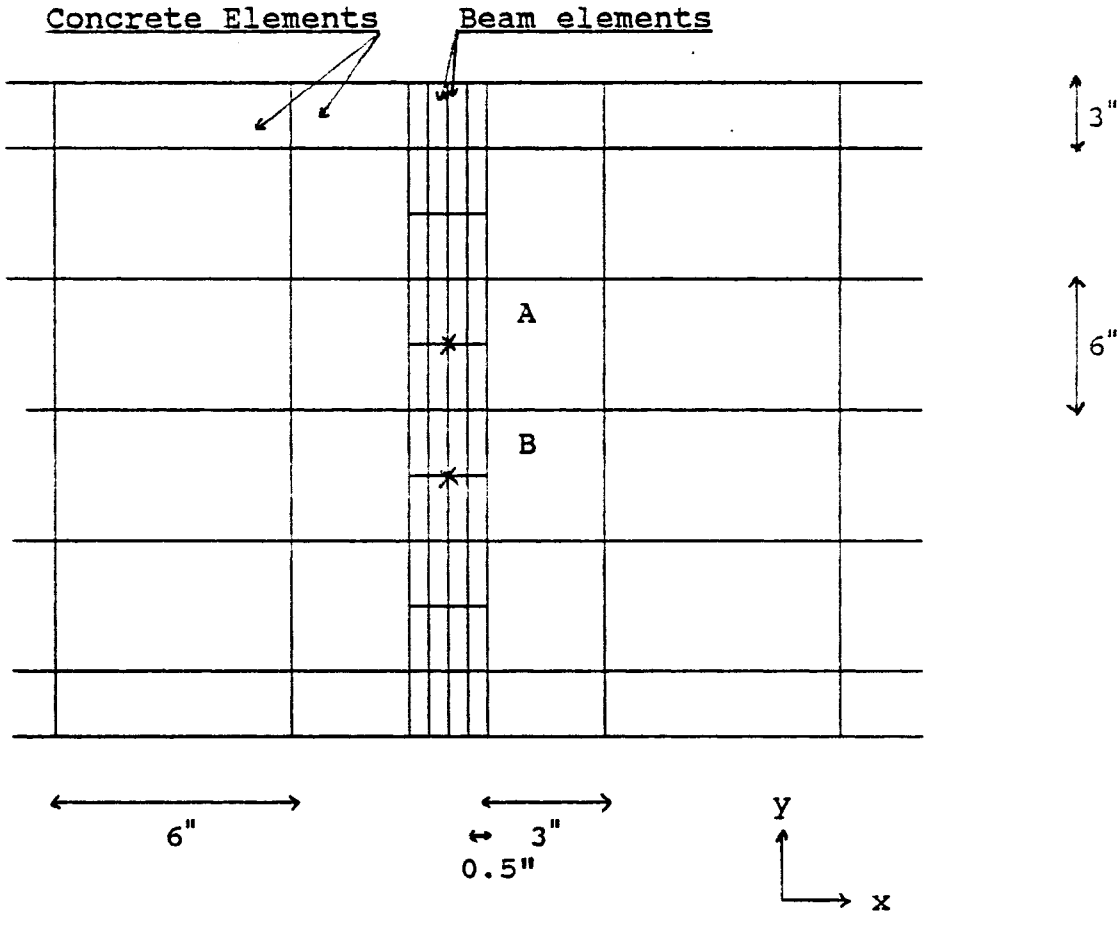

Figure 3.11: Top view for the shear Mechanism

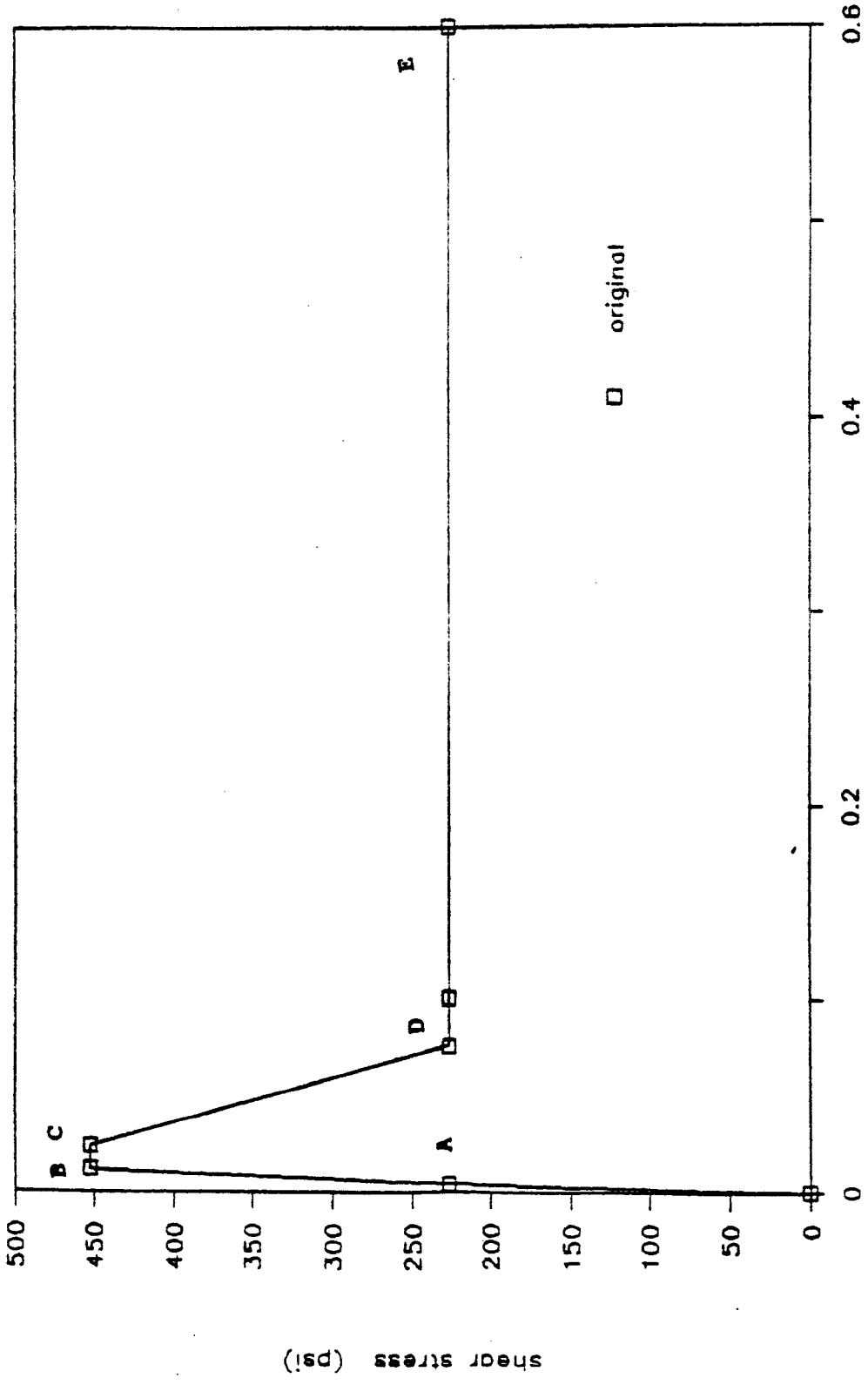

Figure 3.12: Shear Stress-Shear Slip envelope (Hawkin's Model)

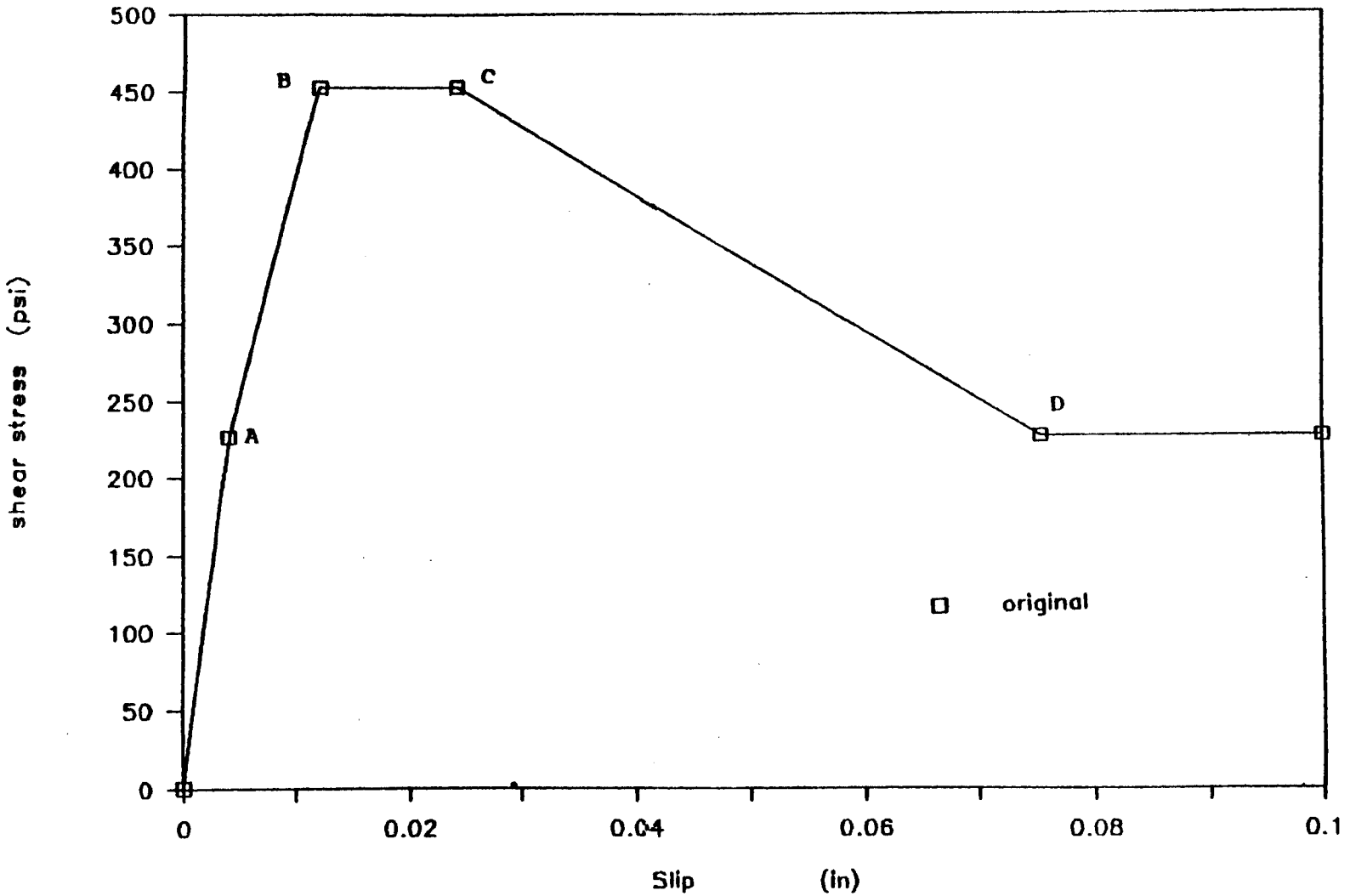

Figure 3.13: Shear Stress-Shear Slip envelope (Hawkin's Model)

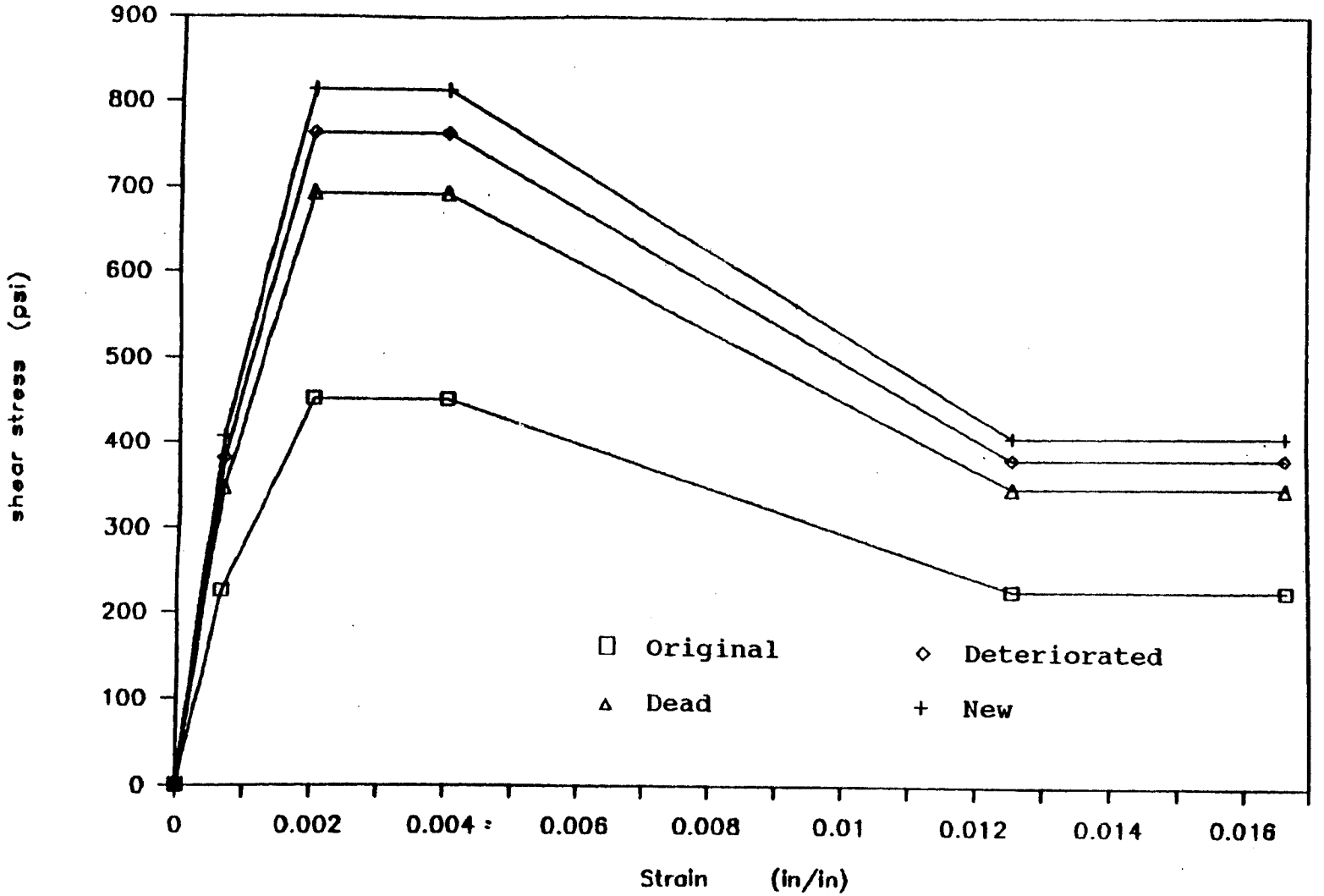

Figure 3.14: Shear Transfer Model (Shear Stress-Shear Strain envelope)

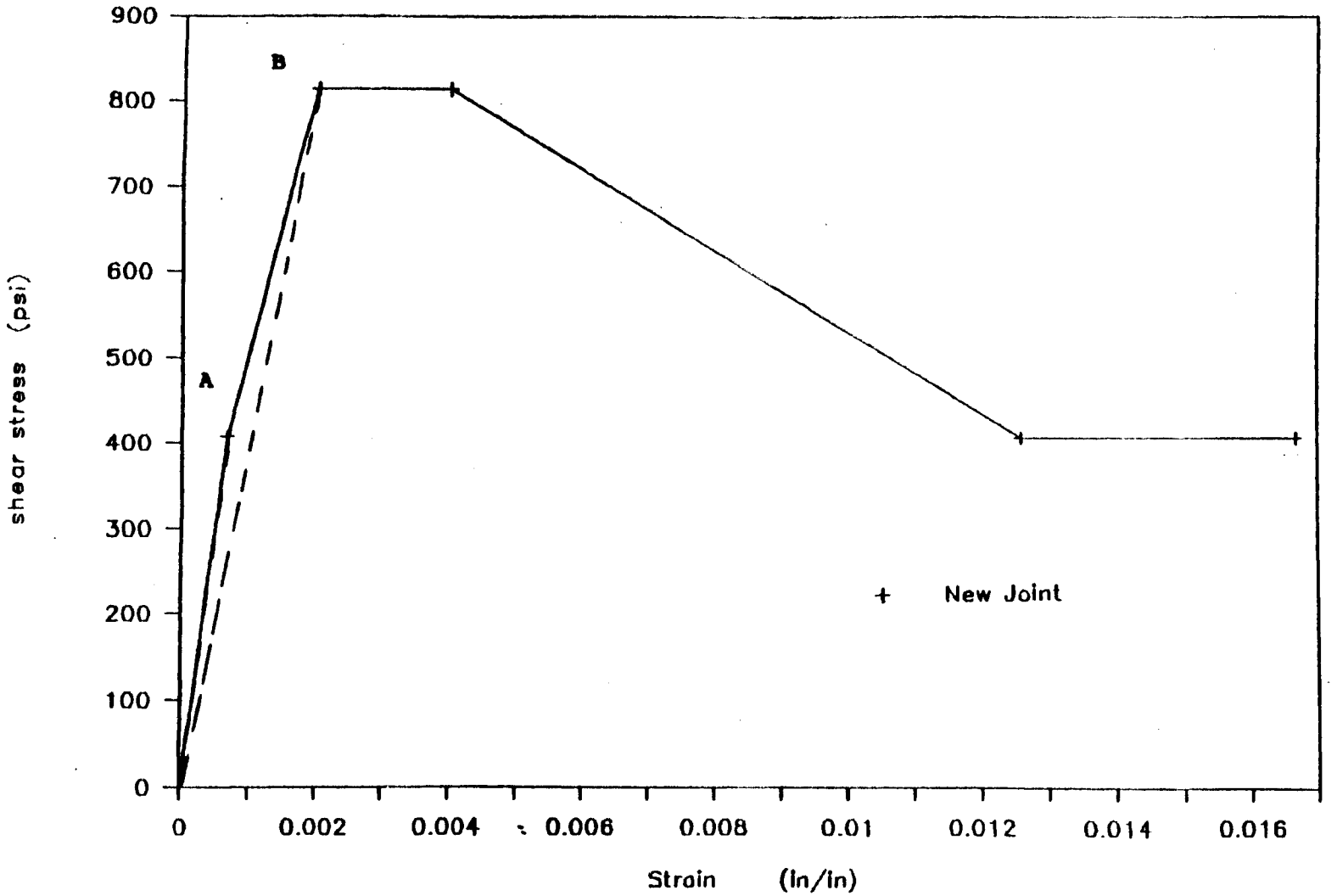

Figure 3.15: Shear Transfer Model (Shear Stress-Shear Strain envelope)

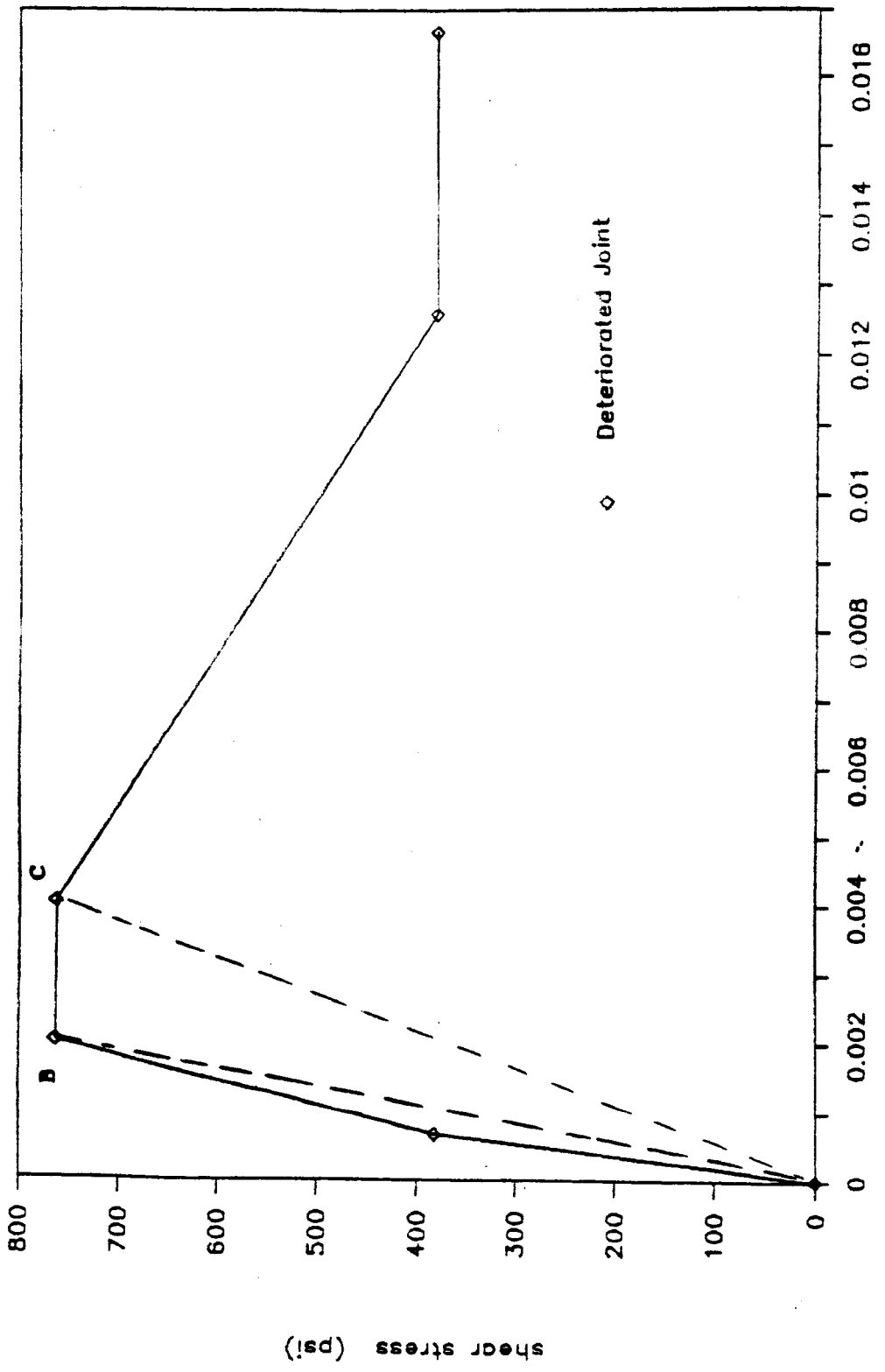

Figure 3.16: Shear Transfer Model (Shear Stress-Shear Strain envelope)

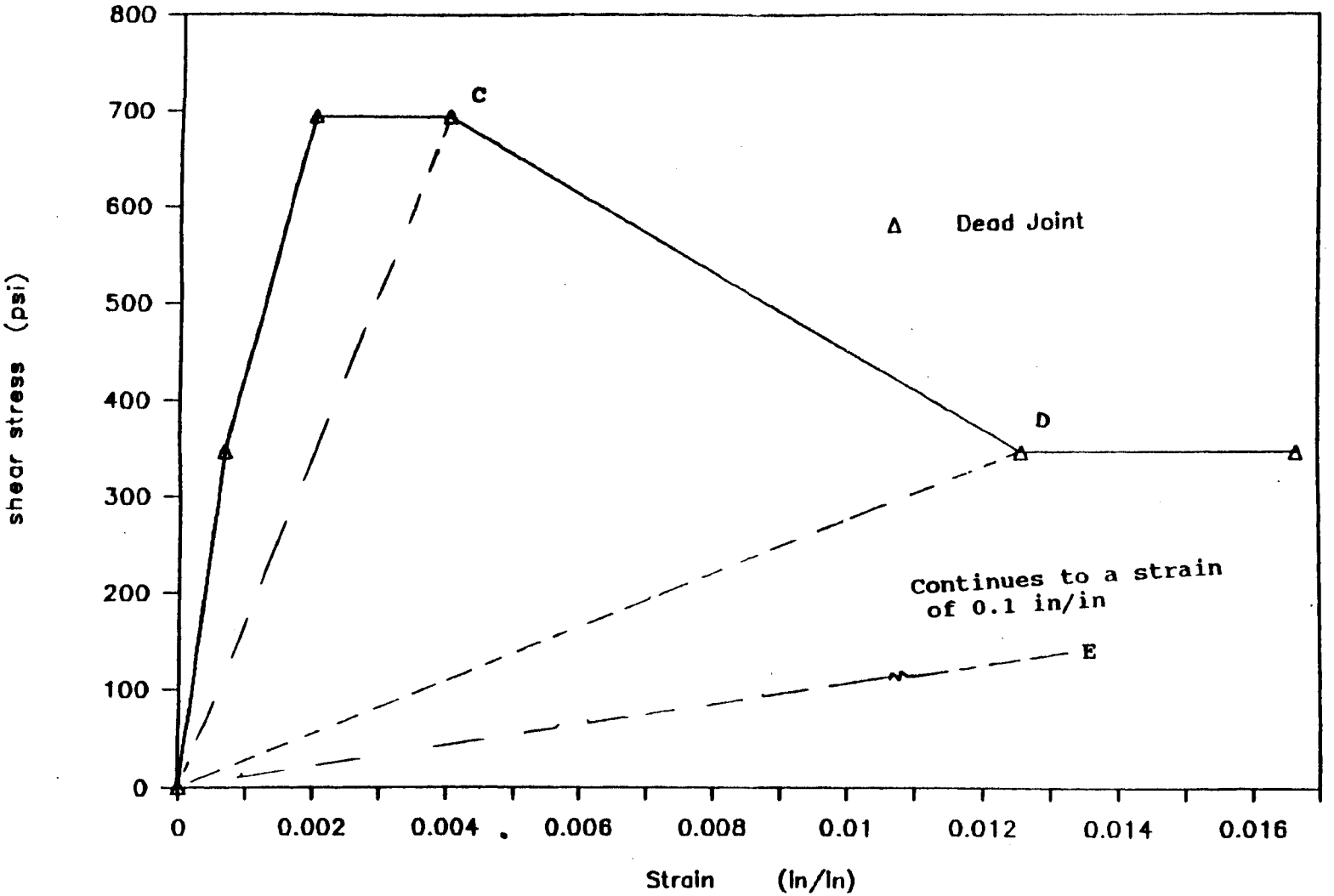

Figure 3.17: Shear Transfer Model (Shear Stress-Shear Strain envelope)

CHAPTER 4

RESULTS

4.1 General

In pavement engineering, nondestructive tests are usually performed to investigate the performance of a joint, and most of these tests use the joint efficiency concept for this purpose. The joint efficiency (JE) is defined by the ratio of the maximum deflection of a point (node) on the unloaded side to the maximum deflection of a point (node) on the loaded side; both nodes are equidistant from the joint plane. The results show that the joint efficiency decreases as the joint deteriorates which corresponded to a decrease in the K value obtained from the Hawkins shear model. The deflection of both loaded and unloaded nodes were not the only information that is obtained from the finite element analyses. The results obtained consisted of the deflections, velocities and accelerations of both nodes which were equidistant (at 3 inches) from the joint plane. The time velocity-curves were smooth, while the time acceleration-curves contained higher frequency components. The plots of deflections, velocities and accelerations versus time are in Appendices A, B, C respectively.

Fourier showed that the frequency content of a periodic time function may be expressed as a sum of weighed sine and cosine functions with harmonically related frequencies. The combination of sine and cosine functions is called Fourier Transform and is expressed mathematically by equation (2.22). The code Asystant+ '87 was used in this analysis for

obtaining the FFT of acceleration-time histories. The Power Spectrum function, which is defined as the squared magnitude of the Fourier Transformation, was obtained for each acceleration record. The Fourier Transformation takes the discrete Fourier Transform of the data processed and returns a complex variable according to the following formula:

$$F(k) = \sum_{j=0}^{n-1} f(j)\, e^{(-2\pi i\, jk/n)} \qquad (4.1)$$

with

$$k = 0,1, \quad ,n-1$$

The plots of the acquired data from the Power Spectrum analysis are provided in Appendix D.

4.2 Model with changing compressive axial force

Three different values of compressive axial force were used, 2000, 4000 and 9500 lbs. These loads were investigated on three different joints: dead, deteriorated and perfect (model 1). The deflections of both the loaded and unloaded nodes showed no influence at all for the case of dead and perfect joints. However, for the case of deteriorated joint, The time-deflection curves for both nodes were very close to each other for the values of axial compression forces of 2000 and 9500 lbs. This difference is utmost 5%, and is explained by the creation of moments from the truss elements which consist the shear transfer mechanism. The plots for deflections, velocities and accelerations for the different axial compressive forces are in appendix E.

4.3 Deflection of loaded and unloaded nodes

From the plots of deflections in appendix B, it is noticed that two peak deflections existed. This resulted from the internal computation in ADINA, and may be explained by the effect of reflection and refraction of shear and dilatational waves at the boundaries. The peak deflection of loaded node is estimated to happen at the following time:

$$T = T_p + 2\ T_c + 2\ T_s$$

in which

T_p = duration of loading pulse.

T_c = time for dilatational waves to travel concrete slab

T_s = time for dilatational waves to travel sand layer

The duration of the loading pulse is 0.81 msec. The duration T_c and T_s are given by the following expressions:

$$T_c = L_c / C_c$$

$$T_s = L_s / C_s$$

in which

L_c = thickness of concrete slab

L_s = thickness of sand layer

C_c = dilatational wave velocity for concrete

C_s = dilatational wave velocity for sand

Using Equation (2.10), C_c and C_s are 124170 and 8920 in/sec, respectively. so

$$T = 0.00081 + 2\ (6/124170) + 2\ (9/8920)$$

$$= 0.00081 + 0.00010 + 0.002$$

$$= 0.00291 \text{ sec}$$

From the above wave analysis the actual peak should be between the two peaks obtained from the FEM analysis. The second peak is probably the actual one, but such a conclusion is not evident. Moreover, it should be noted that the reflection and refraction of shear and dilatational waves from the concrete boundaries also affect the result, but the time for the waves to travel through the concrete elements is very small compared to the case when sand is considered. In the case of new joints, the deflection for the unloaded side is greater than the deflection for the loaded side giving an unrealistic joint efficiency value greater than 1.0. This is believed to happen because the truss elements for the shear transfer mechanism are creating moments, because there is no horizontal elements to transfer the horizontal forces and no sliding is permissible across the joint. As a result neither the first peak nor the second peak provide the exact behavior of the joint, and the average of the two joint efficiencies was considered in this study.

One of the primary roles of joints is to reduce the deflection of the loaded node, and to increase the deflection of the unloaded node due to the load transfer capability. If no load transfer exists across the joint, the deflections of the loaded slab will increase and will result in the loss of serviceability, or breakup. For both peak deflections in the loaded side, Table 4.1 shows that the deflection of a perfect joint is almost half of the deflection for a dead joint. The peak deflections of the loaded node for joint 1 were 0.00616 and 0.00531 inches and they were reduced to 0.0035 and 0.00241 inches, respectively, for the perfect

joint. So, as the joint deteriorates, the deflection of the loaded side increases, as shown in Figure 4.1. However, for the unloaded node, the deflection decreases as the joint deteriorates to reach a very low value in the case of dead joint 1, as shown in Fig 4.2. The peak deflections of the unloaded joint increased from 0.00073 and 0.00033 inches for joint 1 to 0.00344 and 0.00238 inches for the perfect joint. Figure 4.3 shows this relationship for the average peak of both nodes. In Appendix A, the plots for deflections of both loaded and unloaded nodes are provided on the same figures to show the difference between the peaks. The plots of deflection of each node for different joints are also provided in the same Appendix A.

From Tables 4.1 and 4.2, one observes that the maximum deflections for the loaded and unloaded nodes do not occur at the same time, which implies that the nondestructive testing methods (e.g. FWD) may not be accurate enough because these methods measure the joint efficiency from deflections at the same time. This time difference was varying from 0.4 msec for a perfect joint to 0.9 msec for a dead joint, and the existing methods have to be modified for correcting this problem. Also, it is clear that as the joint deteriorates, the time differences between the peaks of both nodes increases (Fig. 4.4).

4.4 Joint Efficiency versus Changing Joint Shear Transfer

As the joint deteriorates, the joint efficiency decreases. The joint efficiency constitutes a certain type of joint. For a value of JE between 85-95%, it constitutes a new joint. For a value of JE less than 60%, the

joint is a dead joint. For values of 65-80% for JE, the joint starts to function improperly and is named deteriorated joint. From the value of average joint efficiency in Table 4.3 and as expected from the classification of joints according to the K value from the Hawkins' shear model, joints 1, 2 and 3 are dead, joints 4 and 5 are deteriorated and joints 6 and 7 are new. Table 4.4 demonstrates that with increasing the K value the JE increases, as shown in Fig 4.5. A value for K of 1,000,000 psi is assumed for a perfect joint for demonstrating the relationship between the shear transfer value K and the joint efficiency.

4.5 Velocities of loaded and unloaded nodes

In the case of deflections, as the joint deteriorates, the deflections of the loaded node increase and the deflections of the unloaded node decrease. For the case of velocities, there are several peaks, either positive or negative. The maximum positive and negative peaks were taken and it is observed that, as the joint deteriorates, the magnitude of both peaks increases for the case of loaded node and decreases for the case of unloaded node. Table 4.5 shows values of peaks for the case of loaded node, and Table 4.6 shows the values of peaks for the unloaded node. For the case of the loaded node, the peaks are occurring approximately at the same time; however for the case of the unloaded node the peaks are delayed as the joints deteriorate. For the loaded node, the magnitudes of the peaks for the case of a perfect joint are almost half of the peak values for a the dead joint 1. For the unloaded nodes, the peaks are increasing from very low values for the case of joint 1 to almost the peak values of the loaded node of the perfect

joint.

4.6 Fast Fourier Transformation analysis

Table 4.7 and Table 4.8 show that, as the joint deteriorates, the peak values of accelerations increase for the case of loaded node and decrease for the unloaded joint. The peak values of accelerations appear to be somewhat random for the case of loaded node and they are delayed as the joint deteriorates for the case of unloaded node. However, the time-acceleration relationships for both nodes also appear to be random and a very appropriate tool for analyzing it is the Fast Fourier Transformation (FFT) which transforms random data to a summation of harmonic sinusoidal functions. From the Power Spectrum Analysis, two frequencies were obtained for each node accelerations.

Table 4.9 gives the values of both frequencies for both nodes of each joint. In structural analysis, the first frequency is always referred to as the fundamental natural frequency of the structure, and it depends on the size and geometry of the structure and the strength parameters of the elements. The loaded node will not give reliable results for the natural frequencies because of the existence of the loading which will have a physical influence on the numerical results for the frequencies (forced vibration vs. free vibration). So the results of the first frequency from the unloaded node are more reliable and are considered in this study. When the spring elements, that represent the shear transfer mechanism, have a low stiffness value, K, each slab is acting separately. This explains the observation that for the dead and deteriorated joints

the natural frequency is 391 Hz, and as the value of K increases for the cases of new joint the frequency increased to 571 Hz (because the slabs are now acting as one slab which is similar to Model 1). However the shear transfer mechanism transfers only shear and the moment and axial effects are not transferred. This corresponds to a softer system, which explains why the first frequency obtained for Model 1 (perfect joint) was higher than the frequency of Model 2 for the cases of new joint.

The only other varying parameter, other than the one influencing the rigid body motion of the system, was the shear transfer stiffness K, so it is expected that it will influence the second frequency. For the loaded side, the second frequency was constant for all joints including the perfect joint. However, for the unloaded side, the second frequency increases as the K value of the shear transfer mechanism increases and as the performance of joint is improving, as shown in Fig 4.6.

4.7 Difference between Model 1 and Model 2

From the joint efficiencies, deflection and velocity peaks and the frequency analysis, it was noticed that Model 1 is just an improved version of the model 2, the only difference was the first frequency obtained from the FFT analysis. That difference is related to the size, and strength parameters. The response of Model 1 is very close to the behavior of the Model 2 when the K value of shear transfer mechanism increases.

4.8 Correlation between the Experimental and Analytical studies

The experimental study of the joint shear behavior was done simultaneously by Palmieri '90. This numerical study was performed before the experimental study and the general trend of the numerical results seem to be very similar to that obtained from the experimental results. Palmieri '90 reported that as the joint condition improved, the joint efficiency increased and the second frequency increased for the loaded and unloaded nodes.

Table 4.1: Maximum Deflection for Loaded Node

	First Peak		Second Peak	
Joint Number	Deflection (in)	Time (msec)	Deflection (in)	Time (msec)
1	- 0.00531	1.34	- 0.00616	3.22
2	- 0.00443	1.29	- 0.00466	3.08
3	- 0.00427	1.28	- 0.00444	3.06
4	- 0.00403	1.27	- 0.00411	2.98
5	- 0.00380	1.27	- 0.00379	2.89
6	- 0.00358	1.26	- 0.00354	2.76
7	- 0.00341	1.26	- 0.00334	2.62
Perfect	- 0.00241	1.50	- 0.00350	3.04

Table 4.2: Maximum Deflection for Unloaded Node

	First peak		Second Peak	
Joint Number	Deflection (in)	Time (msec)	Deflection (in)	Time (msec)
1	- 0.00033	2.27	- 0.00073	4.12
2	- 0.00156	1.84	- 0.00300	3.72
3	- 0.00172	1.77	- 0.00326	3.66
4	- 0.00194	1.70	- 0.00357	3.57
5	- 0.00209	1.61	- 0.00374	3.48
6	- 0.00228	1.58	- 0.00395	3.40
7	- 0.00239	1.54	- 0.00399	3.33
Perfect	- 0.00238	1.38	- 0.00344	2.64

Table 4.3: Joint Efficiencies

Joint Number	First Peak (%)	Second Peak (%)	Average (%)
1	6.21	11.85	9.03
2	35.21	64.38	49.80
3	40.28	73.42	56.85
4	48.13	86.86	67.50
5	55.00	98.68	76.84
6	63.69	111.58	87.64
7	70.09	119.46	94.78
Perfect	98.76	98.29	98.52

Table 4.4: Joint Efficiencies

Joint Number	K value (psi)	Joint Efficiency (%)
1	15,600	9.03
2	140,000	49.80
3	175,000	56.85
4	240,000	67.50
5	350,000	76.84
6	450,000	87.64
7	600,000	94.78
Perfect	1,000,000	98.52

Table 4.5: Maximum Velocities for Loaded Node

	Positive Peak		Negative Peak	
Joint Number	Velocity (in/sec)	Time (msec)	Velocity (in/sec)	Time (msec)
1	10.42	4.32	- 6.50	0.53
2	8.00	3.54	- 6.16	0.54
3	7.76	3.53	- 6.11	0.53
4	7.15	3.48	- 5.98	0.53
5	6.09	3.46	- 5.74	0.53
6	6.25	4.32	- 5.64	0.53
7	7.10	4.32	- 5.46	0.53
Perfect	5.73	3.47	- 5.73	0.52

Table 4.6: Maximum Velocities for Unloaded Node

	Positive peak		Negative Peak	
Joint Number	Velocity (in/sec)	Time (msec)	Velocity (in/sec)	Time (msec)
1	0.76	4.72	- 0.47	3.38
2	5.03	4.51	- 2.93	3.19
3	5.47	4.47	- 3.39	3.15
4	5.67	4.42	- 4.03	3.10
5	5.34	4.38	- 4.42	3.03
6	4.98	3.87	- 4.91	2.99
7	5.05	3.80	- 5.02	2.94
Perfect	3.47	3.55	- 4.01	2.20

Table 4.7: Maximum Accelerations for Loaded Node

	Positive Peak		Negative Peak	
Joint Number	Acceleration (in/sec^2)	Time (msec)	Acceleration (in/sec^2)	Time (msec)
1	30745	4.56	- 40492	4.56
2	32933	1.33	- 38907	4.48
3	32349	4.88	- 36825	4.48
4	33840	1.33	- 32957	4.48
5	29513	4.09	- 37179	5.29
6	33215	4.09	- 39602	5.29
7	34977	4.09	- 35359	5.29
Perfect	25550	3.14	- 23108	3.80

Table 4.8: Maximum Accelerations for Unloaded Node

	Positive Peak		Negative Peak	
Joint Number	Acceleration (in/sec^2)	Time (msec)	Acceleration (in/sec^2)	Time (msec)
1	1785	4.35	- 994	2.94
2	8308	3.69	- 12078	4.83
3	10074	3.65	- 14758	4.80
4	12596	3.59	- 18165	4.74
5	14253	3.56	- 205434	4.69
6	16718	3.37	- 19132	4.66
7	18447	3.26	- 16826	4.63
Perfect	30197	4.93	- 24164	1.81

Table 4.9: Values of frequencies obtained from FFT analysis

	First Frequency		Second Frequency	
Joint Number	Loaded Node	Unloaded Node	Loaded Node	Unloaded Node
1	391	391	1172	977
2	391	391	1172	977
3	586	391	1172	977
4	586	391	1172	977
5	586	391	1172	977
6	586	586	1172	977-1172*
7	586	586	1172	1172
Perfect	586	781	1172	1172

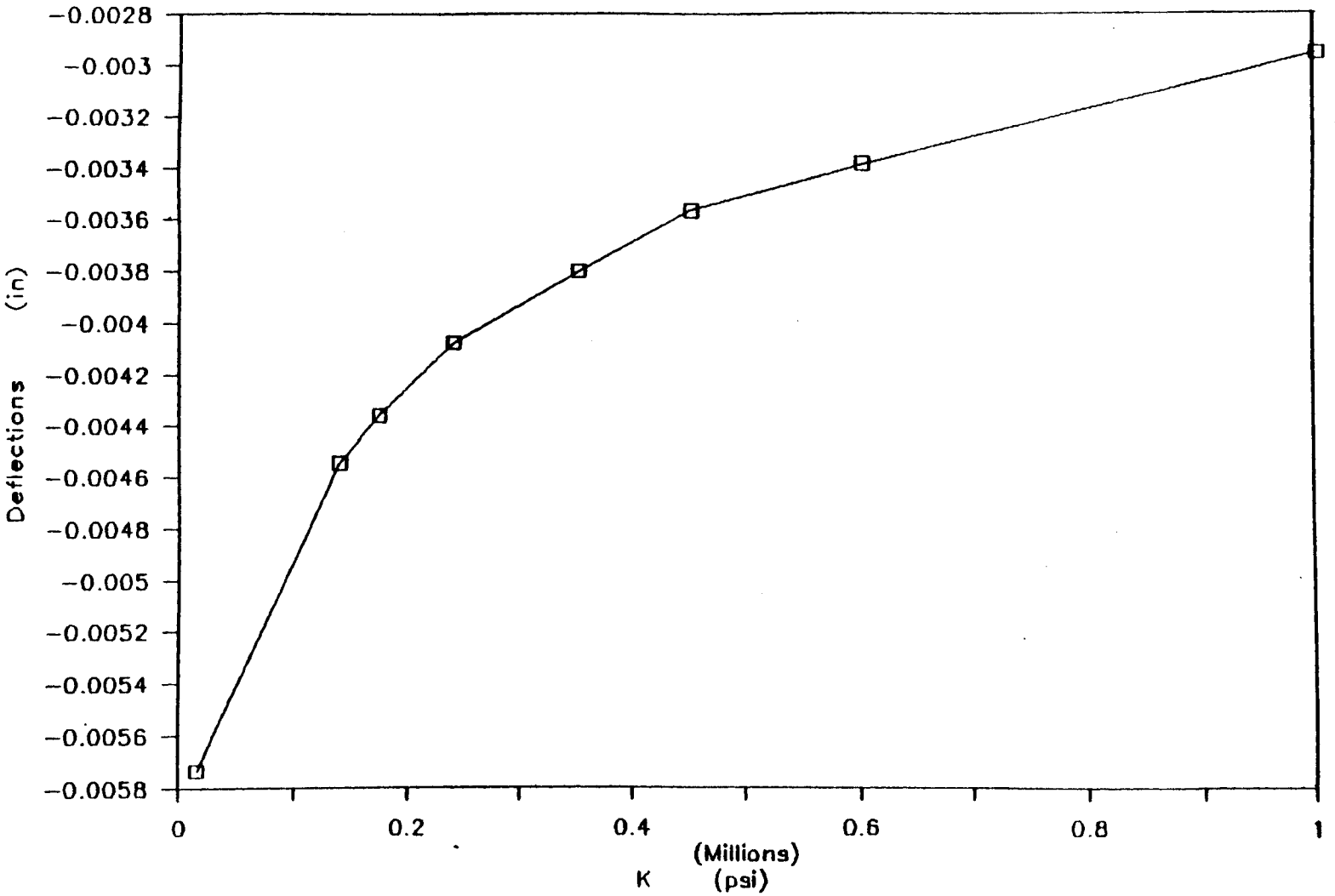

Figure 4.1: Deflections of loaded node vs. Shear Stiffness value, K

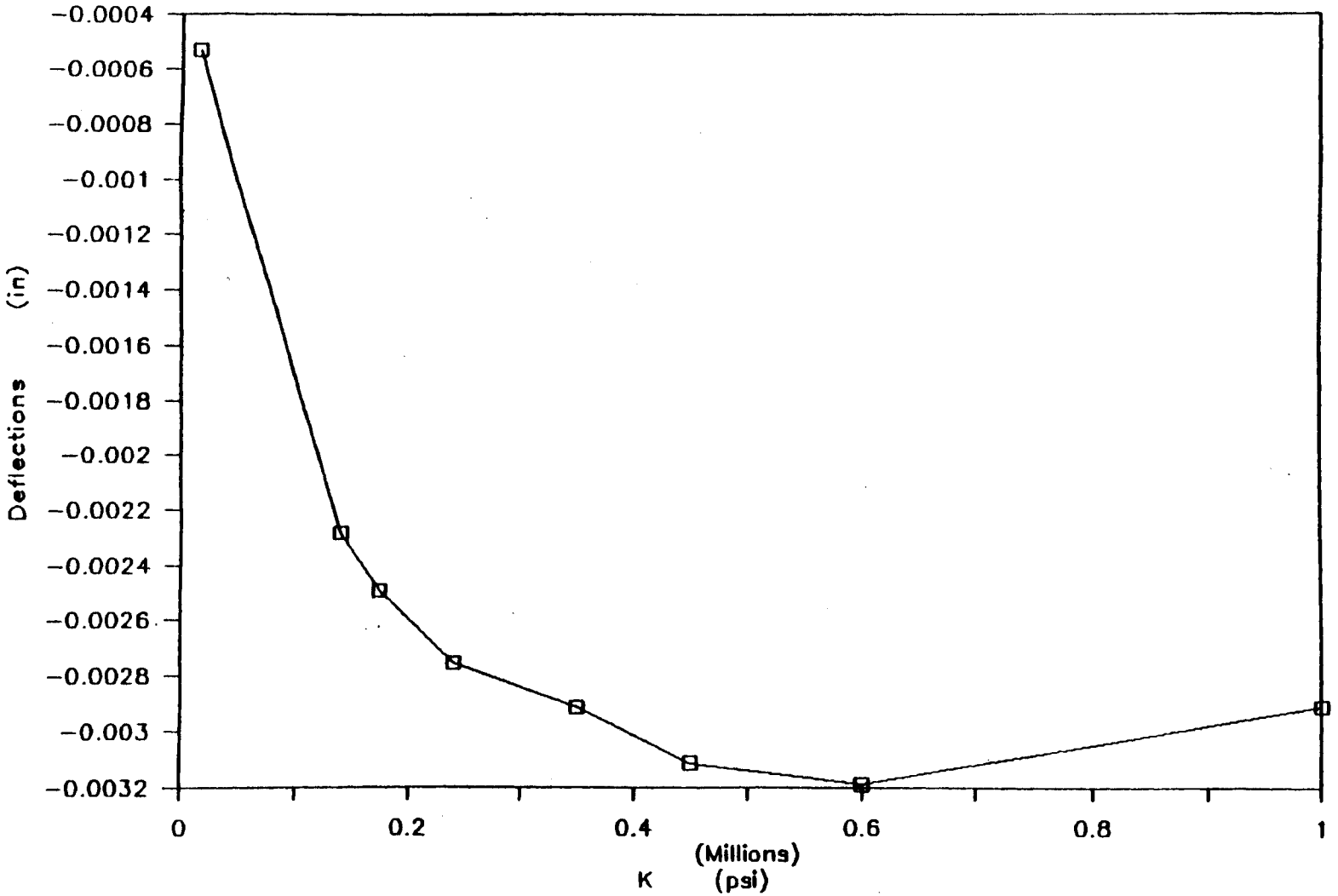

Figure 4.2: Deflections of unloaded node vs. shear stiffness value, K

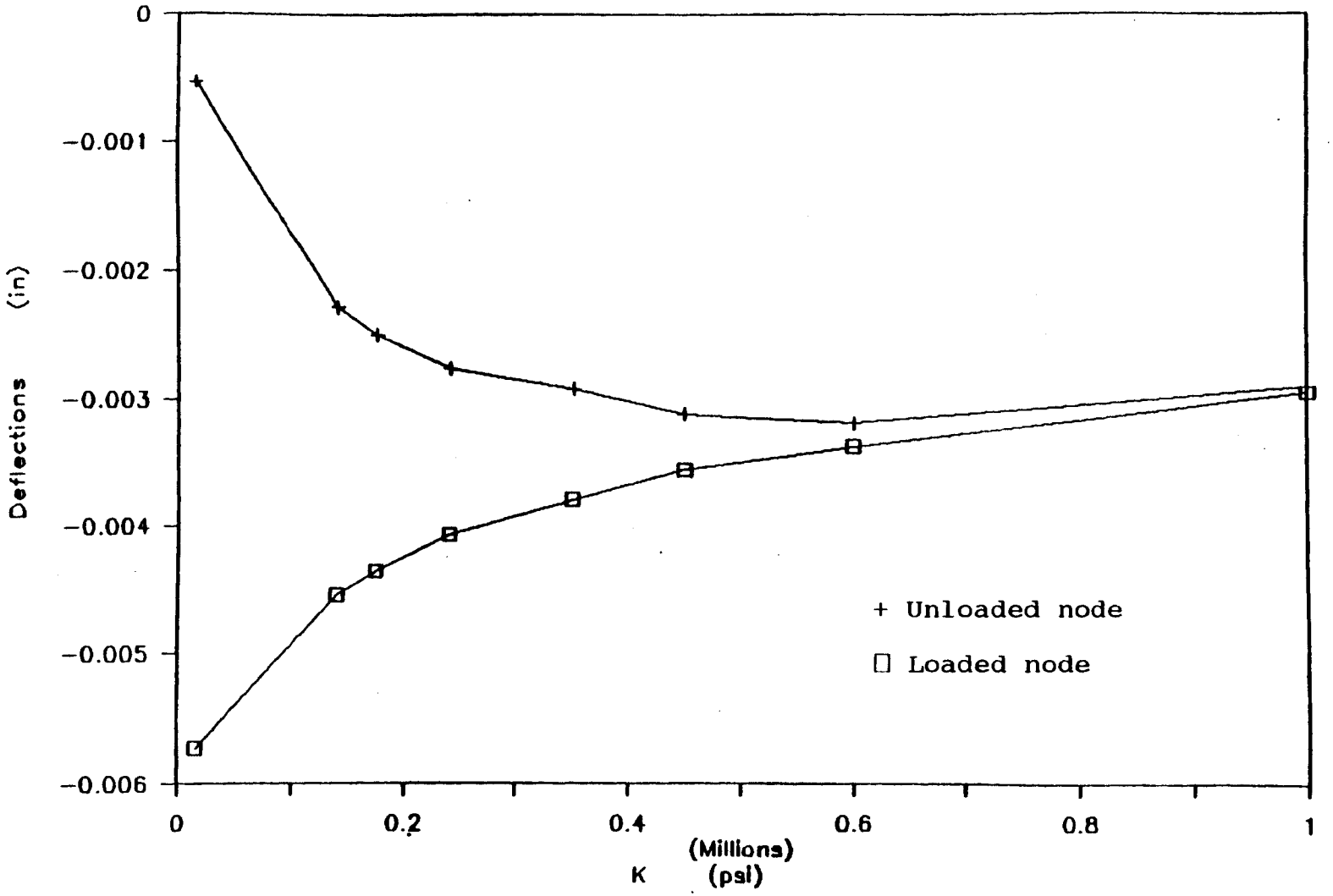

Figure 4.3: Deflections of both nodes vs. shear stiffness value, K

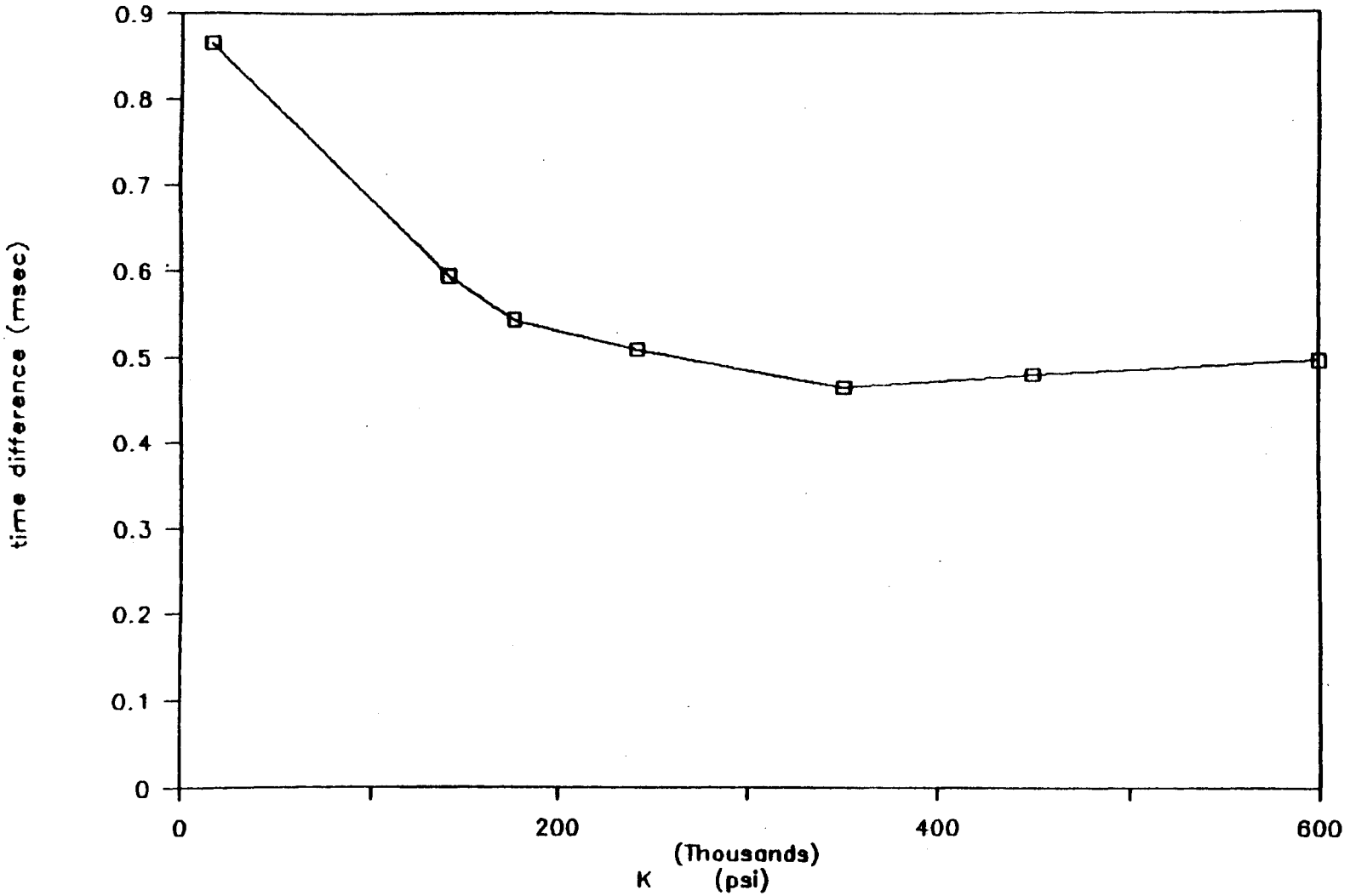

Figure 4.4: Time difference between deflection peaks of loaded and unloaded nodes

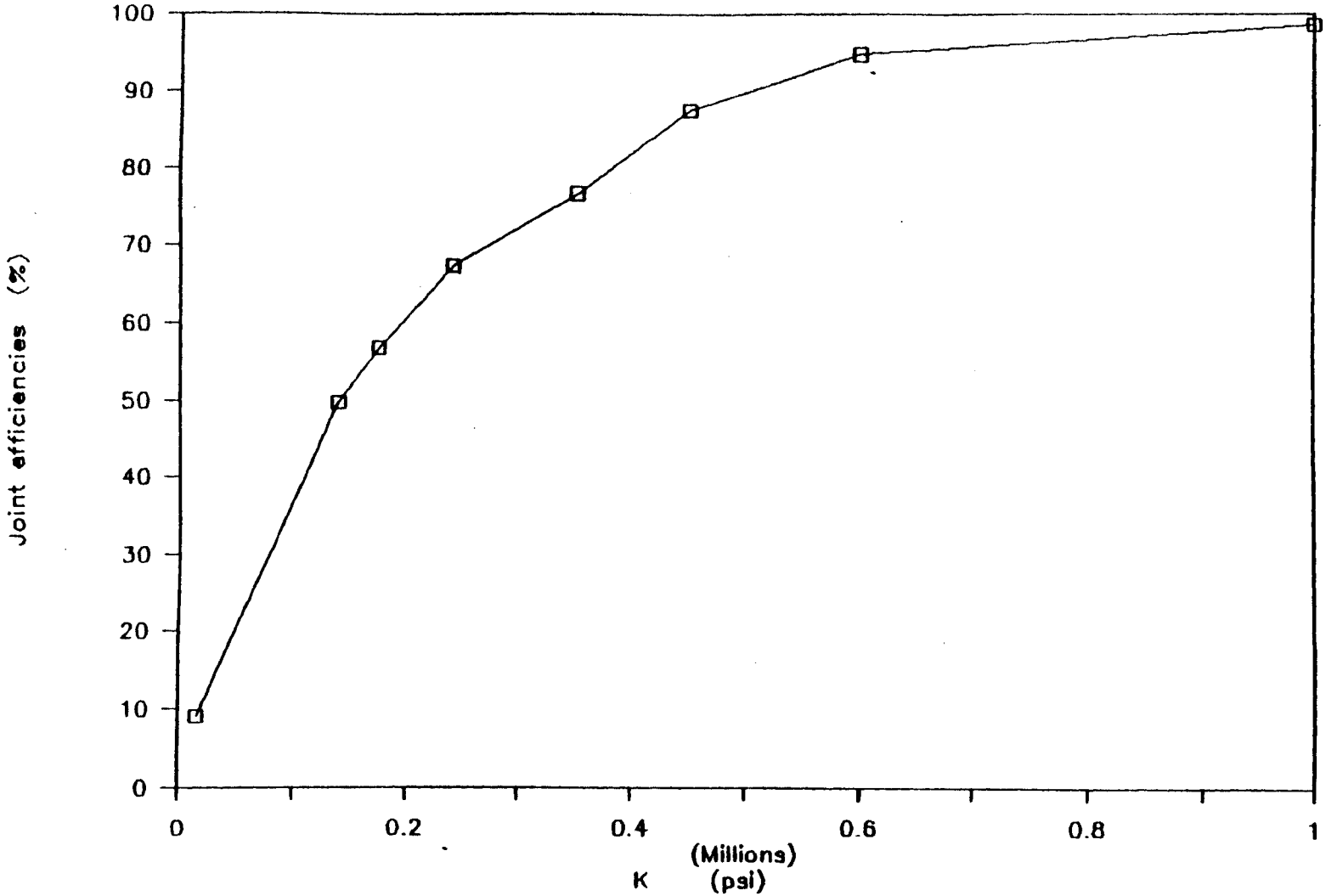

Figure 4.5: Joint Efficiencies vs shear stiffness value, K

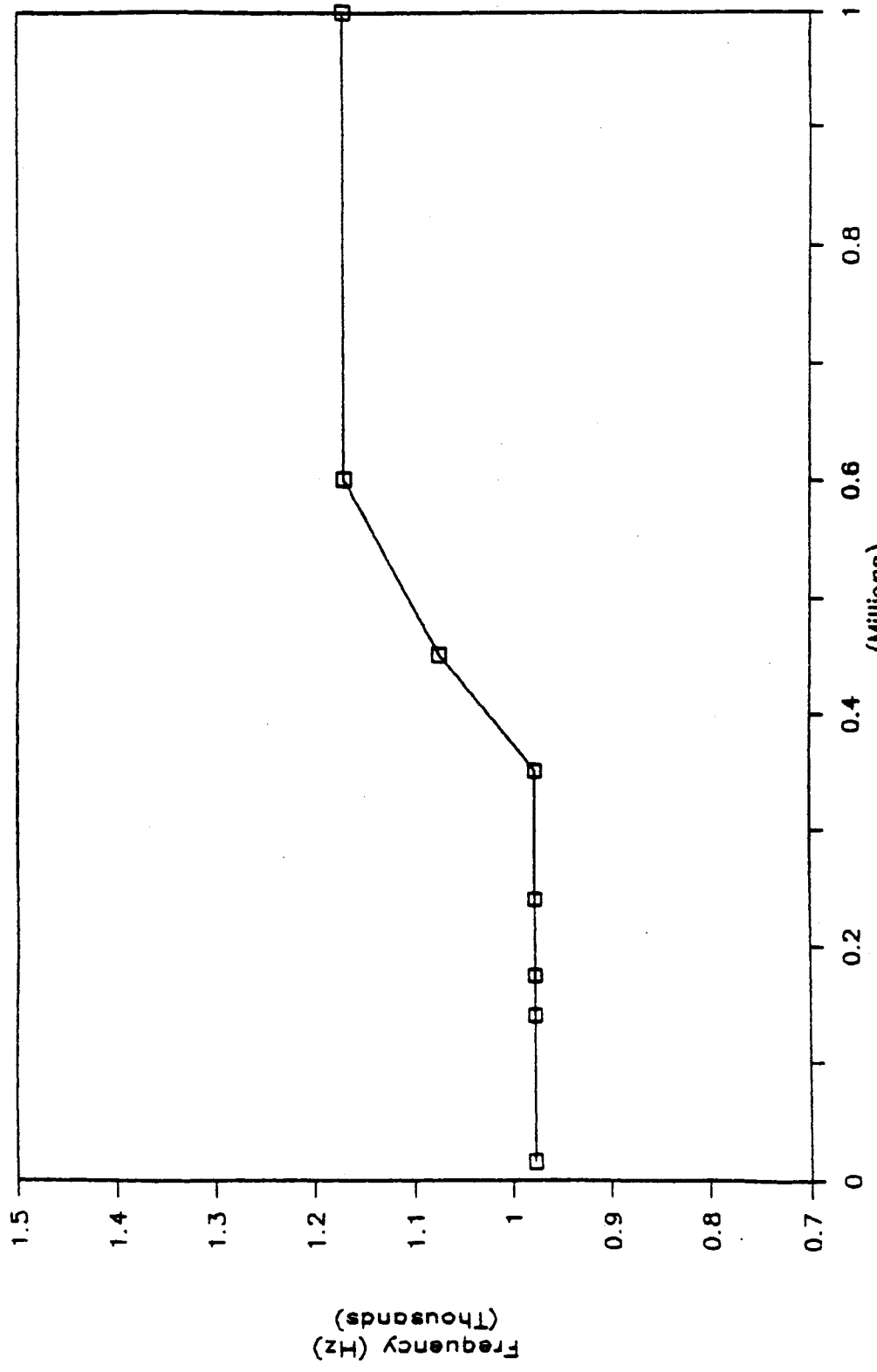

Figure 4.6: Second frequency vs shear stiffness value, K

CHAPTER 5

CONCLUSIONS AND RECOMMENDATIONS

5.1 Conclusions

A numerical method is presented for analyzing rigid pavement joint behavior in the time and in the frequency domains. An explicit shear stress vs. shear slip relationship is employed for defining the shear transfer across the joint. The joint is classified in accordance to its performance, presented by the joint efficiency, and the present results demonstrate the relationship between the internal condition of the joint and the response frequencies under dynamic loading.

The following conclusions are obtained from this study:

1. The present approach documents that the behavior of a joint is related to an explicit joint shear transfer mechanism.

2. The model used to simulate the shear transfer across rigid pavement joints represented accurately the behavior of joints (e.g. joint efficiency and deflections).

3. The frequency domain analysis, using the Fast Fourier Transform, seems to be a useful tool for understanding the behavior of a joint.

4. It seems that a nondestructive testing procedure for rigid pavement joints can be developed by correlating the time domain and the

frequency domain responses.

5. The finite element method can be employed for pavement analysis and for investigating the behavior of joints.

6. The linear three-dimensional analysis gave reasonable information, and it is anticipated that this approach would be more effective if nonlinear effects and in-situ materials properties are considered.

7. From the Fast Fourier Transformation used for this study, it is concluded that the first frequency is related to the structural size and characteristics of the pavement, and the second frequency is related to the shear transfer capability of a joint.

5.2 Recommendations

Based on the results obtained from this study, the following recommendations are made:

1. To continue the present study by performing comparisons with a wide range of rigid pavement joint and material types and seasonal condition to determine a good correlation between the field and numerical results.

2. To extend this study to investigate bridge decks.

3. To develop a clear relationship between the FWD data and the

frequency response approach.

4. To determine and define the effects of in-situ conditions on the results such as type of subgrade, structural parameters and type of bridge deck, temperature and seasonal effects.

5. Include non-linear material properties in the analysis.

6. Prepare charts and tables to relate FWD results and frequency response data to the internal conditions of a joint.

7. Conduct the analysis with lower value of time increment to get better frequency domain results.

REFERENCES

AASHTO, "AASHTO Guide for Design of Pavement Structures", 1986.

ADINA Engineering, "ADINA : A Finite Element Program for Automatic Dynamic Incremental Nonlinear Analysis", Report AE 81-1, Watertown, Mass., Sept. 1981.

Barkan, D. D., "Dynamics of bases and Foundations", McGraw-Hill, 1962.

Bathe, K. J., "Finite Element Procedures in Engineering Analysis", Prentice-Hall, 1982.

Boutrus, S., Davis, T. G., and Mamlouk, M. S.,"Dynamics of Falling Weight Deflectometer", ASCE Journal of Transportation, Vol. 111, No. 6, November 1985.

Bresler, B., and MacGregor, J. G., "Review of Concrete Beams Failing in Shear", ASCE Journal of Structural Division, Vol. 93, February 1976, pp. 343 - 372.

Cloug R. W. and Penzien J., "Dynamics of structures", McGraw-Hill, 1975.

Chou, Y. T., "Stress Analysis of Small Concrete Slabs on Grade", ASCE Journal of Transportation Engineering, Vol. 110, No. 5, September 1984, pp. 481-491.

Chou, Y. T., "Structural Analysis Computer Program for Rigid Multicomponent Pavement Structures with Discontinuities - WESLIQID and WESLAYER", Report GL-81-6, Parts 1-3, U.S. Army Waterways Experiment Station, May 1981.

Churchill R. V., and Brown, J. W. "Fourier Series and Boundary Value Problems", McGraw-Hill, 1978.

Cook R. D., Malkus D. S., and Plesha M. E. "Concepts and Applications of Finite Element Analysis", Wiley, Third Edition, 1989.

Criswell, M. E. "Strength and Behavior of Reinforced Concrete Slab-Column Connections Subjected to Static and Dynamic Loadings", Technical Report N-70-1, U.S. Army Engineer Waterways Experiment Station, Viksburg, Mississippi, 388 pp., December 1970

Das, B. M. "Principles of Foundation Engineering", PWS and Kent, 1984.

Foxworthy, P. T. "Concepts for the Development of a Nondestructive testing and Evaluation System for Rigid Airfield Pavements", Thesis presented to the University of Illinois, Urbana, Ill., in partial fulfillment of the requirements for the degree of Doctor of Philosophy, 1985.

Hawkins N. M., "The Strength of Stud Shear Connections", Civil Engineering Transactions, Institute of Engineers, Australia, December 1974.

Hawkins N. M., "Dynamic Shear Resistance of Reinforced concrete", Report to U.S. Navy, August 1981.

Hoffman, M. S., and Thompson, M. R., "Comparative Study of Selected Nondestructive Testing Devices", TRB, NO. 852, 1982.

Holmquist, T., and Krauthammer T. "A modified Method for the Evaluation of Direct Shear Capacity in Reinforced Concrete Slabs Under the Effect of Dynamic loads", Structural Eng, Report No. 83-02, University of Minnesota, May 1984.

Huang, Y., and Wang, S. T., "Finite Element Analysis of Concrete Slabs and its Implication for Rigid Pavement design", Highway Research Record

No. 671, Transportation Research Board, 1978.

Ioannidis, A. M., Barenberg, E. J., and Thompson, M. R., "Finite Element Model with Stress Dependent Support", Presented at the Annual TRB Meeting, January 1984.

Kiger, S. A., and Slawson, T. R. "Dynamic Shear Failure in One-Way Slabs", Proceedings of Fifth Engineering Mechanics Division Specialty Conference, Edited by A. P. Boresi and K. P. Chong, ASCE Engineering Mechanics Division, August 1984

Kolsky, H., "Stress Waves in Solids", Dover, 1963.

Krauthammer T., Bazeoz,N., and Holmquist, T. J. "Modified SDOF Analysis of RC box Type Structures", Proc. ASCE Journal of Structural Engineering, Vol. 112, No. 4, pp. 726-744, April, 1986.

Krauthammer T., and Western K. L., "Joint Shear Transfer Effects on Pavement Behavior", ASCE, Journal of Transportation Engineering, Vol. 114, No 5, September 1988.

Mattock, A. H. and Hawkins, N. M. "Shear Transfer in Reinforced Concrete-Recent Research", PCI Journal, pp. 55-75, April 1972.

Mattock, A. H. "Effect of Moment and Tension Across the Shear Plane on Single Direction Shear transfer Strength in Monotholic Concrete", Report No. SM-74-3, Department of Civil Engineering, University of Washington, October 1974.

Mattock, A. H. "Effect of Aggregate Type on Single Direction Shear transfer Strength in Monotholic Concrete", Report No. SM-72-2, Department of Civil Engineering, University of Washington, August 1974.

Mattock, A. H. "Shear Transfer Under Monotholic Loading Across an Interface between Concrete Cast at Different Times", Report No. SM-76-3 , Department of Civil Engineering, University of Whashington, September 1976.

Mattock, A. H. "Effect of Reinforcing Bar Size on Shear Transfer Across a Crack in Concrete", Report No. SM-77-2, Department of Civil Engineering, University of Washington, September 1977.

Moore W. M., Hanson D. I., and Hall J. W. Jr, "An Introduction to Nondestructive Structural Evaluation of Pavements", Transportation Research Board, N. 189, January 1978.

Murtha, R. N., and Holland, T. J. "Analysis of WES FY82 Dynamic Shear Test Structures", Technical Memorandum 51-83-02 Defense Nuclear Agency, December 1982

Murtha, R. N., and Crawford, J. "Dynamic Shear Failure Prediction of Shallow-Buried Reinforced Concrete Slabs", Technical Memorandum 51-81-04, Civil Engineering Laboratory, Port Hueneme, California, May 1981.

Newmark, N. M. "Design of Structure for Dynamic Loads including The Effect of Vibration and Ground Shock", Symposium on Scientific Problems of Protective Construction, Zurich, July 1963.

Newmark N. M., and Rosenblueth, R., "Fundamentals of Earthquake Engineering", Prentice-Hall, 1971.

Palmieri, L. "Vibration Spectroscopy for Rigid Pavement Joint Assessment", M.S. Thesis , University of Minnesota, August, 1990.

Park, R., and Pauley, T., "Reinforced Concrete Structures", Wiley, 1975.

Pauw, A., "Static Modulus of Elasticity of Concrete as Affected by Density", ACI Journal, Vol. 57, pp. 679 - 689, December 1960.

Rinehart, J. S., "Stress Transient in Solids", HyperDynamics, 1975.

Richart, F. E. Jr., Hall J. R. JR., and Woods, R. D., "Vibrations of Soils and Foundations", Prentice-Hall, 1970.

Ross, T. J. "Direct Shear Failure in Reinforced Concrete Beams Under Impulsive Loading", Air Force Weapon Laboratory, Kirkland Air Force Base, Report No. AFWL-TR-83-84, September 1983.

Soroushian, P., and Obaseki, K. "Strain Rate-Dependent Interaction diagram for Reinforced Concrete Section", Proceedings, ACI Journal, vol. 83, No. 1, pp. 108-116, February 1986.

Stearns D. S. "Digital Signal Analysis", Hayden Book Co., 1975.

Tabatabaie,A. M., and Barenberg, E. J., "Finite Element Analysis of Jointed or Cracked Concrete Pavement", Transportation Research Record No. 671, Transportation Research Board, 1978.

Tabatabaie, A. M., and Barenberg, E. J., "Structural Analysis of Concrete Pavement Systems", ASCE, Journal of Transportation Engineering Division, Vol. 106 No. TE5, September 1980.

Talar, H. P.,"The Fundamental Behavior of Reinforced Concrete Beams in Bending and Shear", Shear in Reinforced Concrete, Vol. 1 (SP-42), Detroit: ACI, 1974.

Tolsov G. P., "Fourier Series", Dover, 1962.

Yoder, E. J., and Witczak, M. W., "Principles of Pavement Design", 1975.

Walraven J. C. and Reinhardt, H. W. "Theory and Experiments on the Mechanical Behavior of Cracks in Plain and Reinforced Concrete Subjected to Shear Loading", Heron, vol 26, No. 1, 1981.

Wang, C. K., and Salmon, C. G., "Reinforced Concrete Design", Harper and Row, Fourth Edition, 1985.

Appendix A: Time - Displacement Plots

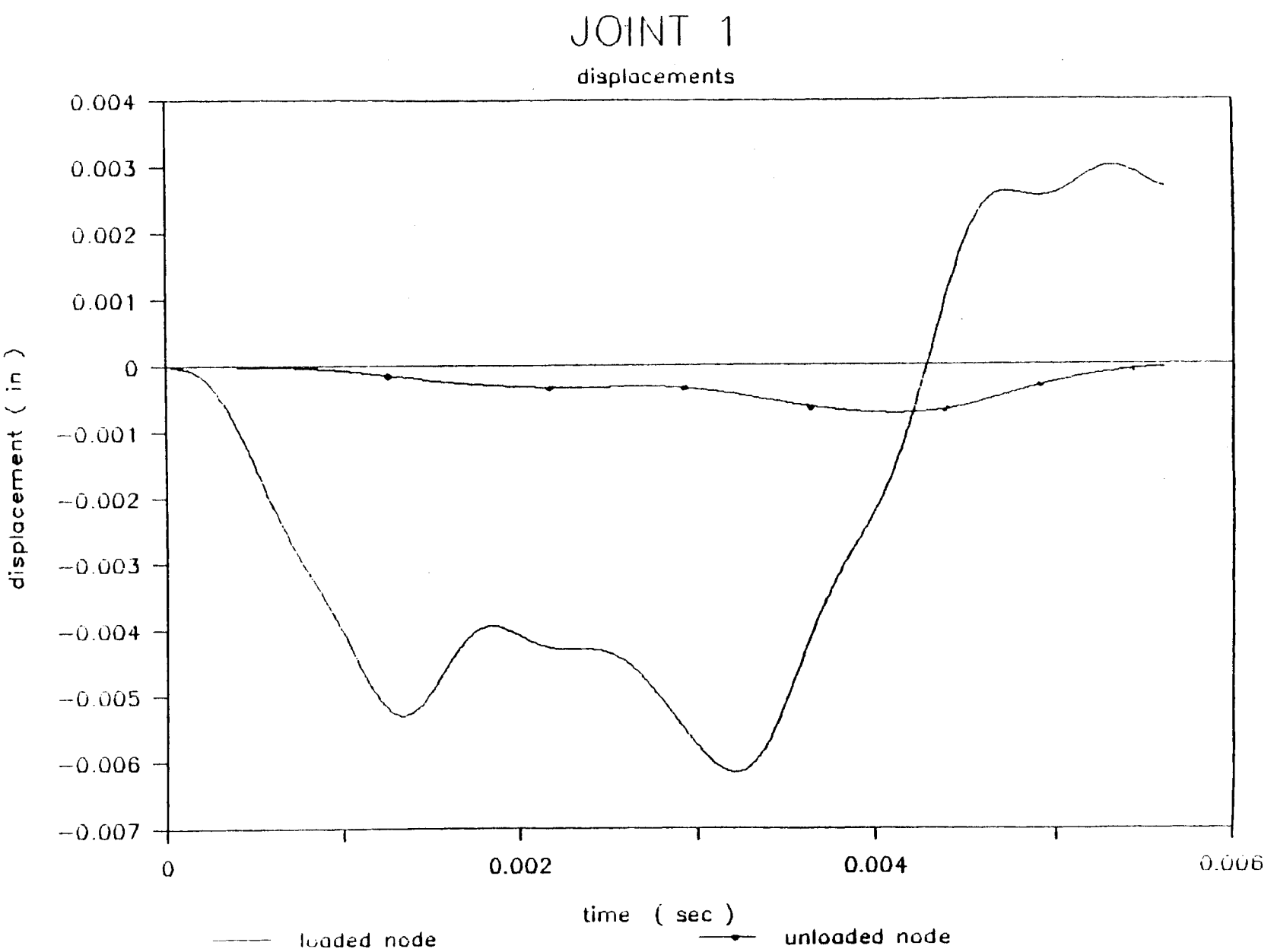
JOINT 1
displacements
0.004
0.003
0.002
0.001
0
-0.001
-0.002
-0.003
-0.004
-0.005
-0.006
-0.007
displacement (in)
0
0.002
0.004
0.006
time (sec)
loaded node
unloaded node

A1

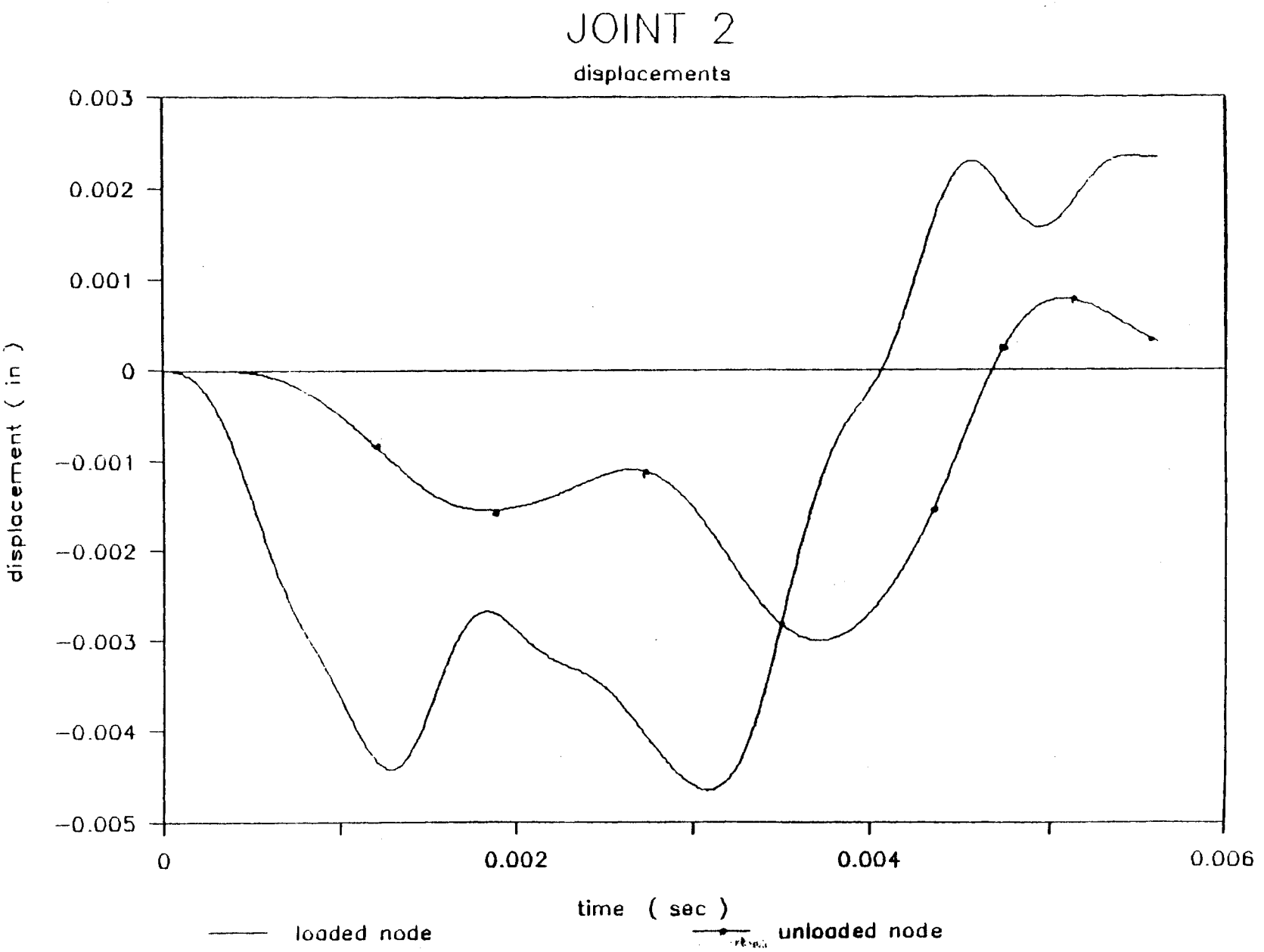
JOINT 2
displacements
0.003
0.002
0.001
0
-0.001
-0.002
-0.003
-0.004
-0.005
displacement (in)
0
0.002
0.004
0.006
time (sec)
loaded node
unloaded node

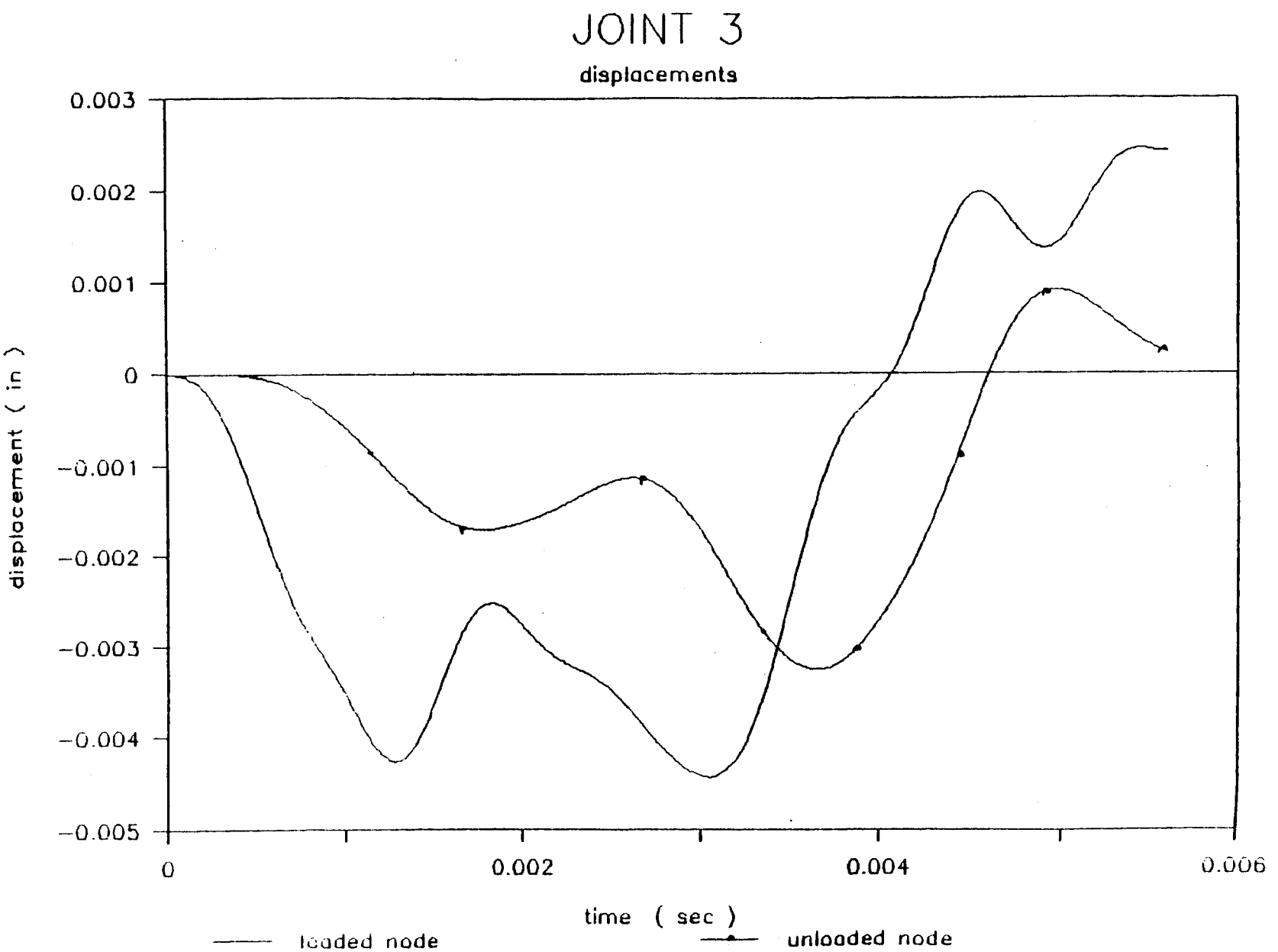
JOINT 3
displacements
0.003
0.002
0.001
0
−0.001
−0.002
−0.003
−0.004
−0.005
displacement (in)
0
0.002
0.004
0.006
time (sec)
loaded node
unloaded node

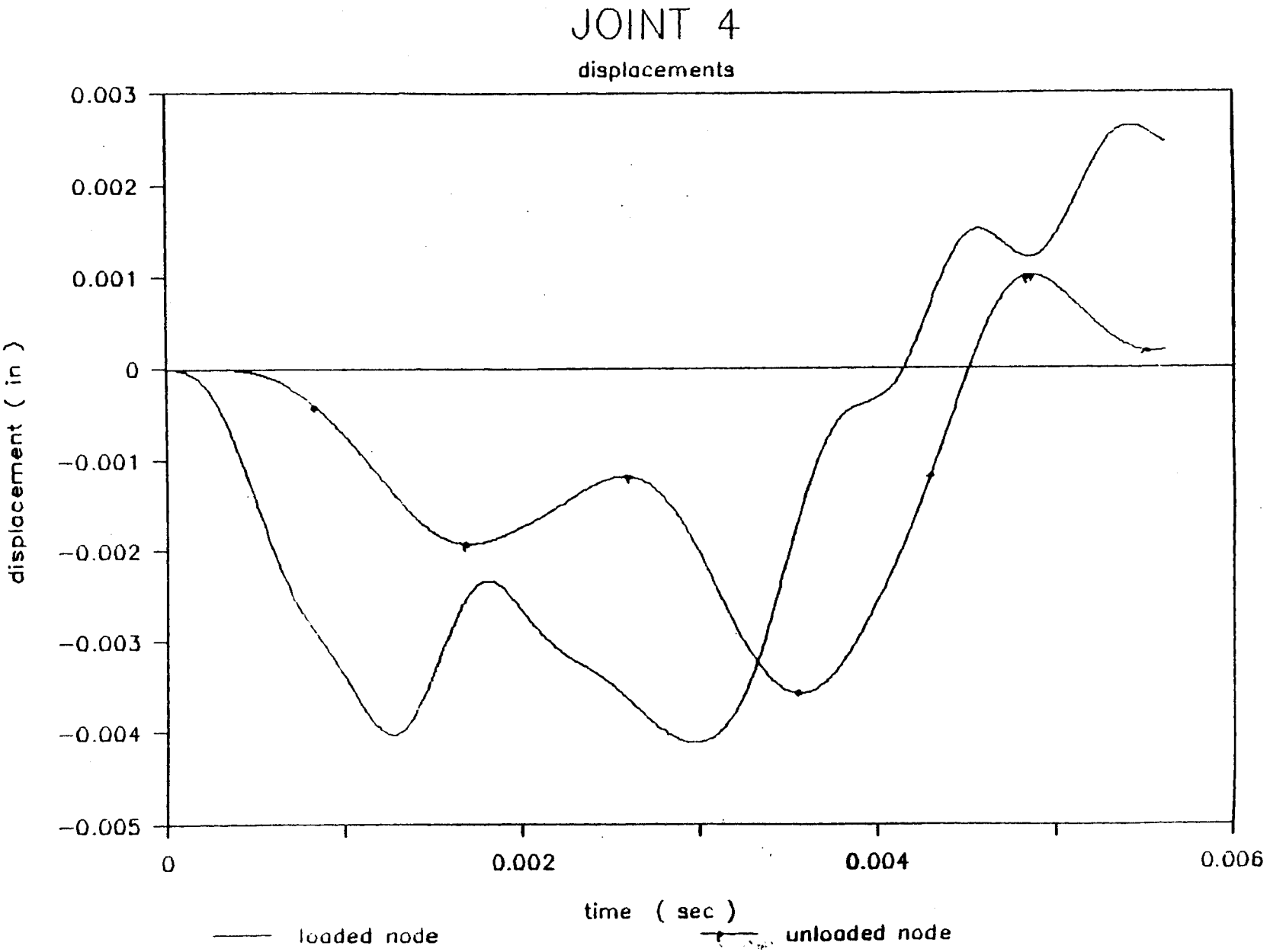
JOINT 4
displacements
0.003
0.002
0.001
0
-0.001
-0.002
-0.003
-0.004
-0.005
displacement (in)
0
0.002
0.004
0.006
time (sec)
loaded node
unloaded node

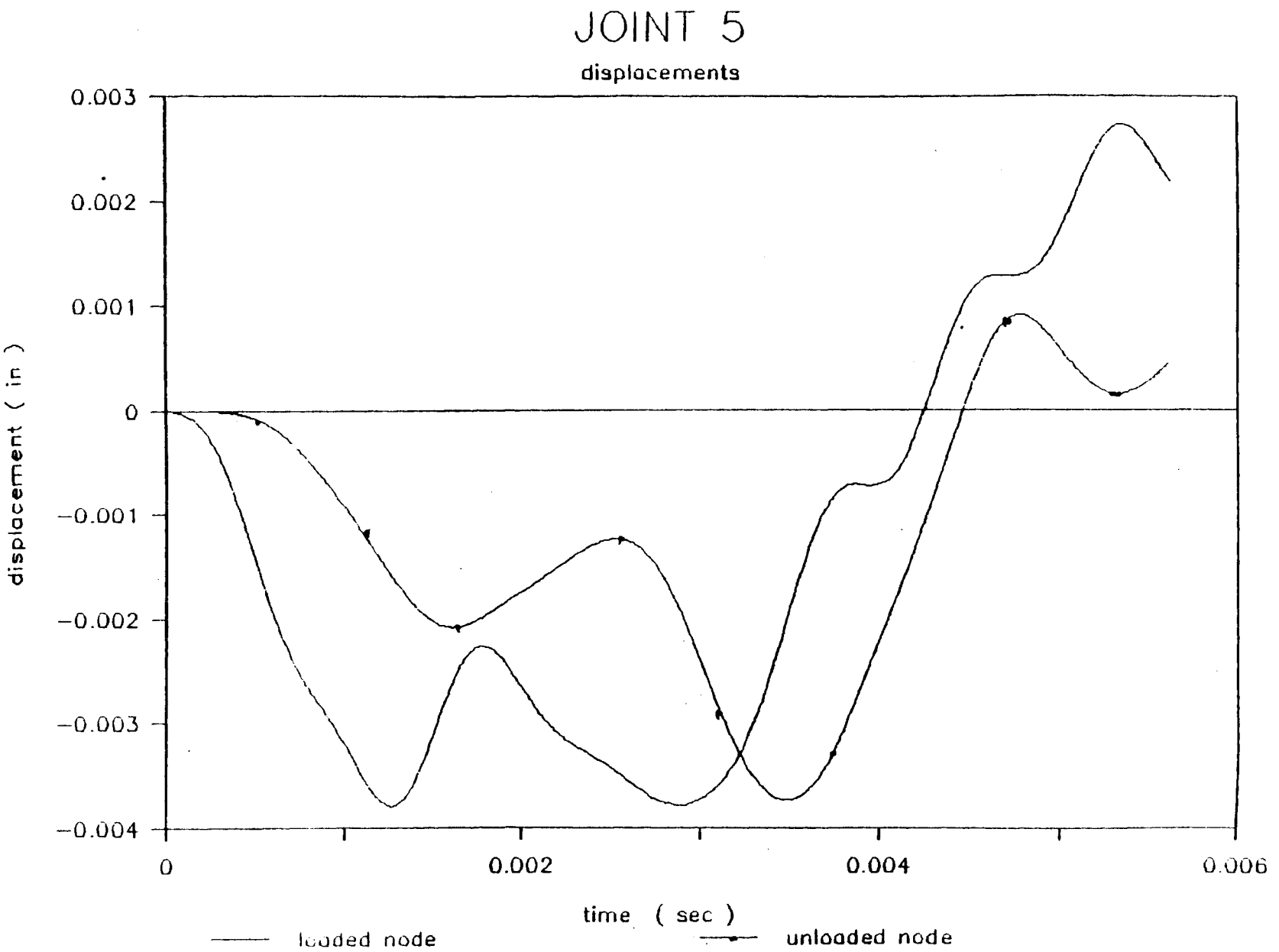
JOINT 5
displacements
0.003
0.002
0.001
0
-0.001
-0.002
-0.003
-0.004
displacement (in)
0
0.002
0.004
0.006
time (sec)
loaded node
unloaded node

A5

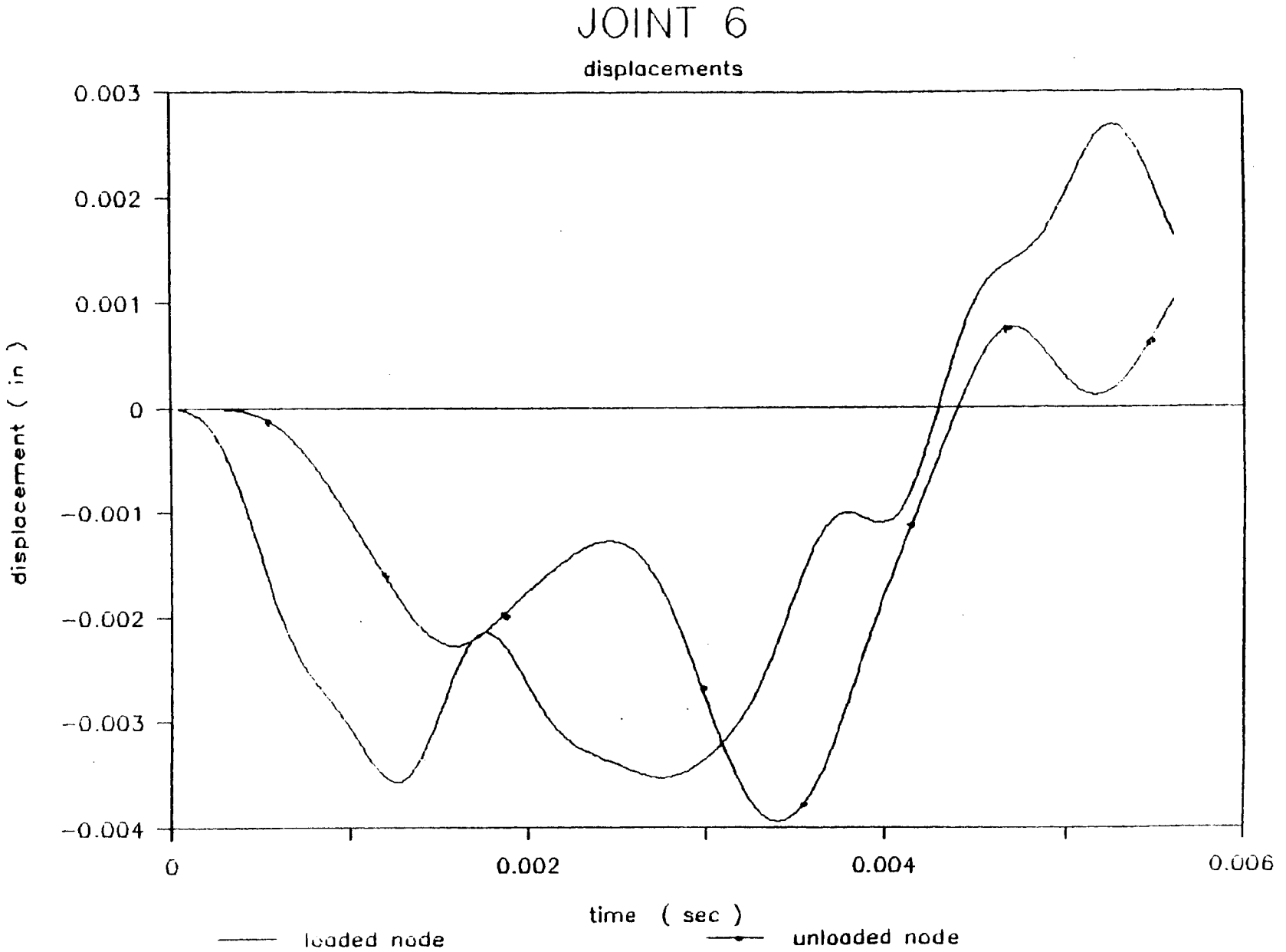
JOINT 6
displacements
0.003
0.002
0.001
0
-0.001
-0.002
-0.003
-0.004
displacement (in)
0
0.002
0.004
0.006
time (sec)
loaded node
unloaded node

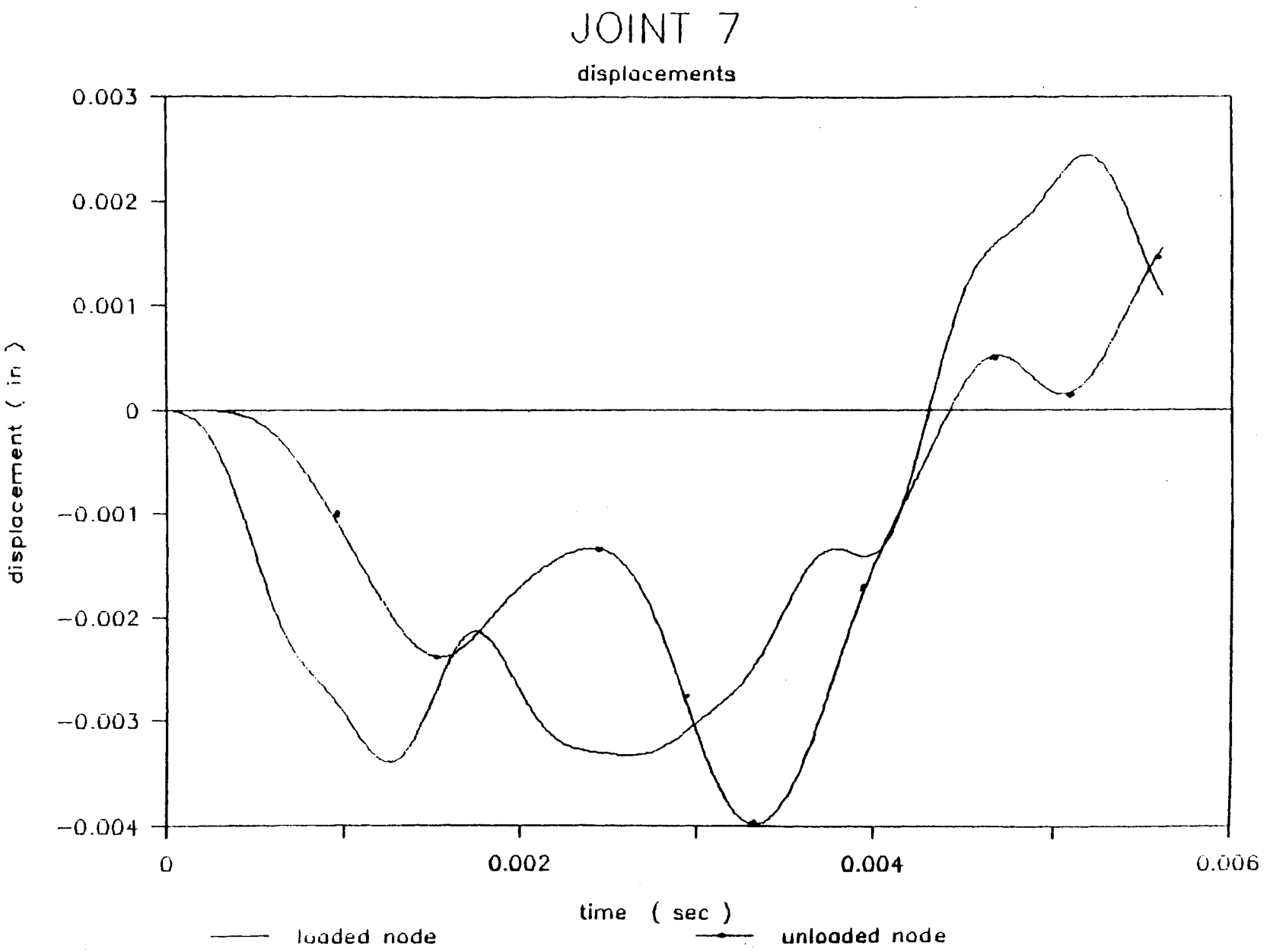
JOINT 7
displacements
0.003
0.002
0.001
0
−0.001
−0.002
−0.003
−0.004
displacement (in)
0
0.002
0.004
0.006
time (sec)
loaded node
unloaded node

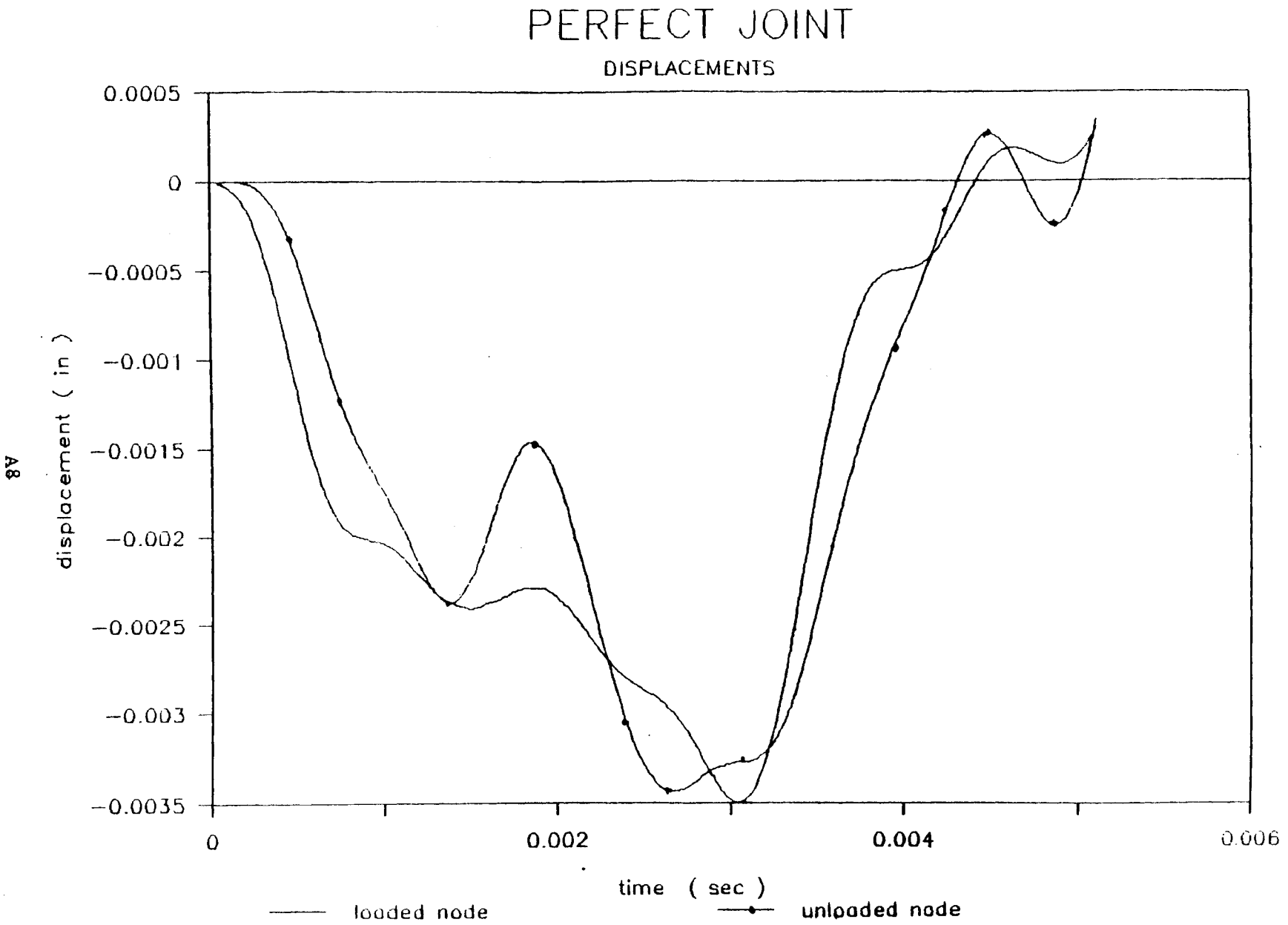
PERFECT JOINT
DISPLACEMENTS
0.0005
0
-0.0005
-0.001
-0.0015
-0.002
-0.0025
-0.003
-0.0035
displacement (in)
0
0.002
0.004
0.006
time (sec)
loaded node
unloaded node

A8

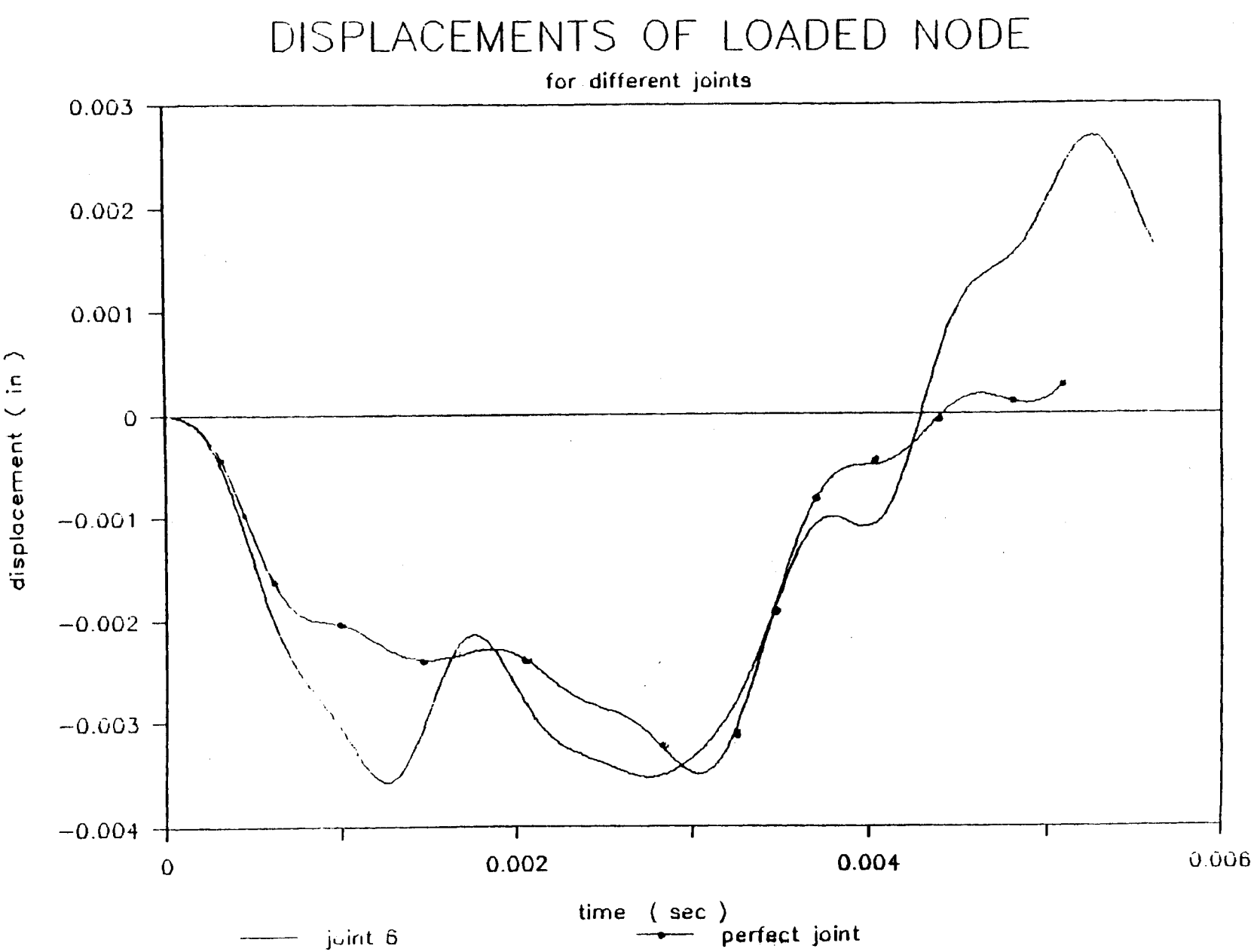
DISPLACEMENTS OF LOADED NODE
for different joints
0.003
0.002
0.001
0
-0.001
-0.002
-0.003
-0.004
displacement (in)
0
0.002
0.004
0.006
time (sec)
joint 6
perfect joint

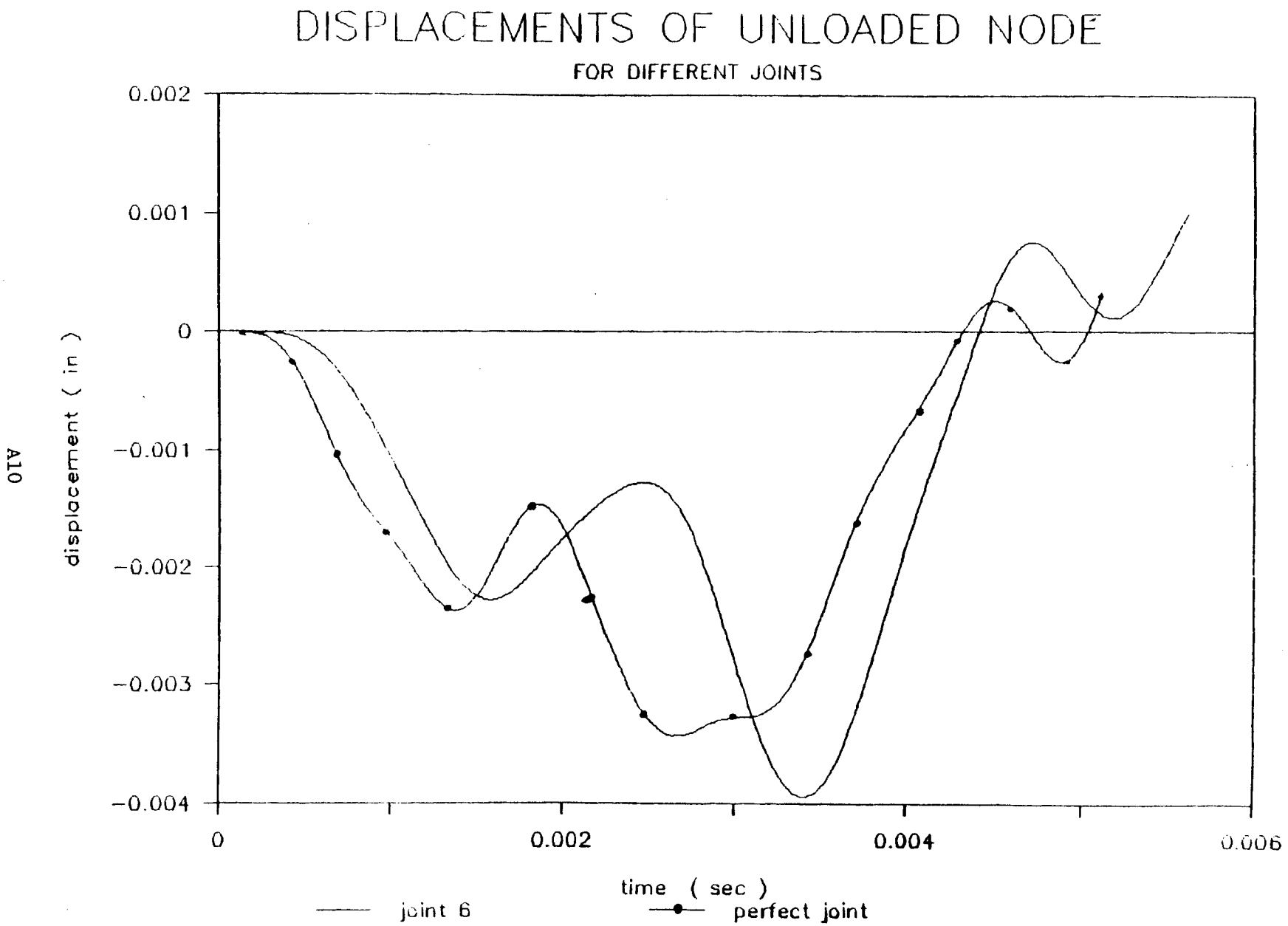
DISPLACEMENTS OF UNLOADED NODE
FOR DIFFERENT JOINTS
0.002
0.001
0
-0.001
-0.002
-0.003
-0.004
displacement (in)
0
0.002
0.004
0.006
time (sec)
joint 6
perfect joint

A10

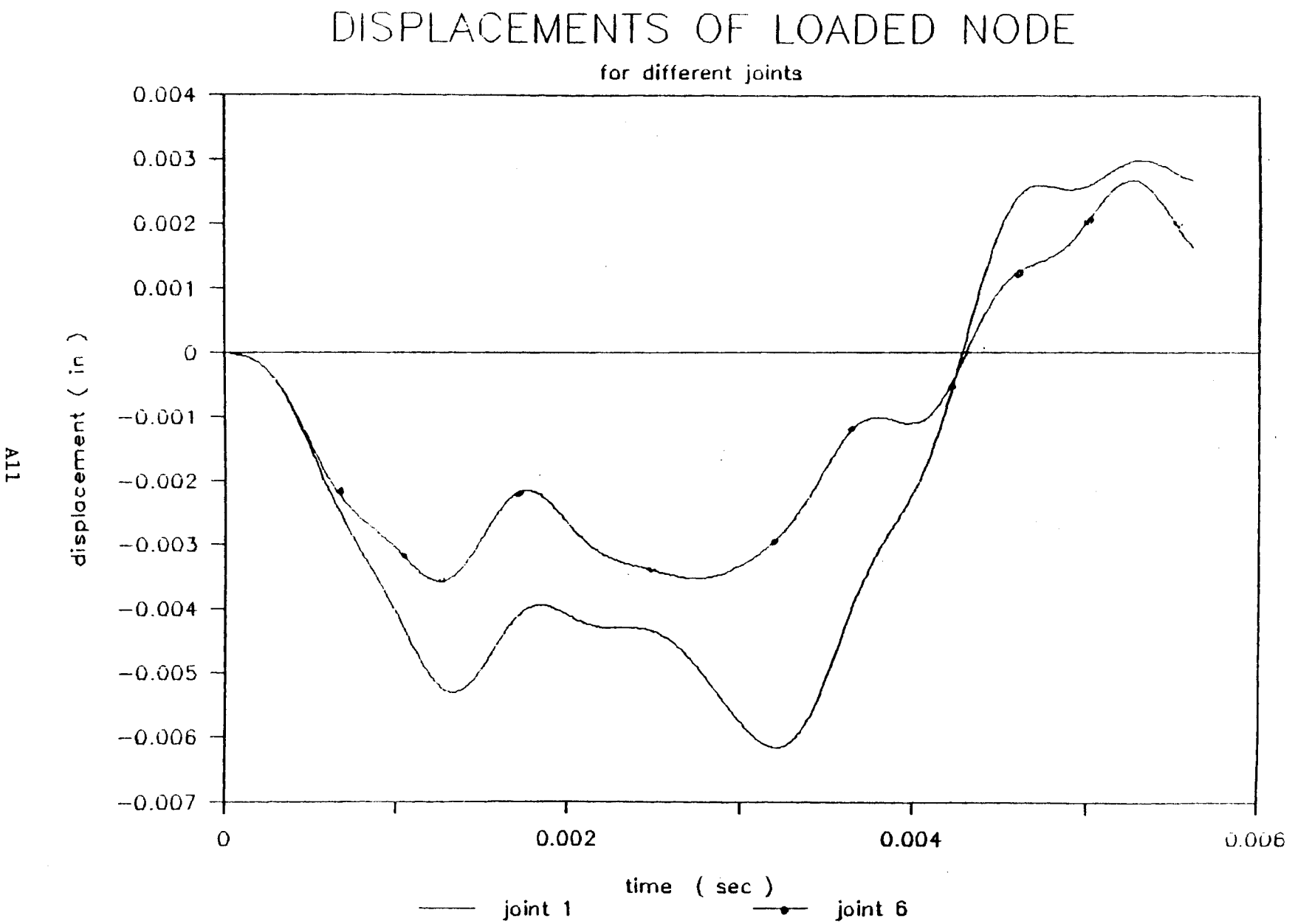
DISPLACEMENTS OF LOADED NODE
for different joints
0.004
0.003
0.002
0.001
0
-0.001
-0.002
-0.003
-0.004
-0.005
-0.006
-0.007
displacement (in)
0
0.002
0.004
0.006
time (sec)
joint 1
joint 6

A11

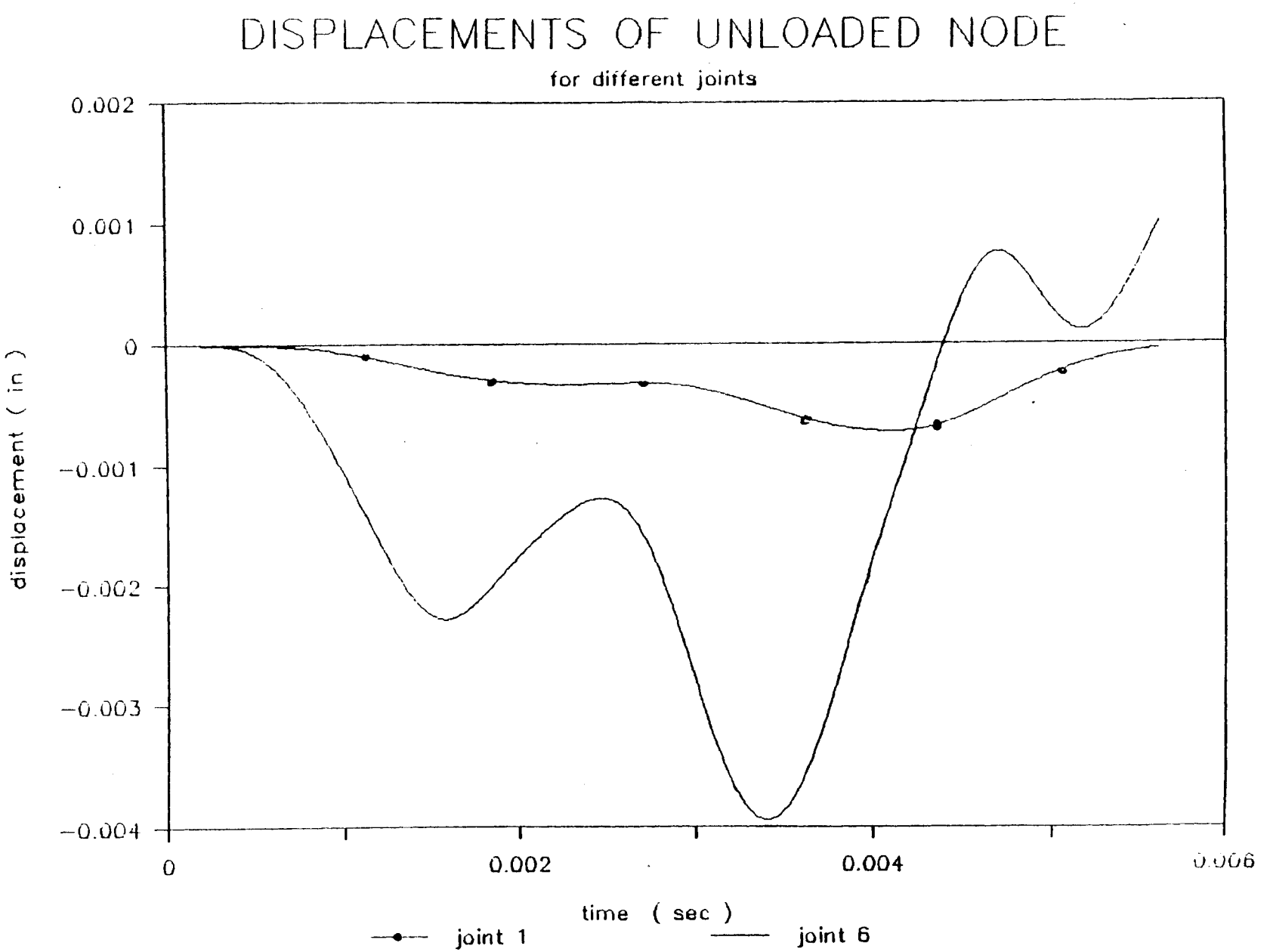
DISPLACEMENTS OF UNLOADED NODE
for different joints
0.002
0.001
0
−0.001
−0.002
−0.003
−0.004
displacement (in)
0
0.002
0.004
0.006
time (sec)
joint 1
joint 6

A12

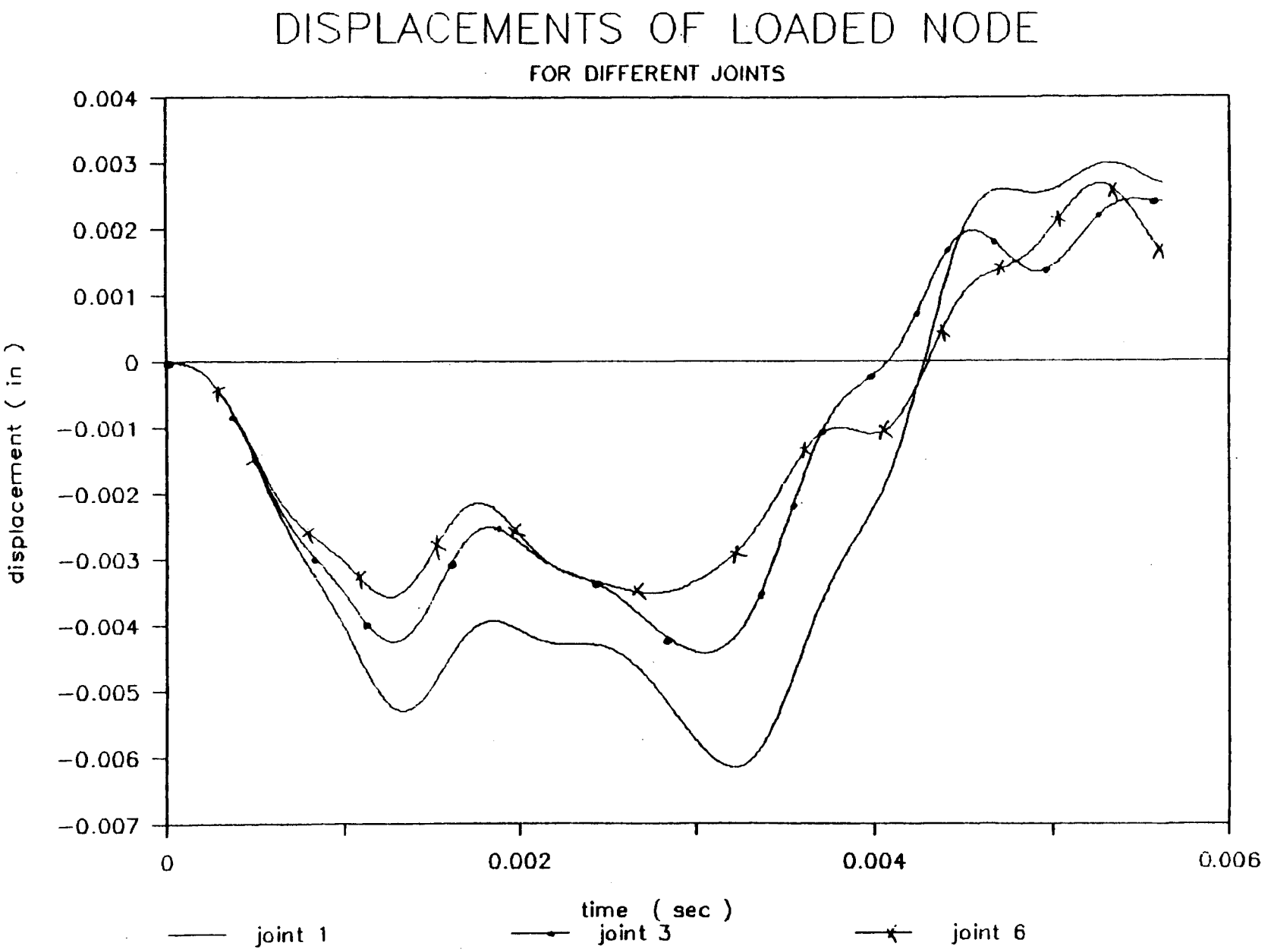
DISPLACEMENTS OF LOADED NODE
FOR DIFFERENT JOINTS
0.004
0.003
0.002
0.001
0
-0.001
-0.002
-0.003
-0.004
-0.005
-0.006
-0.007
displacement (in)
0
0.002
0.004
0.006
time (sec)
joint 1
joint 3
joint 6

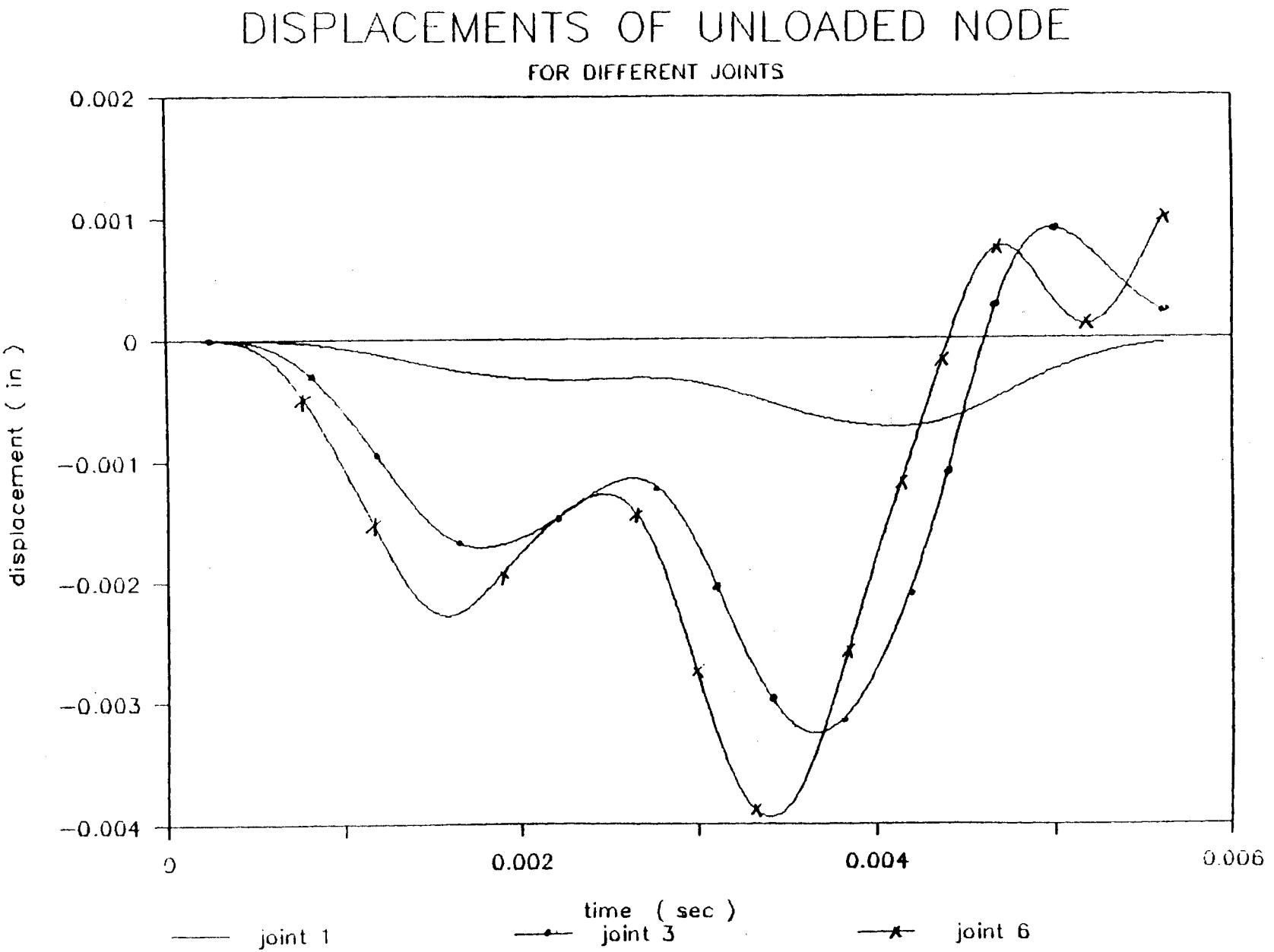
DISPLACEMENTS OF UNLOADED NODE
FOR DIFFERENT JOINTS
0.002
0.001
0
-0.001
-0.002
-0.003
-0.004
displacement (in)
0
0.002
0.004
0.006
time (sec)
joint 1
joint 3
joint 6

Appendix B: Time - Velocity Plots

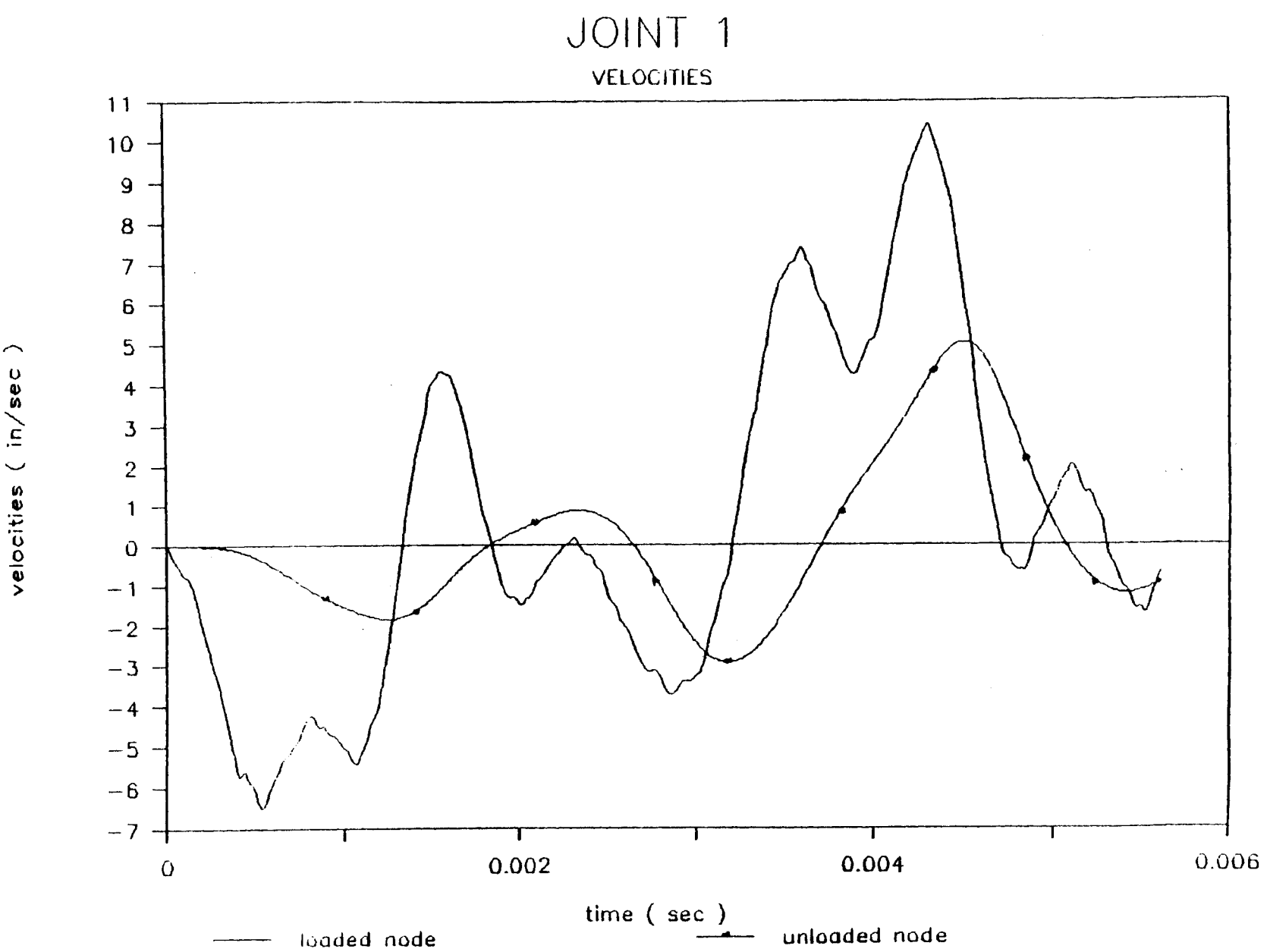
JOINT 1
VELOCITIES
11
10
9
8
7
6
5
4
3
2
1
0
-1
-2
-3
-4
-5
-6
-7
velocities (in/sec)
0
0.002
0.004
0.006
time (sec)
loaded node
unloaded node

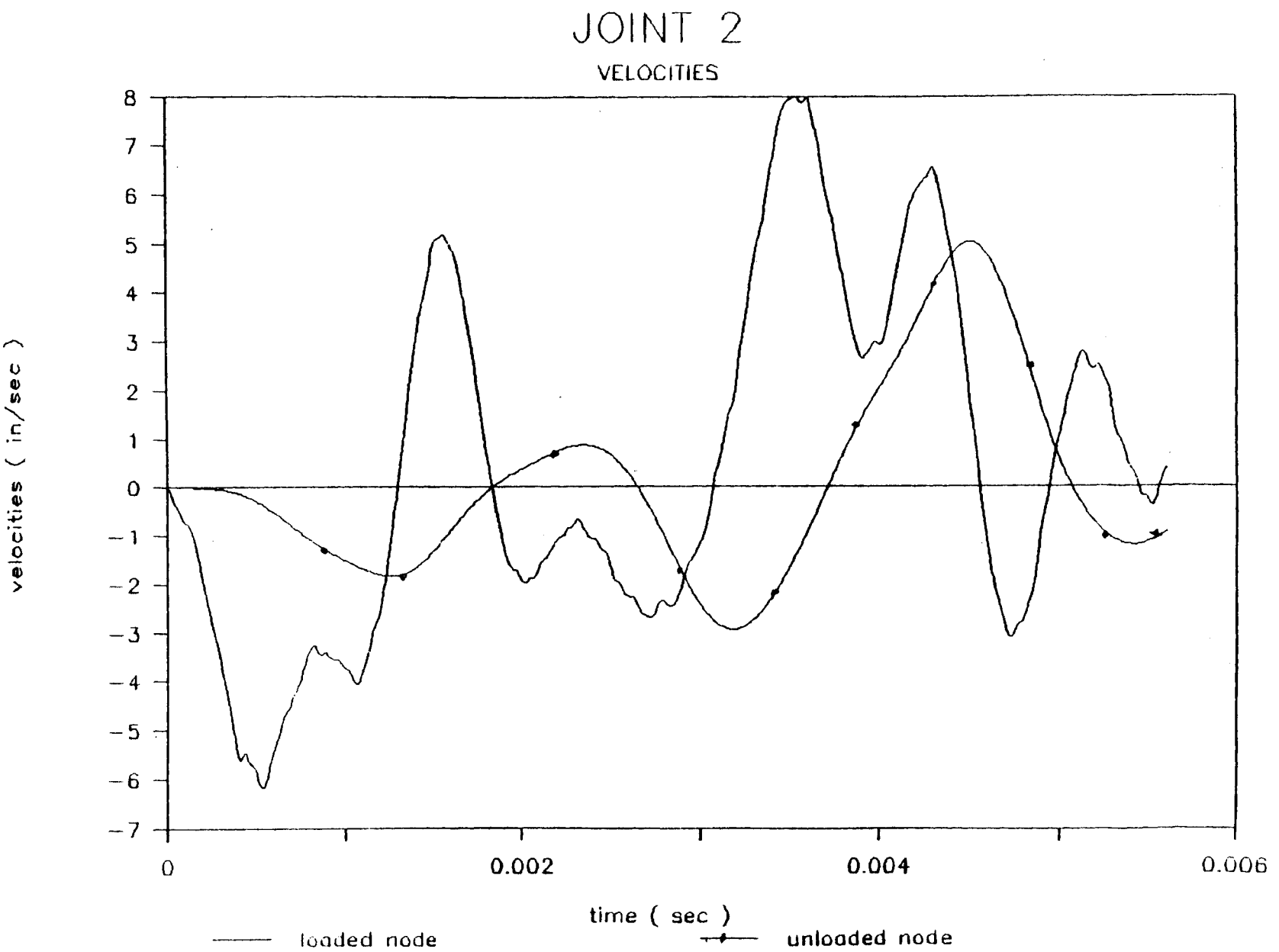
JOINT 2
VELOCITIES
velocities (in/sec)
8
7
6
5
4
3
2
1
0
−1
−2
−3
−4
−5
−6
−7
0
0.002
0.004
0.006
time (sec)
loaded node
unloaded node

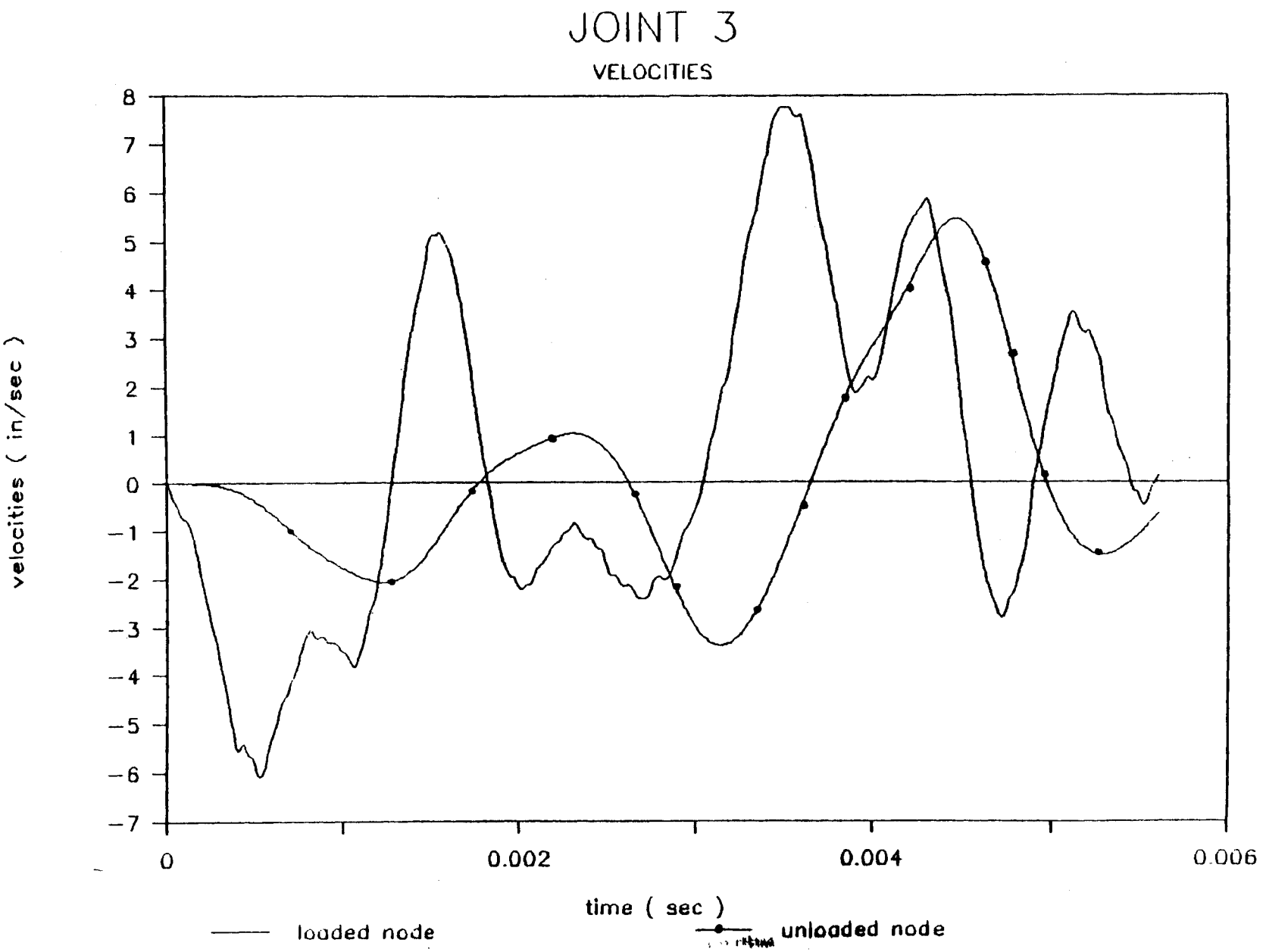
JOINT 3
VELOCITIES
velocities (in/sec)
8
7
6
5
4
3
2
1
0
−1
−2
−3
−4
−5
−6
−7
0
0.002
0.004
0.006
time (sec)
loaded node
unloaded node

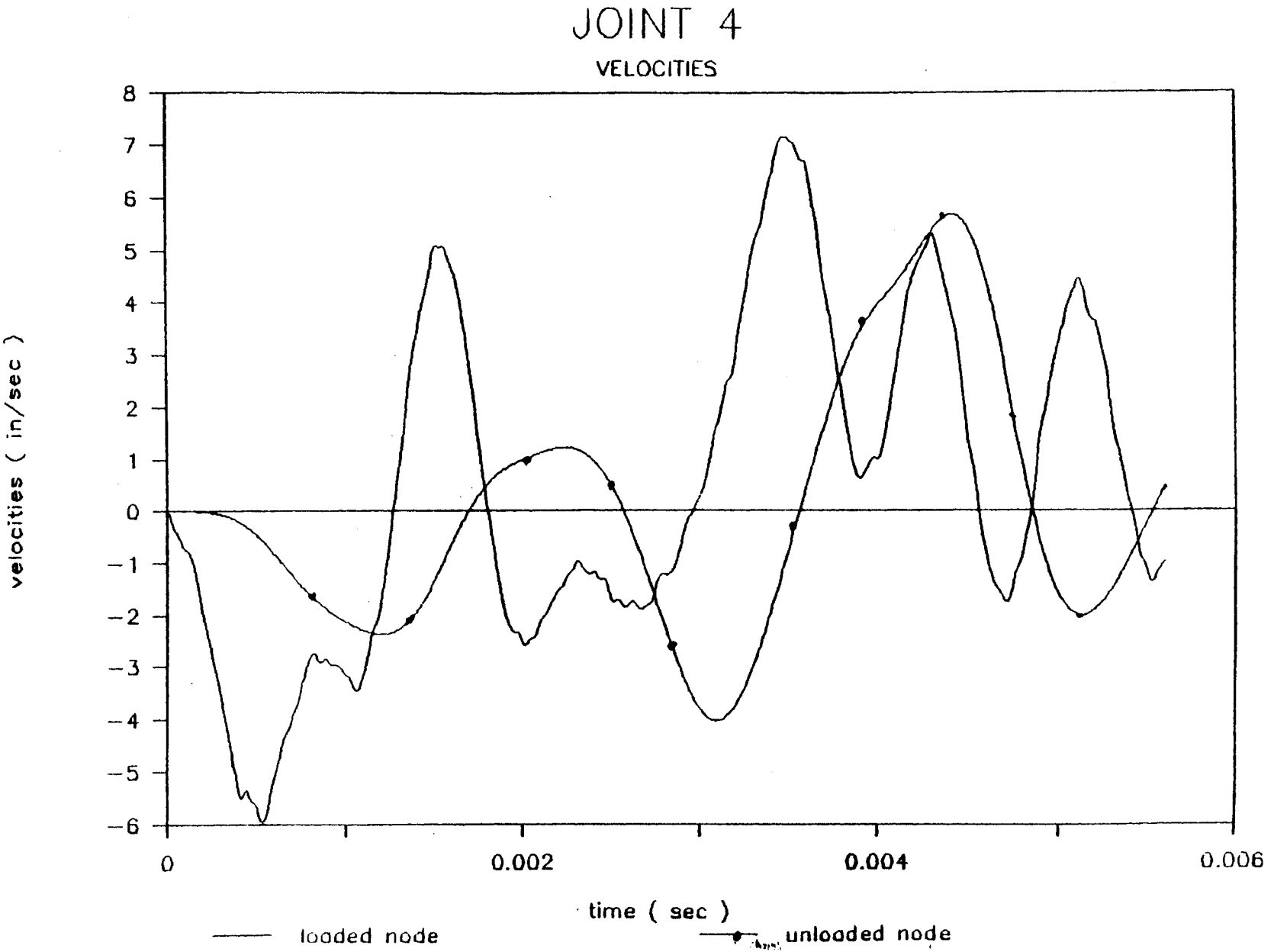
JOINT 4
VELOCITIES
velocities (in/sec)
8
7
6
5
4
3
2
1
0
−1
−2
−3
−4
−5
−6
0
0.002
0.004
0.006
time (sec)
loaded node
unloaded node

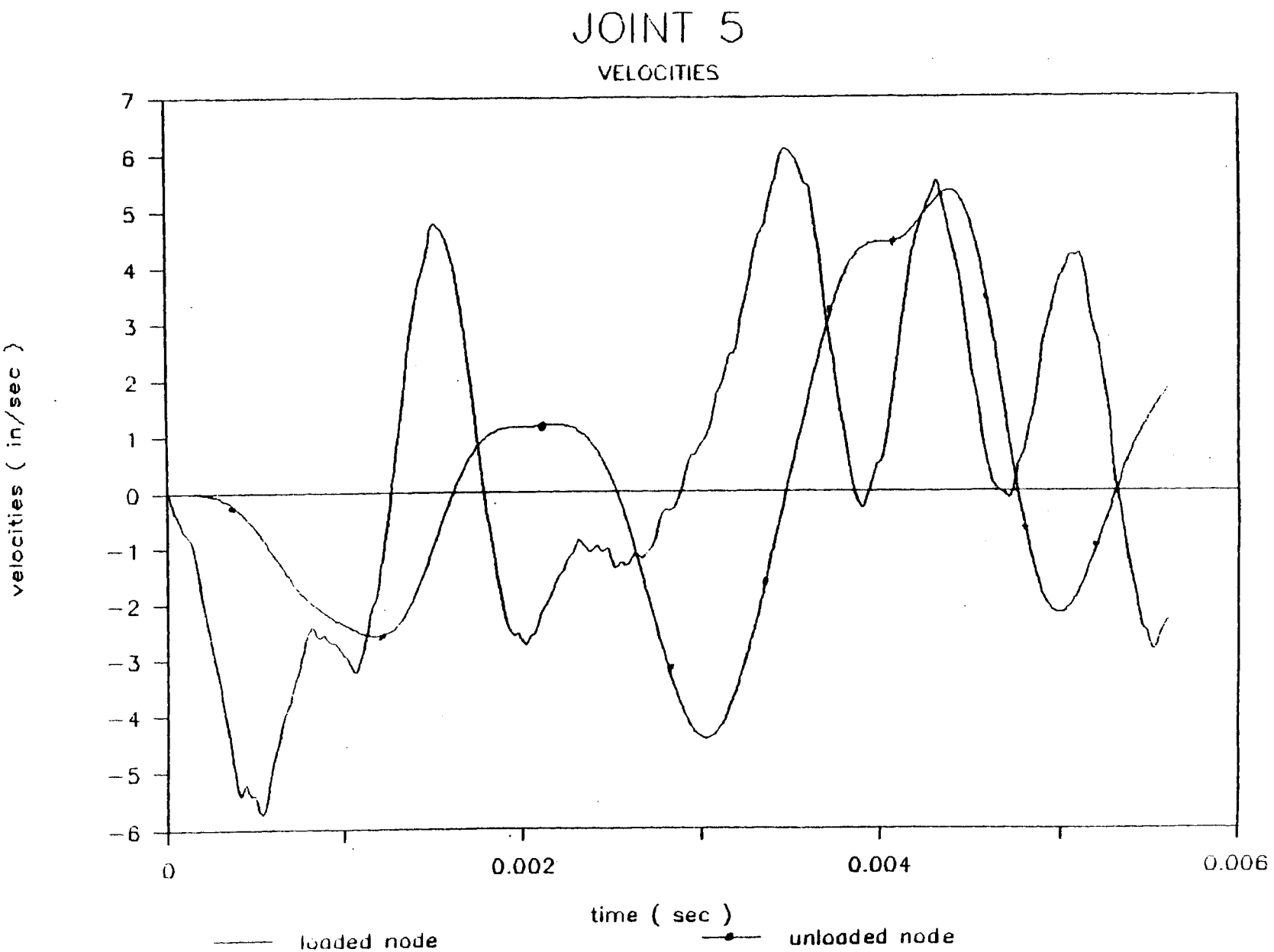
JOINT 5
VELOCITIES
velocities (in/sec)
7
6
5
4
3
2
1
0
−1
−2
−3
−4
−5
−6
0
0.002
0.004
0.006
time (sec)
loaded node
unloaded node

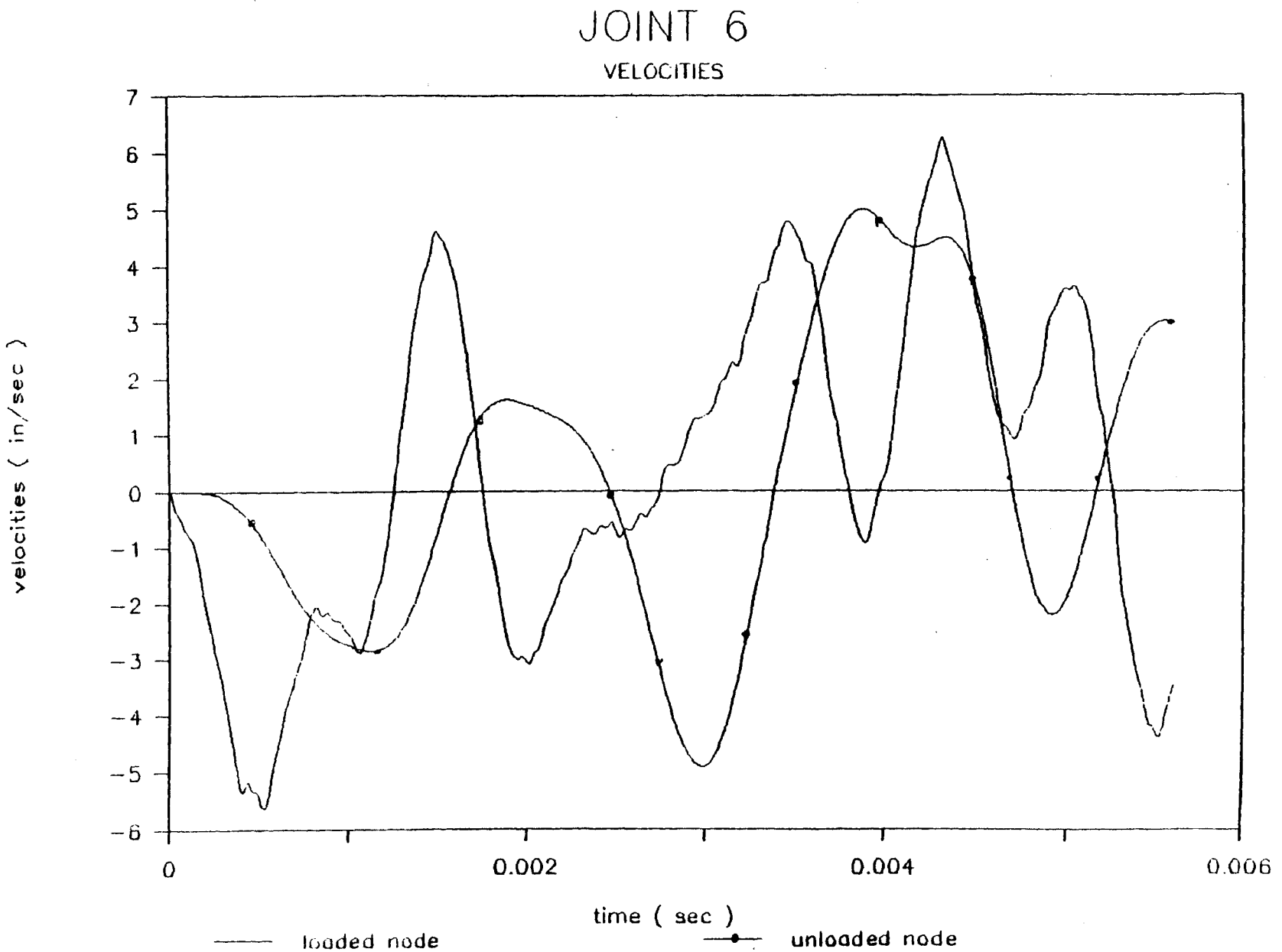
JOINT 6
VELOCITIES
velocities (in/sec)
7
6
5
4
3
2
1
0
-1
-2
-3
-4
-5
-6
0
0.002
0.004
0.006
time (sec)
loaded node
unloaded node

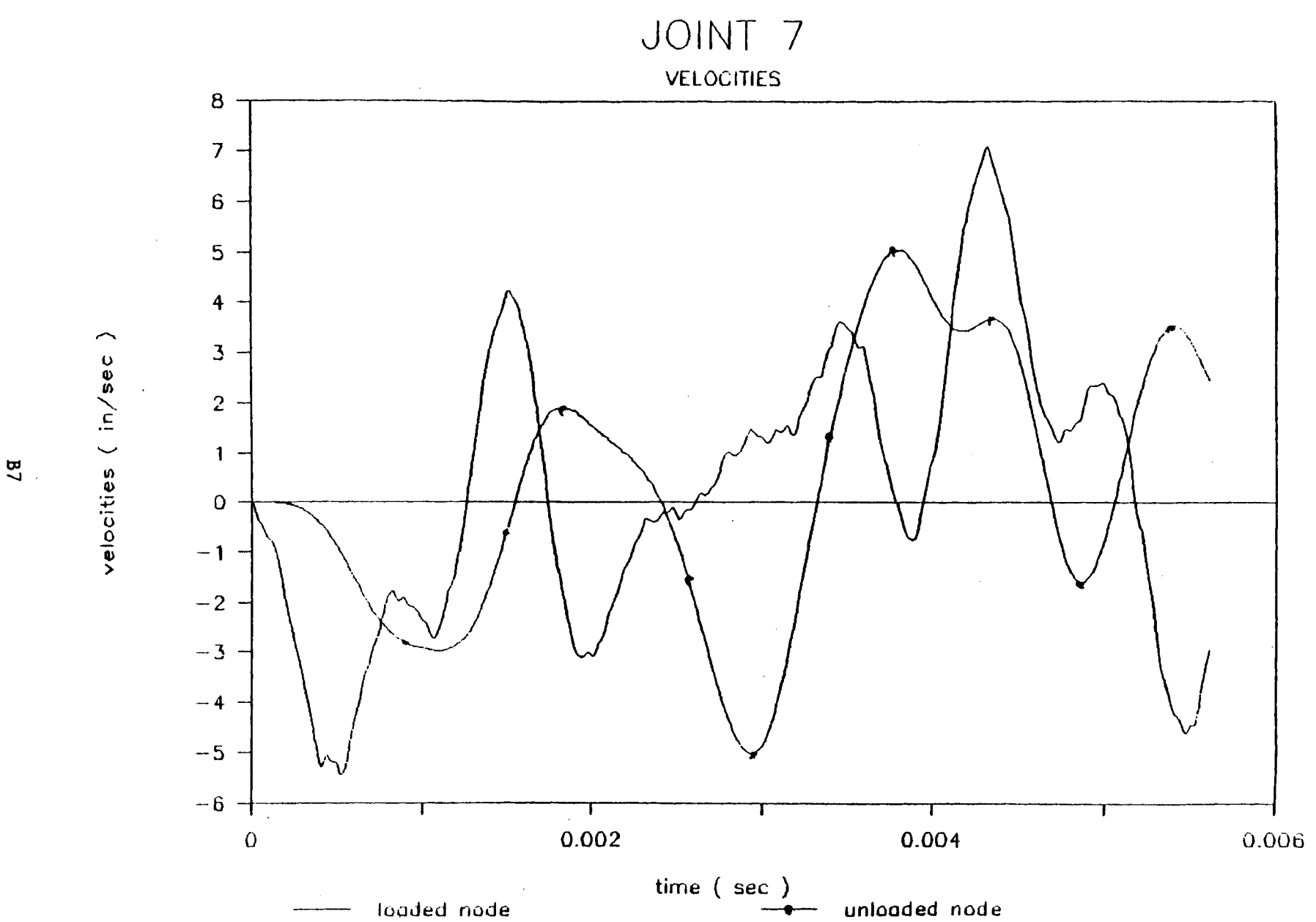
JOINT 7
VELOCITIES
8
7
6
5
4
3
2
1
0
-1
-2
-3
-4
-5
-6
velocities (in/sec)
0
0.002
0.004
0.006
time (sec)
loaded node
unloaded node

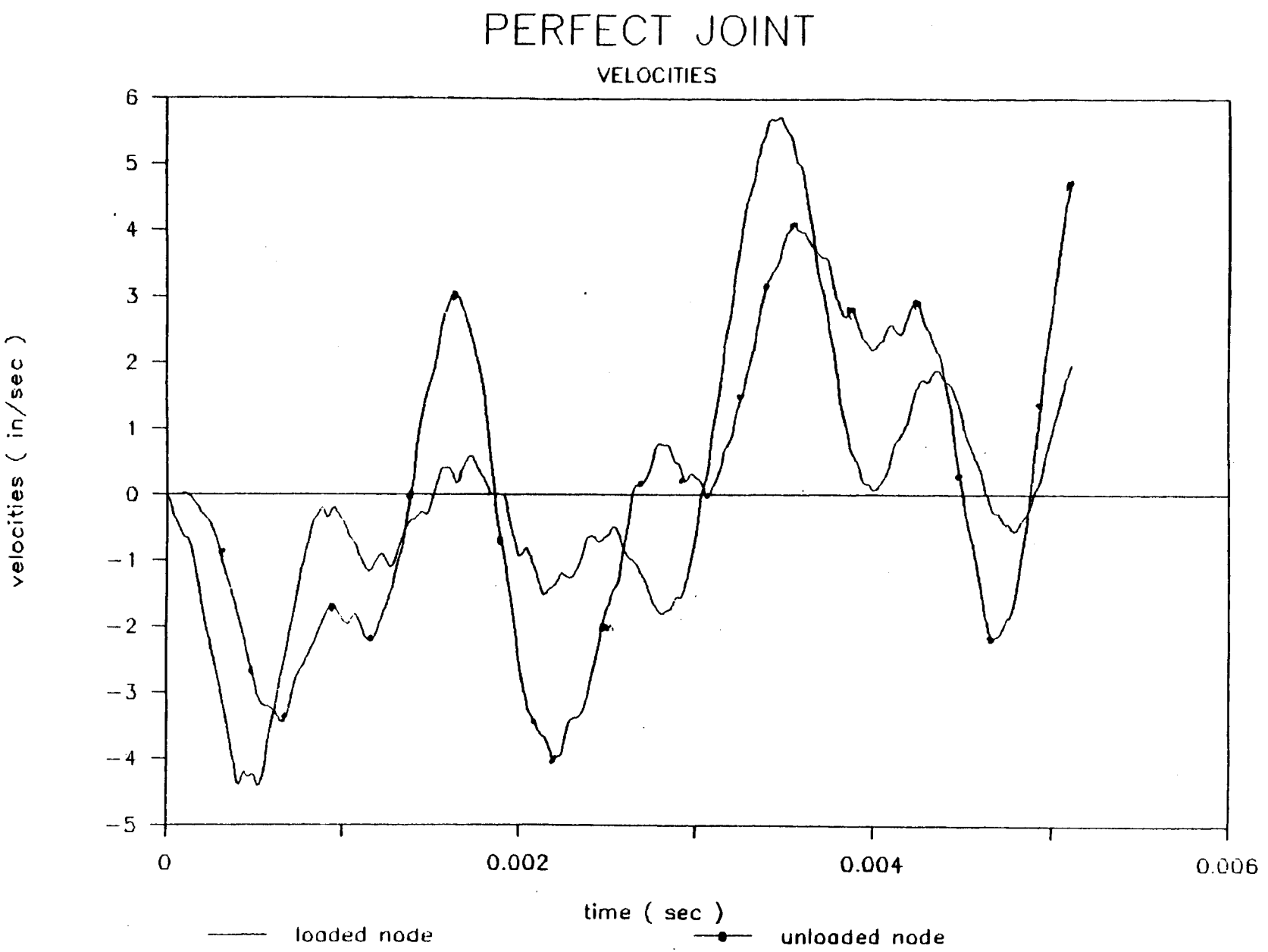
PERFECT JOINT
VELOCITIES
6
5
4
3
2
1
0
−1
−2
−3
−4
−5
velocities (in/sec)
0
0.002
0.004
0.006
time (sec)
loaded node
unloaded node

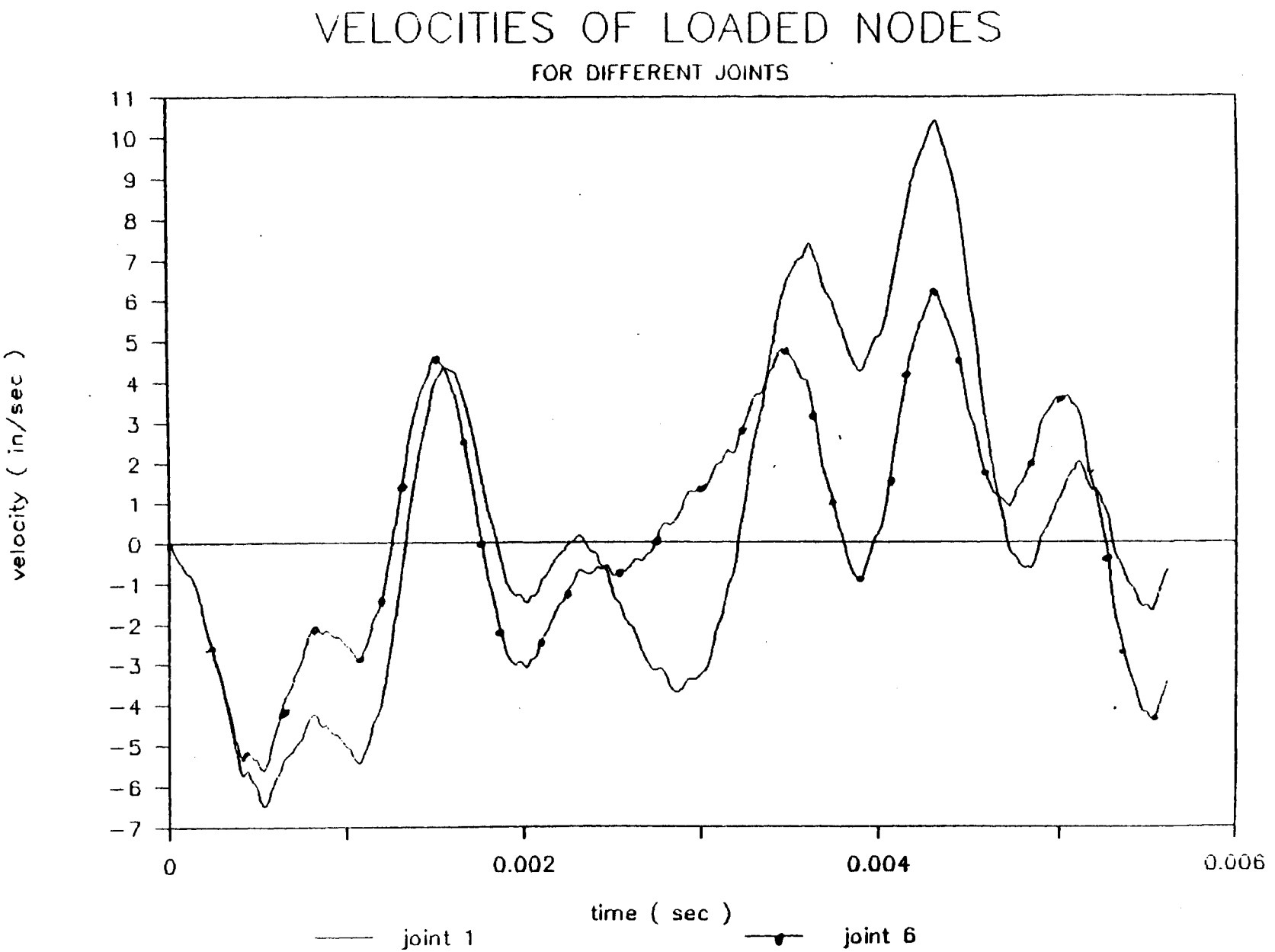
VELOCITIES OF LOADED NODES
FOR DIFFERENT JOINTS
velocity (in/sec)
11
10
9
8
7
6
5
4
3
2
1
0
-1
-2
-3
-4
-5
-6
-7
0
0.002
0.004
0.006
time (sec)
joint 1
joint 6

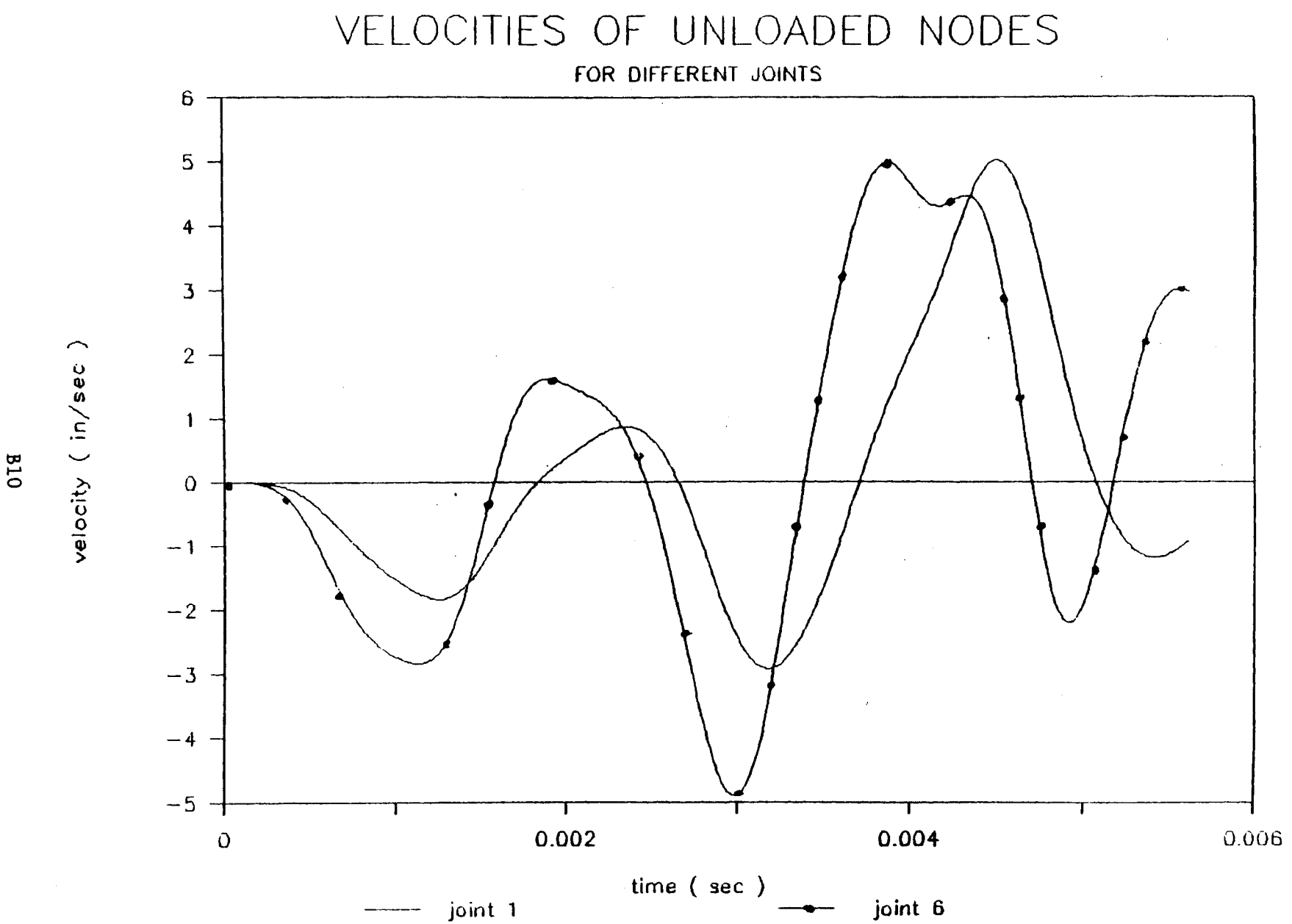
VELOCITIES OF UNLOADED NODES
FOR DIFFERENT JOINTS
velocity (in/sec)
6
5
4
3
2
1
0
-1
-2
-3
-4
-5
0
0.002
0.004
0.006
time (sec)
joint 1
joint 6

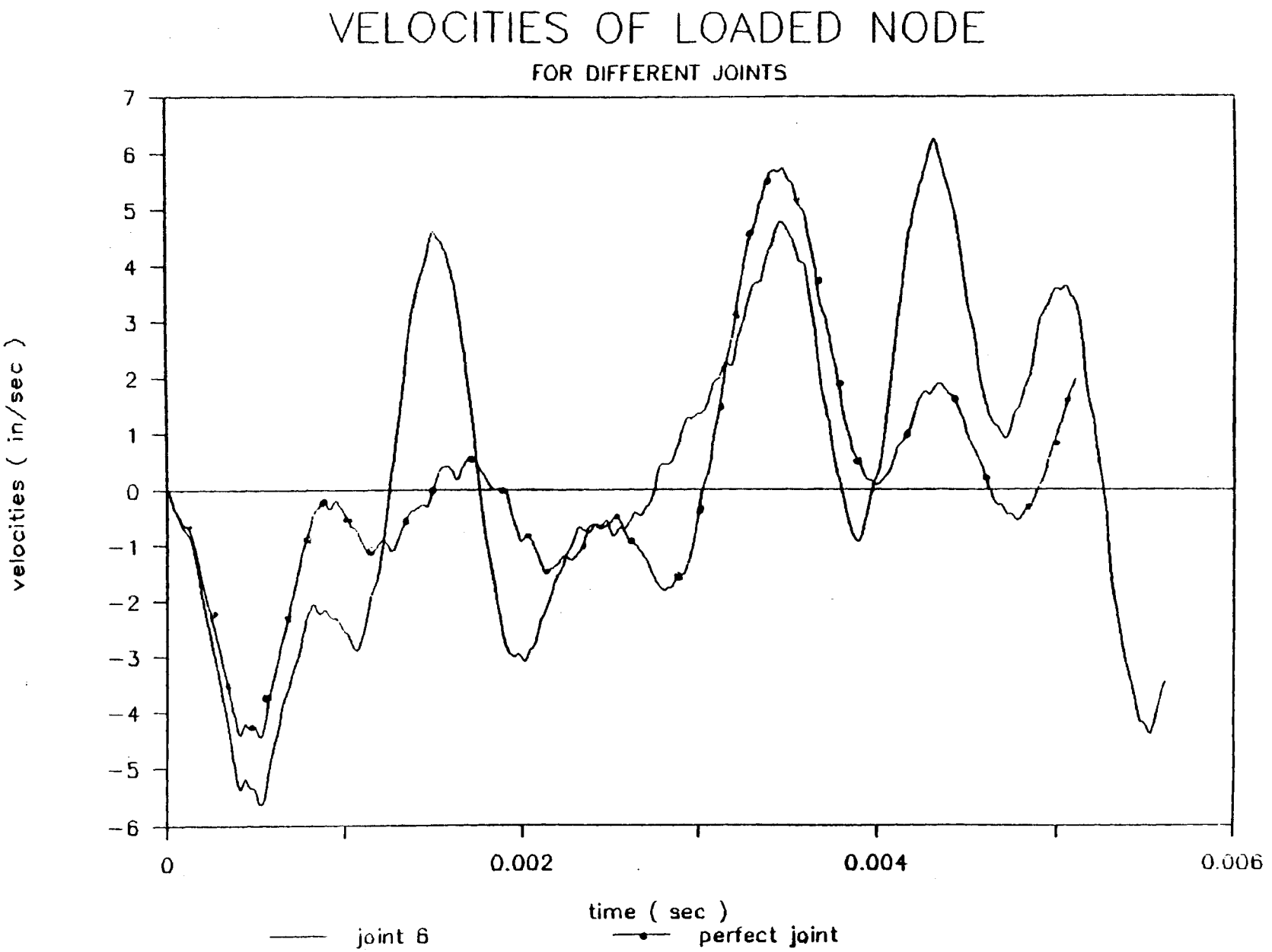
VELOCITIES OF LOADED NODE
FOR DIFFERENT JOINTS
velocities (in/sec)
7
6
5
4
3
2
1
0
-1
-2
-3
-4
-5
-6
0
0.002
0.004
0.006
time (sec)
joint 6
perfect joint

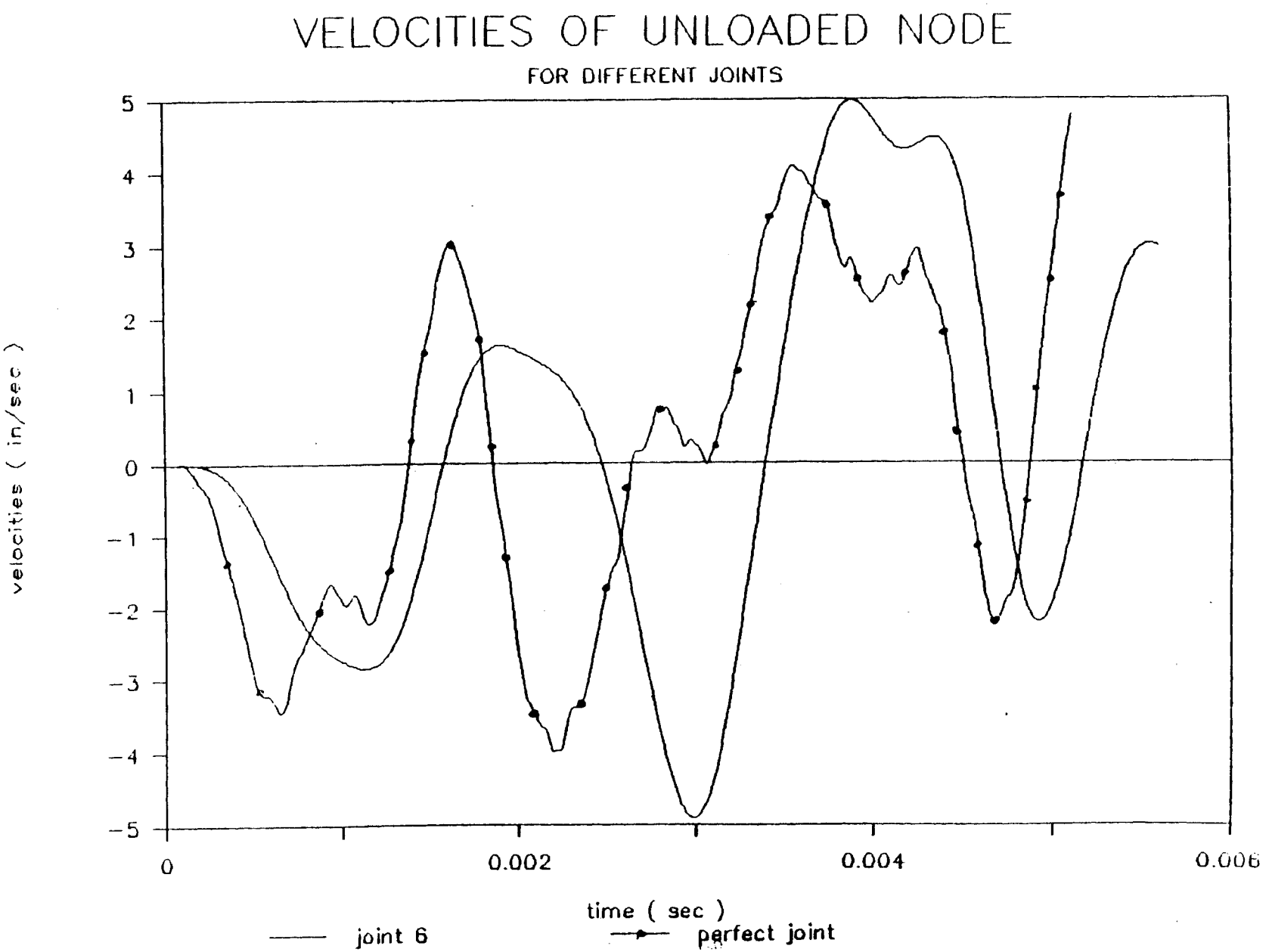
VELOCITIES OF UNLOADED NODE
FOR DIFFERENT JOINTS
velocities (in/sec)
5
4
3
2
1
0
-1
-2
-3
-4
-5
0
0.002
0.004
0.006
time (sec)
joint 6
perfect joint

Appendix C: Time - Acceleration Plots

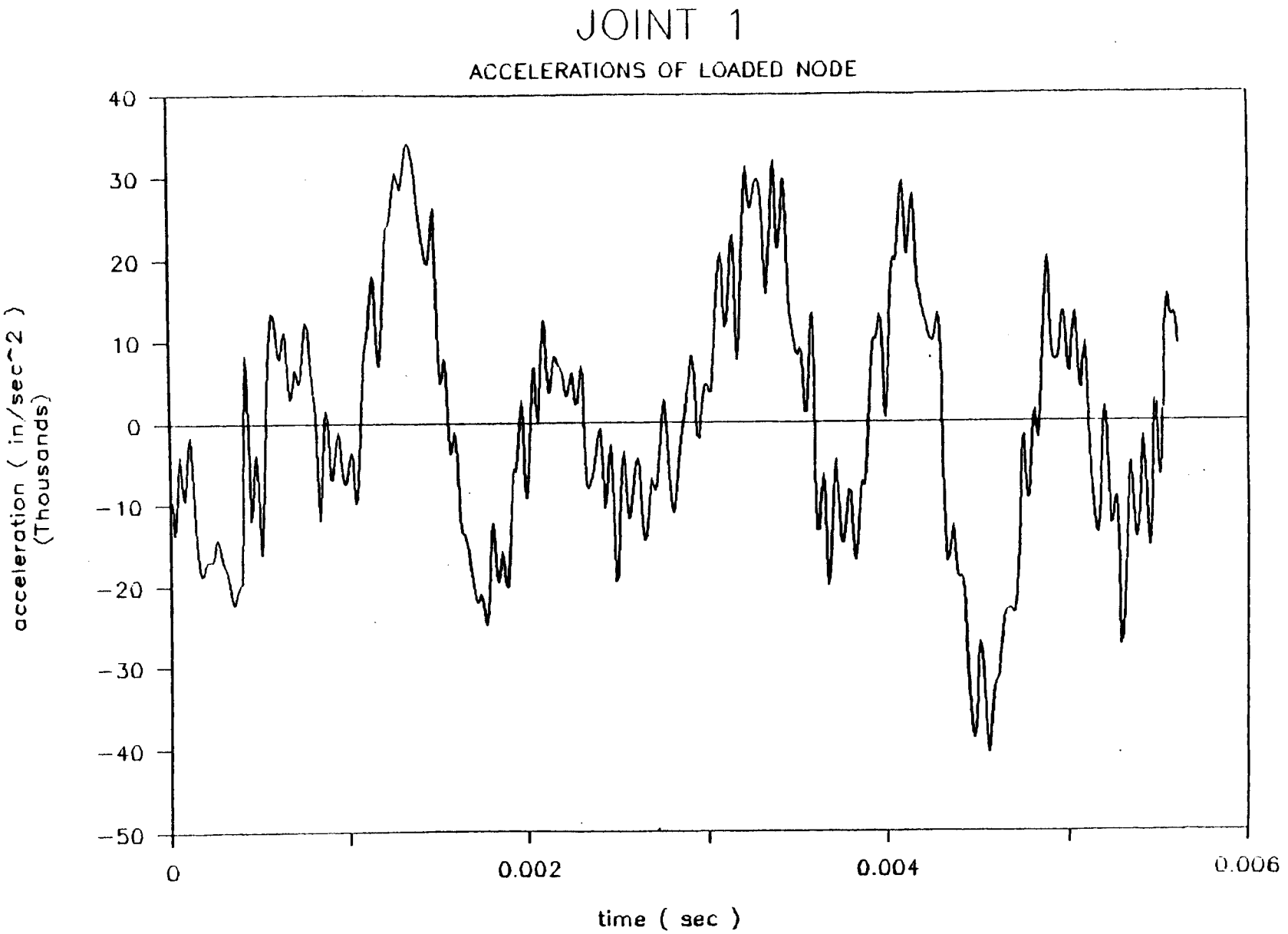
JOINT 1
ACCELERATIONS OF LOADED NODE
acceleration (in/sec^2)
(Thousands)
40
30
20
10
0
-10
-20
-30
-40
-50
0
0.002
0.004
0.006
time (sec)

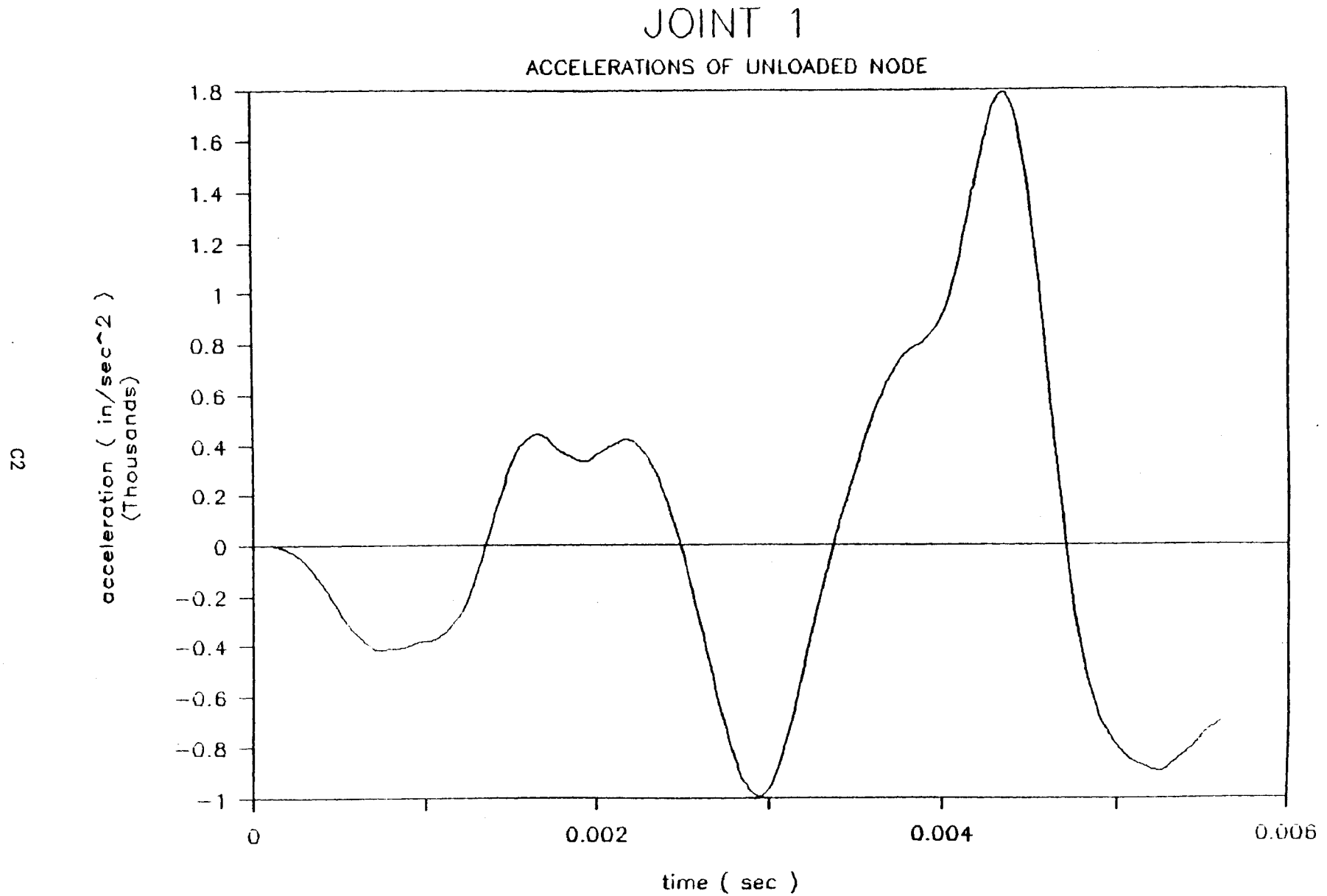
JOINT 1
ACCELERATIONS OF UNLOADED NODE
acceleration (in/sec^2)
(Thousands)
1.8
1.6
1.4
1.2
1
0.8
0.6
0.4
0.2
0
-0.2
-0.4
-0.6
-0.8
-1
0
0.002
0.004
0.006
time (sec)

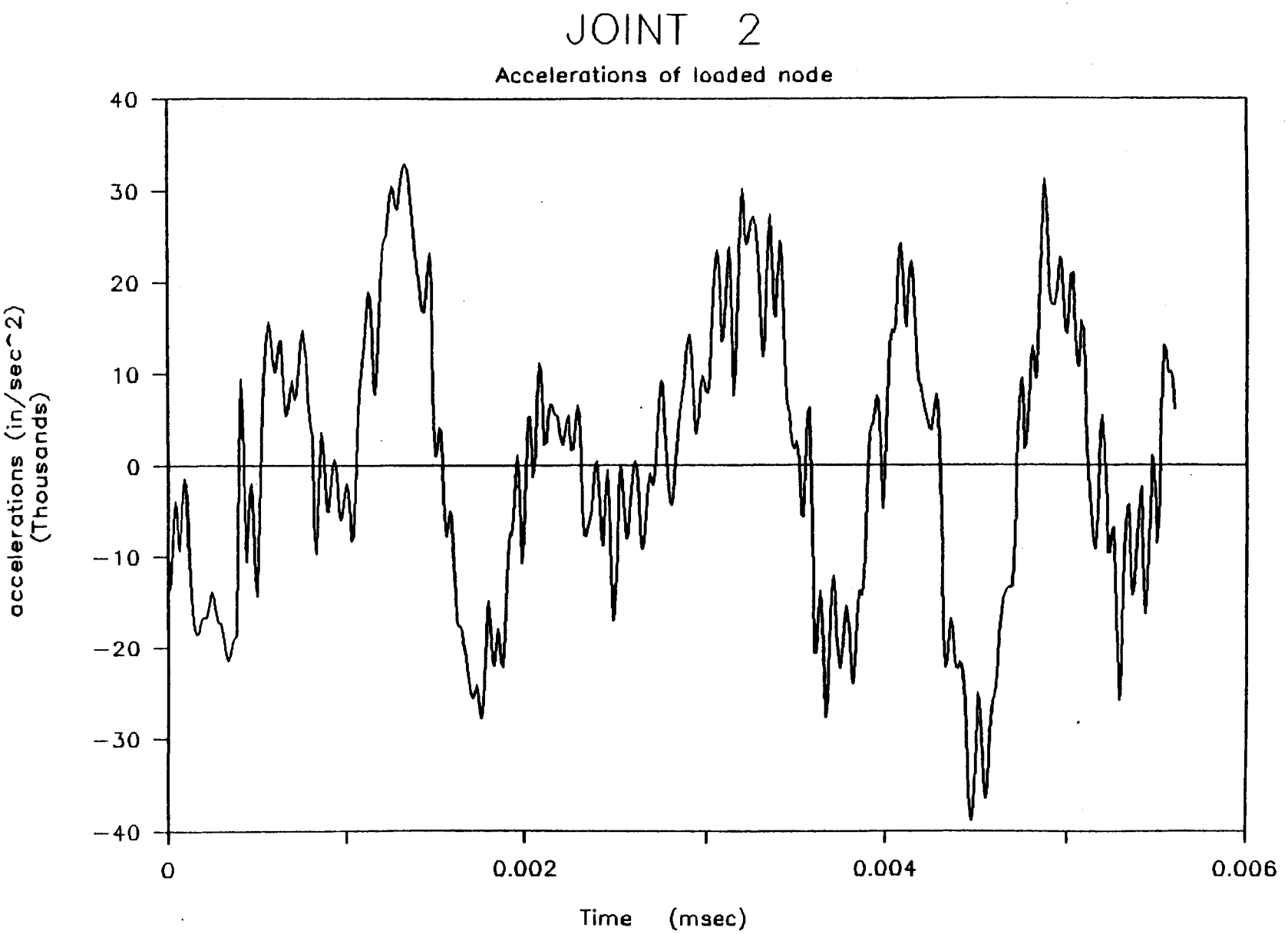
JOINT 2
Accelerations of loaded node
40
30
20
10
0
−10
−20
−30
−40
accelerations (in/sec^2)
(Thousands)
0
0.002
0.004
0.006
Time (msec)

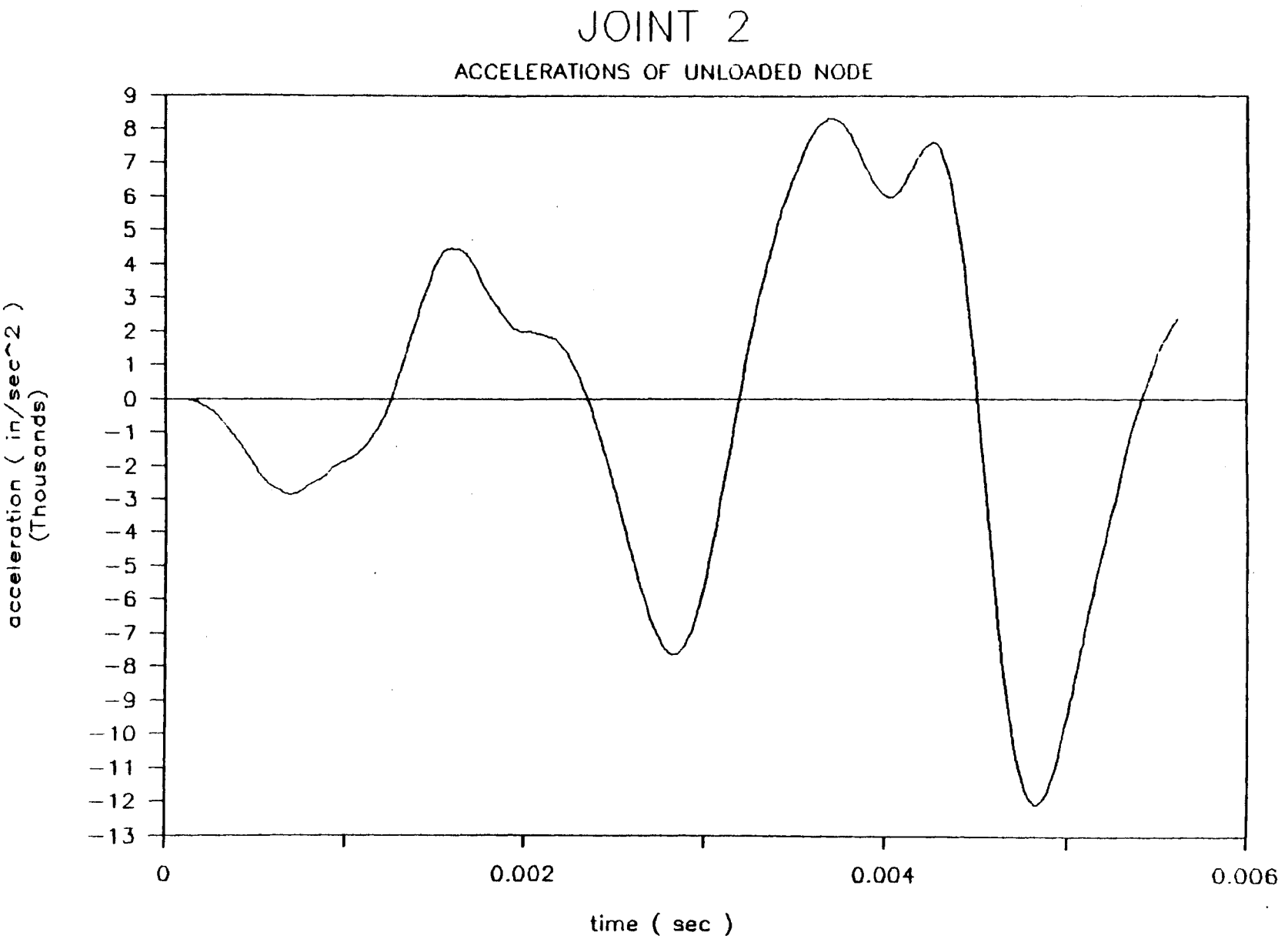
JOINT 2
ACCELERATIONS OF UNLOADED NODE
acceleration (in/sec^2)
(Thousands)
9
8
7
6
5
4
3
2
1
0
-1
-2
-3
-4
-5
-6
-7
-8
-9
-10
-11
-12
-13
0
0.002
0.004
0.006
time (sec)

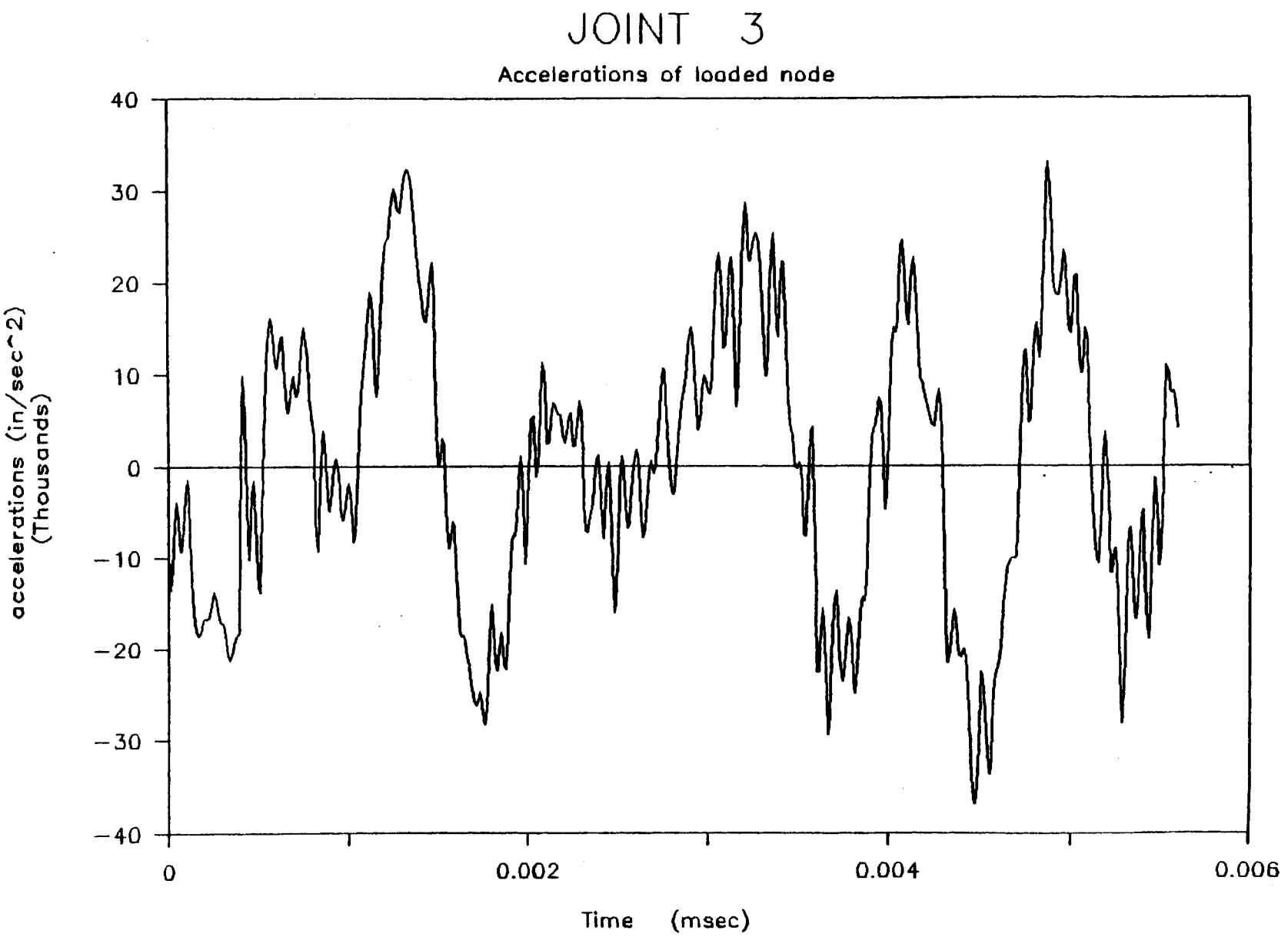
JOINT 3
Accelerations of loaded node
accelerations (in/sec^2)
(Thousands)
40
30
20
10
0
-10
-20
-30
-40
0
0.002
0.004
0.006
Time (msec)

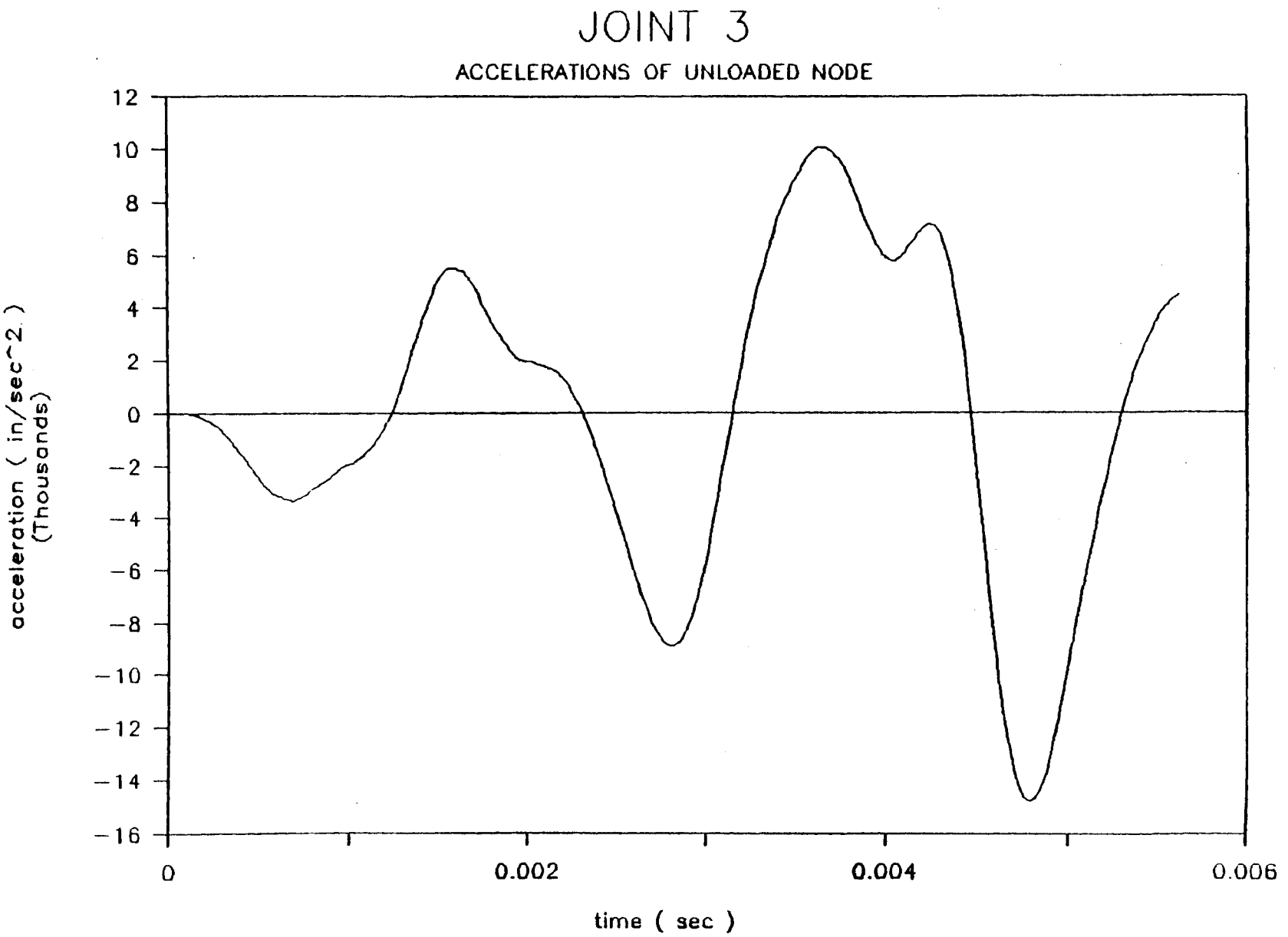
JOINT 3
ACCELERATIONS OF UNLOADED NODE
acceleration (in/sec^2)
(Thousands)
12
10
8
6
4
2
0
-2
-4
-6
-8
-10
-12
-14
-16
0
0.002
0.004
0.006
time (sec)

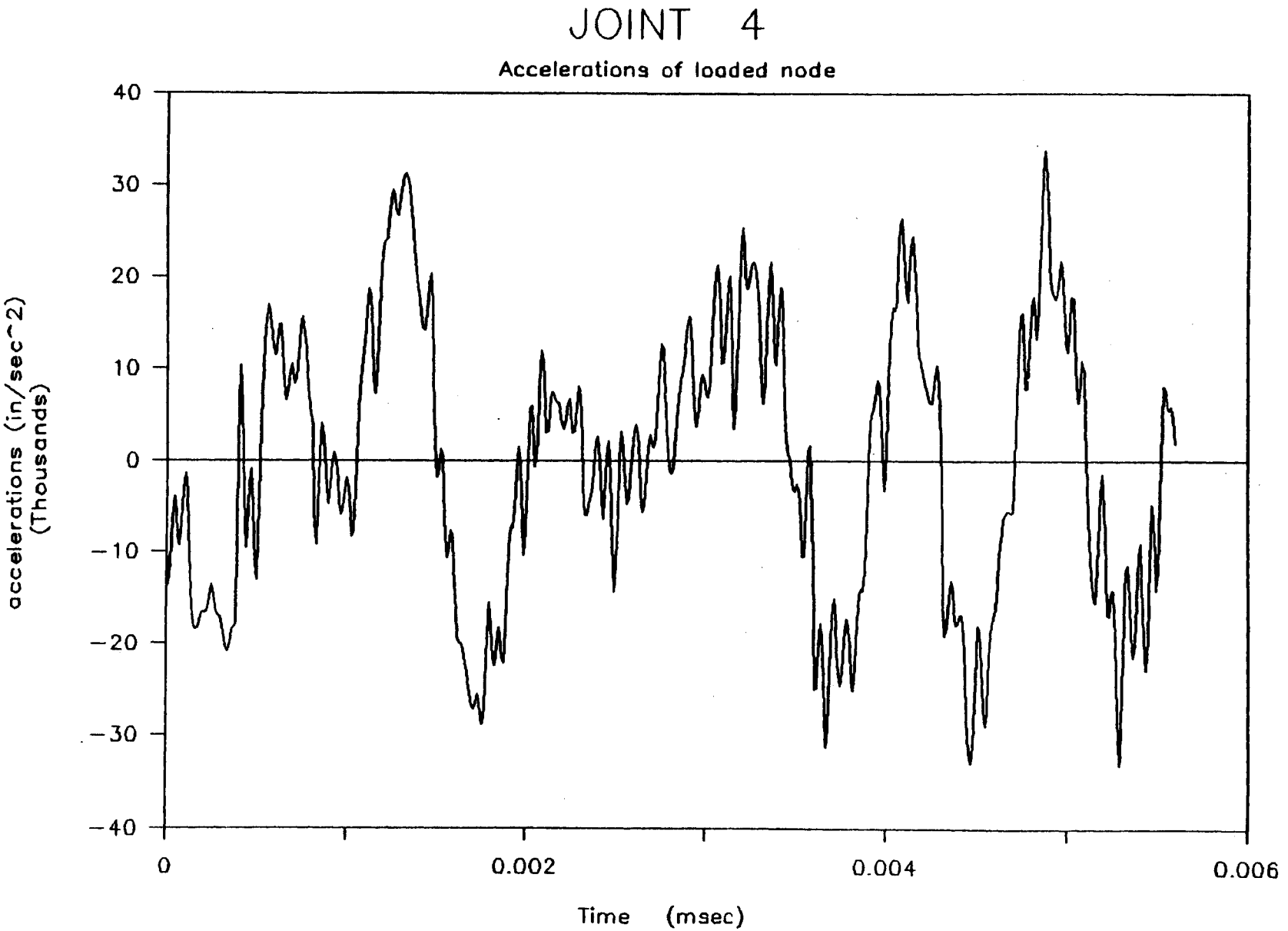
JOINT 4
Accelerations of loaded node
40
30
20
10
0
-10
-20
-30
-40
accelerations (in/sec^2)
(Thousands)
0
0.002
0.004
0.006
Time (msec)

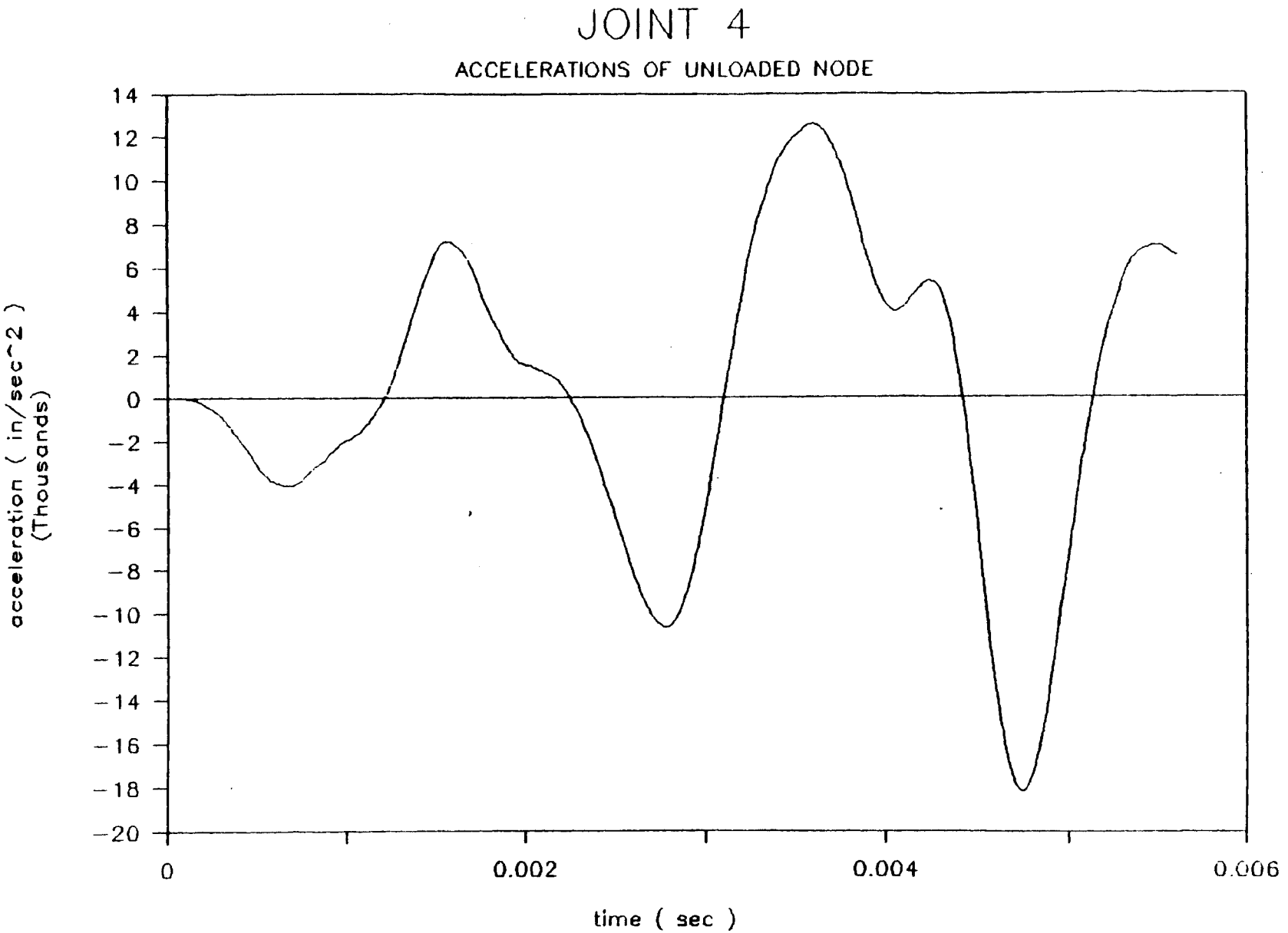
JOINT 4
ACCELERATIONS OF UNLOADED NODE
acceleration (in/sec^2)
(Thousands)
14
12
10
8
6
4
2
0
-2
-4
-6
-8
-10
-12
-14
-16
-18
-20
0
0.002
0.004
0.006
time (sec)

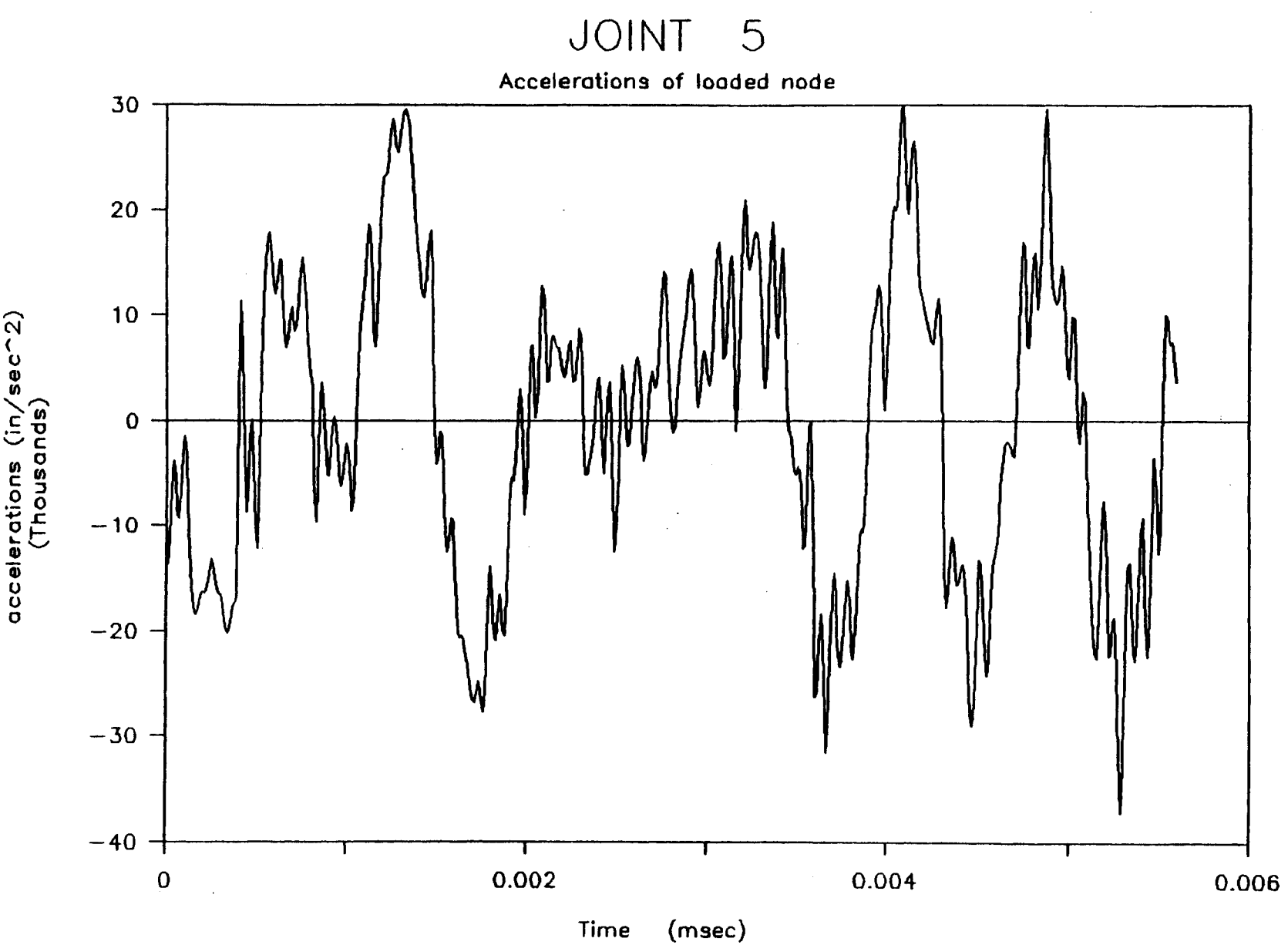
JOINT 5
Accelerations of loaded node
accelerations (in/sec^2)
(Thousands)
30
20
10
0
-10
-20
-30
-40
0
0.002
0.004
0.006
Time (msec)

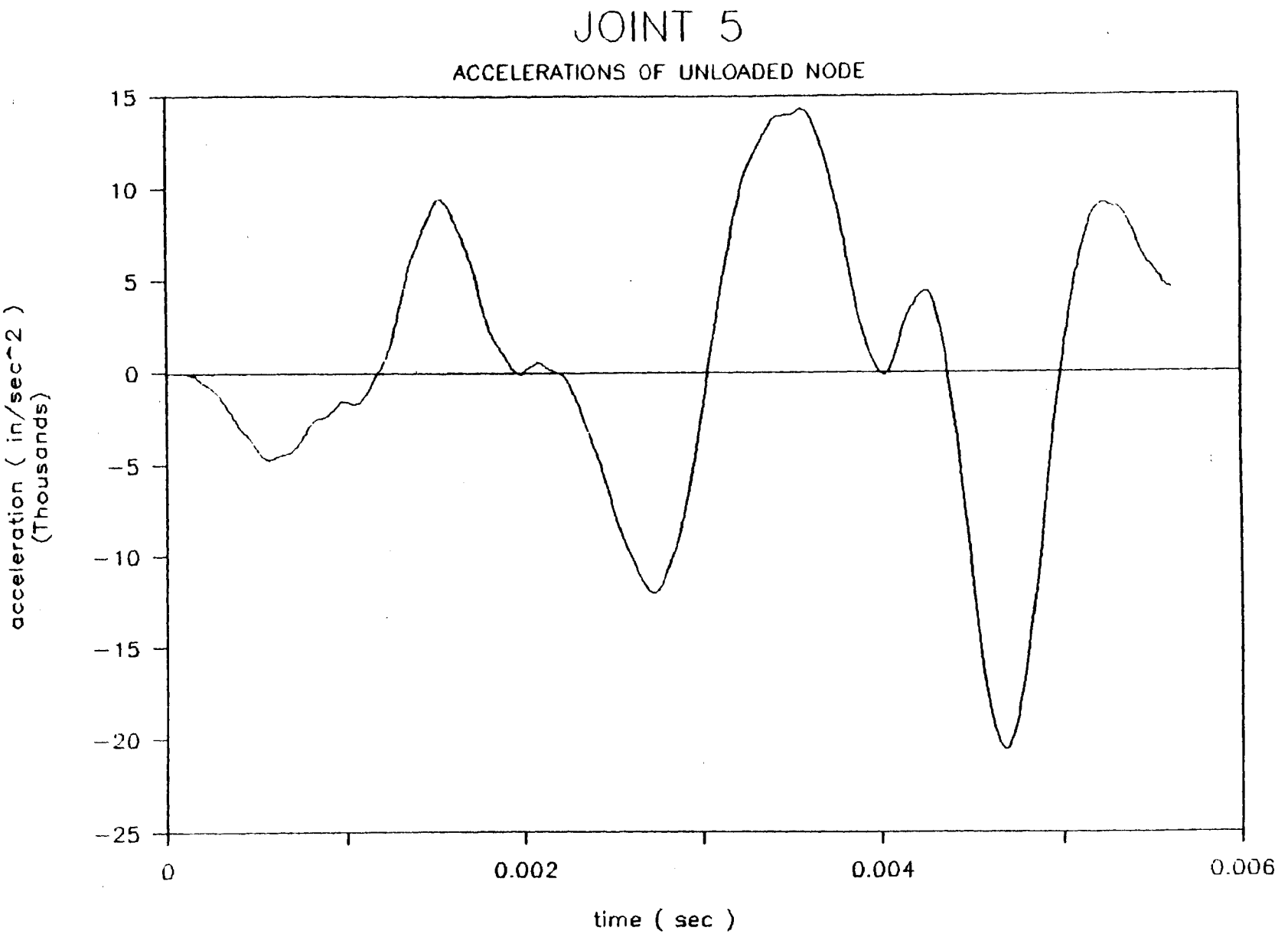
JOINT 5
ACCELERATIONS OF UNLOADED NODE
acceleration (in/sec^2)
(Thousands)
15
10
5
0
-5
-10
-15
-20
-25
0
0.002
0.004
0.006
time (sec)

C10

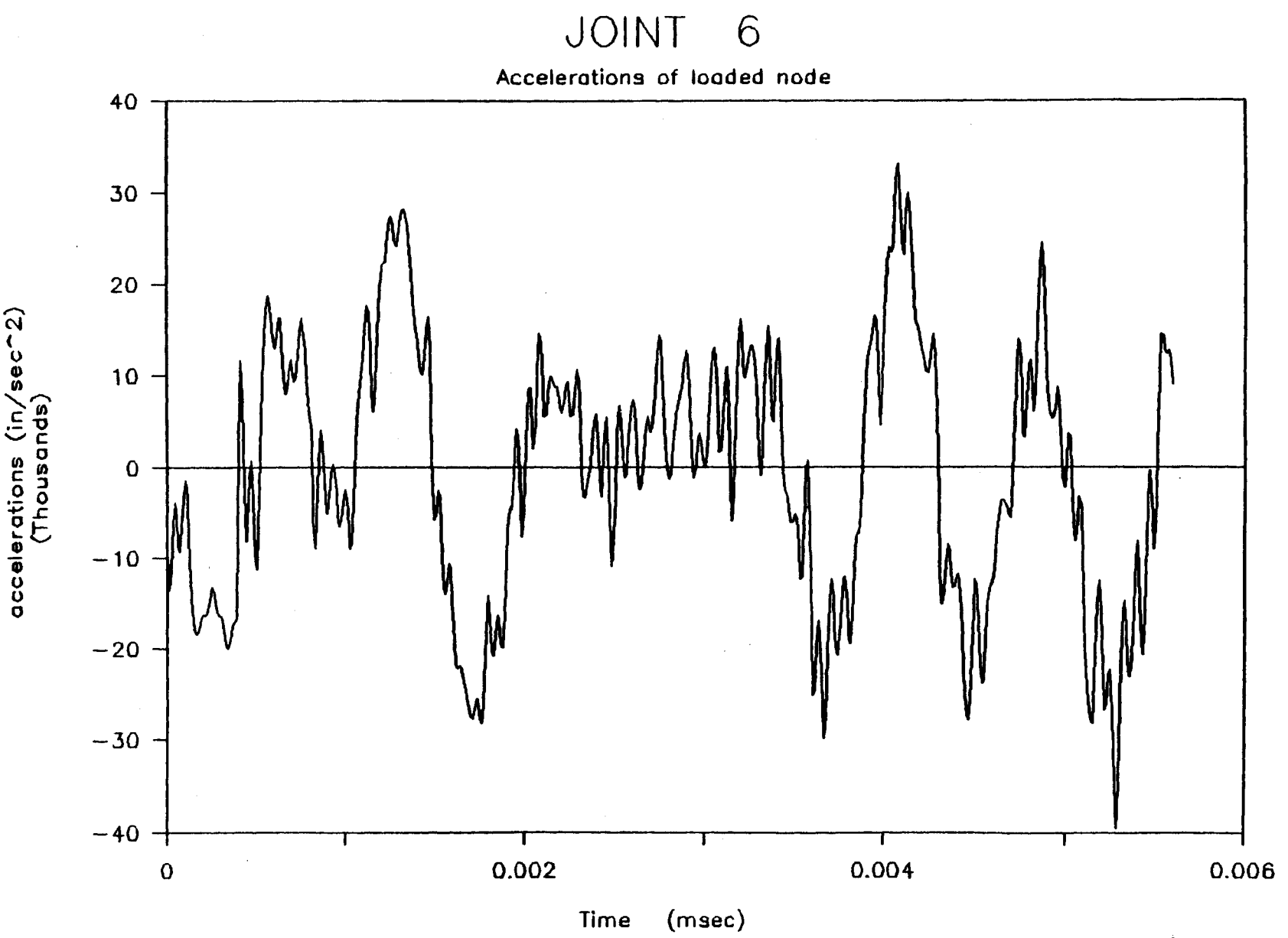
JOINT 6
Accelerations of loaded node
accelerations (in/sec^2)
(Thousands)
40
30
20
10
0
-10
-20
-30
-40
0
0.002
0.004
0.006
Time (msec)

C11

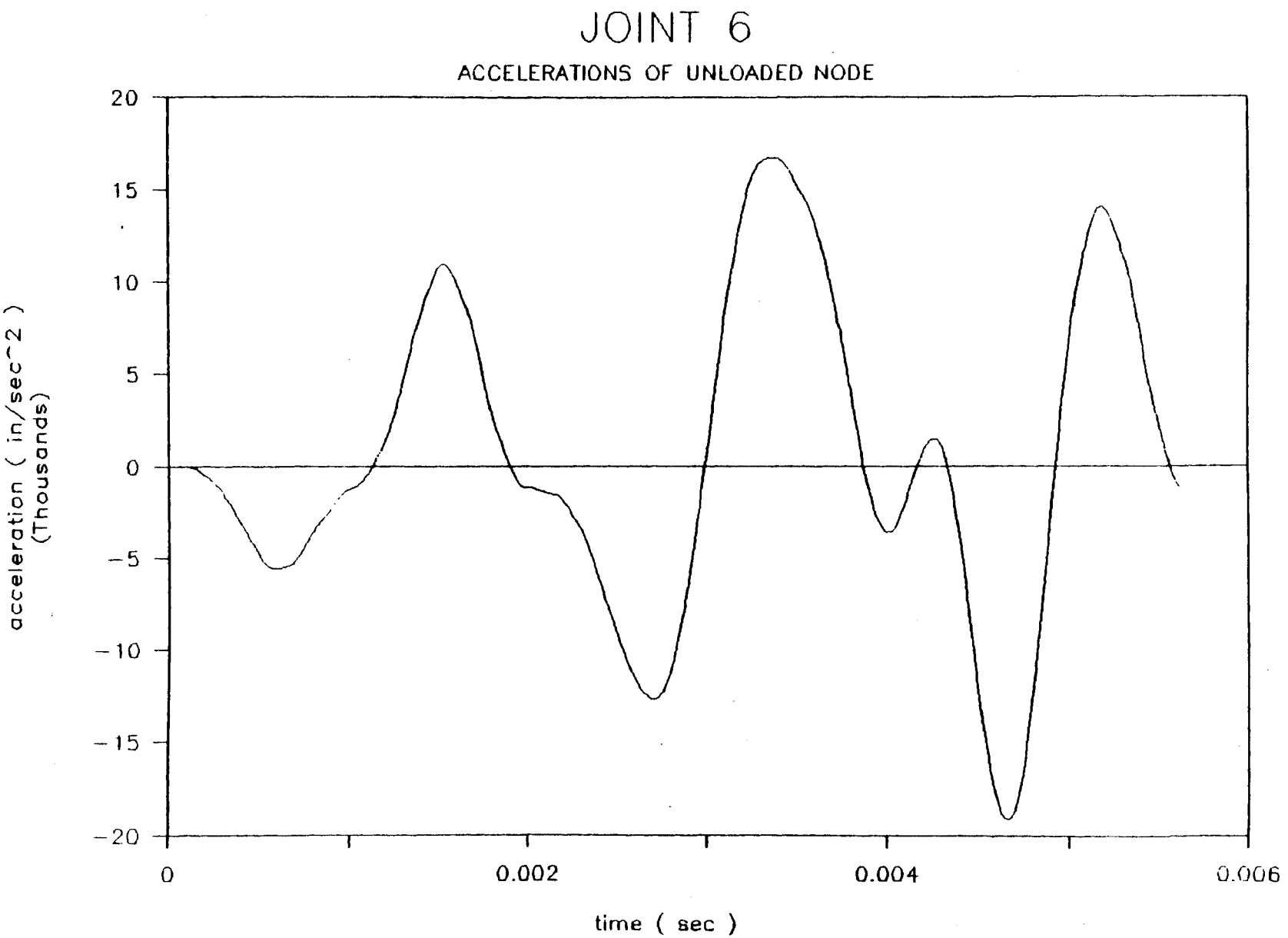
JOINT 6
ACCELERATIONS OF UNLOADED NODE
acceleration (in/sec^2)
(Thousands)
20
15
10
5
0
-5
-10
-15
-20
0
0.002
0.004
0.006
time (sec)

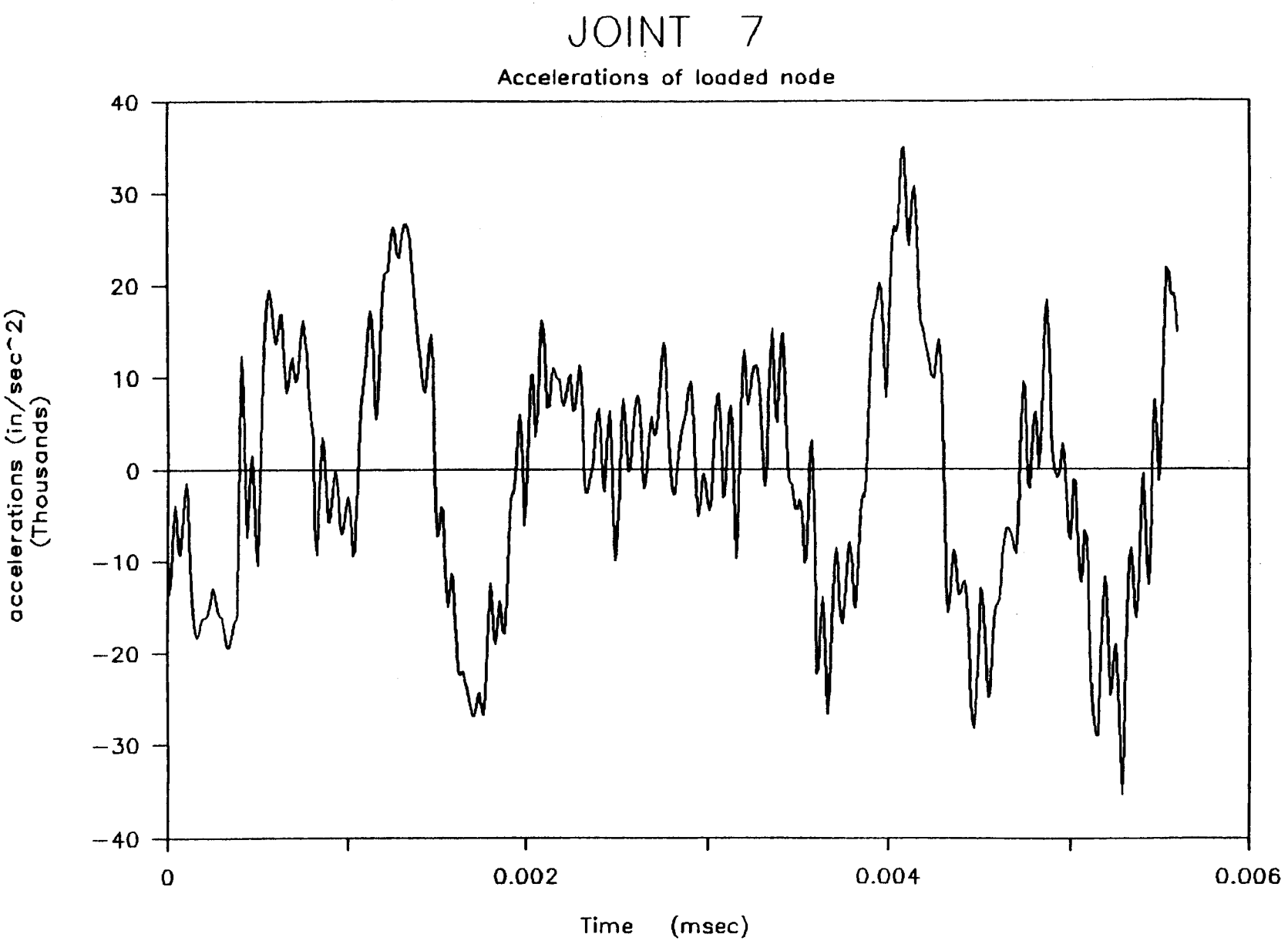
JOINT 7
Accelerations of loaded node
accelerations (in/sec^2)
(Thousands)
40
30
20
10
0
-10
-20
-30
-40
0
0.002
0.004
0.006
Time (msec)

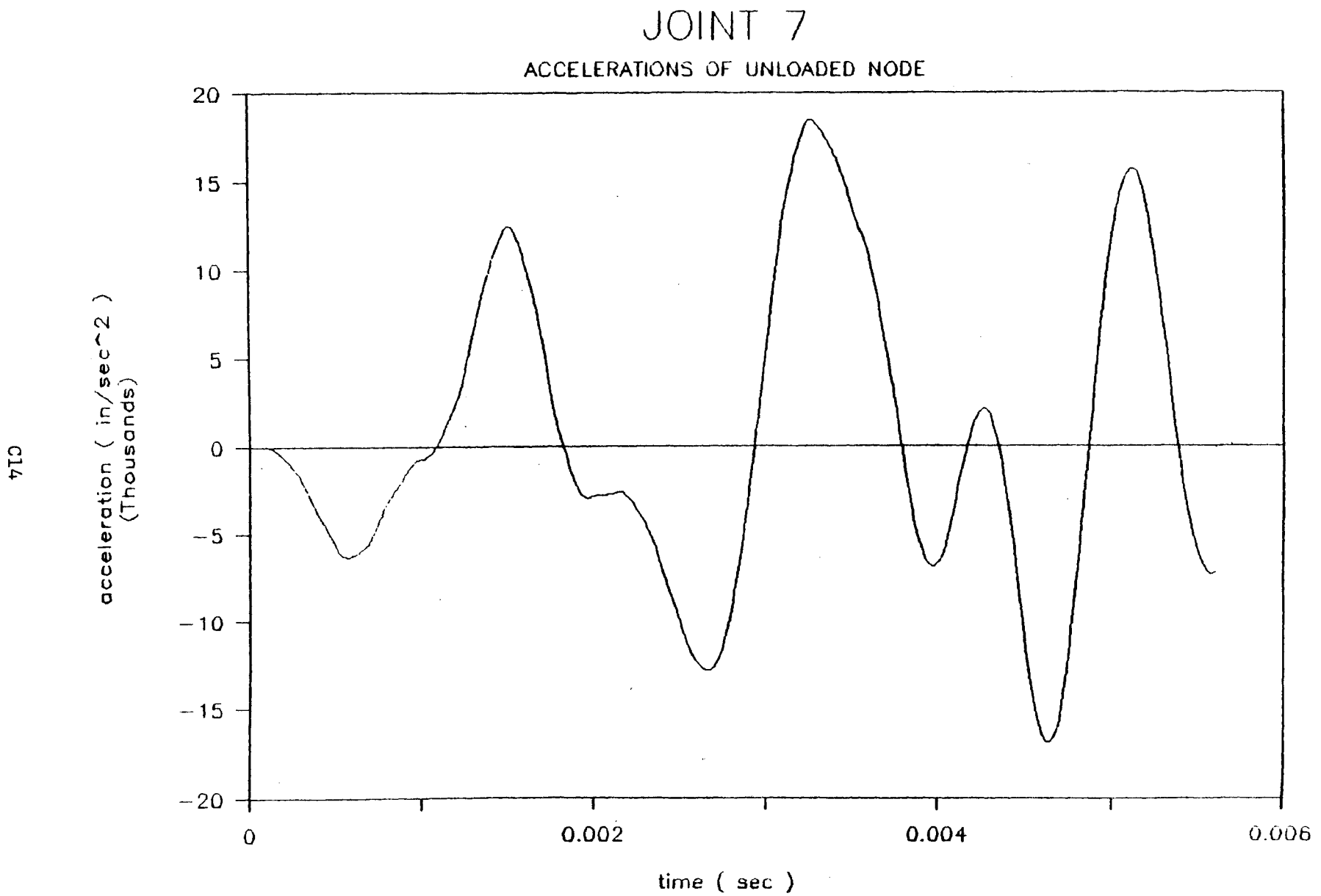
JOINT 7
ACCELERATIONS OF UNLOADED NODE
acceleration (in/sec^2)
(Thousands)
20
15
10
5
0
-5
-10
-15
-20
0
0.002
0.004
0.006
time (sec)

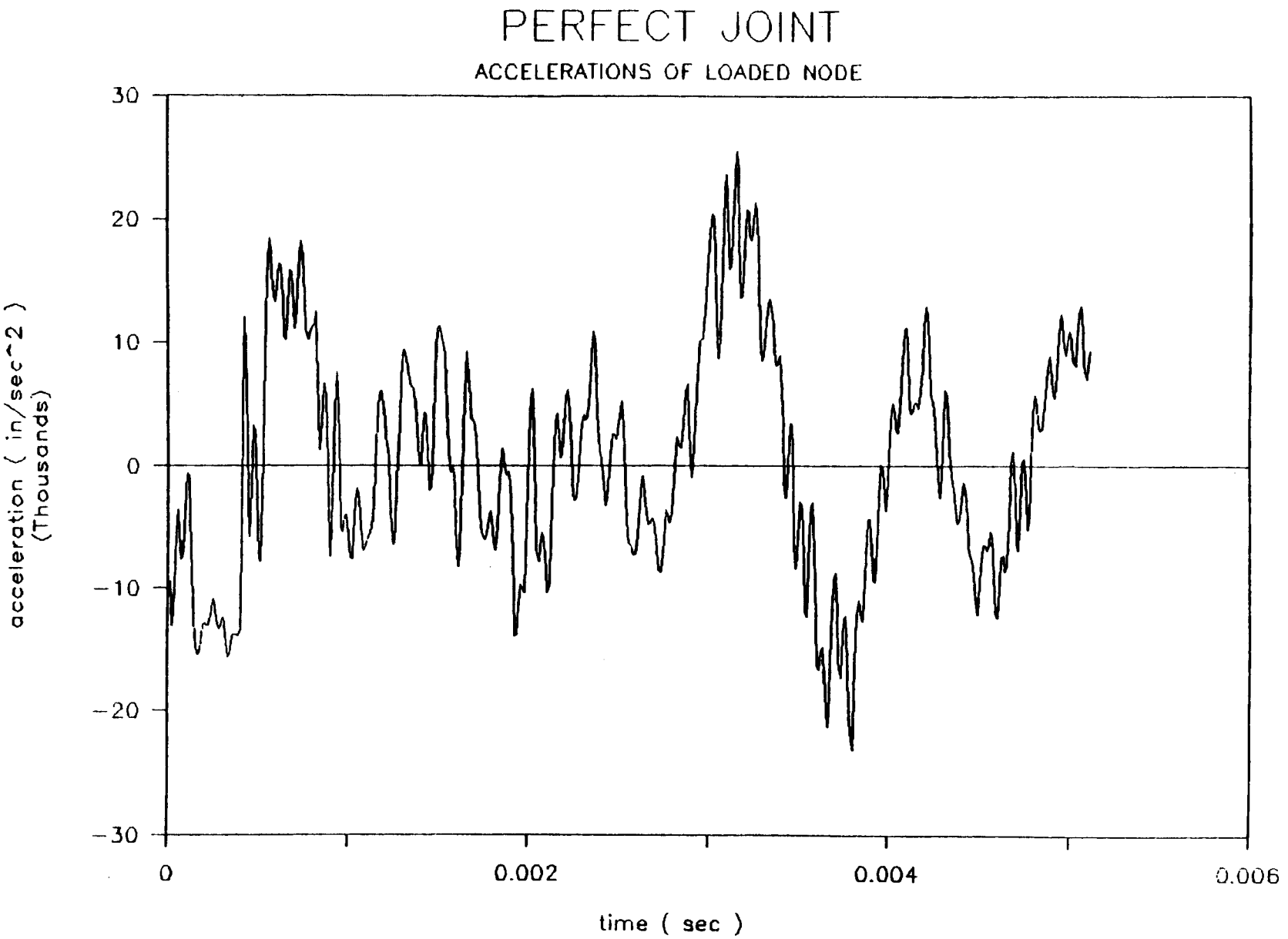
PERFECT JOINT
ACCELERATIONS OF LOADED NODE
acceleration (in/sec^2)
(Thousands)
30
20
10
0
-10
-20
-30
0
0.002
0.004
0.006
time (sec)

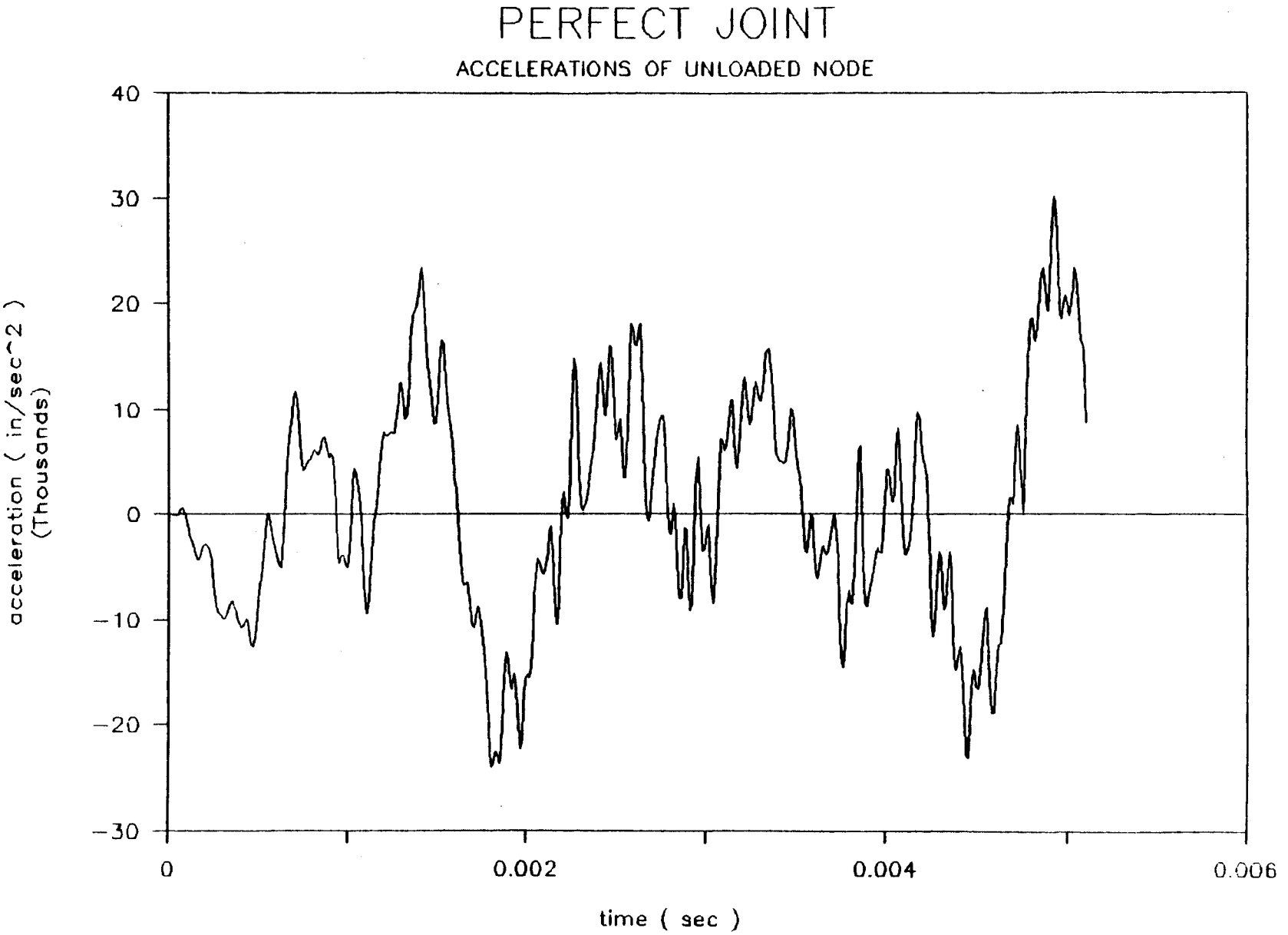
PERFECT JOINT
ACCELERATIONS OF UNLOADED NODE
acceleration (in/sec^2)
(Thousands)
40
30
20
10
0
-10
-20
-30
0
0.002
0.004
0.006
time (sec)

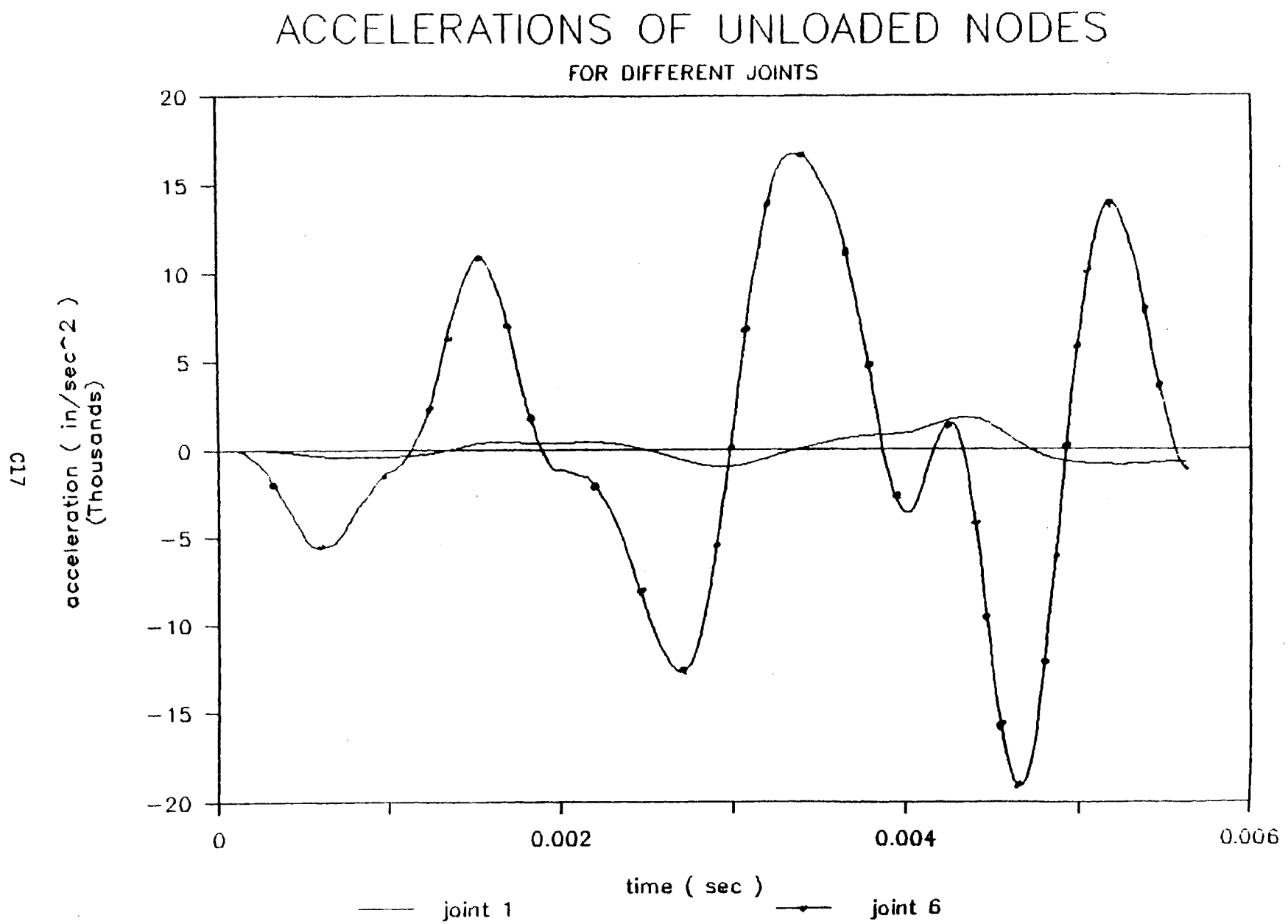
ACCELERATIONS OF UNLOADED NODES
FOR DIFFERENT JOINTS
20
15
10
5
0
-5
-10
-15
-20
acceleration (in/sec^2)
(Thousands)
0
0.002
0.004
0.006
time (sec)
joint 1
joint 6

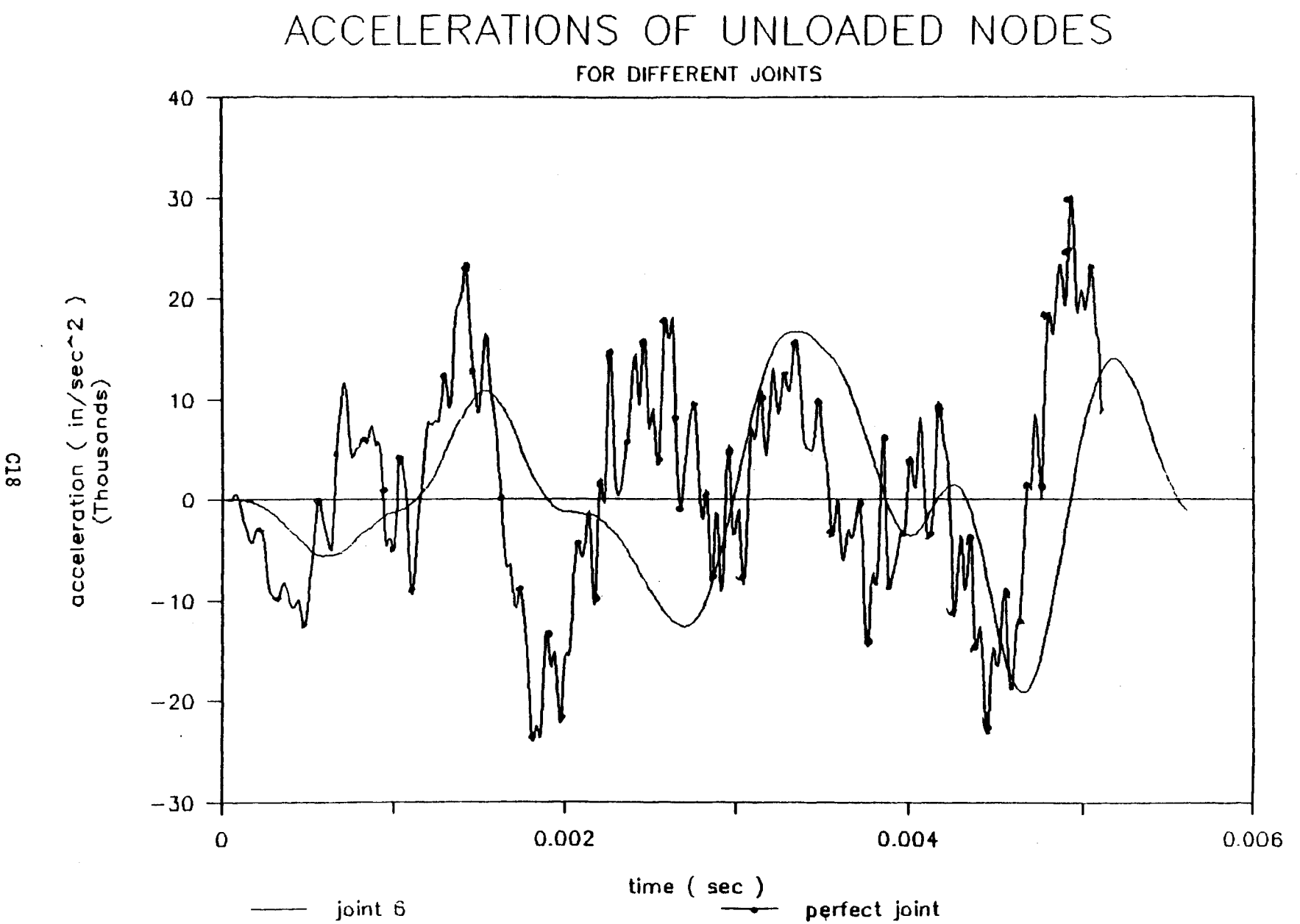
ACCELERATIONS OF UNLOADED NODES
FOR DIFFERENT JOINTS
acceleration (in/sec^2)
(Thousands)
40
30
20
10
0
-10
-20
-30
0
0.002
0.004
0.006
time (sec)
joint 6
perfect joint

Appendix D: Power Spectrum Plots

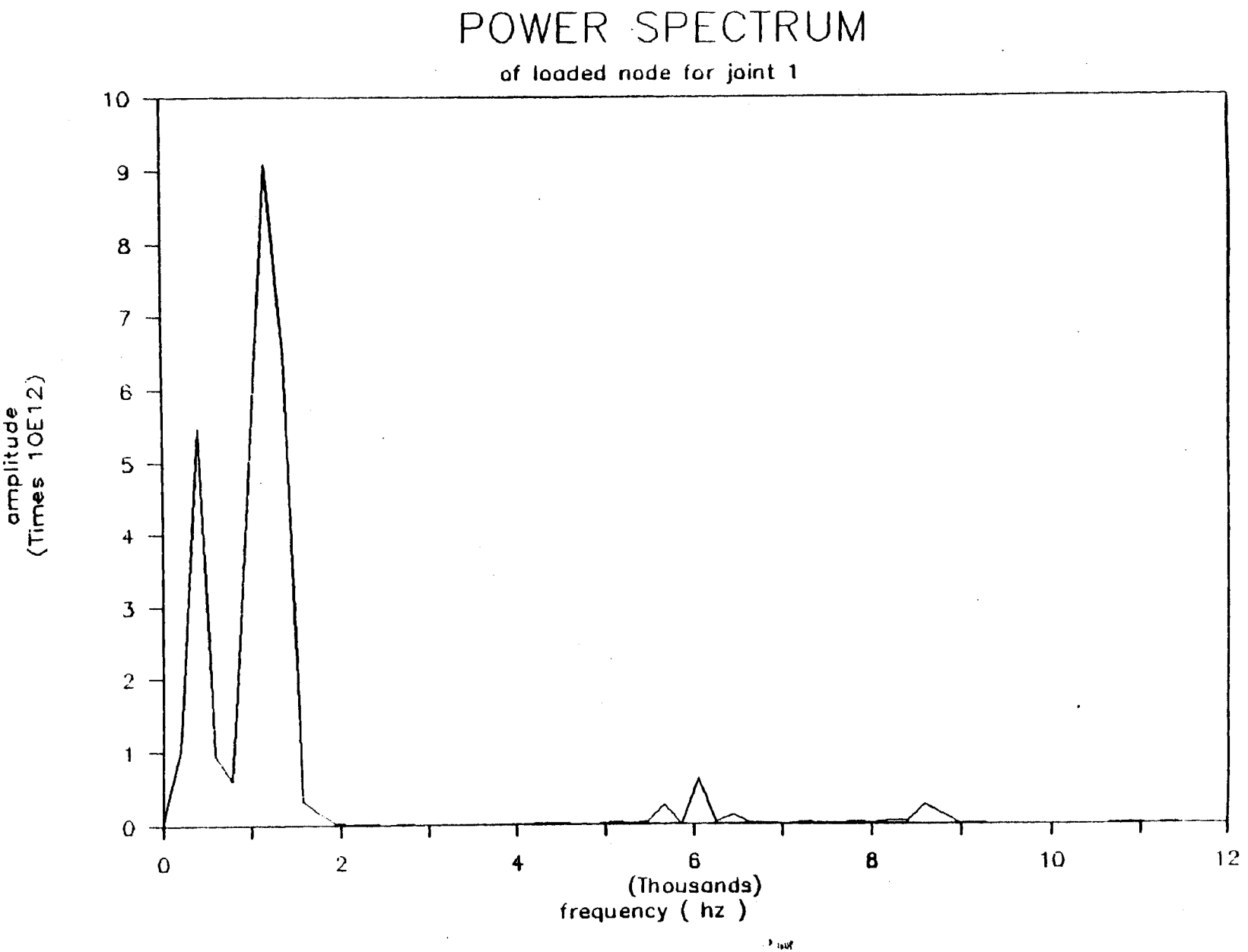
POWER SPECTRUM
of loaded node for joint 1
amplitude
(Times 10E12)
0
1
2
3
4
5
6
7
8
9
10
0
2
4
6
8
10
12
(Thousands)
frequency (hz)

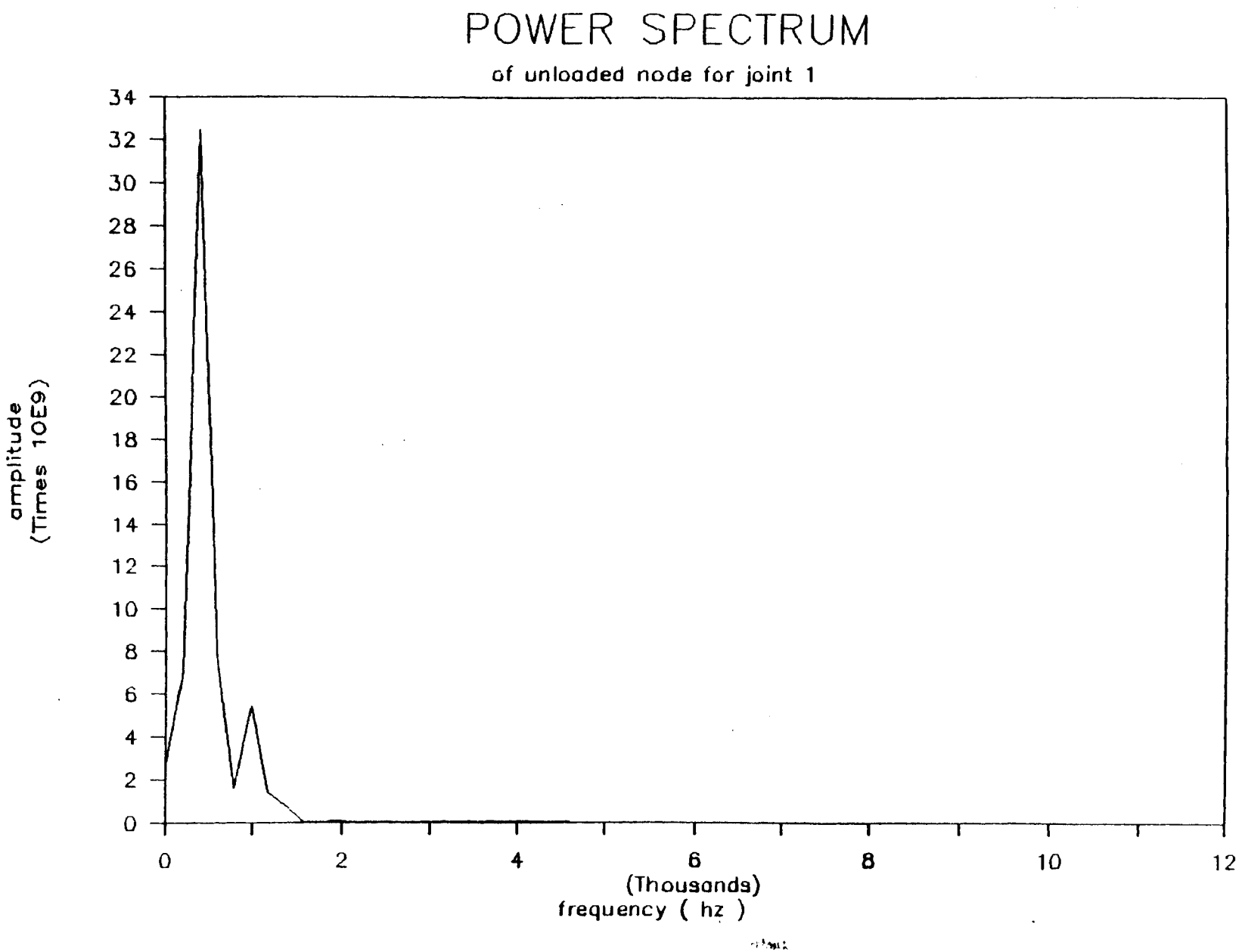
POWER SPECTRUM
of unloaded node for joint 1
amplitude
(Times 10E9)
34
32
30
28
26
24
22
20
18
16
14
12
10
8
6
4
2
0
0
2
4
6
8
10
12
(Thousands)
frequency (hz)

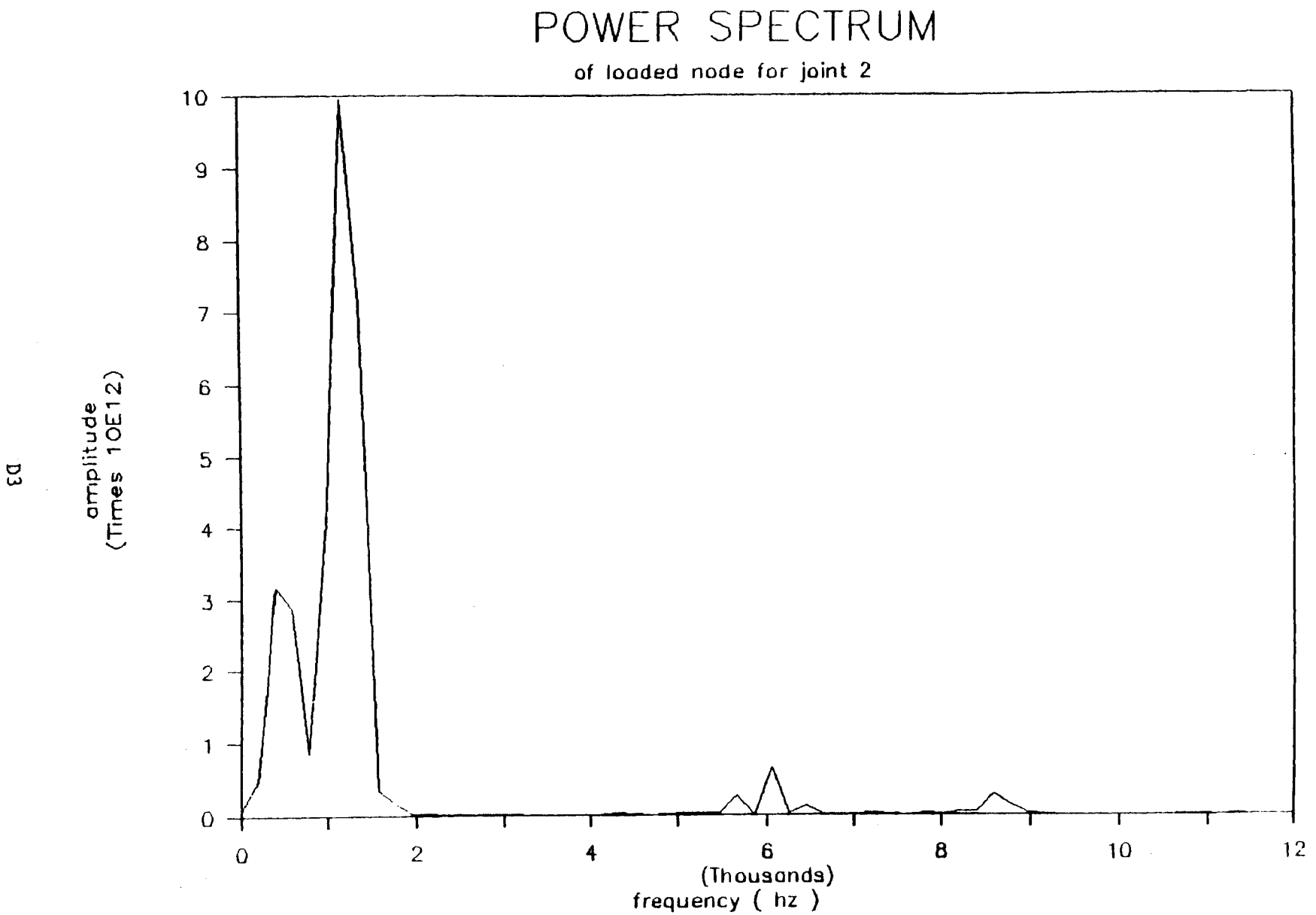
POWER SPECTRUM
of loaded node for joint 2
amplitude
(Times 10E12)
10
9
8
7
6
5
4
3
2
1
0
0
2
4
6
8
10
12
(Thousands)
frequency (hz)

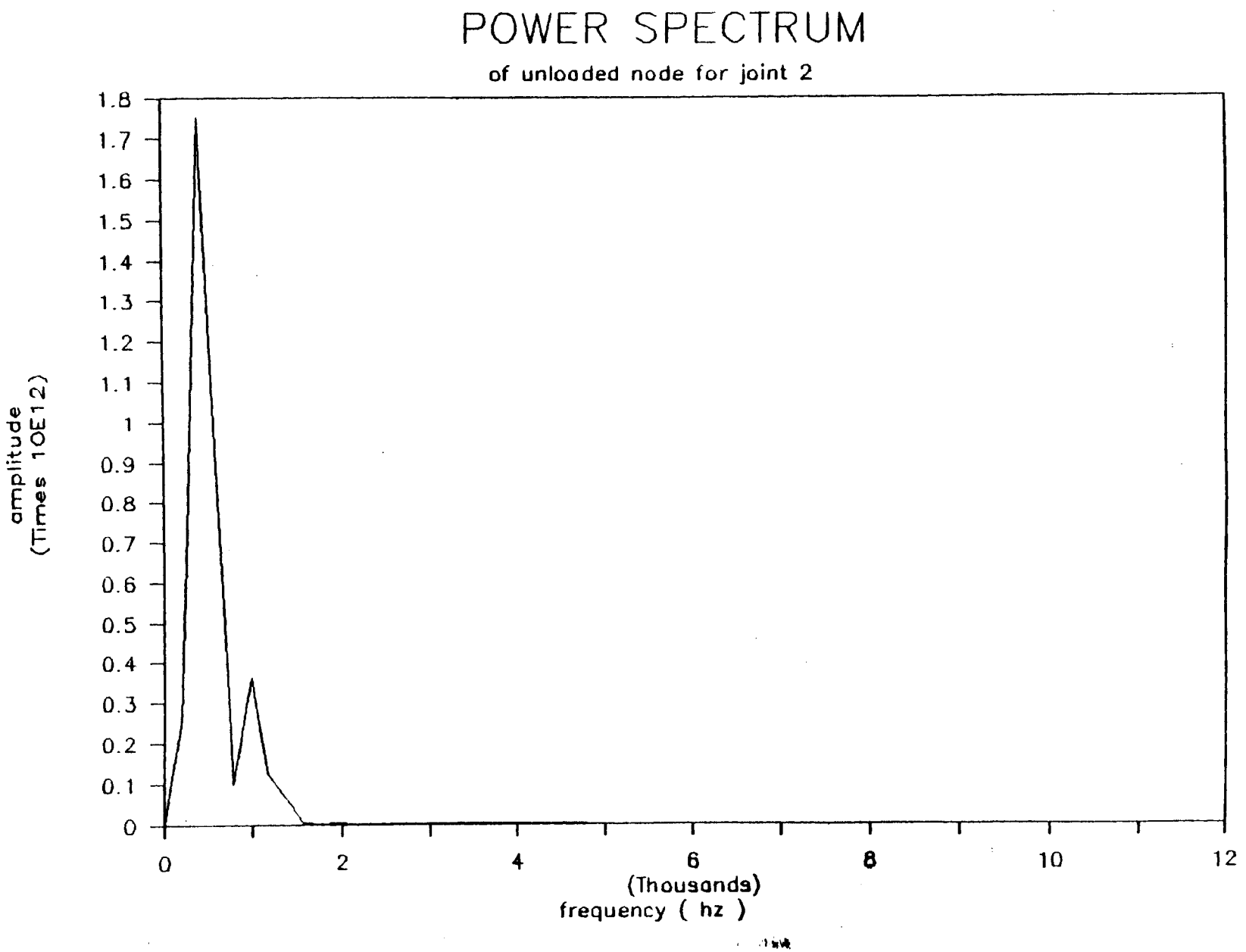
POWER SPECTRUM
of unlooded node for joint 2
amplitude
(Times 10E12)
1.8
1.7
1.6
1.5
1.4
1.3
1.2
1.1
1
0.9
0.8
0.7
0.6
0.5
0.4
0.3
0.2
0.1
0
0
2
4
6
8
10
12
(Thousands)
frequency (hz)

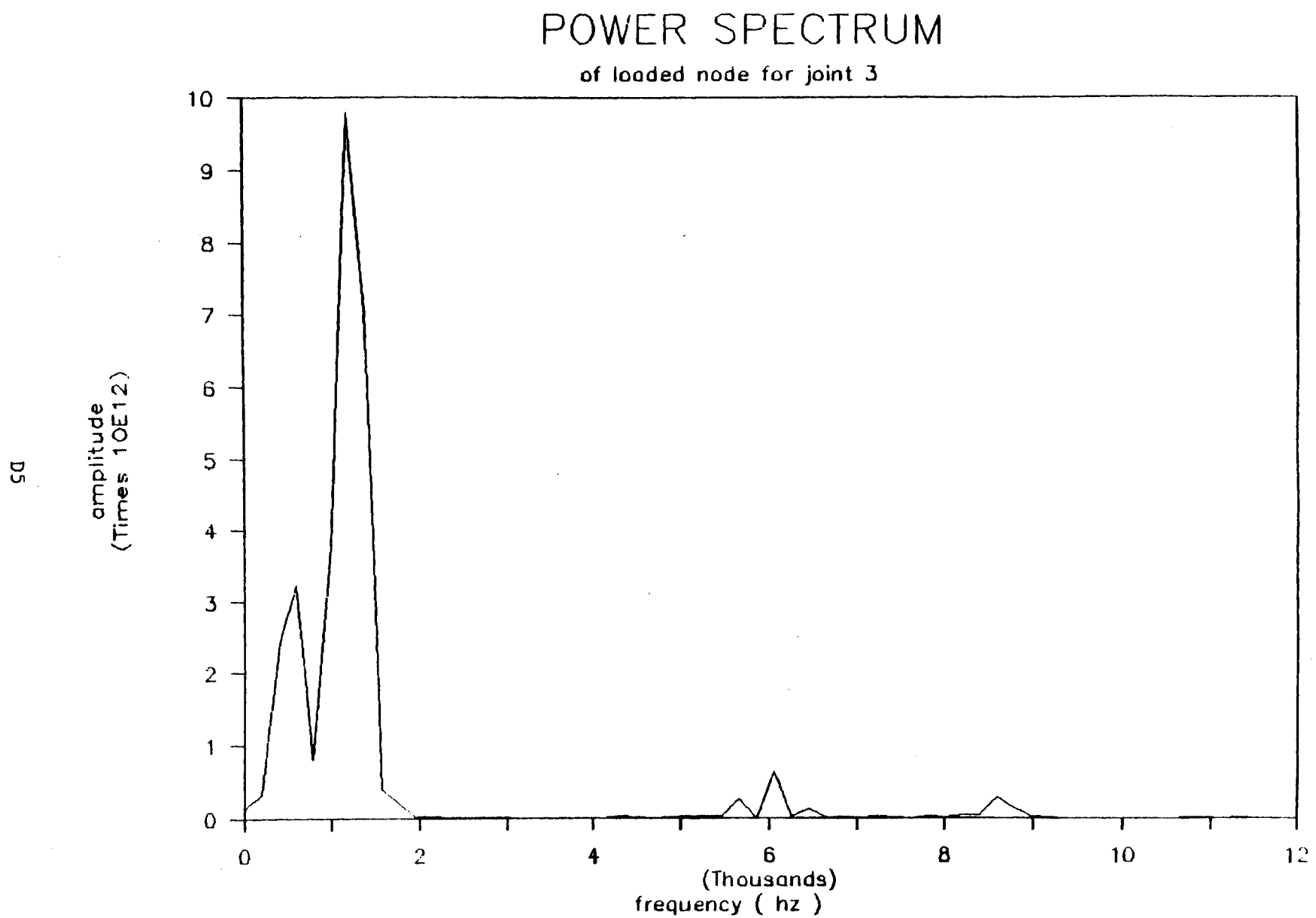
POWER SPECTRUM
of loaded node for joint 3
amplitude
(Times 10E12)
10
9
8
7
6
5
4
3
2
1
0
0
2
4
6
8
10
12
(Thousands)
frequency (hz)

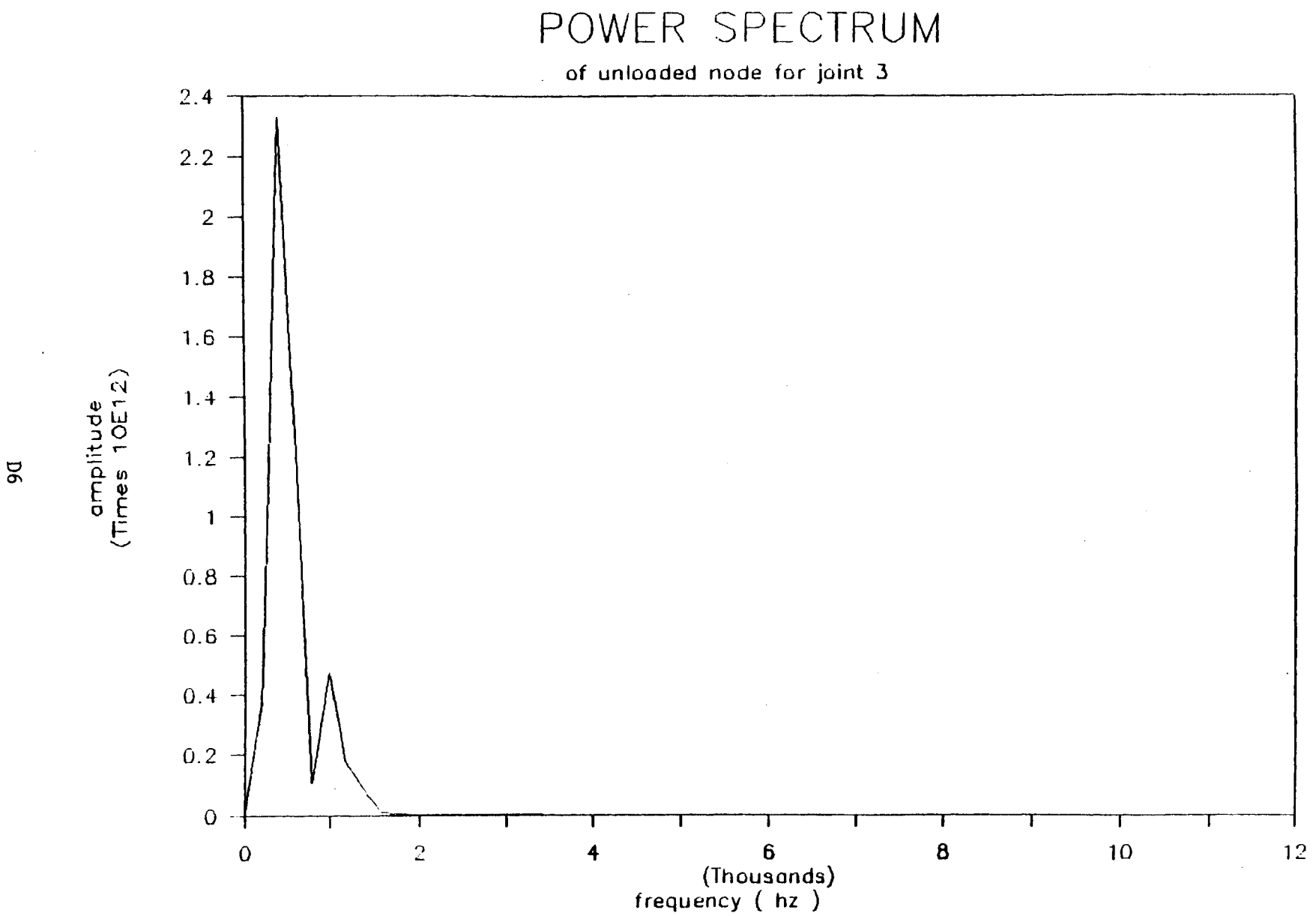
POWER SPECTRUM
of unloaded node for joint 3
amplitude
(Times 10E12)
2.4
2.2
2
1.8
1.6
1.4
1.2
1
0.8
0.6
0.4
0.2
0
0
2
4
6
8
10
12
(Thousands)
frequency (hz)

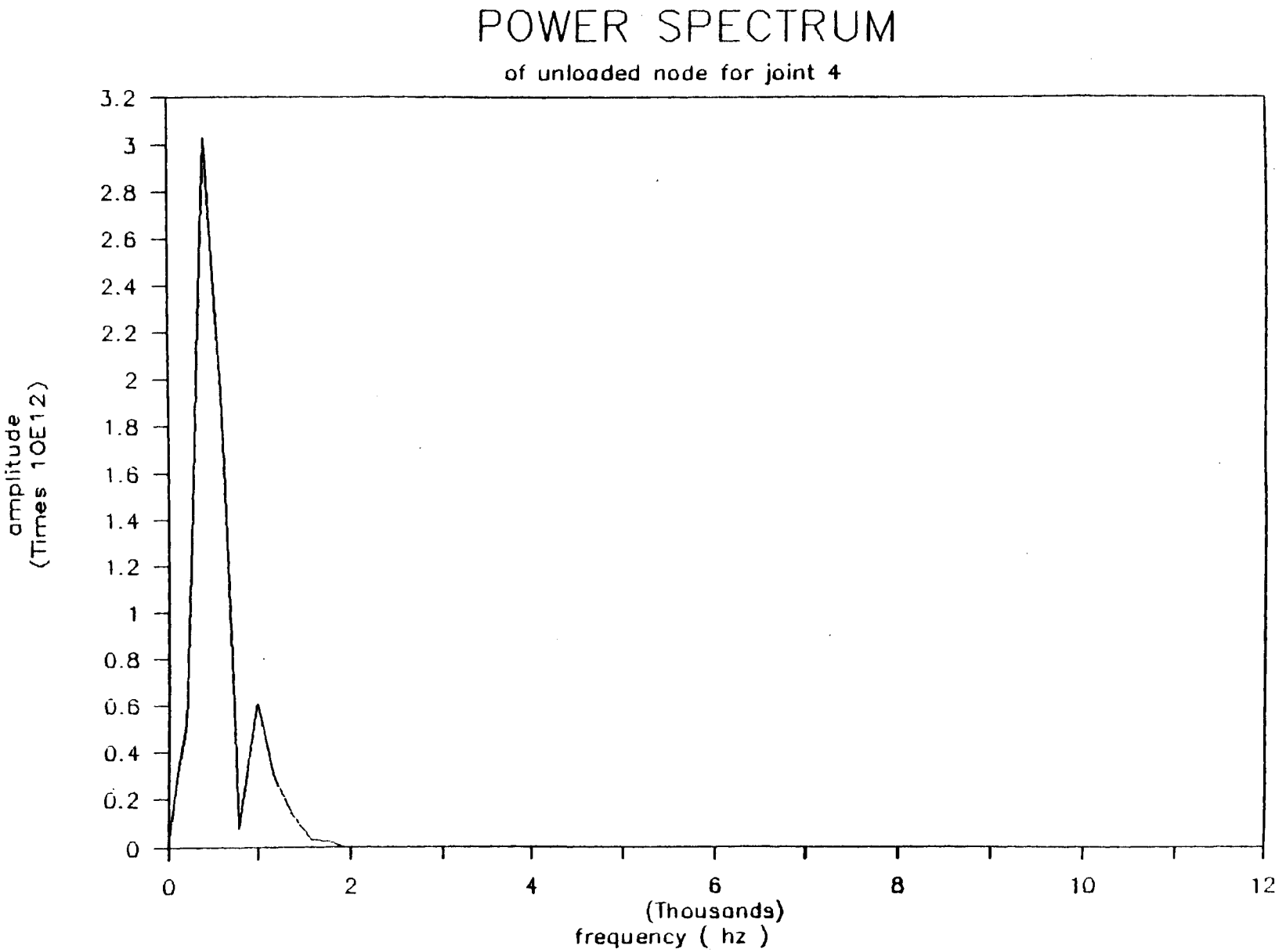
POWER SPECTRUM
of unloaded node for joint 4
amplitude
(Times 10E12)
3.2
3
2.8
2.6
2.4
2.2
2
1.8
1.6
1.4
1.2
1
0.8
0.6
0.4
0.2
0
0
2
4
6
8
10
12
(Thousands)
frequency (hz)

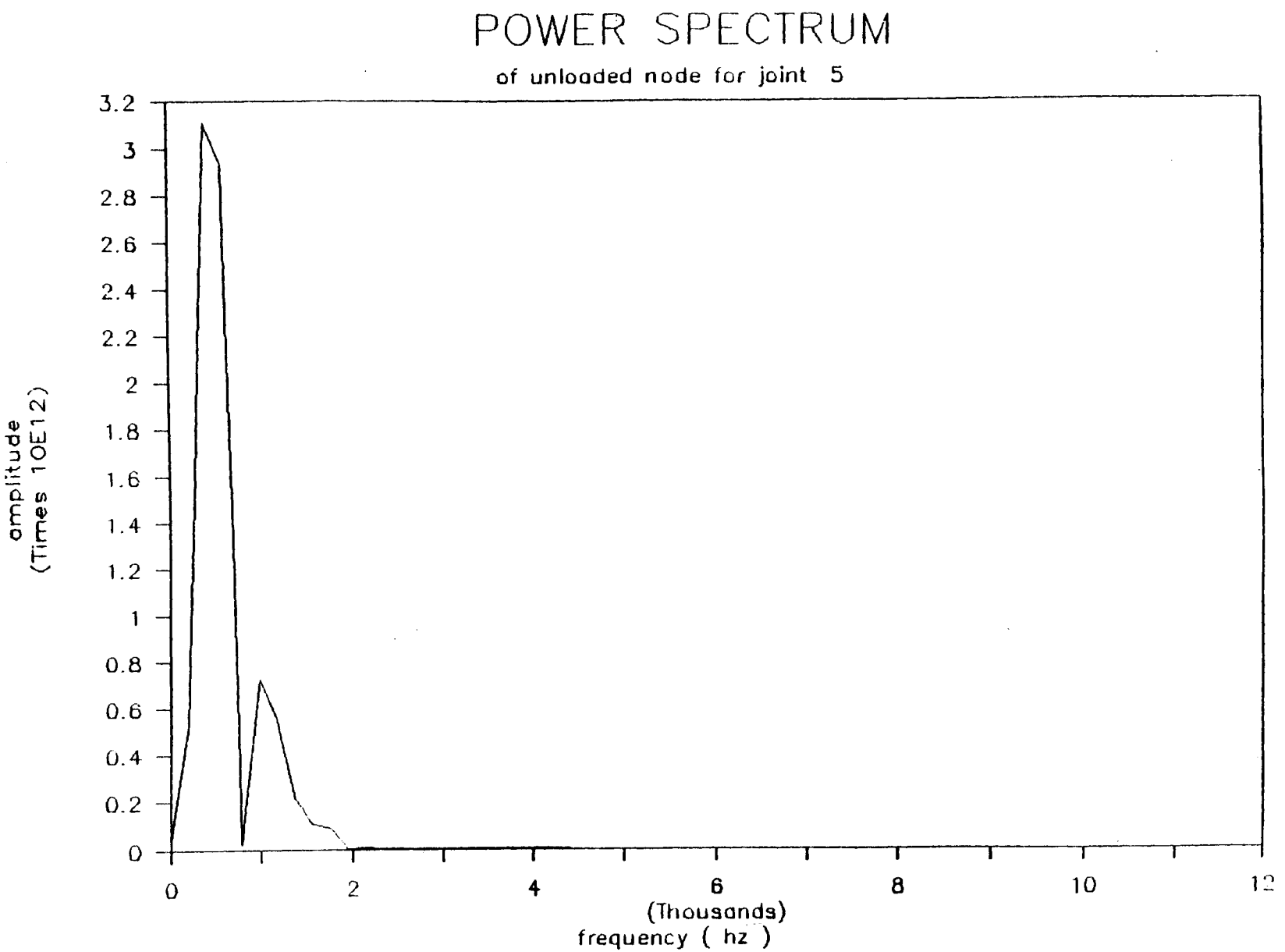
POWER SPECTRUM
of unloaded node for joint 5
amplitude
(Times 10E12)
3.2
3
2.8
2.6
2.4
2.2
2
1.8
1.6
1.4
1.2
1
0.8
0.6
0.4
0.2
0
0
2
4
6
8
10
12
(Thousands)
frequency (hz)

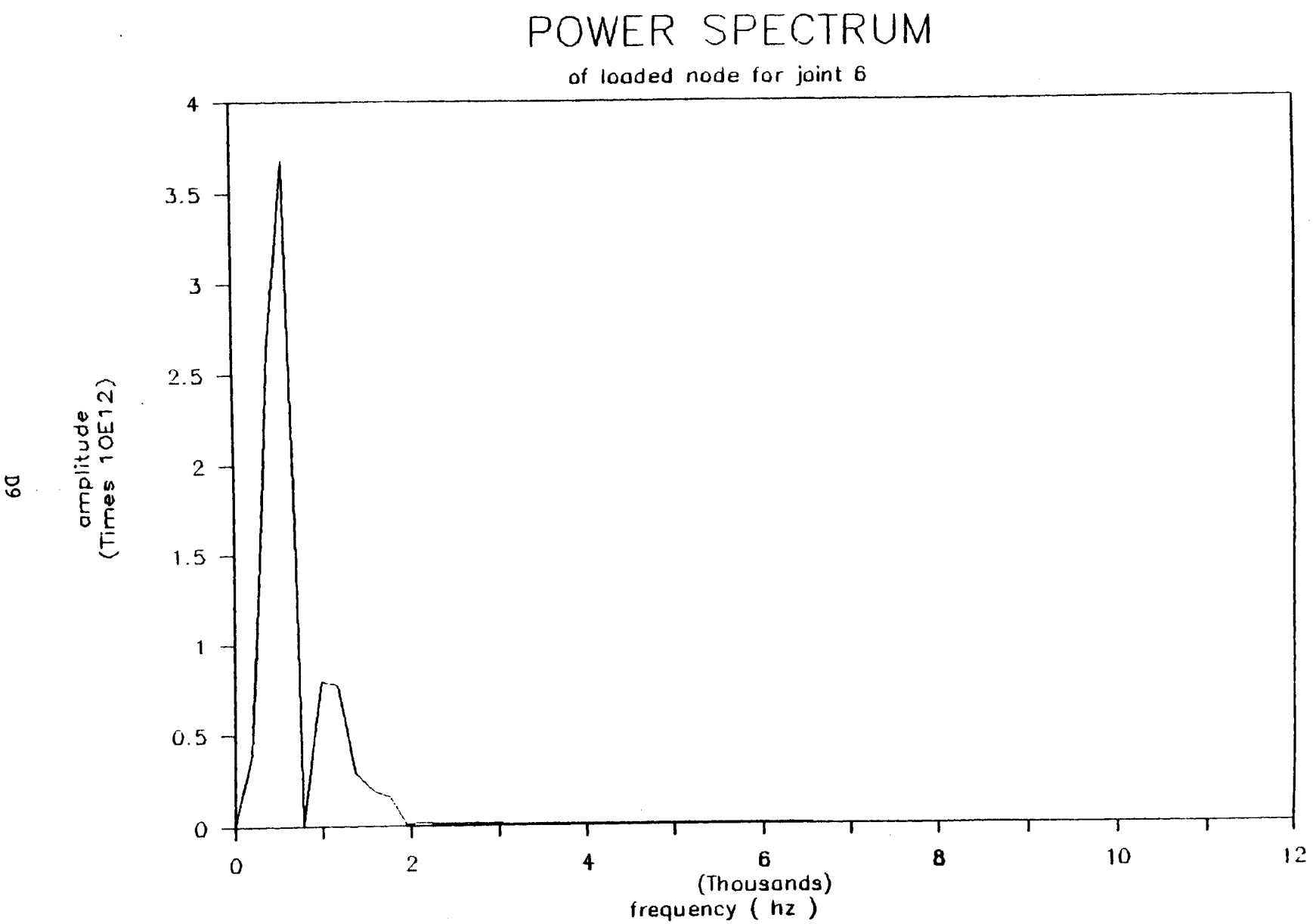
POWER SPECTRUM
of loaded node for joint 6
amplitude
(Times 10E12)
4
3.5
3
2.5
2
1.5
1
0.5
0
0
2
4
6
8
10
12
(Thousands)
frequency (hz)

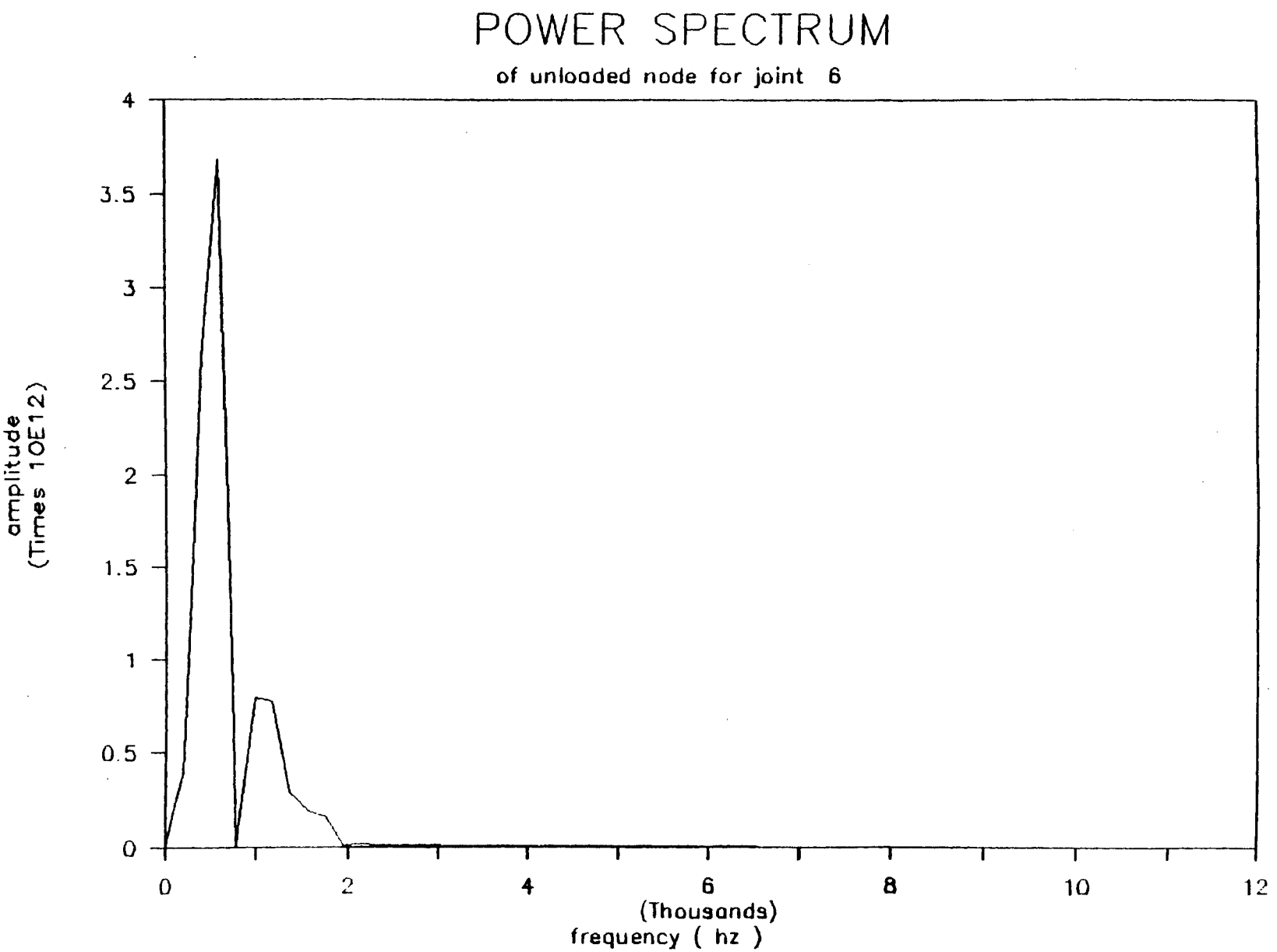
POWER SPECTRUM
of unlooded node for joint 6
amplitude
(Times 10E12)
4
3.5
3
2.5
2
1.5
1
0.5
0
0
2
4
6
8
10
12
(Thousands)
frequency (hz)

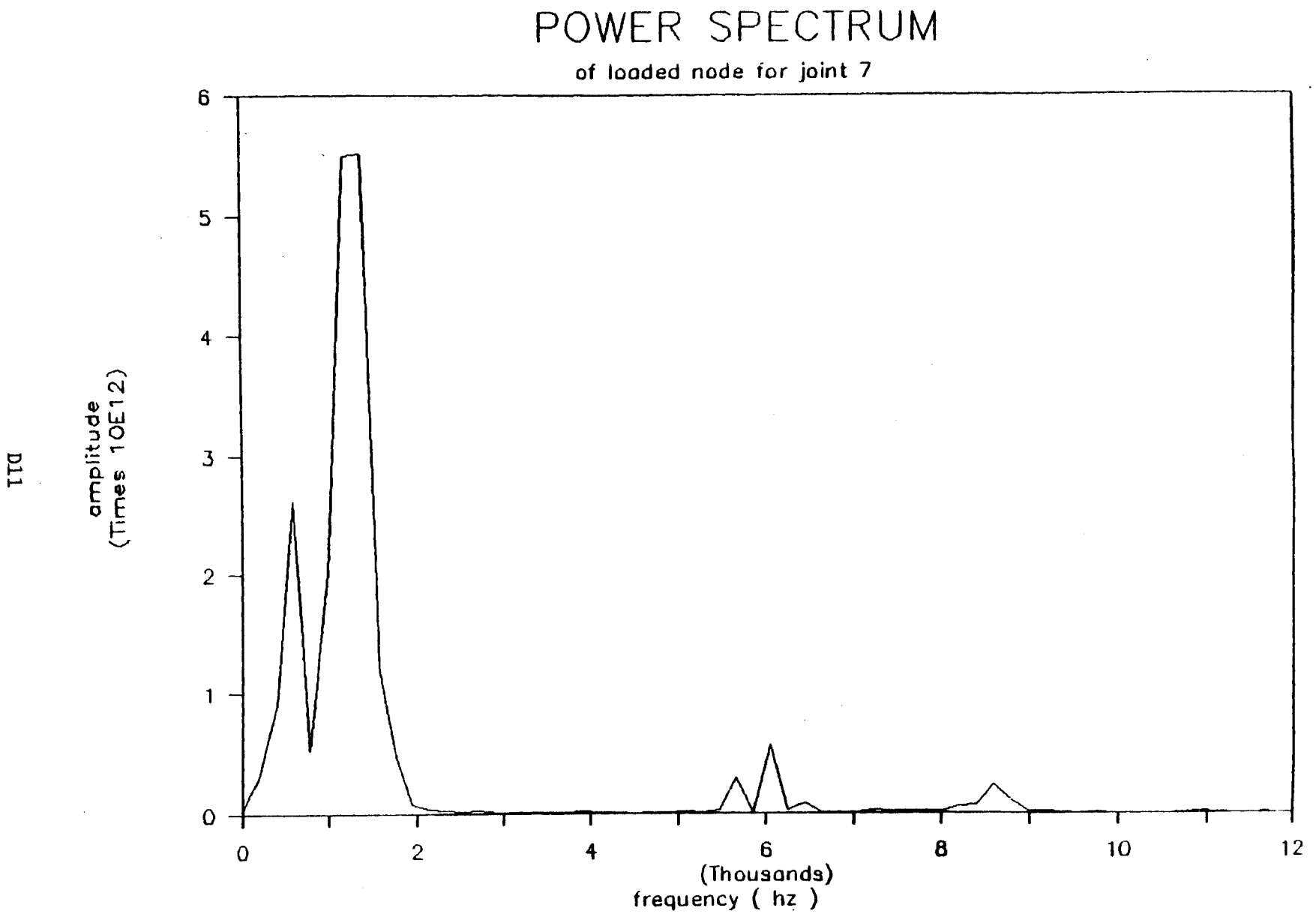
POWER SPECTRUM
of loaded node for joint 7
amplitude
(Times 10E12)
0
1
2
3
4
5
6
0
2
4
6
8
10
12
(Thousands)
frequency (hz)

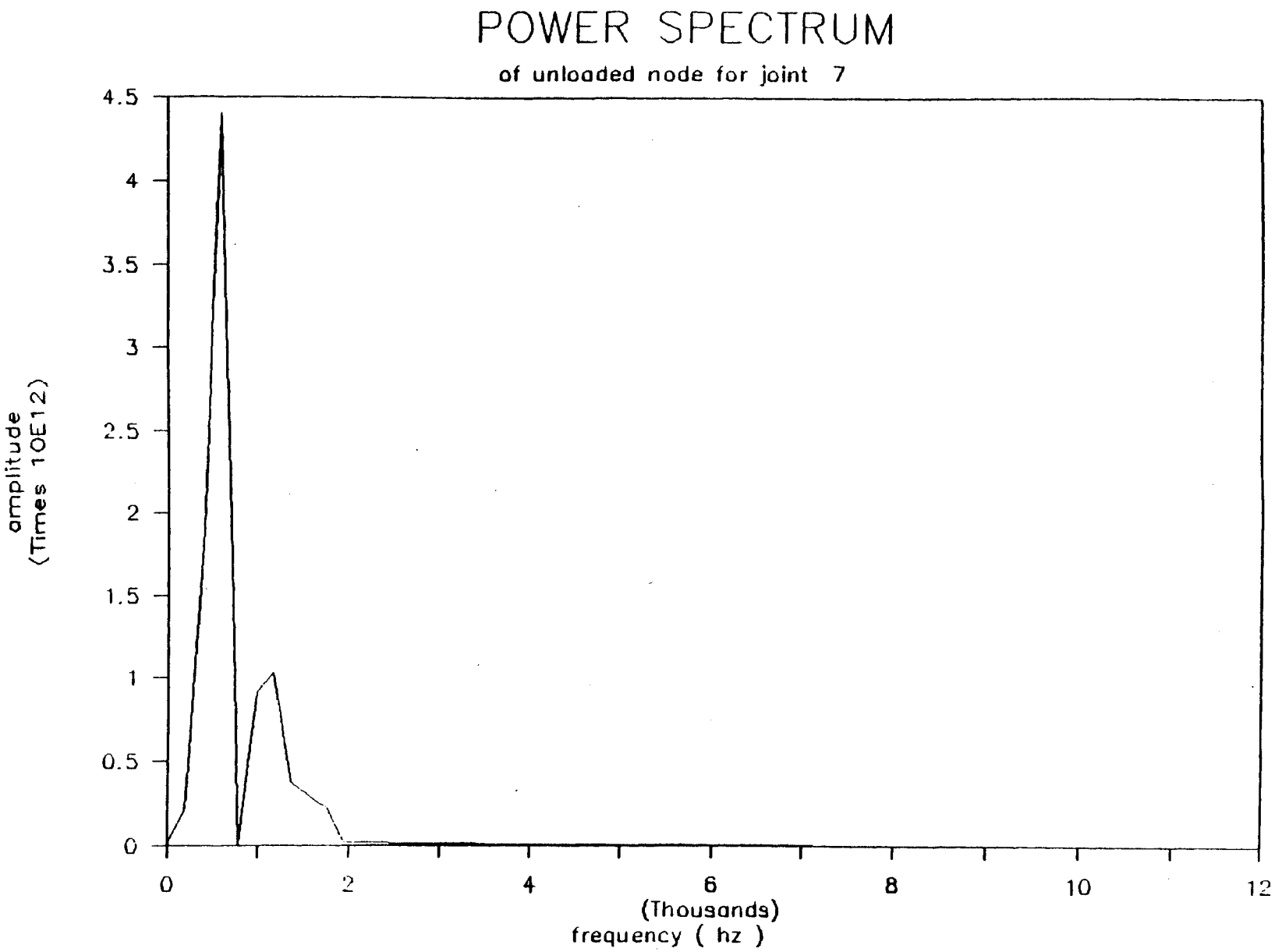
POWER SPECTRUM
of unloaded node for joint 7
amplitude
(Times 10E12)
4.5
4
3.5
3
2.5
2
1.5
1
0.5
0
0
2
4
6
8
10
12
(Thousands)
frequency (hz)

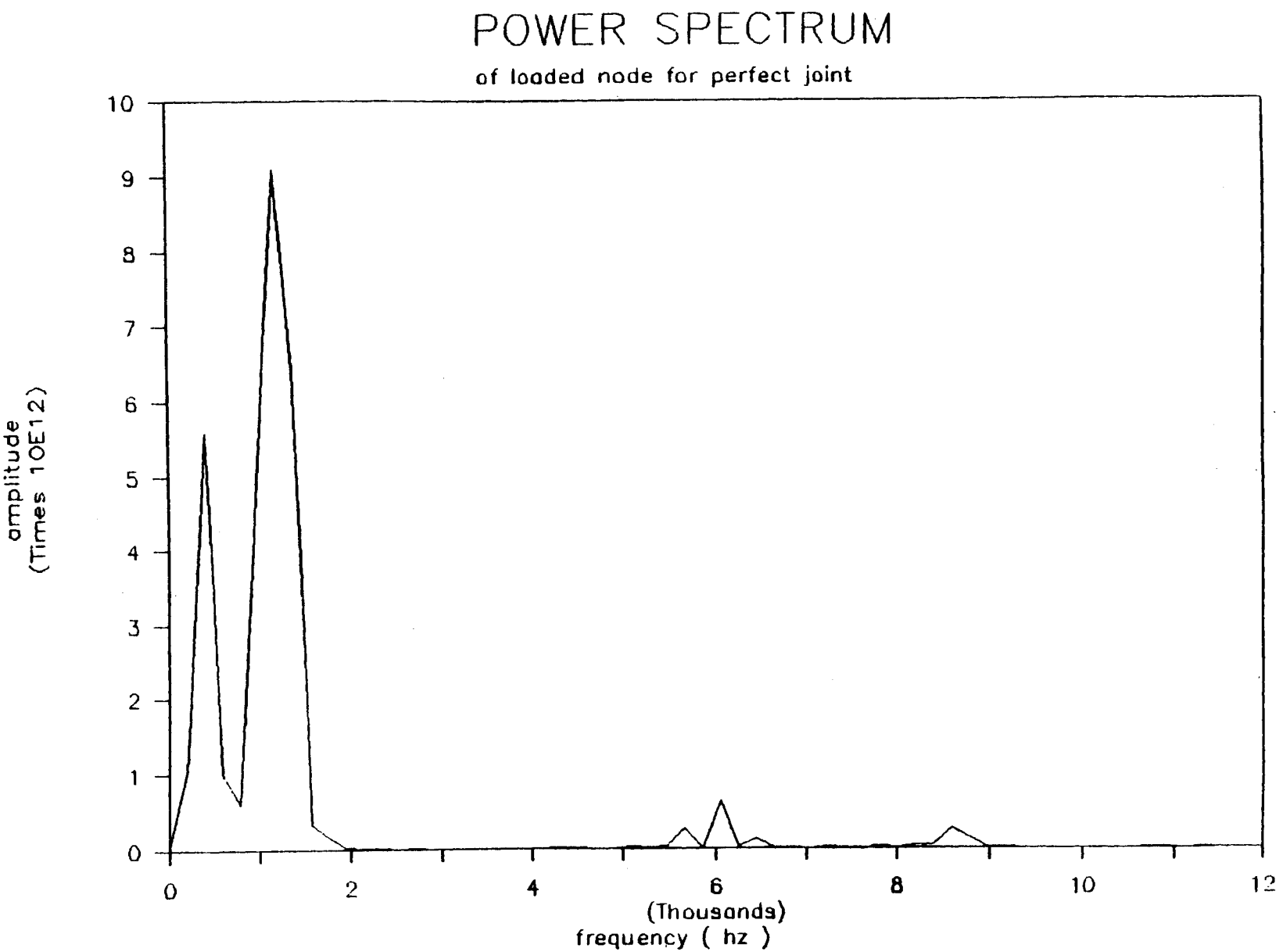
POWER SPECTRUM
of loaded node for perfect joint
amplitude
(Times 10E12)
10
9
8
7
6
5
4
3
2
1
0
0
2
4
6
8
10
12
(Thousands)
frequency (hz)

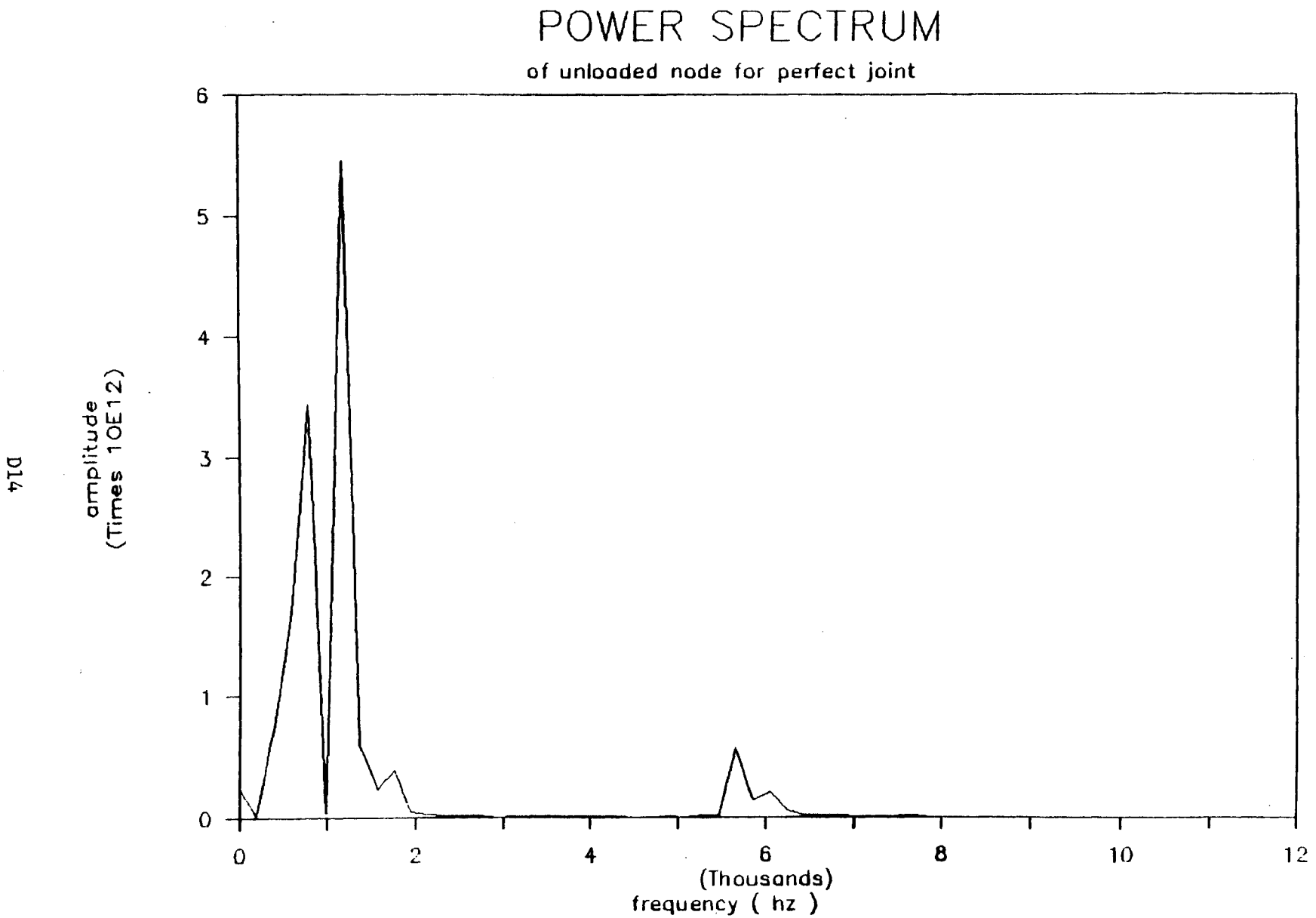
POWER SPECTRUM
of unloaded node for perfect joint
amplitude
(Times 10E12)
0
1
2
3
4
5
6
0
2
4
6
8
10
12
(Thousands)
frequency (hz)

Appendix E: Time Domain Plots for Different Axial Loads

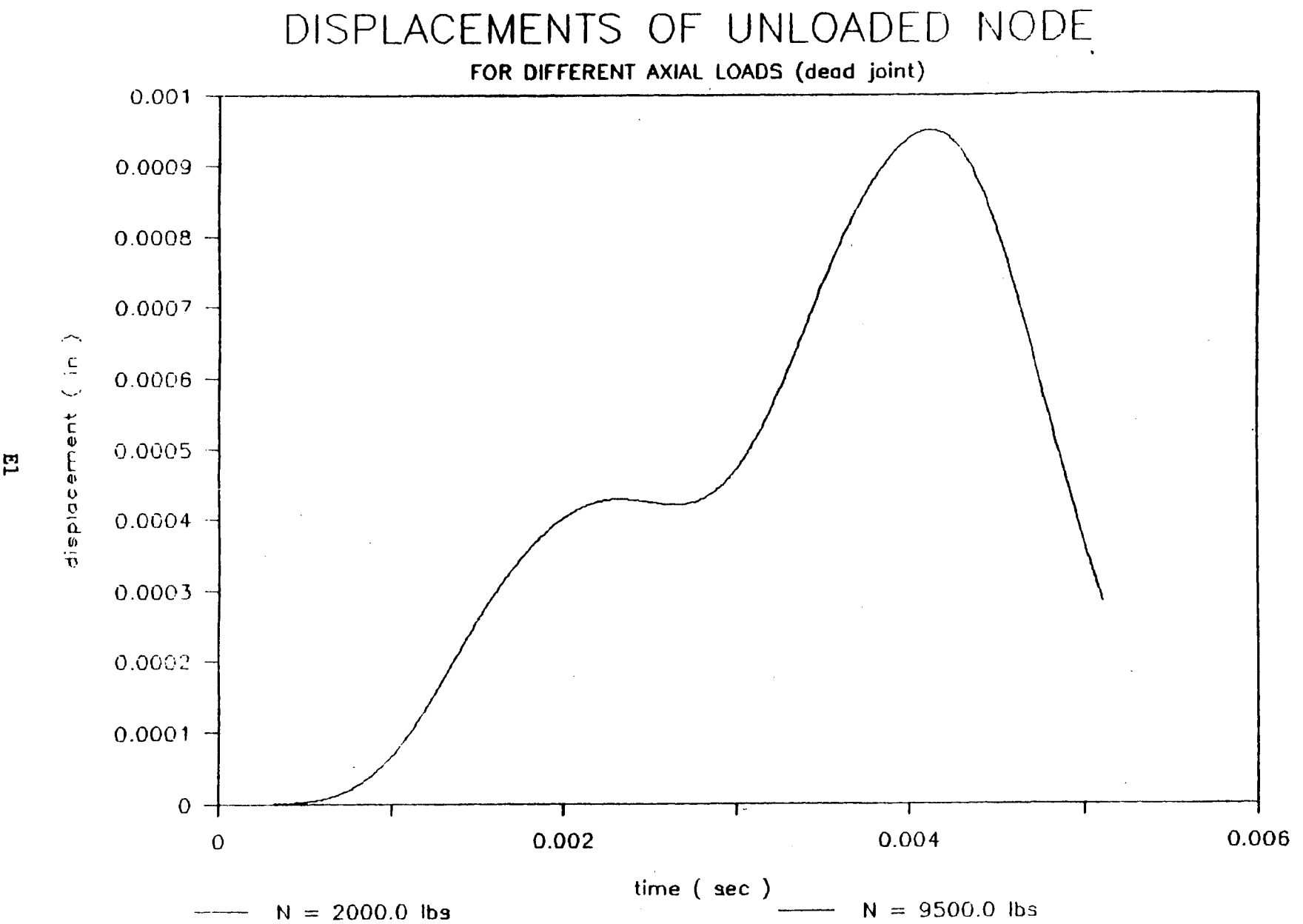
DISPLACEMENTS OF UNLOADED NODE
FOR DIFFERENT AXIAL LOADS (dead joint)
0.001
0.0009
0.0008
0.0007
0.0006
0.0005
0.0004
0.0003
0.0002
0.0001
0
displacement (in)
0
0.002
0.004
0.006
time (sec)
N = 2000.0 lbs
N = 9500.0 lbs

E1

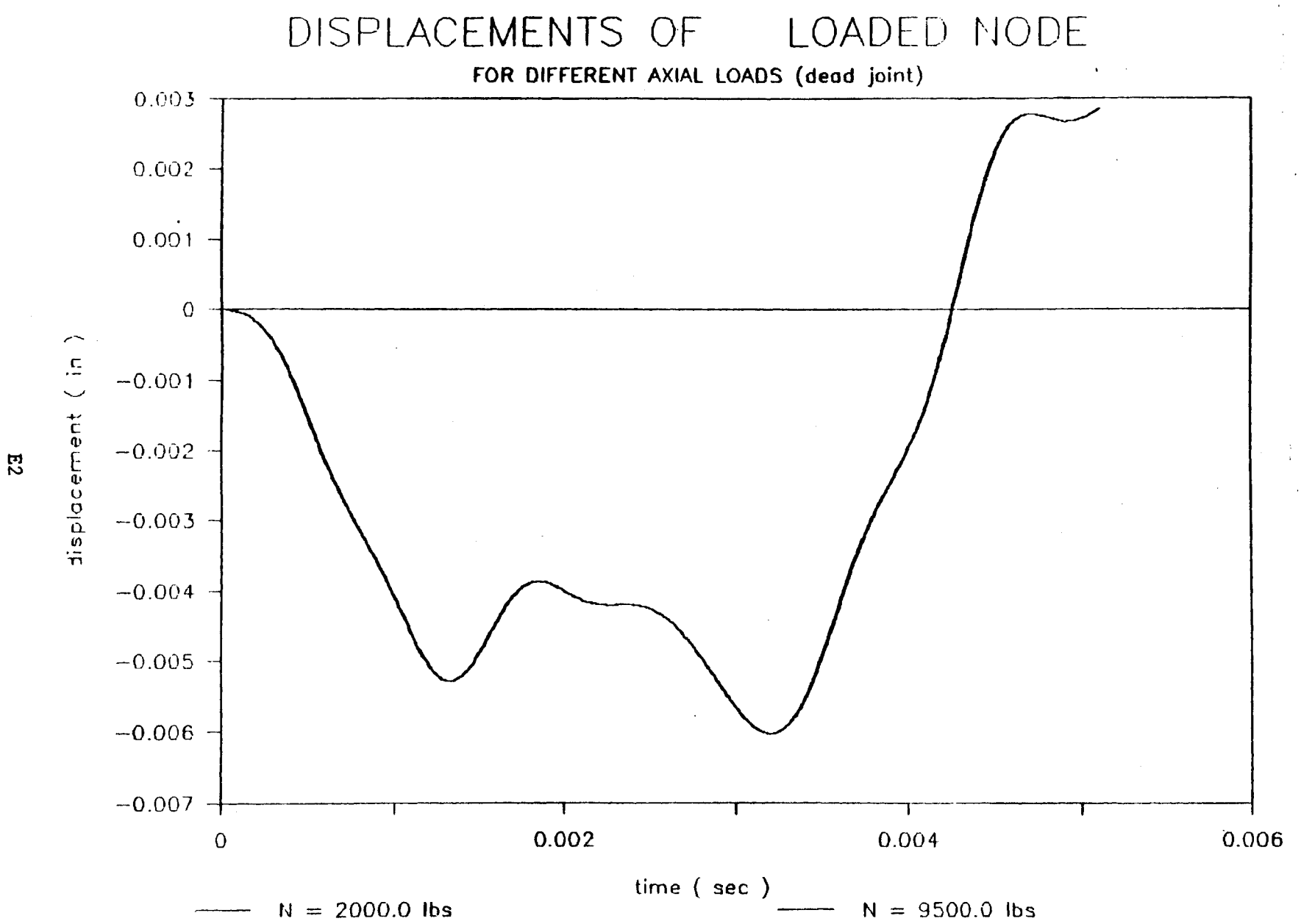
DISPLACEMENTS OF LOADED NODE
FOR DIFFERENT AXIAL LOADS (dead joint)
0.003
0.002
0.001
0
-0.001
-0.002
-0.003
-0.004
-0.005
-0.006
-0.007
displacement (in)
0
0.002
0.004
0.006
time (sec)
N = 2000.0 lbs
N = 9500.0 lbs

E2

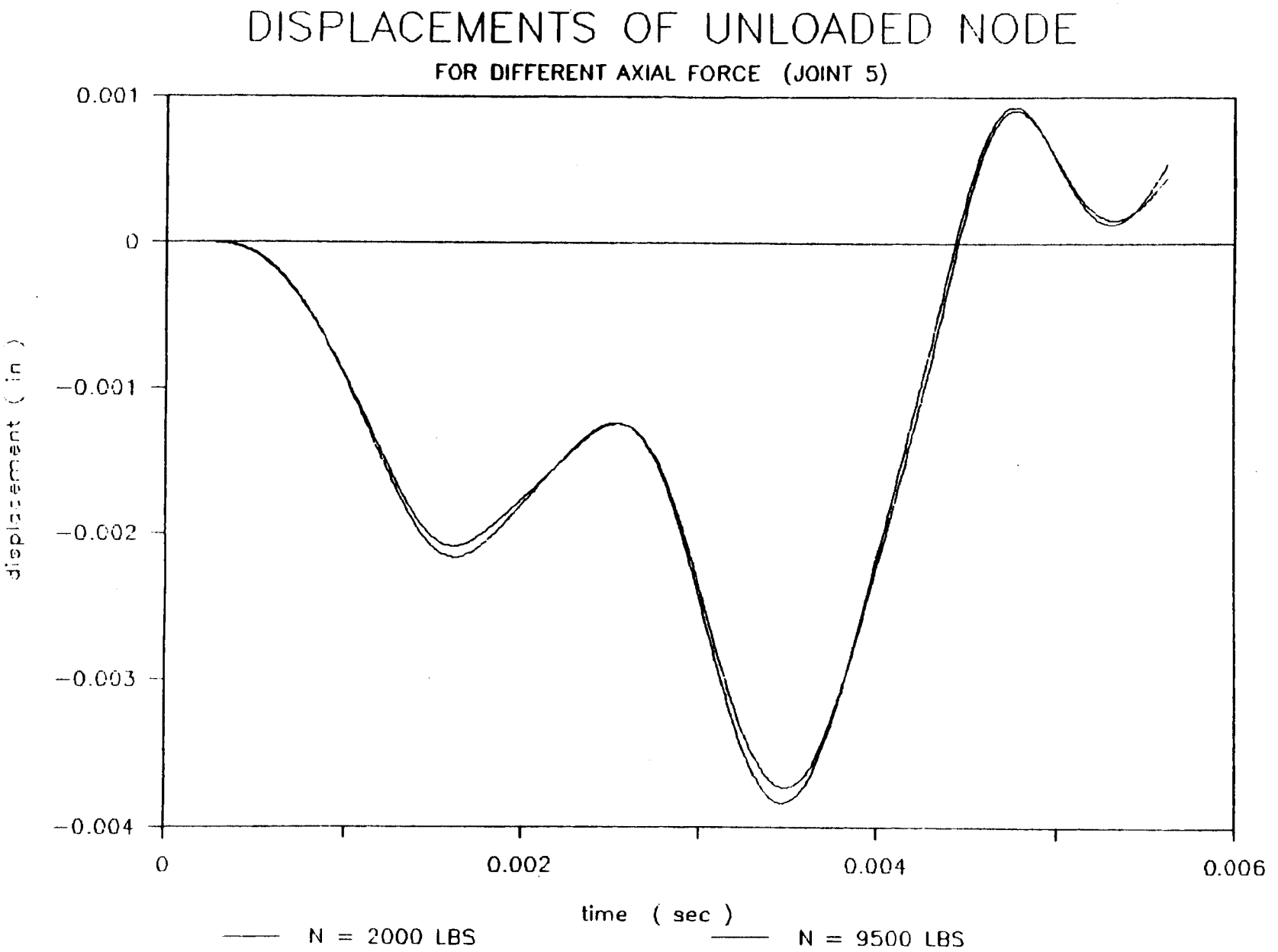
DISPLACEMENTS OF UNLOADED NODE
FOR DIFFERENT AXIAL FORCE (JOINT 5)
0.001
0
−0.001
−0.002
−0.003
−0.004
displacement (in)
0
0.002
0.004
0.006
time (sec)
N = 2000 LBS
N = 9500 LBS

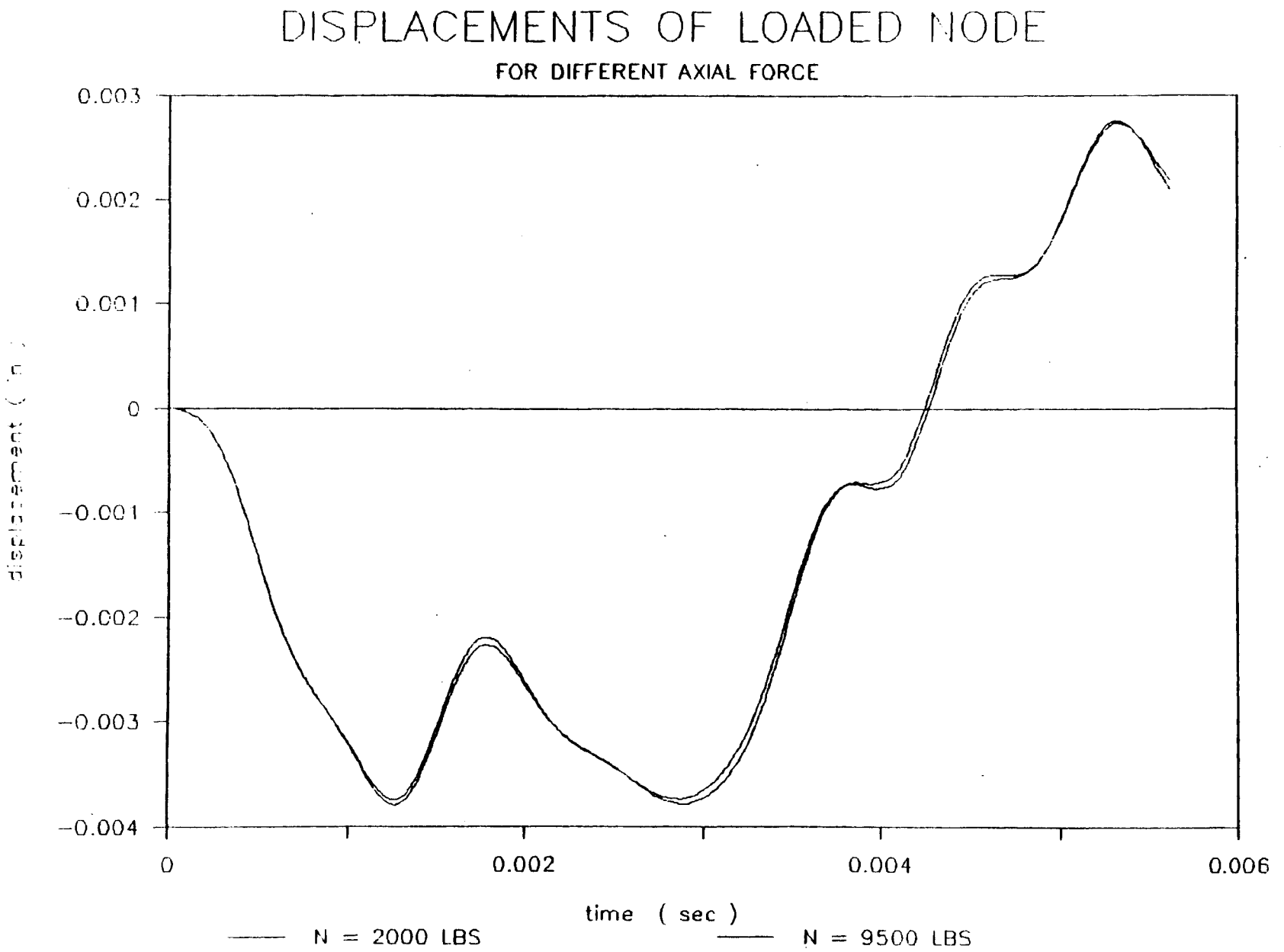
DISPLACEMENTS OF LOADED NODE
FOR DIFFERENT AXIAL FORCE
0.003
0.002
0.001
0
-0.001
-0.002
-0.003
-0.004
0
0.002
0.004
0.006
time (sec)
N = 2000 LBS
N = 9500 LBS

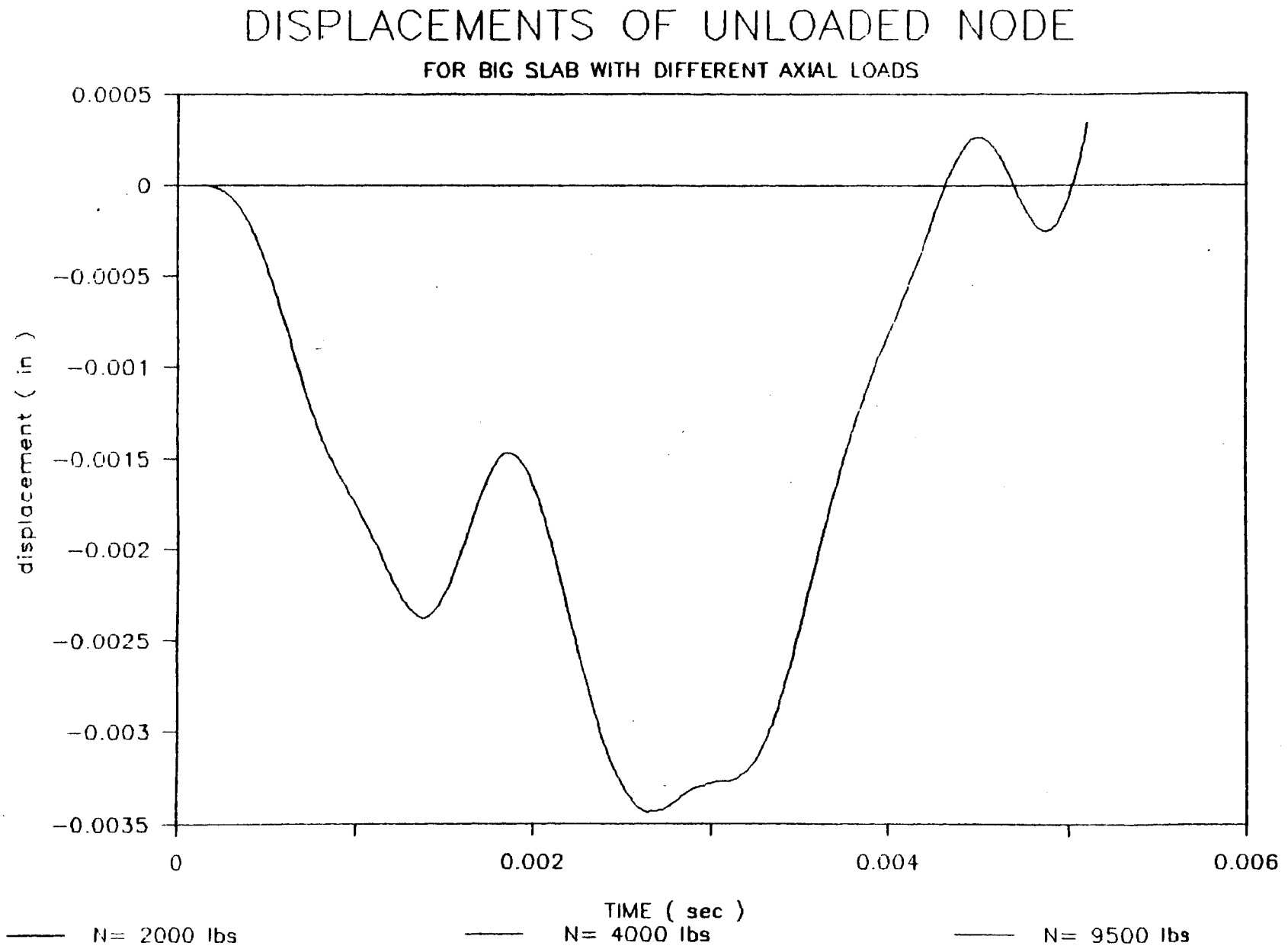
DISPLACEMENTS OF UNLOADED NODE
FOR BIG SLAB WITH DIFFERENT AXIAL LOADS
0.0005
0
-0.0005
-0.001
-0.0015
-0.002
-0.0025
-0.003
-0.0035
displacement (in)
0
0.002
0.004
0.006
TIME (sec)
N= 2000 lbs
N= 4000 lbs
N= 9500 lbs

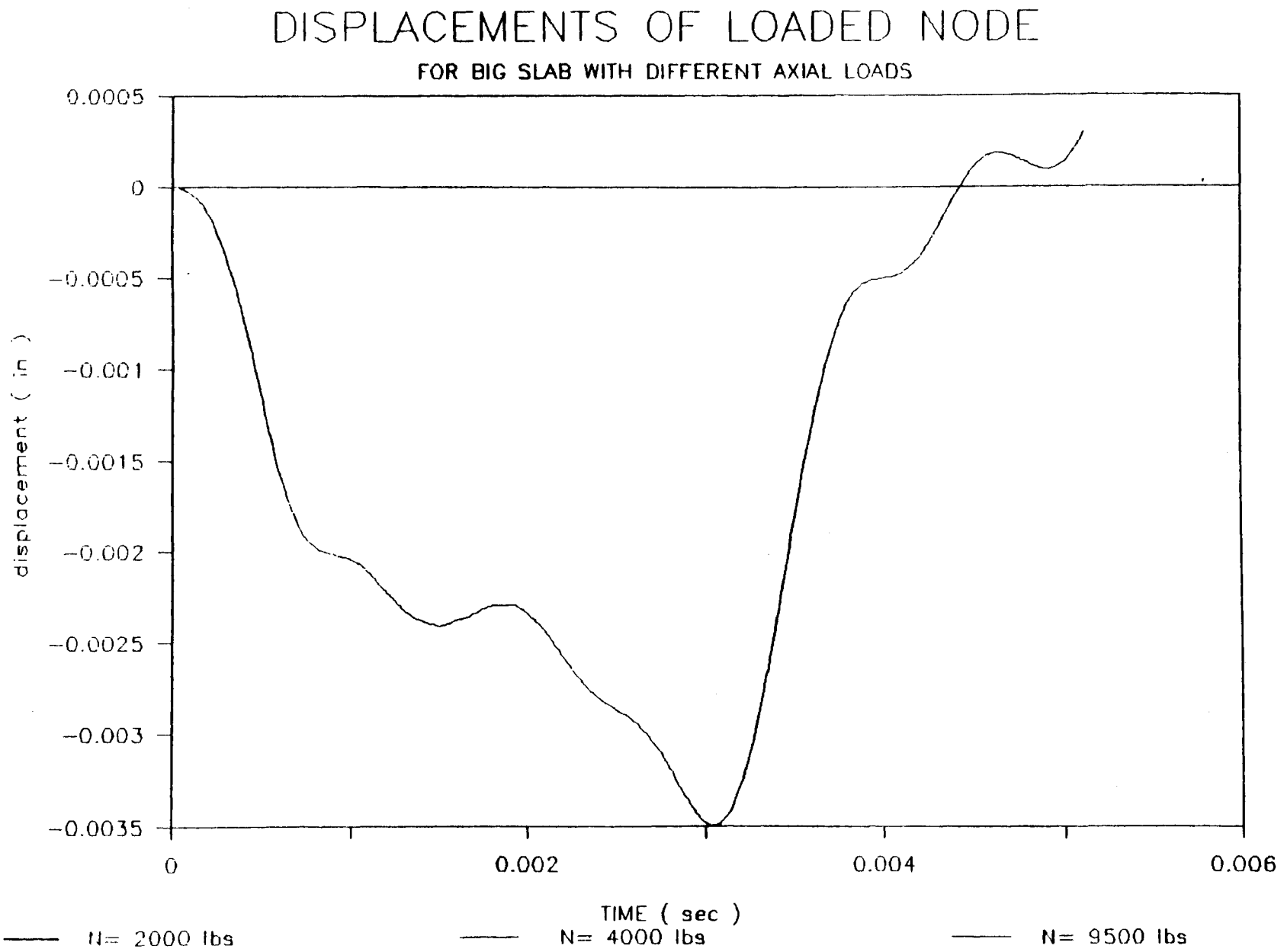
DISPLACEMENTS OF LOADED NODE
FOR BIG SLAB WITH DIFFERENT AXIAL LOADS
0.0005
0
-0.0005
-0.001
-0.0015
-0.002
-0.0025
-0.003
-0.0035
displacement (in)
0
0.002
0.004
0.006
TIME (sec)
N= 2000 lbs
N= 4000 lbs
N= 9500 lbs

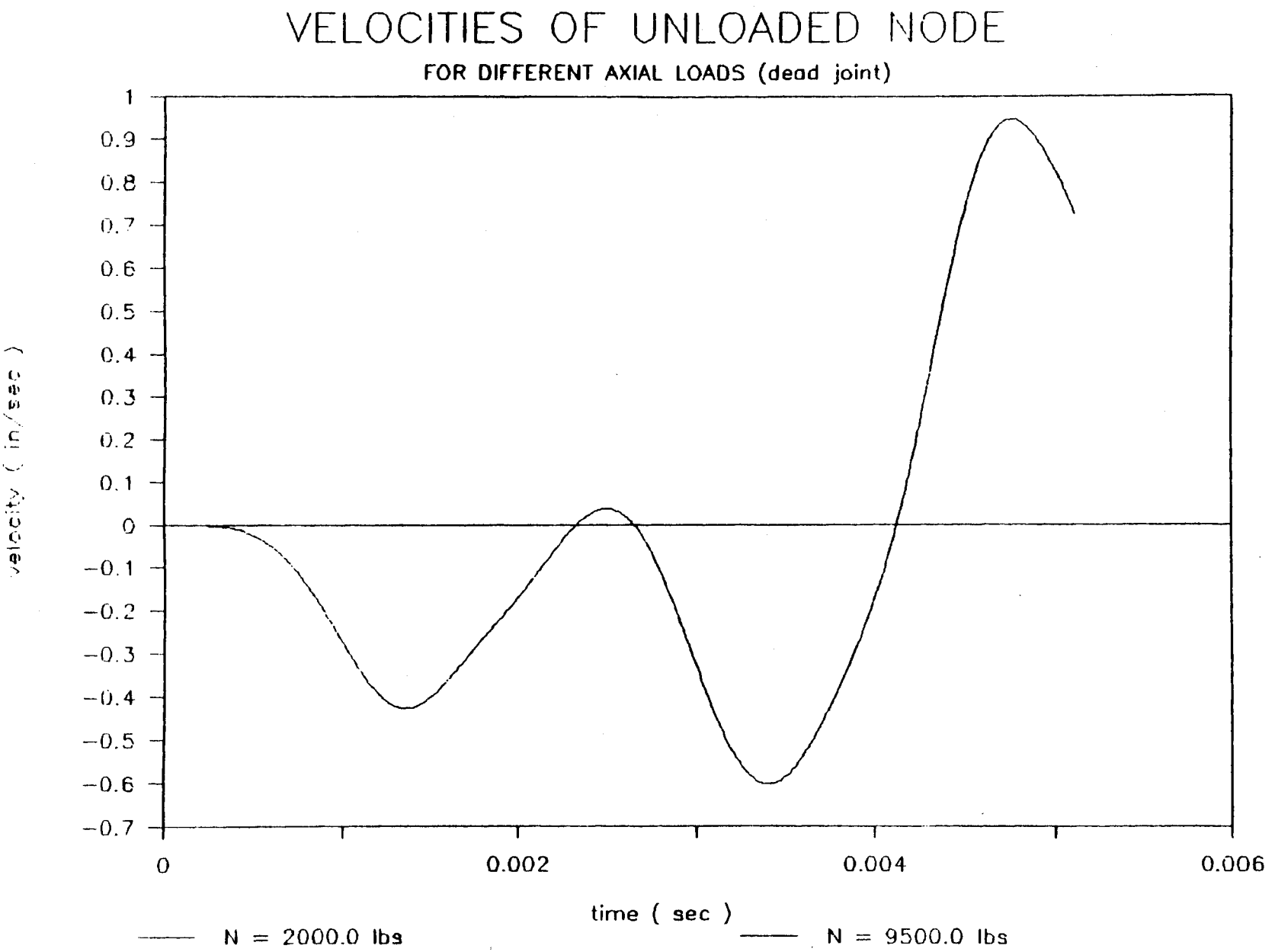
VELOCITIES OF UNLOADED NODE
FOR DIFFERENT AXIAL LOADS (dead joint)
velocity (in/sec)
1
0.9
0.8
0.7
0.6
0.5
0.4
0.3
0.2
0.1
0
−0.1
−0.2
−0.3
−0.4
−0.5
−0.6
−0.7
0
0.002
0.004
0.006
time (sec)
N = 2000.0 lbs
N = 9500.0 lbs

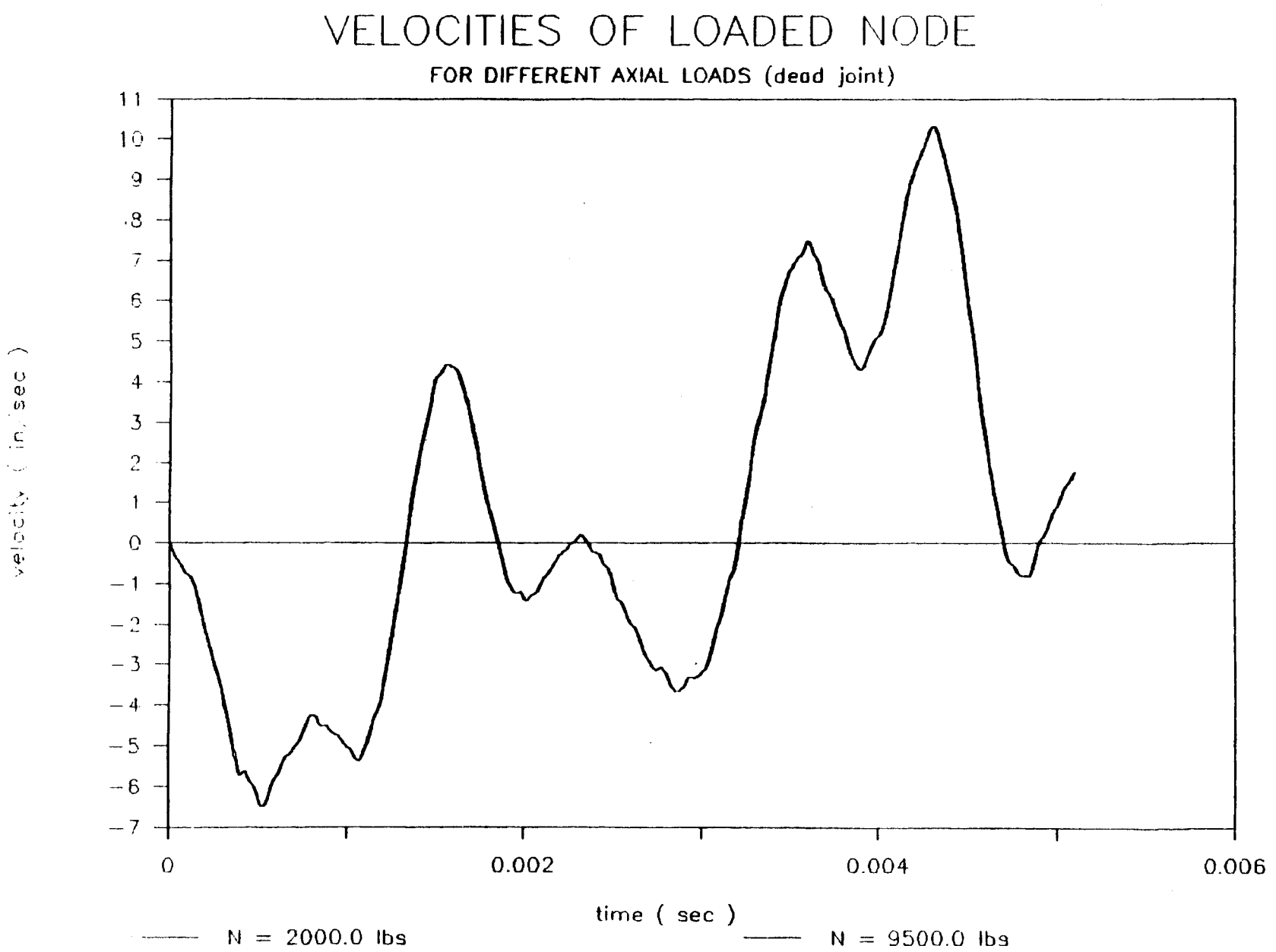
VELOCITIES OF LOADED NODE
FOR DIFFERENT AXIAL LOADS (dead joint)
11
10
9
8
7
6
5
4
3
2
1
0
−1
−2
−3
−4
−5
−6
−7
0
0.002
0.004
0.006
time (sec)
N = 2000.0 lbs
N = 9500.0 lbs

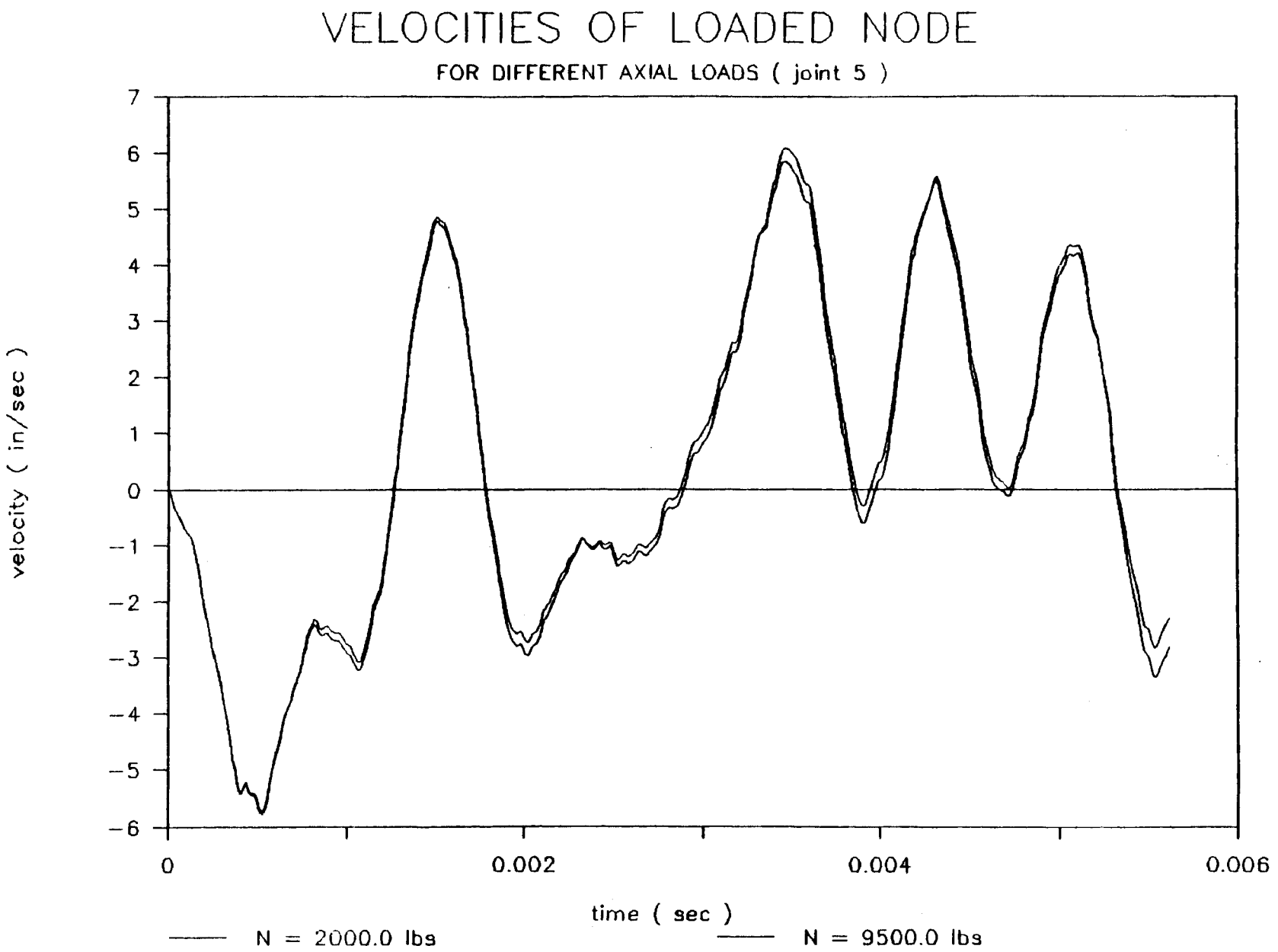
VELOCITIES OF LOADED NODE
FOR DIFFERENT AXIAL LOADS (joint 5)
velocity (in/sec)
7
6
5
4
3
2
1
0
−1
−2
−3
−4
−5
−6
0
0.002
0.004
0.006
time (sec)
N = 2000.0 lbs
N = 9500.0 lbs

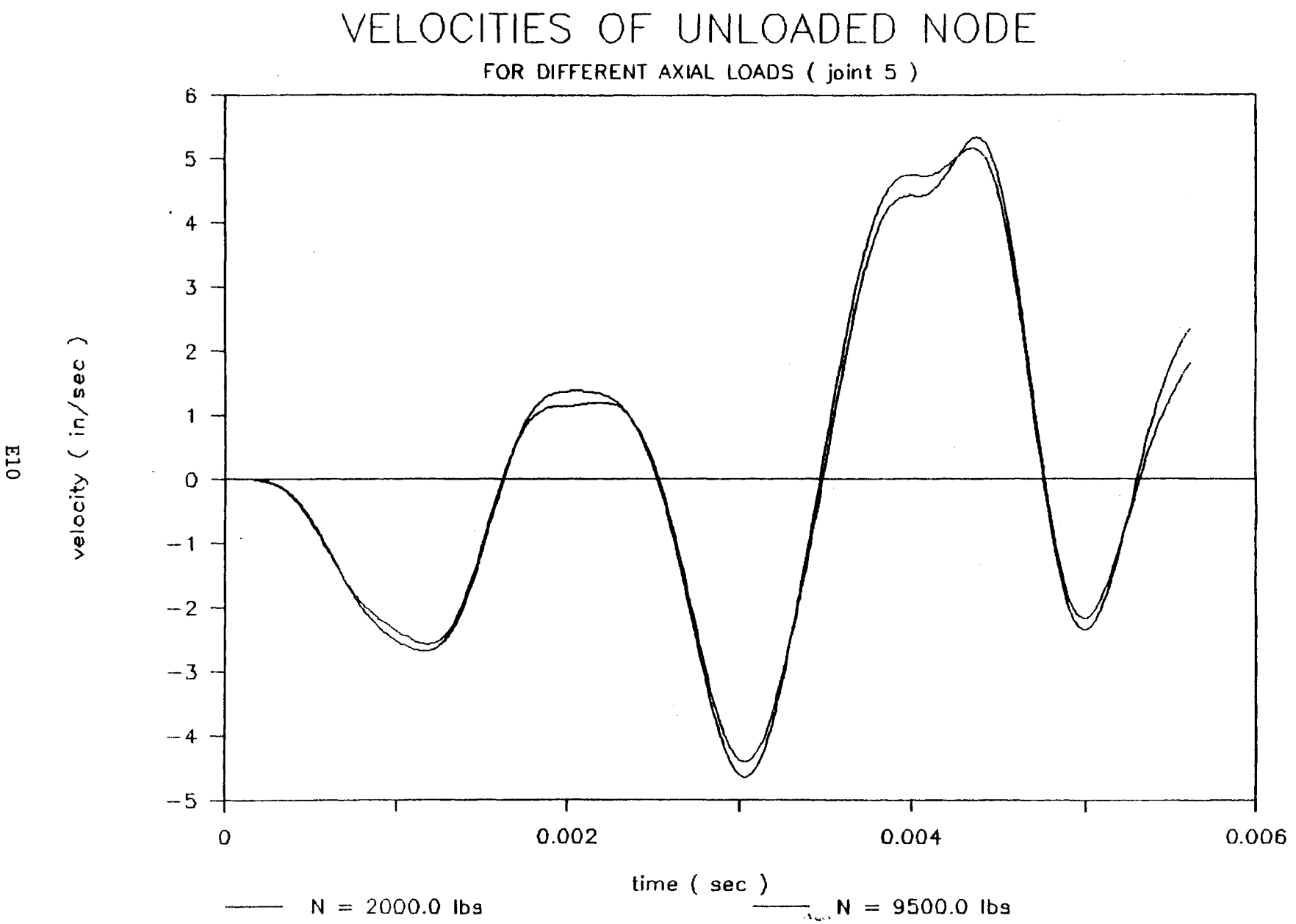
VELOCITIES OF UNLOADED NODE
FOR DIFFERENT AXIAL LOADS (joint 5)
velocity (in/sec)
E10
6
5
4
3
2
1
0
-1
-2
-3
-4
-5
0
0.002
0.004
0.006
time (sec)
N = 2000.0 lbs
N = 9500.0 lbs

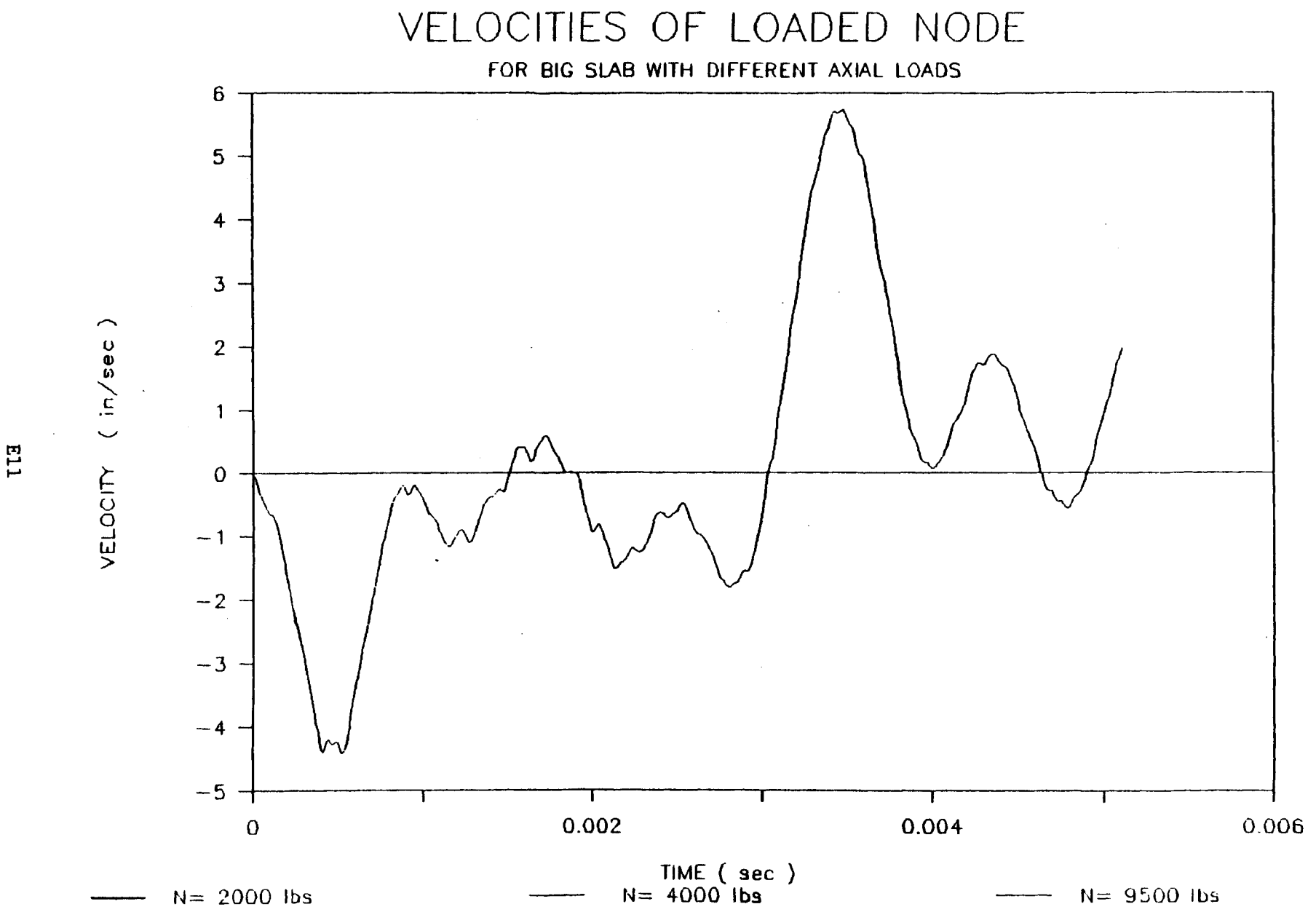
VELOCITIES OF LOADED NODE
FOR BIG SLAB WITH DIFFERENT AXIAL LOADS
VELOCITY (in/sec)
6
5
4
3
2
1
0
-1
-2
-3
-4
-5
0
0.002
0.004
0.006
TIME (sec)
N= 2000 lbs
N= 4000 lbs
N= 9500 lbs

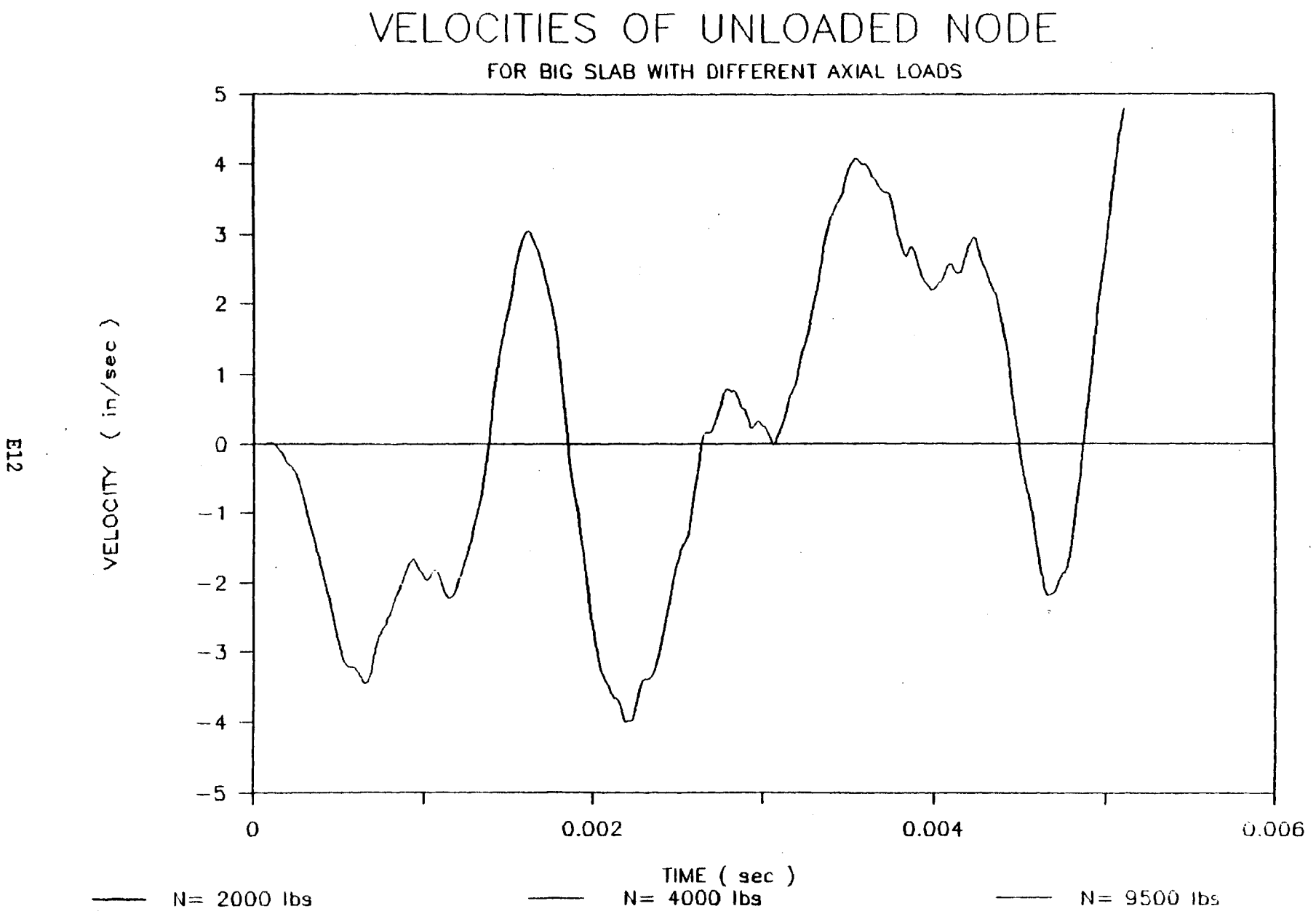
VELOCITIES OF UNLOADED NODE
FOR BIG SLAB WITH DIFFERENT AXIAL LOADS
VELOCITY (in/sec)
5
4
3
2
1
0
-1
-2
-3
-4
-5
0
0.002
0.004
0.006
TIME (sec)
N= 2000 lbs
N= 4000 lbs
N= 9500 lbs

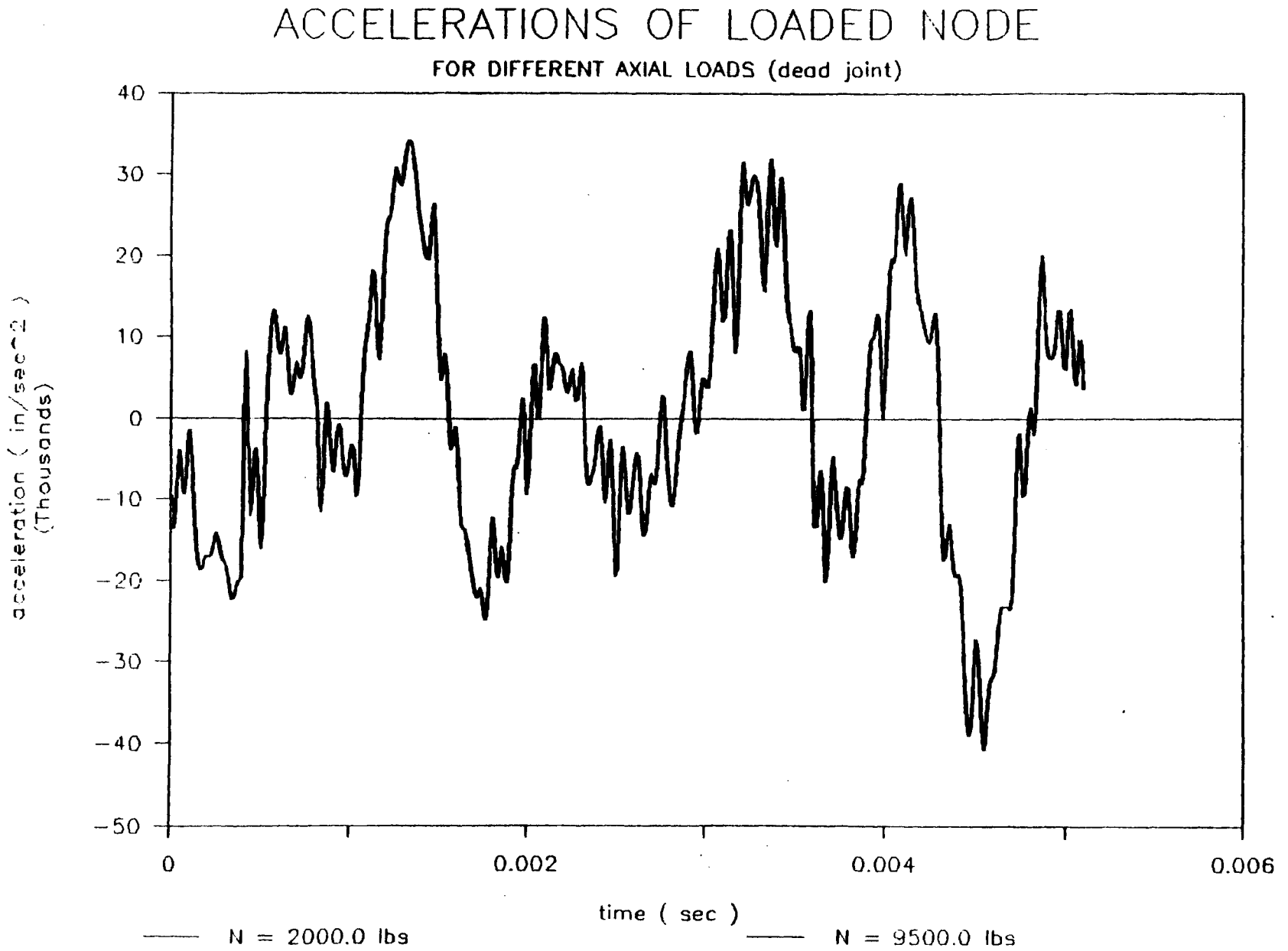
ACCELERATIONS OF LOADED NODE
FOR DIFFERENT AXIAL LOADS (dead joint)
acceleration (in/sec^2)
(Thousands)
40
30
20
10
0
-10
-20
-30
-40
-50
0
0.002
0.004
0.006
time (sec)
N = 2000.0 lbs
N = 9500.0 lbs

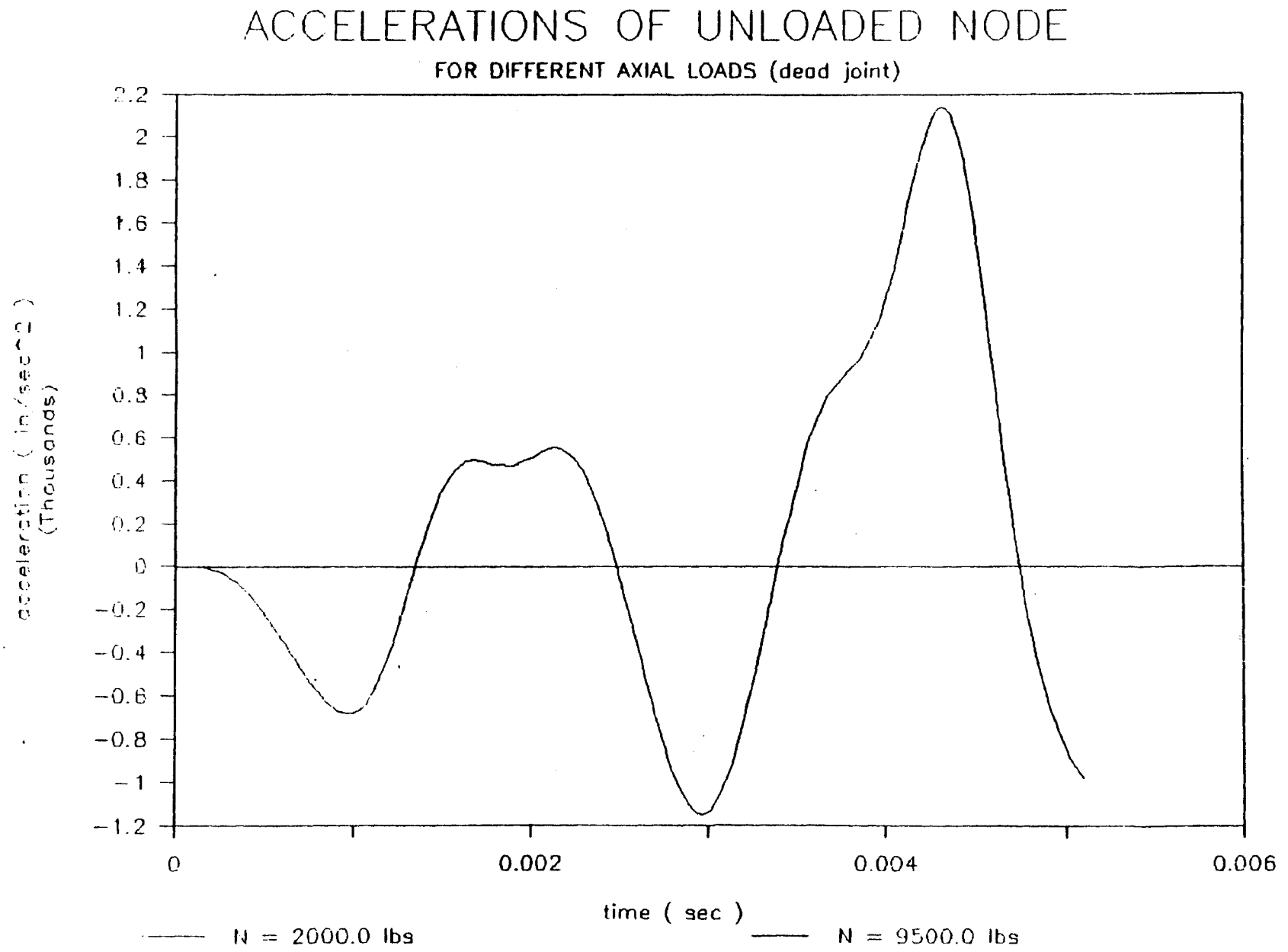
ACCELERATIONS OF UNLOADED NODE
FOR DIFFERENT AXIAL LOADS (dead joint)
acceleration (in/sec^2)
(Thousands)
2.2
2
1.8
1.6
1.4
1.2
1
0.8
0.6
0.4
0.2
0
-0.2
-0.4
-0.6
-0.8
-1
-1.2
0
0.002
0.004
0.006
time (sec)
N = 2000.0 lbs
N = 9500.0 lbs

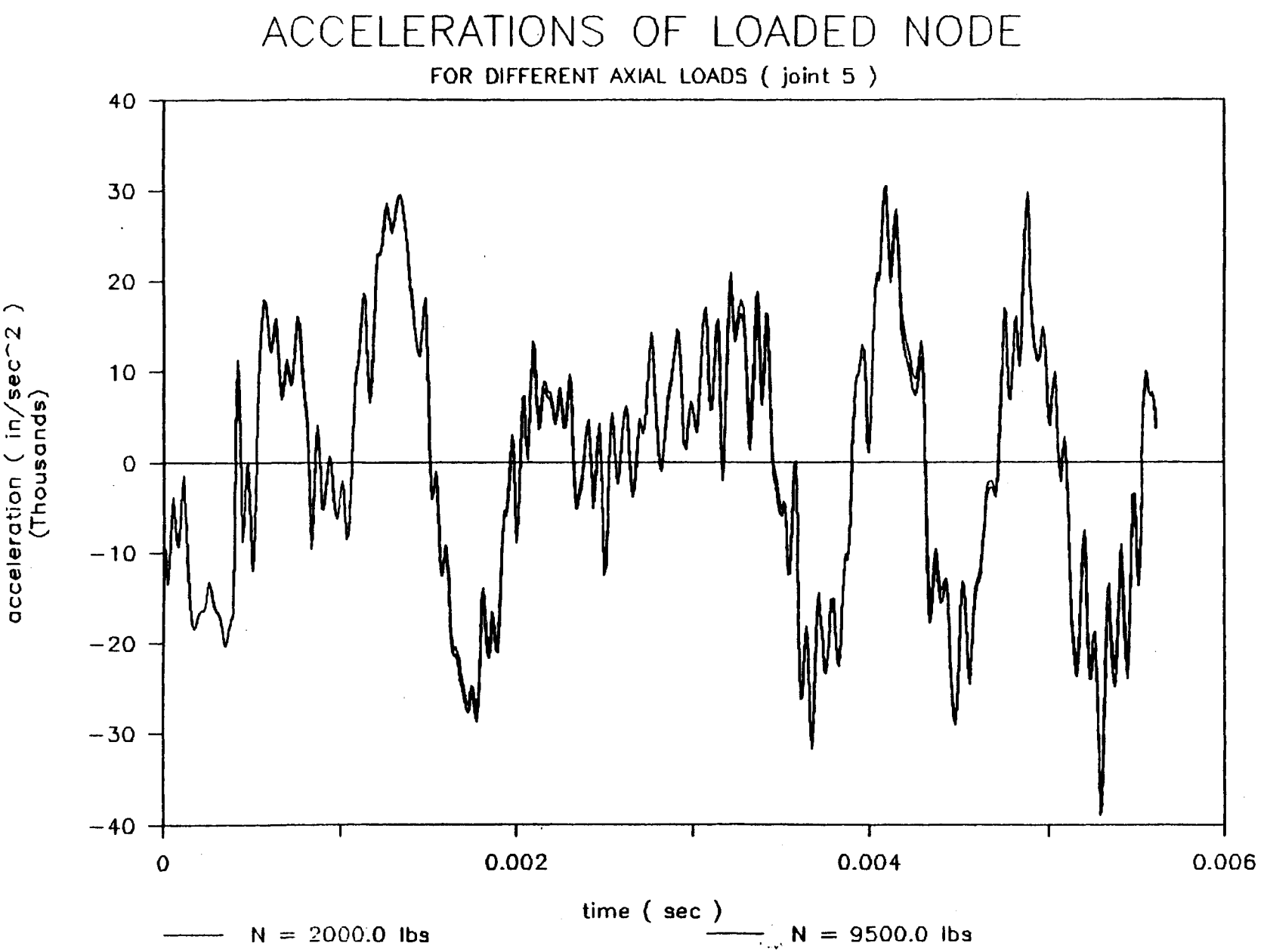
ACCELERATIONS OF LOADED NODE
FOR DIFFERENT AXIAL LOADS (joint 5)
acceleration (in/sec^2)
(Thousands)
40
30
20
10
0
-10
-20
-30
-40
0
0.002
0.004
0.006
time (sec)
N = 2000.0 lbs
N = 9500.0 lbs

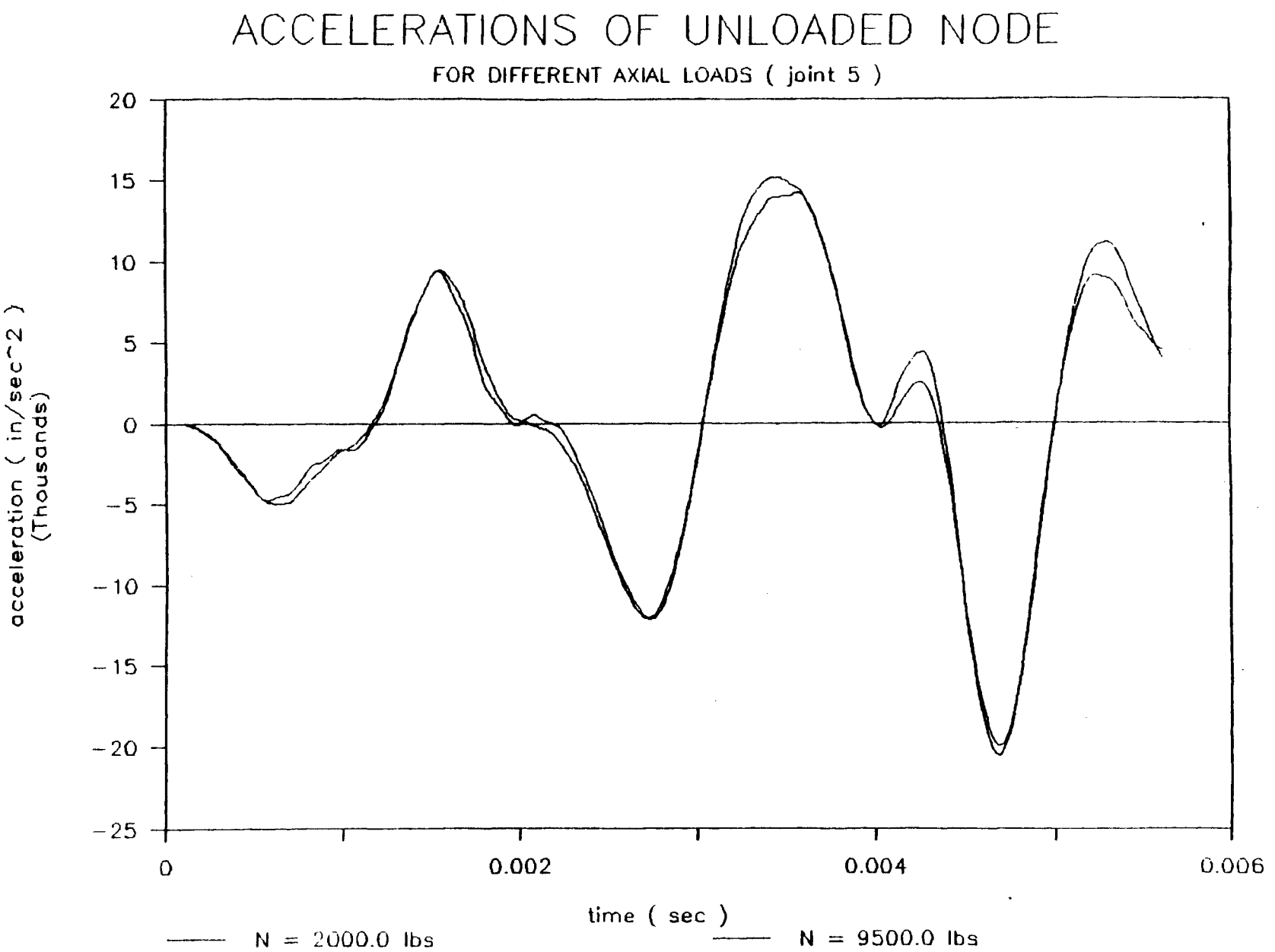
ACCELERATIONS OF UNLOADED NODE
FOR DIFFERENT AXIAL LOADS (joint 5)
acceleration (in/sec^2)
(Thousands)
20
15
10
5
0
-5
-10
-15
-20
-25
0
0.002
0.004
0.006
time (sec)
N = 2000.0 lbs
N = 9500.0 lbs

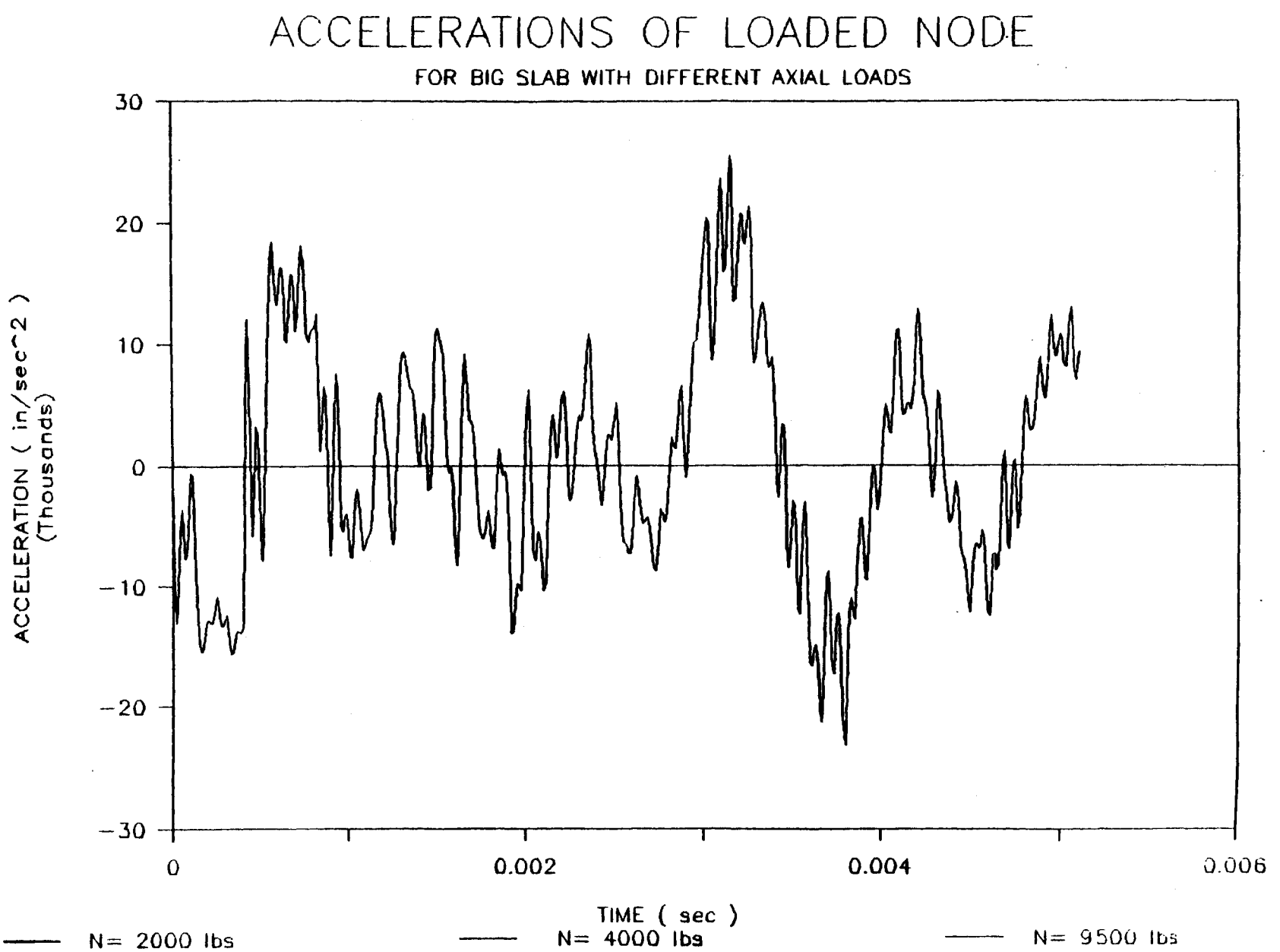
ACCELERATIONS OF LOADED NODE
FOR BIG SLAB WITH DIFFERENT AXIAL LOADS
ACCELERATION (in/sec^2)
(Thousands)
30
20
10
0
-10
-20
-30
0
0.002
0.004
0.006
TIME (sec)
N= 2000 lbs
N= 4000 lbs
N= 9500 lbs

ACCELERATIONS OF UNLOADED NODE

FOR BIG SLAB WITH DIFFERENT AXIAL LOADS